Liquid Sloshing in Containers: its Utilisation and Control

Jeremy Graeme Anderson

A thesis submitted to Victoria University of Technology
for the Doctor of Philosophy Degree (Mechanical Engineering)

2000

ACKNOWLEDGMENTS

I would like to thank the supervisors of this thesis, Associate Professor Özden Turan and Dr. Eren Semercigil. I thank them for their advice, encouragement and friendship. I learnt a great deal from them.

During my candidature I was a recipient of an Australian Postgraduate Award. The financial support of this scholarship was greatly appreciated. I was also given the opportunity to teach in the Department of Mechanical Engineering and then in the School of the Built Environment. I would like to thank Victoria University of Technology for this financial help and teaching experience. To the staff and other postgraduate students, it was a pleasure to work with such a professional team.

Finally, to my wife Rachael and my family, I sincerely thank you for your support.

Jeremy Graeme Anderson

ABSTRACT

Sloshing is the oscillation of a contained liquid. In the first part of this thesis, the interaction between liquid sloshing and a mechanical oscillator has been exploited to control resonant vibrations of the oscillator. A deep-liquid-level sloshing absorber is presented as a practical alternative to the damped tuned absorber. In addition, a numerical simulation procedure is introduced as a computer aided design tool.

In many practical applications, it is necessary to suppress liquid sloshing. Such applications include the transportation of liquid cargo, sloshing in fuel tanks of aircraft and spacecraft and earthquake induced sloshing in liquid storage tanks. Hence, the objective of the rest of the thesis is to control sloshing. Baffles cantilevered from the sides of tanks have shown effective sloshing control, provided that the volume of liquid remains approximately constant. Alternatively, a simple floating control device consisting of two plates in a dumb-bell arrangement has shown effective control at varying liquid levels.

In some practical applications, the addition of such devices may not be possible due to geometric constraints. For such cases, the interaction between liquid sloshing and flexible container walls may be exploited to control liquid sloshing. The advantages of using a flexible container are twofold. Firstly, liquid sloshing is reduced. Secondly, if flexibility of the container is achieved by reducing the wall thickness, a lighter container is used, saving material and cost.

TABLE OF CONTENTS

TABLE OF CONTENTS

LIST OF TABLES

LIST OF FIGURES

LIST OF FIGURES

LIST OF FIGURES

LIST OF FIGURES

LIST OF FIGURES

Page

Chapter 1

INTRODUCTION

The term sloshing generally refers to relatively low frequency but large amplitude oscillations of a liquid in a container. The investigations in this thesis are divided into three separate areas. Firstly, liquid sloshing has been utilised for the purposes of controlling structural vibrations. Secondly, the focus has been to control liquid sloshing with simple, passive controllers that can be added to existing containers. Thirdly, the use of container flexibility has been examined as a means to control liquid sloshing. The general objective is to contribute to the understanding of sloshing motion in engineering applications. To present the specific objectives of this thesis, a brief description of the content of each chapter is given next. Each chapter is self-contained, starting with its own introduction and literature review.

Liquid sloshing has been utilised in the literature in Tuned Liquid Dampers (TLD), to suppress wind induced vibrations of tall structures in a number of applications. A TLD is a passive control device that can suppress structural vibrations using liquid motion. There are a number of advantages to using this device, such as low cost of manufacture and installation and low maintenance. No weight penalty to the structure exists when the design of the damper is incorporated with a storage tank for water supply. However, existing storage tanks typically have deep liquid levels that induce standing sloshing waves. Prior to this thesis, standing sloshing waves had been shown to have inherently poor energy dissipation characteristics. It is this phenomenon that is the focus of Chapter 2. In Chapter 2, a deep liquid sloshing absorber is used to effectively control structural oscillations. Energy dissipation is achieved by strategically placing baffles in the container. The proposed modifications are simple, inexpensive and can easily be added to many types of storage containers in practical applications. Hence, the significance of the new work presented in Chapter 2 is in its showing that deep liquid sloshing absorbers can be modified to effectively control structural oscillations. Previously, such sloshing absorbers were typically restricted to shallow liquid depths only.

The detrimental effects of liquid sloshing are experienced in areas such as transportation of liquid cargo, earthquake induced sloshing in liquid storage tanks and the fuel tanks of aircraft. If not controlled effectively, sloshing may spoil sensitive items, such as suspension type food, wine and chemical liquids during transportation. More importantly, liquid sloshing can cause loss of dynamic stability and manoeuvrability of the transportation vehicle. In earthquake prone parts of the world, liquid sloshing due to ground motion can cause spillage and may lead to structural failure. Therefore, it is important to control sloshing to prevent loss of life and property. Although there has been wide interest in the modelling of liquid sloshing, only few attempted to model the control of liquid sloshing. In Chapter 3, experiments and numerical predictions are presented to show that cantilever baffles extending from the walls of rigid tanks can provide effective control of liquid sloshing. One of the significant contributions in Chapter 3 is that the control action of different sized cantilever baffles is presented in a non-dimensional form to be used for design purposes.

Cantilever baffles may not be suitable for all practical applications as their effectiveness depends on the location of the fixed baffles on the side of the container.

For cases where the liquid volume in the container changes, there may be a significant deterioration of the control action of fixed baffles. In such cases, simple floating devices may prove successful. Chapter 3 also focuses on an experimental investigation of a floating device, named a dumb-bell controller, to suppress liquid sloshing when the liquid level is expected to change over time. Due to the floating nature of dumb-bell controllers, it is shown that effective sloshing control may be maintained even when the volume of liquid in the tank is varied, and this is another significant contribution in Chapter 3. It is clear that the specifications of practical problems involving the suppression of liquid sloshing, will ultimately govern the type of control technique employed.

The addition of passive control devices to control liquid sloshing may not be possible in all applications due to structural constraints. Therefore, in Chapter 4, numerical predictions and experimental observations are given for sloshing control using the flexibility of the container. Oscillations of the container are induced intentionally by tuning the structural natural frequencies to that of liquid sloshing. Such tuned cases suggest effective control of the liquid. Hence, the work in Chapter 4 may provide quite significant benefits in applications involving the transportation of liquid cargo. Ultimately, the containers used to transport liquid cargo may act as sloshing controllers. In addition, if the container walls are made flexible by reducing the wall thickness, then significant reductions may be made to the mass of the container. The significance of Chapter 4 is in presenting this novel concept of exploiting container flexibility.

In Chapter 5, the conclusions of the thesis are summarised. In addition, three appendices are included in this thesis. The predictions in Chapter 2 for a sloshing absorber were done using a commercially available computational fluid dynamics code, CFX4.1. The two files written in the CFX environment to model the sloshing absorber are in Appendix 1. Throughout the thesis, the theoretical sloshing frequency is determined and compared with predictions or experiments. The derivation of the theoretical sloshing frequency from Milne-Thomson (1968) is included in Appendix 2, for completeness. As a starting point to modelling dumb-bell type controllers, some initial numerical predictions are given in Appendix 3 to determine the control action of a single floating plate.

Chapter 2

A STANDING-WAVE TYPE SLOSHING ABSORBER TO CONTROL TRANSIENT OSCILLATIONS†

2.1. INTRODUCTION

The problem of interest in this chapter is the control of excessive vibrations of a mechanical oscillator in response to an initial displacement. Tuned vibration absorbers are frequently used for this purpose, and if damping is included in the tuned absorber, the control action is quite effective. The problem, however, is that inclusion of an energy dissipation element necessitates frequent maintenance in practice. In this chapter, a deep liquid sloshing absorber is presented as a practical alternative to the damped tuned absorber. In addition, a numerical simulation procedure is introduced as a computer aided design tool.

In contrast to a tuned absorber, a sloshing absorber accomplishes energy dissipation through sloshing. Therefore, it may be virtually maintenance free. Also, for practical applications, this type of absorber can be an advantage where existing water storage tanks can be modified to control vibrations of the supporting structure. Numerical simulations and experimental observations are presented in this chapter to compare the performances of a sloshing absorber and a conventional tuned absorber. The scaling parameters of liquid sloshing in containers are shown to be applicable to a system consisting of a sloshing absorber and the structure to be controlled. In addition, numerical predictions of the velocity field and liquid free surface shape in a

† The work presented in this chapter has been published in Anderson et al. 1999a and 1999b.

sloshing absorber are exploited to determine the optimum sloshing absorber configuration. The tuned absorber and sloshing absorber are described next in detail.

2.1.1. Tuned Absorber

A tuned absorber, in its standard form, is a mechanical oscillator whose resonant frequency is tuned at a critical frequency of the structure to be controlled. Comprehensive treatment of this classical subject may be found in standard textbooks such as in Hunt (1979) and in Snowdon (1968). Figure 2.1. schematically illustrates such a system. The primary system with mass m_1, damping c_1 and stiffness k_1 represents the structure to be controlled, whereas the auxiliary oscillator with m_2, c_2 and k_2 is the tuned absorber. Tuning is usually accomplished by designing the natural frequency of the absorber to be the same as that of the structure to be controlled: $(k_1 / m_1)^{1/2} = (k_2 / m_2)^{1/2}$. Some slight deviations from this basic relationship may occur when using significant values of c_2.

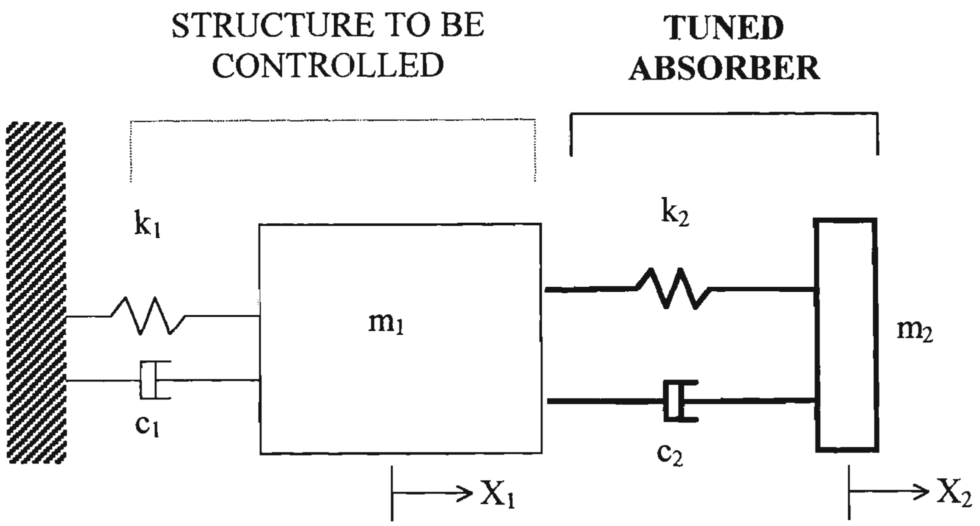

Figure 2.1. A tuned vibration absorber and the structure to be controlled.

With an undamped tuned absorber, control may be very effective when the structure to be controlled is excited harmonically at the tuning frequency. However, this effectiveness deteriorates drastically in the case of transient disturbances. In transient cases, the oscillatory energy may be transferred readily to the absorber due to strong interaction. This energy returns to the structure resulting in a poor control action, unless some means of energy dissipation is provided in the absorber. A damper, c_2, may be included in the absorber to improve performance. Optimum values of damping are derived in Snowdon (1968), and the response of a tuned vibration absorber is discussed in detail here in Section 2.2. Inclusion of a damper, however, presents problems of frequent maintenance and reduces the practical value of the controller. A sloshing absorber may be a simple alternative to the conventional tuned absorber to avoid such problems.

2.1.2. Sloshing Absorber

Most of the earlier work in the field of sloshing has been directed to understanding the physics of the phenomenon for the purposes of suppressing it. The objective in this study is to intentionally induce sloshing of a liquid in a container which is in turn attached onto a resonant structure. In such a configuration, fluid forces may be used to counteract and suppress structural oscillations (Anderson et al. 1998a). The proposed sloshing absorber is shown in Figure 2.2, when attached on the same structure as in Figure 2.1. In Figure 2.2(a), the sloshing absorber has no baffles. Alternatively, Figure 2.2(b) shows a sloshing absorber with a pair of baffles cantilevered from the vertical walls of the container. The use of sloshing absorbers with baffles is discussed in detail later in Section 2.3. For now, Figure 2.2 is used to show that the principle of this particular structural control technique is similar to that of a classical tuned vibration absorber (Anderson et al. 1998b). However, a distinct potential advantage of the proposed approach is that existing liquid storage tanks may be employed for structural control purposes. For cases where the sloshing controller is an added component to reduce structural oscillations, its inherent characteristic of requiring virtually no maintenance is a significant practical advantage.

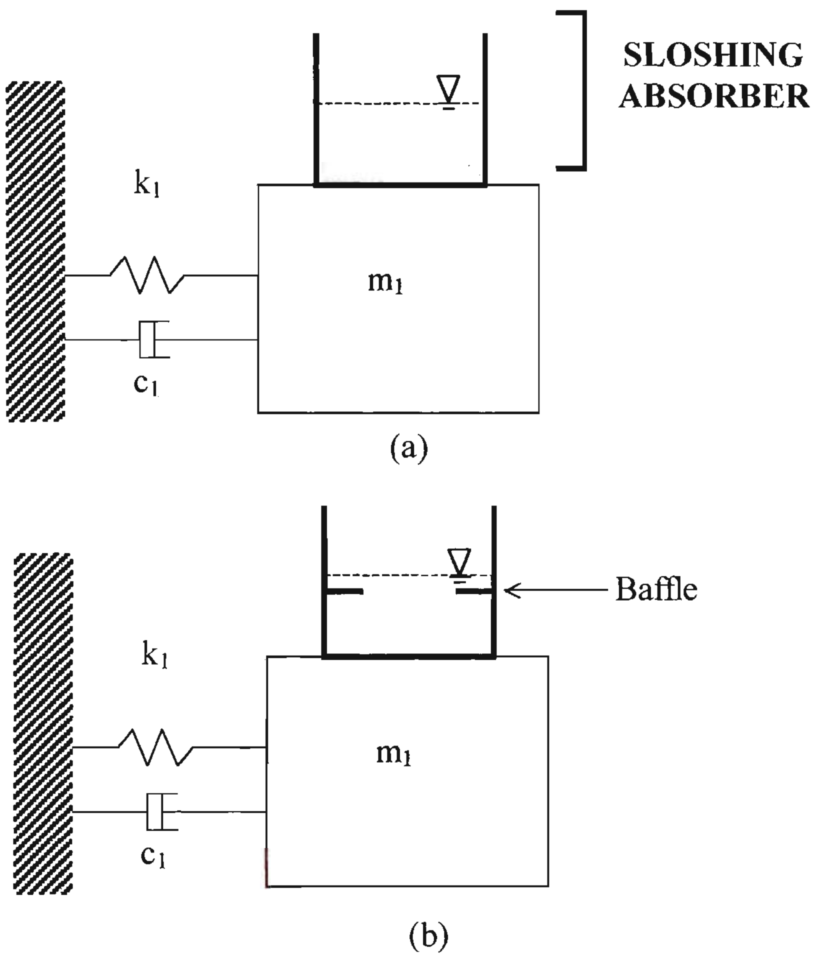

Figure 2.2. The proposed sloshing absorber attached on the structure to be controlled: (a) a sloshing absorber without baffles and (b) with a pair of cantilever baffles.

2.1.3. Use of Liquid Sloshing for Structural Control

The concept of using sloshing forces for structural control has been suggested earlier. Fujii et al. (1990) reported using liquid motion in a circular container to reduce wind-induced oscillations at Nagasaki Airport Tower and Yokohama Marine Tower to about half of the uncontrolled values. Abe et al. (1996) reported effective control of structural vibrations using a U-tube with a variable orifice passage. Modi and Welt (1984) pioneered research on Nutation Dampers and their applications in tall structures. Seto and Modi (1997) also presented work to use fluid-structure interaction to control wind induced instabilities.

In sloshing controllers, plain water, which has poor energy dissipation characteristics, is usually used as the working fluid. In order to improve energy dissipation, Kaneko and Yoshida (1994) suggested employing a net to obstruct the flow of liquid during sloshing, and reported optimum levels of obstruction for best structural control. Warnitchai and Pinkaew (1998) predicted the effect of flow damping devices such as vertical poles, blocks and nets on sloshing in rectangular tanks for the purpose of controlling structural oscillations. In their formulation, the liquid was assumed to be inviscid, incompressible and irrotational. Surface tension effects were neglected.

Shallow liquid levels in a container are likely to induce travelling sloshing waves with desirable energy dissipation. For this reason, earlier work invariably dealt with shallow liquid levels in the tuned sloshing absorbers. Even in the work of Kaneko and Yoshida (1994) which employs a relatively larger depth than those of the others, the water depth is approximately equal to 35% of the length of the container. Such a small depth may be quite limiting for some geometries such as liquid storage tanks in tall structures. This particular point is addressed in this study with water depth of the absorber comparable to the length of the container.

Deep liquid levels cause a standing sloshing wave at the fundamental mode. Without additional measures, the suppression effect of a standing sloshing wave is quite limited. For such cases, the oscillatory energy of the structure could be easily transferred to the sloshing liquid, if there is a strong interaction. A strong interaction is assured when the sloshing frequency is close to the natural frequency of the structure. However, if there is no dissipative mechanism in the sloshing absorber, this transferred energy in the liquid may travel back to the structure to excite it quite easily. Oscillation of energy between the structure and the liquid, produces a beating envelope of oscillations of the structure. Such a beat drastically reduces the control effect, which is discussed in more detail later in this chapter (Kaneko and Yoshida, 1994, Anderson et al. 1998b).

To improve the performance of a standing wave sloshing absorber, fixed plate baffles are employed in the liquid container, as shown in Figure 2.2(b). Similar baffles were investigated earlier by Muto et al. (1988) where the purpose was to suppress liquid sloshing when the liquid container was excited by external means. In Chapter 3, the effectiveness of baffle plates to suppress sloshing is demonstrated. In contrast, in Chapter 2, baffle plates are used to modify the energy dissipation characteristics of a sloshing absorber to improve the control of structural oscillations.

Next, the response of a tuned vibration absorber is presented in Section 2.2, followed by a detailed experimental and numerical treatment of the response of sloshing absorbers with two baffle plates in Section 2.3. In this section, the tuned absorber is also compared with a sloshing absorber. Practical applications and scaling of sloshing absorbers are given in Section 2.4. An optimum sloshing absorber, which has only one baffle, is presented in Section 2.5.

2.2. RESPONSE OF TUNED VIBRATION ABSORBER

The performance of a conventional tuned absorber is examined in this section. A tuned absorber and the structure to be controlled are shown in Figure 2.1. The mass of the structure and mass of the absorber are 28 kg and 2.8 kg, respectively. The stiffness of the springs used for the structure and absorber are 5826 N/m and 579 N/m respectively. The structure to be controlled is undamped, $c_1 = 0$. The system parameters are summarised in Table 2.1.

The structure was given an initial displacement of 1.3 mm, and then the free vibration response of the system was determined. As shown in detail in Section 4.3.2, the response of a structure for a transient disturbance is a good indication of that for random excitation such as an earthquake. The reason for this behaviour, of course, is that random excitation may be envisaged as being made up of a series of transient disturbances in time. For this reason, transient system response has been used in this chapter in assessing the effectiveness of a tuned vibration absorber, as well as those of double and single baffle sloshing absorbers.

The solution of the equations of motion of the system shown in Figure 2.1 was obtained by numerically integrating the coupled system of two differential equations of motion, one for each mass. A standard fourth order Runge-Kutta procedure was followed. The time step was taken to be smaller than 1/40th of the shortest expected period of oscillations. Details of this procedure can be found in standard textbooks such as Rao (1990).

Histories of the displacement of m_1 (——) and the control force (——) of the tuned absorber on m_1, are shown in Figure 2.3. The horizontal axis represents non-dimensional time, t / T_0, where T_0 is the natural period of the structure to be controlled alone. The control force is comprised of the spring force, $k_2(X_2-X_1)$, and the damper force $c_2(\dot{X}_2-\dot{X}_1)$, of the tuned absorber, where X_1 and $\dot{X}_1$ and X_2 and $\dot{X}_2$ are the displacement and velocities of the masses m_1 and m_2, respectively . In Figure 2.3(a), the absorber is undamped, whereas in Figures 2.3(b) to 2.3(d), the value of critical damping ratio of the absorber, ξ_2, is 0.025, 0.19 and 1.24. Here, the critical damping ratio of the absorber, is defined as, $\xi_2 = \dfrac{c_2}{2\sqrt{m_2 k_2}}$.

In Figure 2.3(a), for the undamped tuned absorber, the oscillatory energy periodically travels back and forth between the structure to be controlled and the absorber. Due to this strong interaction, which is the result of tuning the absorber to the natural frequency of the structure, an initial displacement of 1.3 mm rapidly decays to very small values around 1.8 periods. At this instant, the absorber oscillates quite violently as indicated by the large control force. Starting from about 2 natural periods, however, the structure receives the absorber's energy back, resulting in as large displacements as its initial displacement. This exchange of energy, produces periodic beats of the envelopes of both displacement and force oscillations. The beat of the two histories are almost perfectly out of phase, indicating where most of the oscillatory energy is at a particular time.

In Figure 2.3(b), some light damping, $\xi_2 = 0.025$, is included in the tuned absorber, producing a significant difference from the results in Figure 2.3(a). The strong interaction and the resulting beat are still quite clear in Figure 2.3(b). However, the peak amplitudes decay gradually as a result of energy dissipated due to damping. When ξ_2 is increased to 0.19 in Figure 2.3(c), the beat disappears completely leaving a very effective control action. Oscillations virtually stop after 8 periods. In Figure 2.3(d), when ξ_2 is 1.24, the effective control in Figure 2.3(c) deteriorates quite drastically. Due to having too large a resistance between the oscillator and the absorber, the absorber is no longer able to oscillate freely with respect to the structure to be controlled. The limited relative motion still dissipates some energy, resulting in a slow rate of decay of the oscillation envelope. Any further increase in the value of ξ_2 would worsen the situation, eventually locking m_2 on m_1 and reverting to an undamped oscillator.

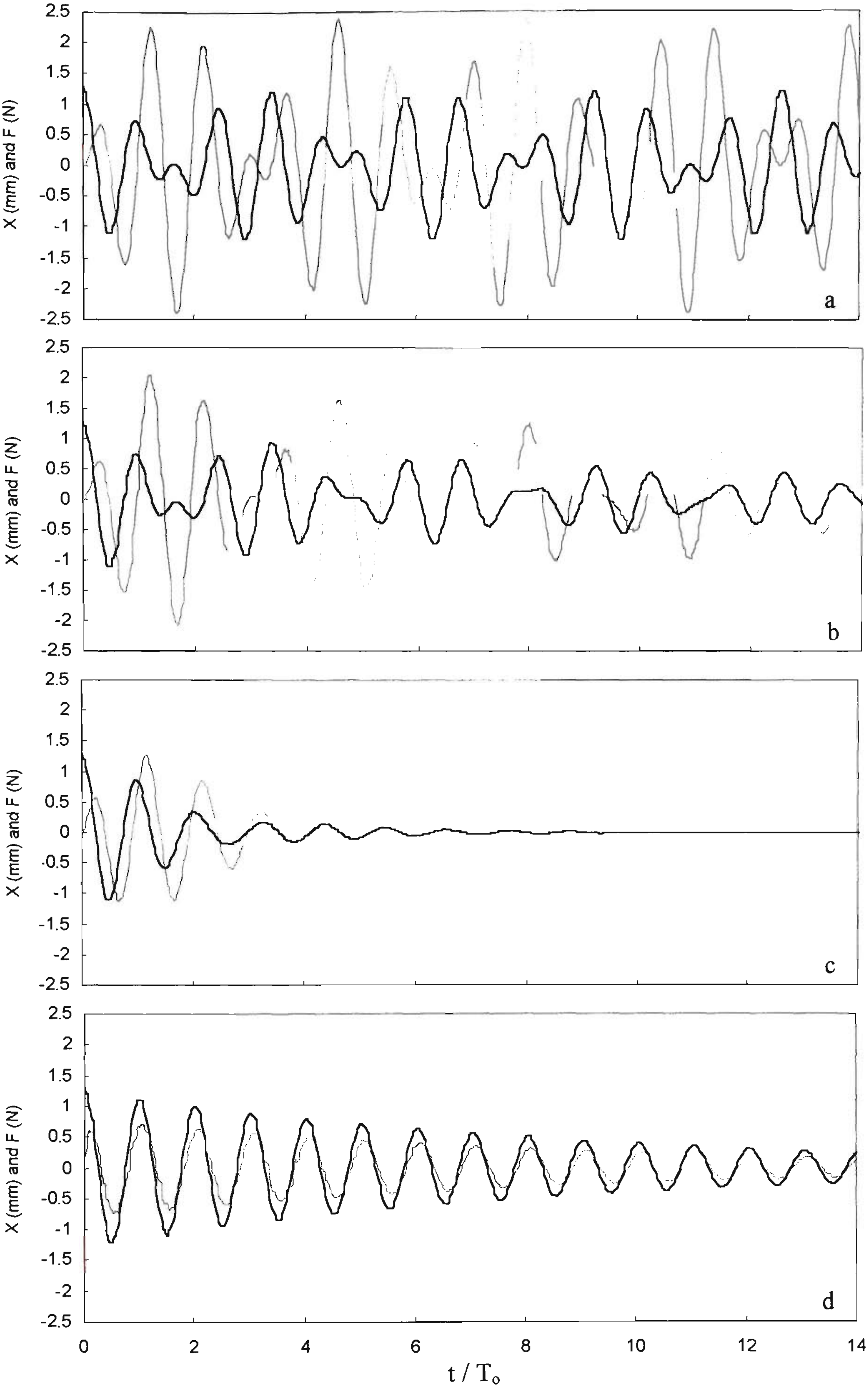

Figure 2.3. Displacement (——) and force (——) histories of the tuned absorber for (a) ξ_2=0, (b) ξ_2=0.025, (c) ξ_2=0.19 and (d), ξ_2=1.24, respectively.

A conventional tuned absorber is certainly capable of producing an effective control action for a value of ξ_2 around 0.19. This ξ_2 value is in close agreement with the optimum value suggested in Snowdon (1968). For such optimally damped cases, the control is so effective that the total energy of the system is dissipated within eight periods after the initial disturbance. Such tuned absorbers have been used in towers and bridges (Abiru et al. 1991). Viscous damping is introduced using hydraulic mechanisms which are rather complex and demand continual maintenance. Avoiding such a need for maintenance should certainly be an advantage in application. The sloshing absorber discussed in the next section, is proposed to gain such an advantage.

2.3. SLOSHING ABSORBER

To examine the response of a structure with a sloshing absorber as shown in Figure 2.2, first, a liquid container was attached to the oscillator. Then, baffle plates were added to the container to improve the control performance. Many different baffle configurations were simulated with the suggested sloshing absorber. For a sloshing absorber with two baffles, the baffle length was varied between 2 mm and 30 mm. The vertical position of the baffles was also varied from 10 mm above the static liquid height to 20 mm below the liquid surface (submerged). The same baffle sizes were also investigated for a sloshing absorber with one baffle. From the trials with two baffles, it was clear that with a single baffle, vertical baffle positions ranging from on the liquid surface to 20 mm below (submerged) needed to be evaluated.

Baffle configurations were evaluated numerically and verified experimentally. The results presented here show the trends of the control effect of a sloshing absorber on the structure. In Section 2.3.1, the experimental procedure is outlined first. Then, the numerical model is described in Section 2.3.2. The experimental and numerical results are compared and the resulting trends are discussed in Section 2.3.3 for a sloshing absorber with a pair of baffles.

2.3.1. Experiments

The sloshing absorber consisted of a rectangular container of 130 mm length by 210 mm width, as shown in Figure 2.4. The container was filled with water to a depth of 100 mm, corresponding to a mass of approximately 2.8 kg. As indicated in Figure 2.4, the length of the container used for the sloshing absorber was longer in the Z direction than in the X direction for two-dimensionality. The sloshing absorber was orientated on the structure to be controlled such that a sloshing wave was induced in the XY plane. The chosen dimensions of the sloshing absorber resulted in a virtually two-dimensional sloshing wave with little motion in the Z direction. The experimental setup is shown in Figure 2.5.

The structure consisted of a mass of 27.9 kg supported on four 390 mm long mild steel columns of 3.5 mm thickness and 22 mm width. The columns were aligned so that they formed an equivalent one-dimensional spring, allowing the motion of the structure in the X direction, as shown in Figure 2.5. The ratio of the mass of water in the container to the mass of the structure was about 10%. The structure exhibited light damping under free vibrations, and it had a natural frequency of 2.6 ± 0.2 Hz. The fundamental sloshing frequency of the liquid in the container was 2.3 ± 0.2 Hz. System parameters are summarised in Table 2.1.

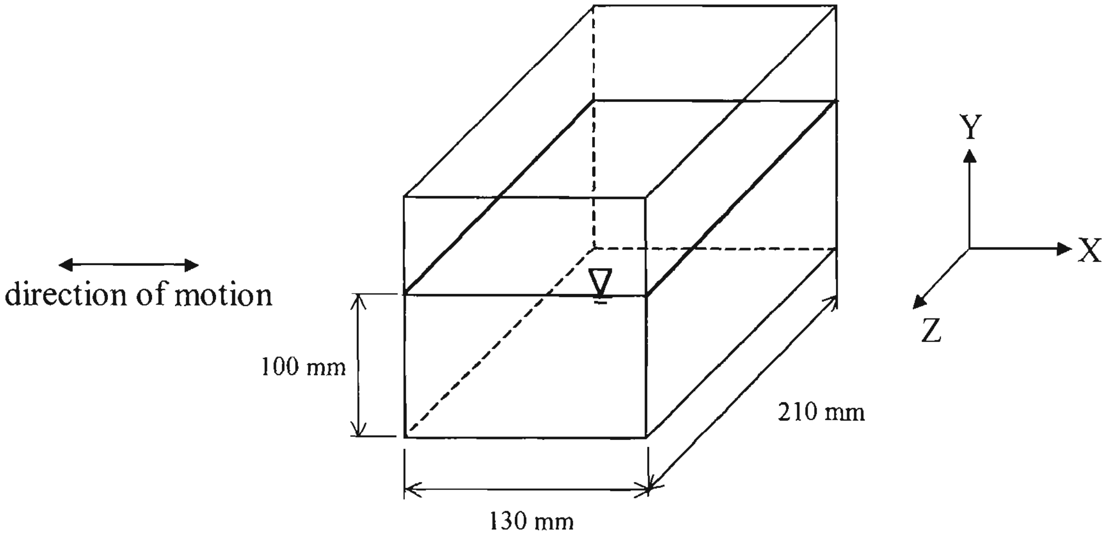

Figure 2.4. An isometric view of the sloshing absorber filled with water to a depth of 100 mm.

Table 2.1. System parameters. In each column, experimental / ***computational*** values are given when they differ. f_n and ξ_{eq} represent the fundamental frequency and the equivalent viscous damping ratio.

	mass (kg)	Stiffness (N/m)	f_n (Hz)	ξ_{eq}
Structure	27.9 / ***28***	7490 / ***6374***	2.6 ± 0.2/ ***2.4***	0.004±0 .002
Tuned Absorber	***2.8***	***585***	***2.3***	
Water	2.8		2.3 ± 0.2 / ***2.2***	

For each test case, the structure was displaced by 1.30 ± 0.05 mm before being released to oscillate freely. This value was chosen to create a reasonable sloshing amplitude in the absorber. The displacement of the structure was tracked with a Keyence LB-12 laser displacement transducer and then recorded. After determining the behaviour of the free vibrations of the structure alone, the rectangular container was secured to the structure. Several series of tests were performed where the liquid motion was first left uncontrolled, and then, it was controlled by different cantilevered baffles attached to the vertical sides of the container.

The baffles were constructed from 3 mm thick plywood, and the surfaces were sealed to reduce water absorption. The performance of the sloshing absorber is shown in Section 2.3.3 for a pair of baffles with cantilevered lengths of 10 mm located at different distances from the liquid surface. Although many other trials were performed with two baffle plates, this particular baffle size was found to provide an optimal control for the chosen sloshing absorber. Hence, only this set of results is needed to show the complete trend in the control action of the sloshing absorber.

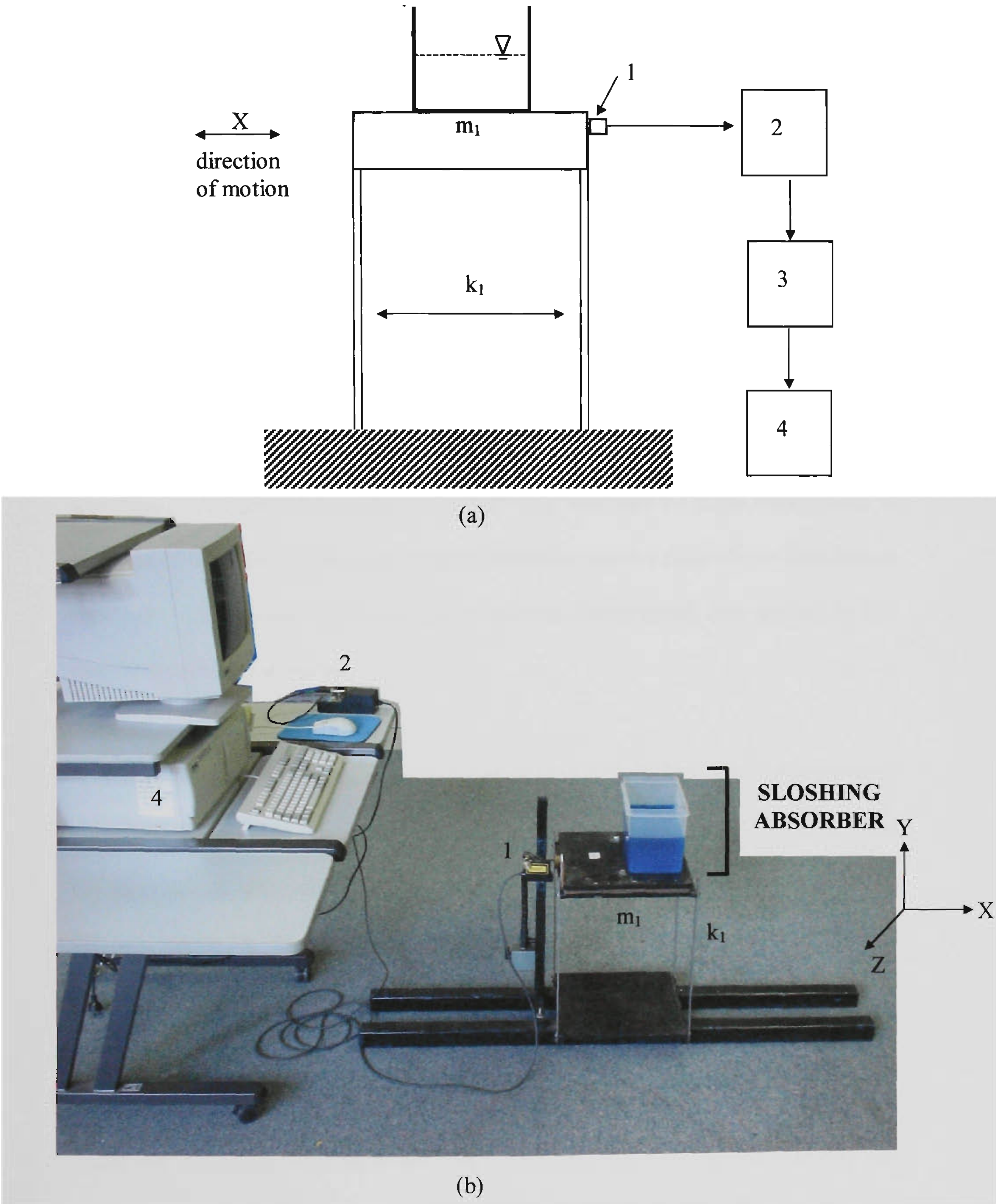

Figure 2.5. (a) Schematic diagram and (b) photograph of the experimental setup.

1. Keyence, LB-12 laser displacement transducer,
2. Keyence LB-72 amplifier and DC power supply,
3. Data Acquisition Analogue to Digital conversion board (DT707T),
4. Personal Computer.

2.3.2. Numerical Model

A two-dimensional numerical model of the sloshing absorber was created using CFX Version 4.1 (CFDS-FLOW3D, 1994). For liquid sloshing, a two-phase model was adopted because of the presence of a liquid-gas interface at the free surface. The Navier-Stokes equations were solved using the Volume of Fluid method (Hirt and Nichols, 1981). Each phase was assumed to be homogeneous, and a clear definition of the liquid free surface was obtained by using a surface sharpening algorithm. Surface tension was not included, and no-slip condition was imposed at solid boundaries. A mass source tolerance of 10^{-6} kg/s was used to judge convergence in single precision. The maximum number of iterations was set to be 50 per time step at each cell. This choice was conservative, because convergence was reached in less than 50 iterations in all cases.

A viscous model was used, in order to maintain the ability to simulate a wide range of cases. As discussed in Section 2.4, an inviscid approach may be sufficient to simulate the particular sloshing absorber used in this investigation. However, viscous effects are not negligible in all cases of sloshing absorbers in practical applications. Therefore, a general numerical tool capable of including viscous effects is useful.

A two-step solution procedure was followed to account for the interaction between the liquid and the structure at each time step. First, the structure to be controlled was given an initial displacement of 1.3 mm. Initially, the control force from the sloshing absorber was zero, since there was no sloshing of the liquid. Hence, the solution started by calculating the displacement of the structure in Figure 2.2. Since a rigid connection existed between the structure to be controlled and the sloshing absorber, the two systems had to experience the same displacement. Therefore, the displacement of the structure was given to the sloshing absorber next within the same time step. The pressure distribution on the container walls was obtained from the CFX solution of the liquid motion for the updated displacement. The force of the sloshing absorber on the structure was obtained by numerically integrating the pressure distribution on the walls of the absorber. The procedure then continued with the calculation of the displacement of the structure in response to the control force from the sloshing absorber.

In order to solve the equation of motion for the structure, a FORTRAN routine was developed within the CFX environment using the Average Acceleration Method (Rao 1990). The equation of motion for the structure to be controlled, is given in Equation 2.1, where $\ddot{X}_1$, $\dot{X}_1$ and X_1 are the acceleration, velocity and displacement of the mass, M_1; k_1 is the stiffness and F(t) is the control force of the sloshing absorber, consisting of the resultant pressure force on the container walls, as a function of time.

$$M_1 \ddot{X}_1 + c_1 \dot{X}_1 + k_1 X_1 = F(t) \tag{2.1}$$

Grid independence was achieved after evaluating a series of mesh refinements. After testing grids of 13 × 14, 26 × 28 and 52 × 56 cells, for the sloshing absorber with no baffles, a grid of 26 × 28 cells was determined to be sufficient. For sloshing absorbers with baffles, a non-uniform grid was needed to provide numerical accuracy in the region near the baffles. A non-uniform grid of 64 × 70 cells was chosen for the simulations, because further addition of cells provided no detectable change to the predicted wave shape. This grid is shown in Figure 2.6. In Figure 2.6, each region of the grid is given a number. The cell size in each of these regions is given in Table 2.2.

For each grid evaluated for the fluid solution, the time step was also varied between 0.00025 s and 0.1 s. A time-step of 0.001 s was determined to be the largest possible for the numerical results to be independent of the time step. The structural solution required a time step of 0.01 s, which was 10 times coarser than that of the fluid solution. The COMMAND and FORTRAN files used to model a sloshing absorber in the CFX environment are included in Appendix 1.

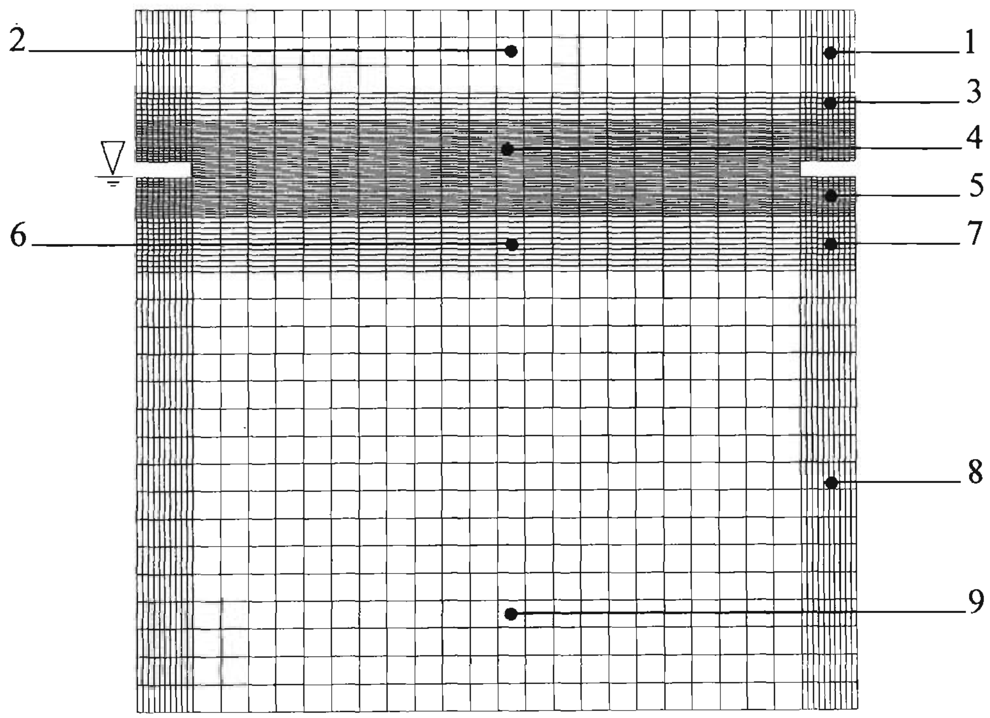

Figure 2.6. Numerical grid of the sloshing absorber showing 10 mm long cantilevered baffles located on the static liquid surface.

Table 2.2. Cell size of each region of the non-uniform grid in Figure 2.6.

Region	1	2	3	4	5	6	7	8	9
Cell Size mm × mm	1 × 5	5 × 5	1 × 1	5 × 0.5	1 × 0.5	5 × 1	1 × 1	1 × 5	5 × 5

Initial numerical predictions were performed to determine the strongest interaction between the structure and the liquid. "Tuning" was observed for a frequency ratio of 0.95. This value represents the ratio of the fundamental sloshing frequency (when the container is alone), to the structural natural frequency (including the added liquid mass). Although other frequency ratios were tried between 0.8 and 1.2, the interaction between the sloshing absorber and the structure to be controlled was strongest for a tuning ratio of 0.95. This frequency ratio agrees with those in Hayama and Iwabuchi (1986) and Fujii et al. (1990). The mass of the oscillator, m_1, was set to 30.8 kg (consisting of 28 kg mass of the structure and 2.8 kg mass of the water). The stiffness of the spring, k_1, was 6374 N/m. Structural damping was set to zero. Parameters of the numerical model corresponding to those of the experiments are listed in Table 2.1.

2.3.3. Results

In Figures 2.7(a) to 2.7(d), the numerically predicted (——) and experimentally observed (-----) displacement histories of the oscillator are given along with the numerically predicted sloshing force (——) on the oscillator for an absorber without baffles and then with baffles at different positions. Again, the time is non-dimensionalised with the period of the oscillator alone. Both experimentally and computationally, the displacement history of the oscillator starts with an initial displacement of 1.3 mm. At the start, the total energy of the combined system is the potential energy stored in the spring of the oscillator due to its initial displacement. In the following paragraphs, numerical predictions are discussed before the comparison with experiments.

In Figure 2.7(a), after the oscillator is released from 1.3 mm, its amplitude decays while the amplitude of the sloshing force increases as the sloshing motion develops. After approximately 3.5 natural periods, the displacement experiences its smallest amplitude whereas the sloshing force is at its largest value. This phenomenon indicates an exchange of energy between the oscillator and the sloshing liquid. In contrast to the situation at the start, now most of the energy is with the sloshing liquid. This exchange continues as the energy is transferred back to the oscillator, around 6.3 periods, and back to the liquid, around 9 periods, forming a "beat" envelope of oscillations.

Strong interaction of the oscillator with liquid sloshing is desirable during the initial stages. This strong interaction assures that the oscillatory energy is taken away from the structure to be controlled. However, as mentioned earlier, the liquid level used in this study results in a standing sloshing wave, which has virtually no effective means of dissipating energy. Hence, the energy in the absorber returns to the oscillator, producing a poor control effect. Some additional means of energy dissipation in liquid sloshing must be introduced to improve control.

In Figures 2.7(b) to 2.7(d) histories of the same three parameters are shown as in Figure 2.7(a). However, in these three frames, the sloshing absorber has two baffle plates cantilevered symmetrically from the opposite sides of the container. These plates are all 10 mm long and 3 mm thick. In Figure 2.7(b), the baffles are located 5 mm above the static free surface of the liquid; in Figure 2.7(c) they are submerged 5 mm below the surface, and in Figure 2.7(d) the baffles are on the surface.

In Figure 2.7(b), when the baffle plates are 5 mm above the surface, the response of the system is identical to that of the no baffle case in Figure 2.7(a), until the surface wave reaches a height of 5 mm. This instant is clearly signified around 1.8 periods where the sloshing force displays some discontinuity. The overall difference between Figures 2.7(a) and 2.7(b), however, is quite insignificant. This relative ineffectiveness could be attributed to minimal interaction between the surface of the liquid and the baffle plates since the liquid surface is free from contact with the baffles during most of its cycle.

The best control effect is obtained for the case shown in Figure 2.7(c) when the baffles are 5 mm below the surface. For this case, the disturbance in the flow is able to allow a relatively strong interaction at the start. After the initial strong interaction, however, the sloshing liquid is disturbed enough so that the beat in the envelope of structural oscillations is much less pronounced. In addition, the structural displacements are smaller than 0.25 mm (about one-fifth of the initial displacement) after approximately 5 periods, whereas peak displacements reach up to 1.0 mm for the case in Figure 2.7(a).

In Figure 2.7(d), when the baffles are on the surface, the beat shown in the preceding frames disappears completely. The sloshing force oscillates in almost perfect phase with the oscillator. This in-phase motion between the sloshing liquid and the oscillator, prevents the transfer of energy from the oscillator to the liquid as they move in unison. Therefore, surface baffles modify the sloshing wave too strongly resulting in a poor control action.

In all four frames of Figure 2.7, the experimentally measured displacement of the oscillator is also given for comparison purposes. These experimentally measured displacements follow the same trends as those of the numerical predictions. However, the experimental frequency of oscillations is about 5% smaller in Figure 2.7(a) and 5% higher in Figures 2.7(b) to 2.7(d) than the numerical ones. In addition, especially for the two more effective cases in Figures 2.7(b) and 2.7(c), when the baffles are 5 mm above and below the surface, respectively, the experimentally observed control of the structure is more effective than predicted. This pronounced effectiveness may be attributed to the dissipation of energy due to the surface roughness of the baffles and the container, surface tension effects and light structural damping which are not included in the numerical model. For the case when the baffles are at the surface in Figure 2.7(d), the experimentally measured displacements have just as ineffective a control as the numerical predictions, due to the in-phase motion discussed earlier in the previous paragraph. Even with the differences, the comparisons clearly indicate that the numerical predictions are able to capture the significant trends in the control action. The numerically predicted structural control may be conservative, assuring that the control may well be better in application. Hence, the numerical model is certainly a useful tool to predict performance and to select the promising configurations for practical applications.

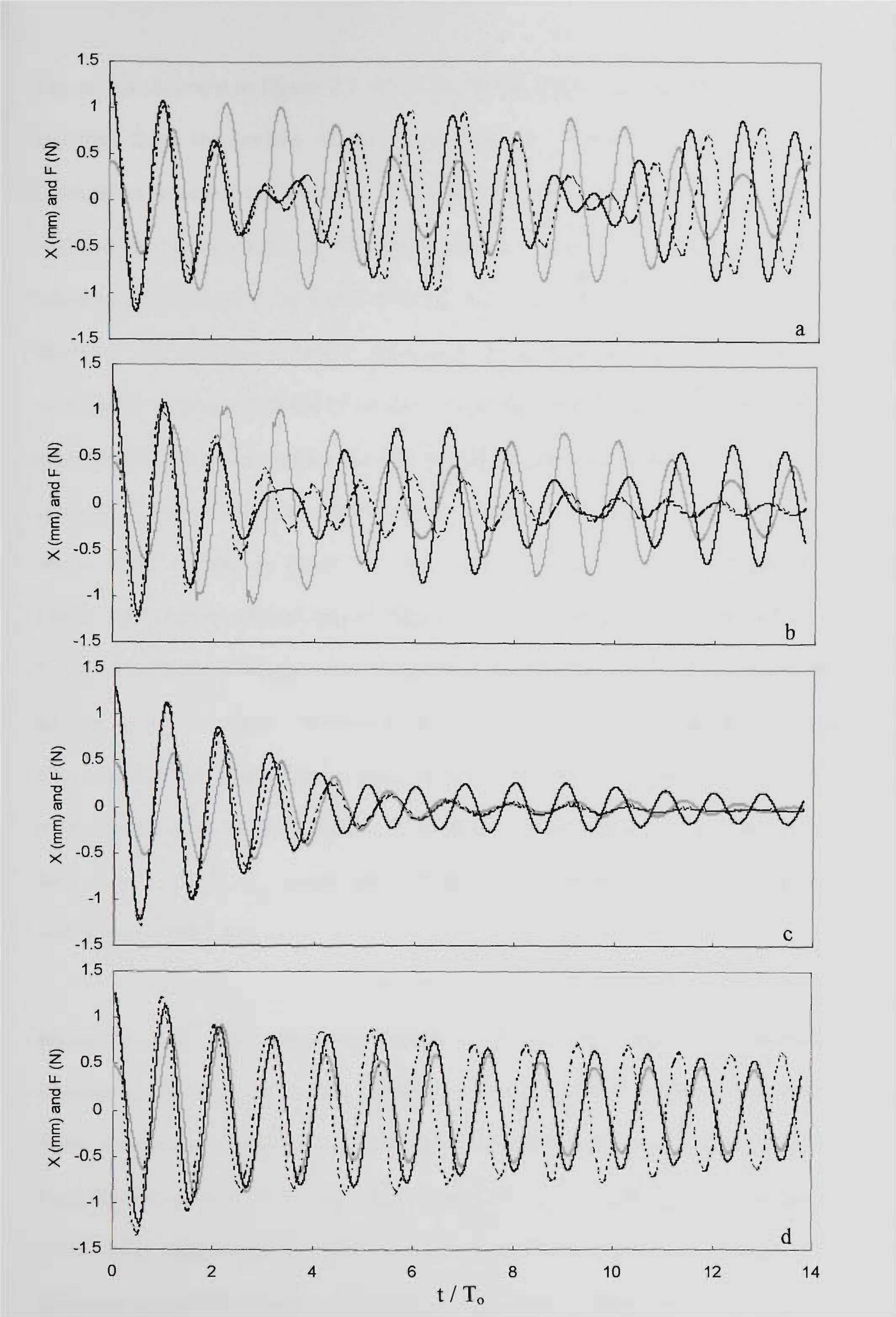

Figure 2.7. Displacement and force histories of the sloshing absorber, (a) without baffles, (b), (c) and (d) with 10 mm baffles, 5 mm above, 5 mm below and on the static liquid surface, respectively.
(——) predicted displacement; (-----) experimental displacement; (——) predicted sloshing force.

The trends observed in Figure 2.7, where the baffle plates are positioned at different locations from the surface of the liquid, may be explained in relation to the information presented in Figure 2.8. The results in Figure 2.8 correspond to the same container as the one used to generate the results in Figure 2.7. In Figure 2.8, what is presented is the control of liquid sloshing and not structural control using liquid sloshing. The container is excited sinusoidally at the fundamental sloshing frequency with a peak-to-peak amplitude of 2.5 mm. Although a full description of the modified experimental setup and results for the control of liquid sloshing will be given in Section 3.2 and Section 3.3, respectively, of Chapter 3, it should be noted here that a setup similar to that in Figure 2.5 was used to obtain the results presented in Figure 2.8. The horizontal axis of Figure 2.8 shows the position of the baffles at 5 mm intervals from 10 mm under the surface (negative values) to 10 mm above the surface (positive values). The numerical predictions are marked with (●), whereas (■) indicates the corresponding experimental observation. The vertical axis, A_c/A_o, represents the ratio of the amplitude of the sloshing wave with a pair of baffles, A_c, to that without baffles, A_o. Hence, any reduction in the sloshing amplitude is reflected with a ratio smaller than 1.0.

Numerical predictions consistently indicate at least a 75% reduction for all baffle locations up to the liquid surface, indicated by 0 mm position on the horizontal axis. Then, the reduction effect deteriorates almost proportionally with the baffle distance from the free surface. As before, experiments (■) show consistently more effective control than what could be predicted numerically (●) for all cases. Similarly, this difference is attributed to the surface tension and wall roughness effects which were not modelled in the numerical simulations. When the baffles were at the surface, no measurable amplitude could be observed experimentally, resulting in perfect sloshing control. For this case, the liquid acted as if it was just an added mass in the container moving in perfect phase with it. For the results presented in Figure 2.7(d), when the same container was attached as the controller on the oscillator, the same overly suppressed sloshing wave was observed which prevented the transfer of energy from the oscillator. As result of this too effective sloshing control, the sloshing absorber behaved similarly to the overdamped tuned absorber in Figure 2.3(d). Figure 2.8 will be re-visited in Section 3.3 of Chapter 3 in relation to the control of liquid sloshing.

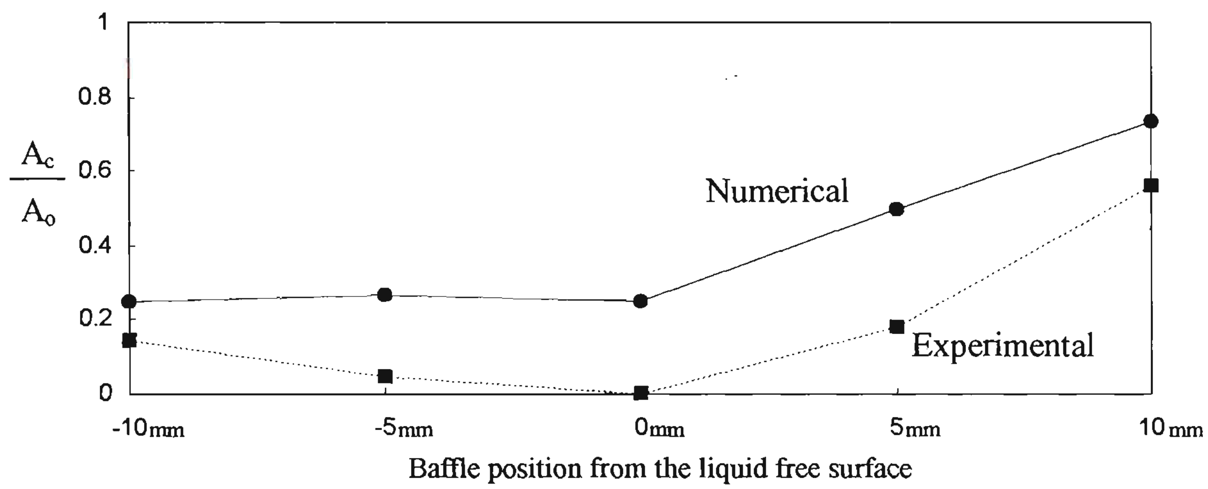

Figure 2.8. Non-dimensional sloshing amplitude plotted against baffle position.

In Figures 2.9 and 2.10, force versus displacement phase plots are given for the tuned absorber and the sloshing absorber, respectively. The diamond shaped phase pattern of the undamped tuned absorber in Figure 2.9(a) is also noticeable in that of the sloshing absorber in Figure 2.10(a). In Figure 2.9(a), the trace of force-displacement is characterised by a series of ellipses formed either in counter-clockwise or in clockwise directions. By changing their direction of rotation, the ellipses cross over one another creating many intersections, representing a poor control action. For the sloshing absorber in Figure 2.10(a), a small amount of energy is dissipated in the fluid. Figure 2.10(b) shows that the performance of the sloshing absorber with baffles above the surface is similar to that of a lightly damped tuned absorber shown in Figure 2.9(b). The optimal cases of both absorbers are given in Figures 2.9(c) and 2.10(c). These phase plots have a distinct counter-clockwise pattern that forms a spiral towards the origin. As indicated by a comparison of Figure 2.10(d) with Figure 2.9(d), the surface baffles make the sloshing absorber behave like an overdamped tuned absorber. In Figure 2.10(d), smaller elliptical areas are enclosed for each cycle of oscillations than the corresponding optimal case in Figure 2.10(c), due to the mostly in-phase trend of the displacement and force. The slope of the longer axis of the ellipses indicates the stiffness of the oscillator. For the tuned absorber, the ellipses are concentric with a constant slope. However, for the sloshing absorber, the slope changes due to the nonlinear nature of liquid sloshing.

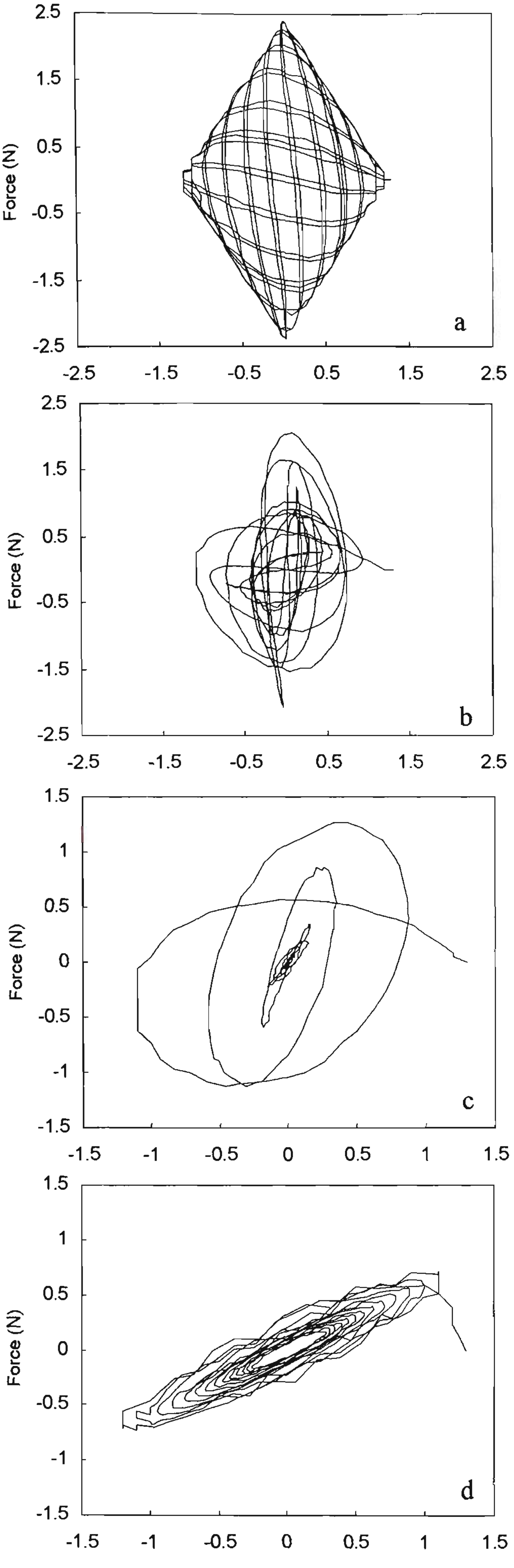

Figure 2.9. Force – displacement phase plots of the same cases as in Figure 2.3.

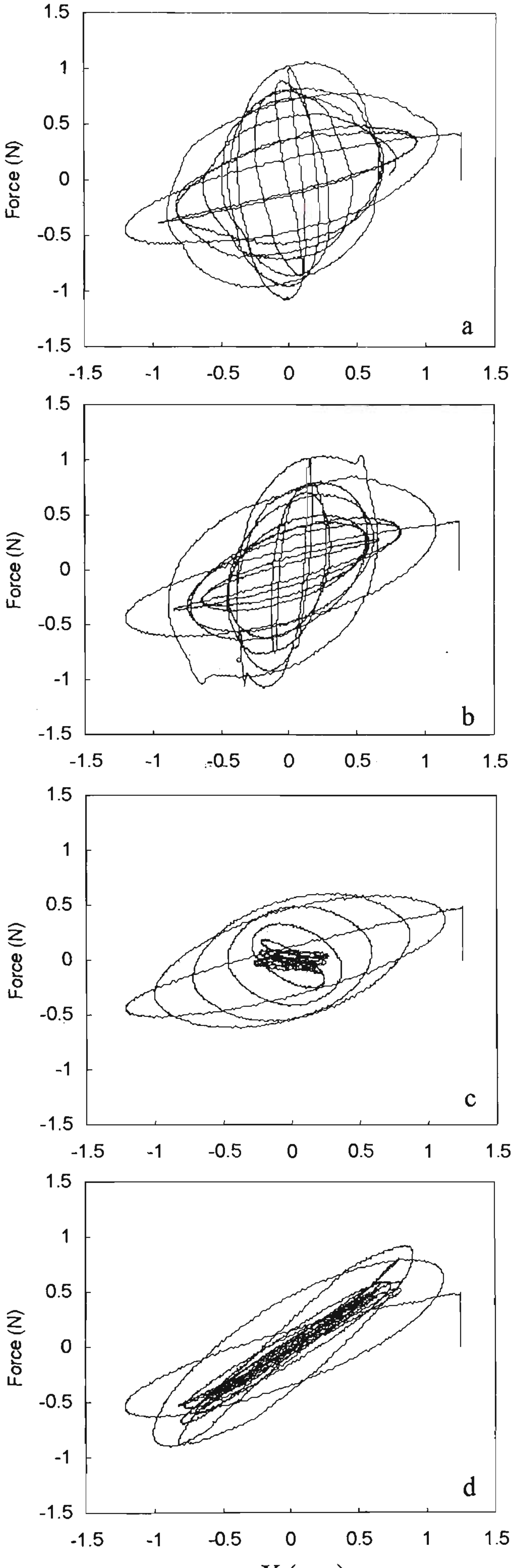

Figure 2.10. Force – displacement phase plots of the same cases as in Figure 2.7.

Histories of the transient energy of the oscillator are shown for the same undamped, lightly damped, optimally damped and overdamped cases from frame (a) to frame (d) in Figures 2.11 and 2.12 for the tuned and the sloshing absorbers, respectively. These histories are obtained from the cumulative product of the velocity of the oscillator and the control force. The product of the control force and oscillator velocity is the instantaneous power in the oscillator. Summing this power over time consequently represents energy. Figure 2.11(a) has large fluctuations of energy due to the strong beat. In Figure 2.11(b), there is some dissipation due to light damping. However, beat instances are clearly marked as the oscillatory energy is exchanged between the structure and the tuned absorber. Figure 2.11(c) corresponds to the optimal damping with a steep slope of decay and no beat. The overdamped tuned absorber results in poor interaction between the structure and the absorber as shown in Figure 2.11(d). Hence, the energy dissipation rate is small.

In Figure 2.12, similar comments are valid for the sloshing absorber as those for the tuned absorber. In Figure 2.12(a) with no baffles, however, the beat period is approximately twice as long as in Figure 2.11(a), and there is some energy loss. In Figure 2.12(b), the energy dissipation rate is marginally enhanced with the beat still clearly apparent when the baffles are 5 mm above the free surface. The most effective dissipation of energy corresponds to the case in Figure 2.12(c) where the baffle plates are 5 mm under the surface. In Figure 2.12(d), sloshing wave is suppressed too effectively with the surface baffles resulting in poor energy exchange and poor rate of energy dissipation. The loss of energy can be attributed to two reasons in the case of a sloshing absorber. First, it can be due to the occasional phase difference between the control force and the structure's velocity. Secondly, it can be due to momentum exchange between the translational and rotational fluid motions over a baffle plate, as described in detail later in Section 2.5.1.

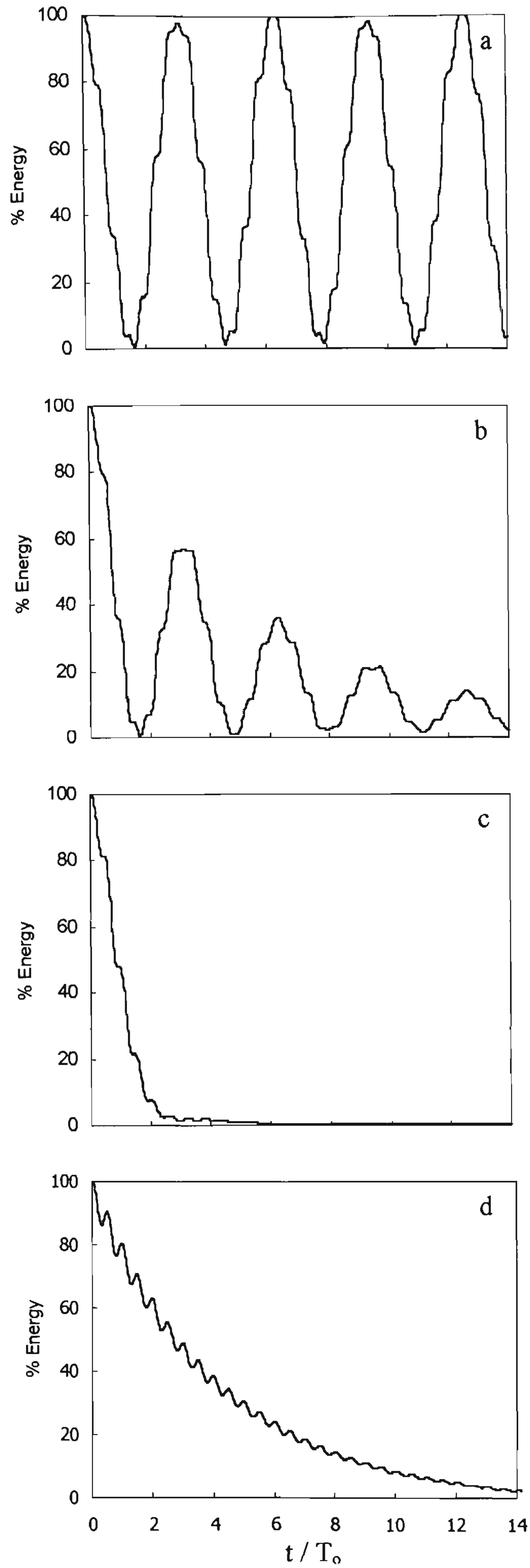

Figure 2.11. %Energy of the structure plotted against non-dimensional time for the same cases as in Figure 2.9.

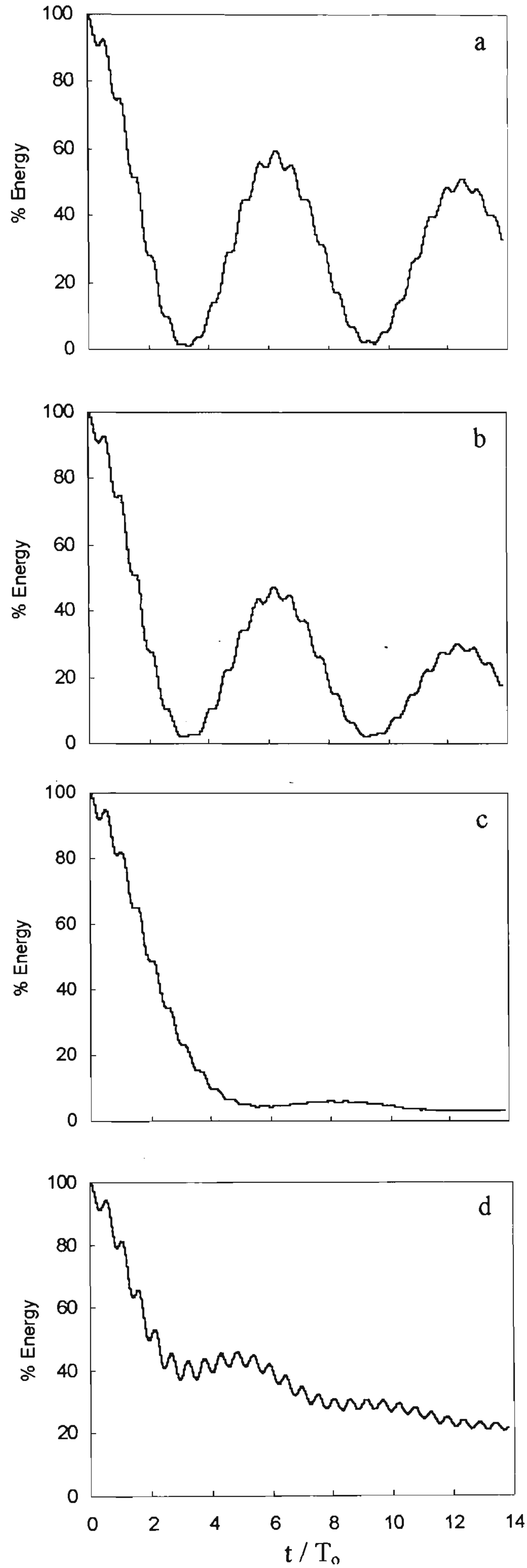

Figure 2.12. %Energy of the structure plotted against non-dimensional time for the same cases as in Figure 2.10.

2.4. ON SCALING AND PRACTICAL APPLICATION

In cases where full-scale experiments are expensive or dangerous, scaled experiments and numerical predictions are needed to determine potentially promising solutions. To this end, scaling is applied to the entire absorber-oscillator system so that the promising results of the simulations presented earlier can be scaled to systems of any practical size, without having to perform new simulations (Anderson et al. 1998c).

Like many other phenomena involving liquids with free surfaces, liquid sloshing can be scaled using Froude, Reynolds, and Euler numbers. Bass et al. (1985) used Froude and Euler scaling to conduct experiments for liquid sloshing of 1/30th to 1/50th size of prototype tanks containing liquefied natural gas. Muto et al. (1988) also used Froude scaling to represent liquid sloshing in a prototype tank with a 1/30th scale model using water as the working fluid. The difference between the present work and the earlier applications is that here, there is significant fluid-oscillator interaction. In addition, there is strong interaction between liquid sloshing and the baffle plates. In this section, the scaling parameters developed for liquid sloshing are applied to a sloshing absorber coupled to a mechanical oscillator. Froude number is used to scale displacement and time. Reynolds and Euler numbers are used to scale viscosity and pressure force, respectively.

Scaling starts by selecting a geometric scale, α, $\alpha=L_m/L_p$ where L is the container length, and the subscripts m and p denote the model and the prototype, respectively. All dimensions of the absorber have this geometric scale between the model and prototype systems. The mass ratio of the liquid to the oscillator is kept the same for the model and the prototype. Having selected α, the mass of the liquid in the scaled absorber can be calculated by maintaining $\rho_m = \rho_p$ where ρ is the liquid density. After determining the dimensions of the prototype absorber, Froude scaling is used for displacement and time scaling. Froude number is the ratio of inertial to gravity forces for flows with free surfaces, and it is defined as:

$$Fr = \frac{V^2}{gX} \tag{2.1}$$

where X and V are the displacement and velocity, respectively, of the coupled absorber-oscillator system, and g is the gravitational acceleration. For a model wave scaled to a prototype wave, Froude scaling (having equal values of the Froude number for both the model and the prototype) results in the following relationships for displacement, X, and velocity, V:

$$\text{Since } X_m = X_p \alpha,$$

$$V_m = V_p \sqrt{\alpha}\,.$$

Hence,

$$T_m = T_p \sqrt{\alpha} \tag{2.2}$$

Here, the relationship for T is used to scale the period of structural oscillations as well as the period of sloshing in the absorber.

The expression governing T can also be obtained using the Strouhal number. Strouhal number is used for oscillating flows, and it represents a velocity ratio. Here, Strouhal number is defined as, $St = \frac{fL}{\sqrt{gL}}$ where f is the sloshing frequency, L is the container length and $\sqrt{gL}$ is the characteristic velocity, (Popov et al. 1992). In this representation, $\sqrt{gL}$ is used to denote the characteristic mean fluid velocity, because the actual mean speed of a standing sloshing wave is about zero, due to the oscillation of the wave about the static liquid position. This form of St is used here for liquid-structure interaction due to controlled sloshing for the purpose of structural control. The period of sloshing can be determined, since $f = \frac{1}{T}$.

Reynolds number, Re, is the ratio of inertial to viscous forces, and it is used here to scale viscous effects. For liquid sloshing, Reynolds number is defined as,

$$Re = \frac{\rho L \sqrt{gL}}{\mu} \tag{2.3}$$

where μ, ρ and L are the absolute liquid viscosity, liquid density and container length in the direction of liquid sloshing, respectively. Here again, as in Strouhal number, $\sqrt{gL}$ is the characteristic velocity. If viscous effects are important, then Re is kept constant, $Re_m = Re_p$, by scaling kinematic viscosity, $v = \frac{\mu}{\rho}$, as $v_m = \alpha^{\frac{3}{2}} v_p$. Bass et al. (1985) reported that for sloshing in tanks containing Liquefied Natural Gas, viscous effects were insignificant if Re was larger than 10^3, and for such cases, viscous scaling need not be considered. This conclusion is in close agreement with the observations given by Popov et al. (1993) for liquid sloshing in horizontal cylindrical road containers. Popov et al. showed that viscosity had no effect for Re in the range 10^5–10^7, and the effect was small for Re in the range $10^3 - 10^5$. Therefore, the liquid in the model absorber need only to have a density similar to that of the liquid in the prototype, and a viscosity low enough to give a Reynolds number of greater than 10^3.

For Re less than 10^3 in the prototype absorber, viscosity will have some effect on liquid sloshing, and scaling of viscosity may be important.

Euler number, Eu, is the ratio of pressure to inertial forces, and it has been used here to scale pressure force on the walls of the absorber due to sloshing. Euler number is,

$$Eu = \frac{P}{\rho V^2} \tag{2.4}$$

where P is pressure. Euler number is the same in the model and prototype absorbers. Therefore, substituting $V_m = V_p\sqrt{\alpha}$ from Equation 2.2 gives,

$$\frac{P_m}{P_p} = \alpha \frac{\rho_m}{\rho_p} \tag{2.5}$$

Since pressure is the distributed load per unit area,

$$\frac{F_m}{F_p} = \alpha^3 \tag{2.6}$$

for $\rho_m=\rho_p$, where F is the pressure force on the container walls, which is the control force on the oscillator. Using this relationship, the force amplitude for the prototype system can be determined from that of the model system. To obtain the force history for the prototype, time scaling is also needed, as defined in Equation 2.2.

As an example, the model used for the analysis presented in the earlier sections of this thesis was scaled to a larger prototype system, using α=0.026. This geometric scale value was chosen to give an absorber of 5000 mm length and 8100 mm width, containing 158,427 kg of water representing a water storage tower as the prototype. The parameters of the model and prototype systems are given in Table 2.3.

To compare the two systems, the displacement and force magnitudes were scaled using Equations 2.2 and 2.6, respectively. Hence, a displacement of 1.3 mm and a force of 0.4 N for the small system corresponded to 50 mm and 22,760 N, respectively, for the larger system.

The validity of scaling was checked by predicting the response of the prototype system. The results obtained for the model system were duplicated identically. These results were presented in Figure 2.7 earlier. Hence, the suggested scaling procedure is useful for this highly non-linear system with strong fluid-oscillator and fluid-baffle plate interactions.

The Reynolds number for the model and prototype cases was 150,000. Therefore, viscous effects were expected to be insignificant. This point was also verified numerically with a case of 10^{-11} Ns/m^2 viscosity and slip wall conditions. Identical results to Figure 2.7 were obtained for this "inviscid" case. Hence, scaling viscosity through the Reynolds number can be relaxed for the chosen example, since $Re>10^3$.

The effect of wall surface roughness and flexibility have not been taken into account in this discussion on scaling. Therefore, the scaling procedure outlined here is for smooth and rigid wall containers. Proper representation of wall roughness requires a Reynolds number defined with the nominal roughness height. The viscous effects associated with wall roughness can be represented with such a Reynolds number (Schlichting, 1979). Wall flexibility, on the other hand, causes the liquid sloshing frequency to be time dependent as shown in Chapter 4, due to varying container length, making the scaling argument of this section invalid.

Table 2.3. System parameters of model (m) and prototype (p) absorber-structure systems.

	Numerical Model	Numerical Prototype
L_1 (mm) Container length (X direction)	130	5000
L_2 (mm) Container length (Z direction)	210	8100
Depth of submerged baffle (mm)	5	192
Baffle length (mm)	10	384
Liquid Depth (mm)	100	3800
Initial Displacement (mm)	1.3	50
Reynolds Number	150000	150000
Liquid Viscosity (Ns/m^2)	0.001	0.24
Liquid Density (kg/ m^3)	1020	1020
Fundamental Sloshing Frequency (Hz)	2.2	0.35
Liquid Mass (kg)	2.8	158427
Structural Mass (kg)	28	1584270
Spring Stiffness (N/m)	6374	9376283
Structural natural frequency (Hz)	2.4	0.39
Time Step (sec)	0.001	0.006

2.5. AN IMPROVED SLOSHING ABSORBER

In this section, a sloshing absorber is re-examined for two reasons. First, an explanation is suggested for the effectiveness of the baffled standing-wave sloshing absorber presented previously in this chapter, and in Anderson et al. (1999b and 1999c). Secondly, based on this explanation, a modified sloshing absorber is described, which has a single baffle, as shown in Figure 2.13.

As indicated at the start of this chapter, the works of Fujii et al. (1990), Abe et al. (1996), Kaneko and Yoshida (1994) and Seto and Modi (1997), dealt with shallow liquid levels in the sloshing absorbers. At shallow depths, a travelling sloshing wave occurs. Travelling sloshing waves are preferable to standing waves because of their energy dissipation characteristics. The poor energy dissipation characteristics of standing sloshing waves have been reported earlier (Kaneko and Yoshida, 1994). In the present investigation, deep liquid levels have been used to intentionally create standing sloshing waves for use in practical situations.

At the fundamental mode, the standing sloshing wave in the absorber is tuned to the natural frequency of the structure to be controlled. As discussed earlier, an optimal tuning ratio exists. Numerical simulations are given in this section to demonstrate the performance of an improved sloshing absorber in controlling the excessive transient vibrations of a resonant structure. As done earlier in assessing the effectiveness of a tuned vibration absorber and double-baffled sloshing absorber, the improved absorber with a single baffle is evaluated for a transient disturbance on the structure.

2.5.1. Numerical Predictions

The same numerical procedure reported earlier in Section 2.3.2 of this chapter is used here. The system parameters are summarised in Table 2.1. The sloshing absorbers evaluated in Section 2.3 have two cantilever baffle plates. One plate is located on each of the left and right vertical walls of the container. The new design configuration for the sloshing absorber has only one baffle plate, and it is shown in Figure 2.13 attached to the structure to be controlled.

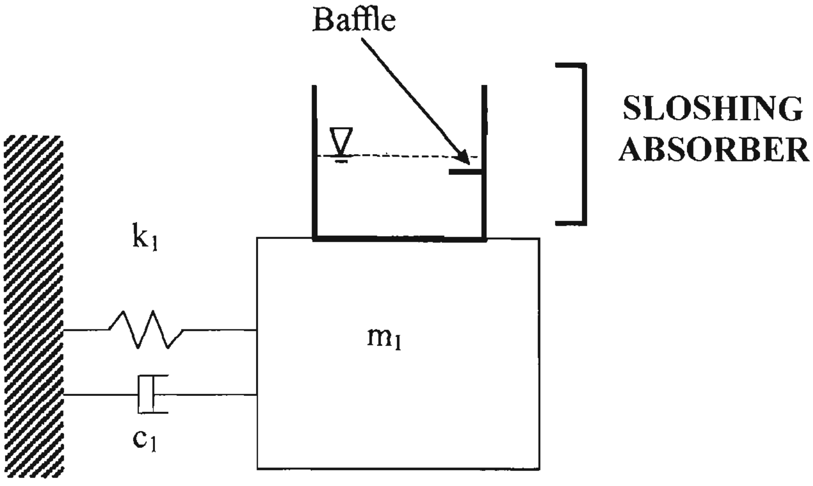

Figure 2.13. A sloshing absorber with one cantilever baffle attached on the structure to be controlled.

In Figure 2.14, histories of the numerically predicted displacement of the oscillator (——) and sloshing force (——) are given for different sloshing absorbers. Similar to Figure 2.7, the vertical axis is the displacement of the structure to be controlled in millimetres and also the force of the sloshing absorber on the structure in Newtons. The horizontal axis is non-dimensional time. In Figure 2.14(a), the sloshing absorber has no baffles. In Figure 2.14(b) the sloshing absorber has two baffles that are 10 mm long and submerged 5 mm below the static liquid surface. These cases are identical to Figures 2.7(a) and 2.7(c), respectively. They are included here to illustrate the improvement of the suggested new design. In Figure 2.14(c) the length of the two baffles is increased to 15 mm and the vertical position shifted to 10 mm below the liquid surface. The new design, which involves a sloshing absorber with one 15 mm baffle submerged 10 mm below the static liquid surface is shown in Figure 2.14(d). Many different sloshing absorbers with only one baffle were evaluated numerically. Only the most promising case is presented here corresponding to optimal structural control.

In Figures 2.15, 2.16, 2.17, and 2.18, vector plots of the liquid velocity are given for the same sloshing absorbers as in Figure 2.14. These velocity vector plots show a series of instantaneous images of the flow field in the sloshing absorber from 2.39 to 3.40 periods. This period of non-dimensional time is marked in Figure 2.14 with two vertical lines. The performance of each sloshing absorber is discussed next with reference to these figures.

In Figure 2.14(a), the sloshing absorber has no baffles. The poor control effect is characterised by a beat in the displacement of the structure. As indicated in relation to Figure 2.7(a), the initial displacement of 1.3 mm decays significantly between 2.39 and 3.40 periods. There is little energy dissipation in the sloshing liquid, and the displacement amplitude returns to almost 1.3 mm at 6 periods. This strong interaction between the sloshing liquid and the structure between 2.39 and 3.40 periods can be explained in relation to the velocity vector plots given in Figure 2.15.

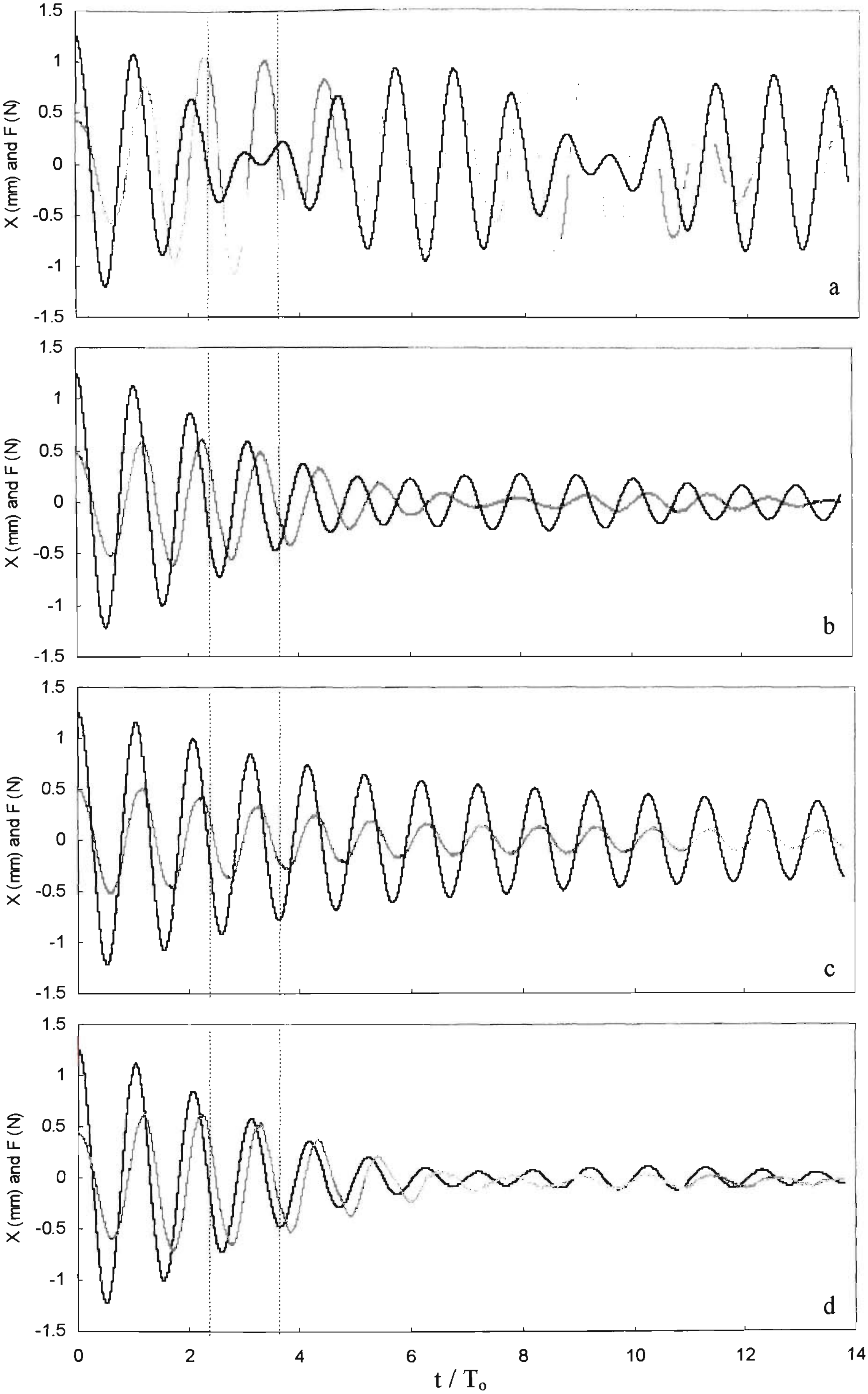

Figure 2.14. Displacement (——) and force (——) histories of the sloshing absorber, (a) without baffles, (b) with two baffles 10 mm long submerged 5 mm below the static liquid surface, (c) with two baffles 15 mm long submerged 10 mm below the static liquid surface and (d) with one baffle 15 mm long submerged 10 mm below the static liquid surface.

In Figure 2.15, vector plots are given of the liquid velocity for the sloshing absorber with no baffles. The liquid free surface is shown by a solid line in each frame. Vectors above and below the free surface represent air and liquid velocities, respectively. The first frame represents the velocity field in the absorber at 2.39 periods, and consecutive frames describe approximately one full period of wave motion to 3.40 periods. From 2.39 to 2.48 periods, the sloshing wave is higher on the right side than on the left side of the container. During this time, the resultant force on the container is to the right. This is also indicated by the positive value of force in Figure 2.14(a). The displacement history shown in Figure 2.14(a) shows that the structure is moving to the left. Therefore, the sloshing force is opposing the motion of the structure.

At 2.58 periods, Figure 2.15 shows that the sloshing wave is approximately flat. At this point, the resultant sloshing force is negligible. The structure has slowed down, and it is about to change direction to start moving to the right. This is indicated by the first turning point in the displacement history in the region of interest, which is marked with the two vertical lines in Figure 2.14(a). In Figure 2.15, the wave continues to climb high on the left wall in frames for 2.67 to 2.94 periods. The resultant sloshing force increases to a maximum to the left at time equals 2.85 periods. This is shown in Figure 2.14(a) by the 1N negative force at this instant. The displacement history shows that the structure is moving to the right. The sloshing force is to the left with a magnitude capable of prematurely stopping the structure and making it change direction at time equals 3.04 periods. This strong interaction continues to time 3.40 periods with the sloshing wave climbing on the right-side wall and creating a resultant sloshing force to the right. At this point, the structure is once again made to stop and change direction.

In Figure 2.15, the characteristic wave shape at the fundamental mode of sloshing in the absorber is shown. This wave shape is referred to as a standing wave, and it has a clear nodal point. This nodal point is located on the liquid free surface at the center of the container, and it is shown in the vector plots as an area of re-circulation. This type of wave has poor energy dissipation characteristics, leading to the performance shown in Figure 2.14(a) or in (Figure 2.7(a)). To improve the performance of the sloshing absorber, cantilever baffles are used. Sloshing absorbers with baffles are discussed next.

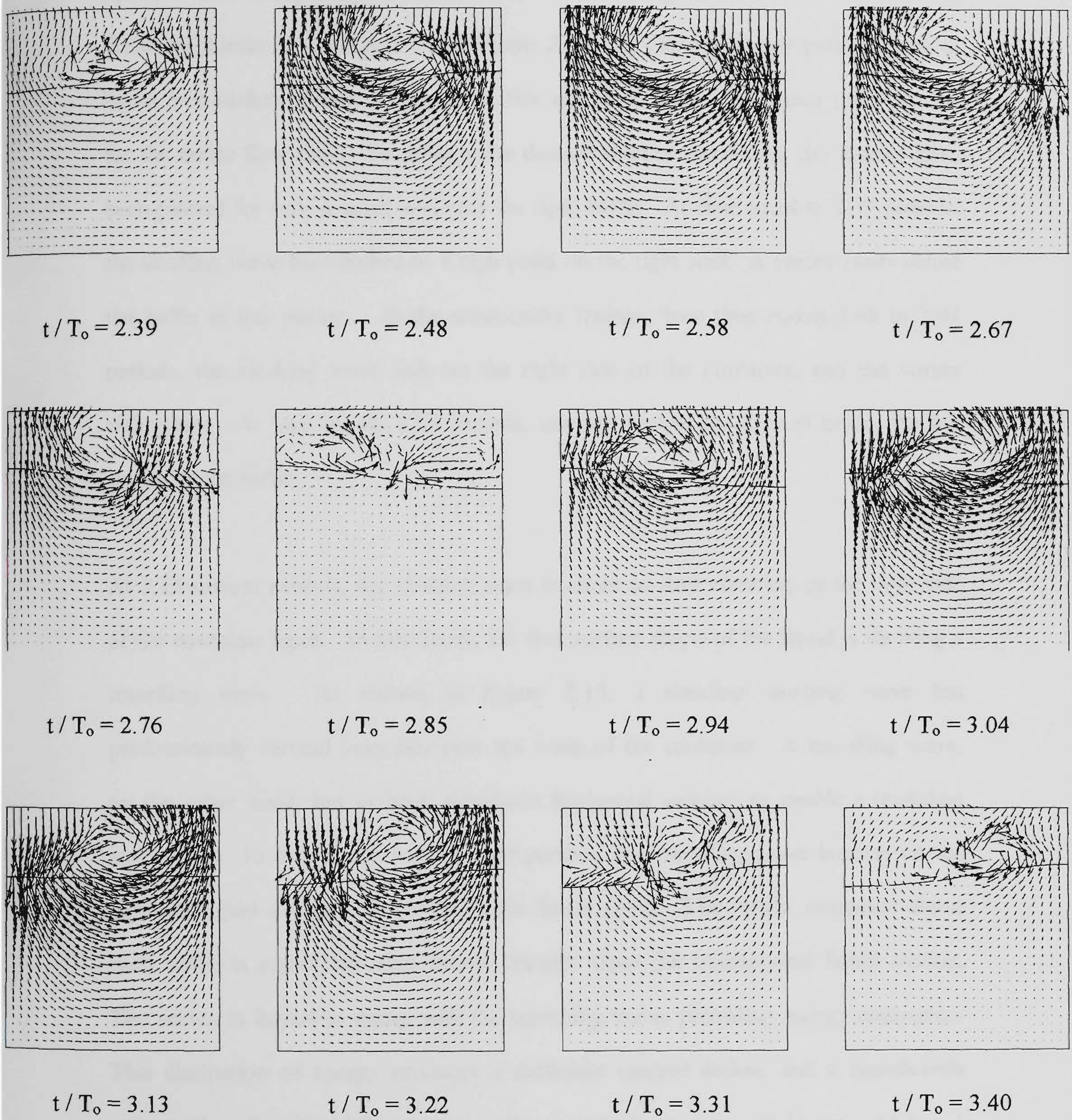

Figure 2.15. Velocity vector plots for a sloshing absorber with no baffles.

In Figure 2.14(b), the force and displacement histories are given for a sloshing absorber with a pair of 10 mm long baffles submerged 5 mm below the static liquid surface. This configuration is the optimum for a sloshing absorber with two baffles as discussed earlier in Section 2.3. In Figure 2.16, the velocity vector plots as well as liquid free surface shapes are given for this absorber. Here, the vector plots are not for the entire flow field. To achieve the desired level of resolution, the vectors have been plotted for only a small area near the right baffle. At time equal to 2.39 periods, the sloshing wave has climbed to a high point on the right wall. A vortex exists above the baffle at this instant. In the consecutive frames, from time equals 2.48 to 2.94 periods, the sloshing wave falls on the right side of the container, and the vortex disappears. At time equals 2.85 periods, another vortex has formed below the left corner of the baffle.

At 3.13 natural periods, the sloshing wave is about to start climbing up the right side of the container again. In this frame, the free surface shape of the liquid is showing a travelling wave. As shown in Figure 2.15, a standing sloshing wave has predominantly vertical velocities near the walls of the container. A travelling wave, on the other hand, has to have significant horizontal velocity to enable a travelling wave front. In frames for 3.13 to 3.40 periods, the travelling wave impacts on the right wall, and a vortex above the baffle forms again. The vortex formation above each baffle is associated with energy transfer from the translational liquid motion. The vortex is forced to decay with the travelling wave, providing energy dissipation. This dissipation of energy produces a sufficient control action, and it significantly reduces the vibration of the structure after 6 periods, as shown in Figure 2.14(b). A travelling wave is likely to develop when the liquid depth is shallow compared with the length of the container. As the length of the baffles is increased, a region above the baffles is created where a travelling wave is likely to form.

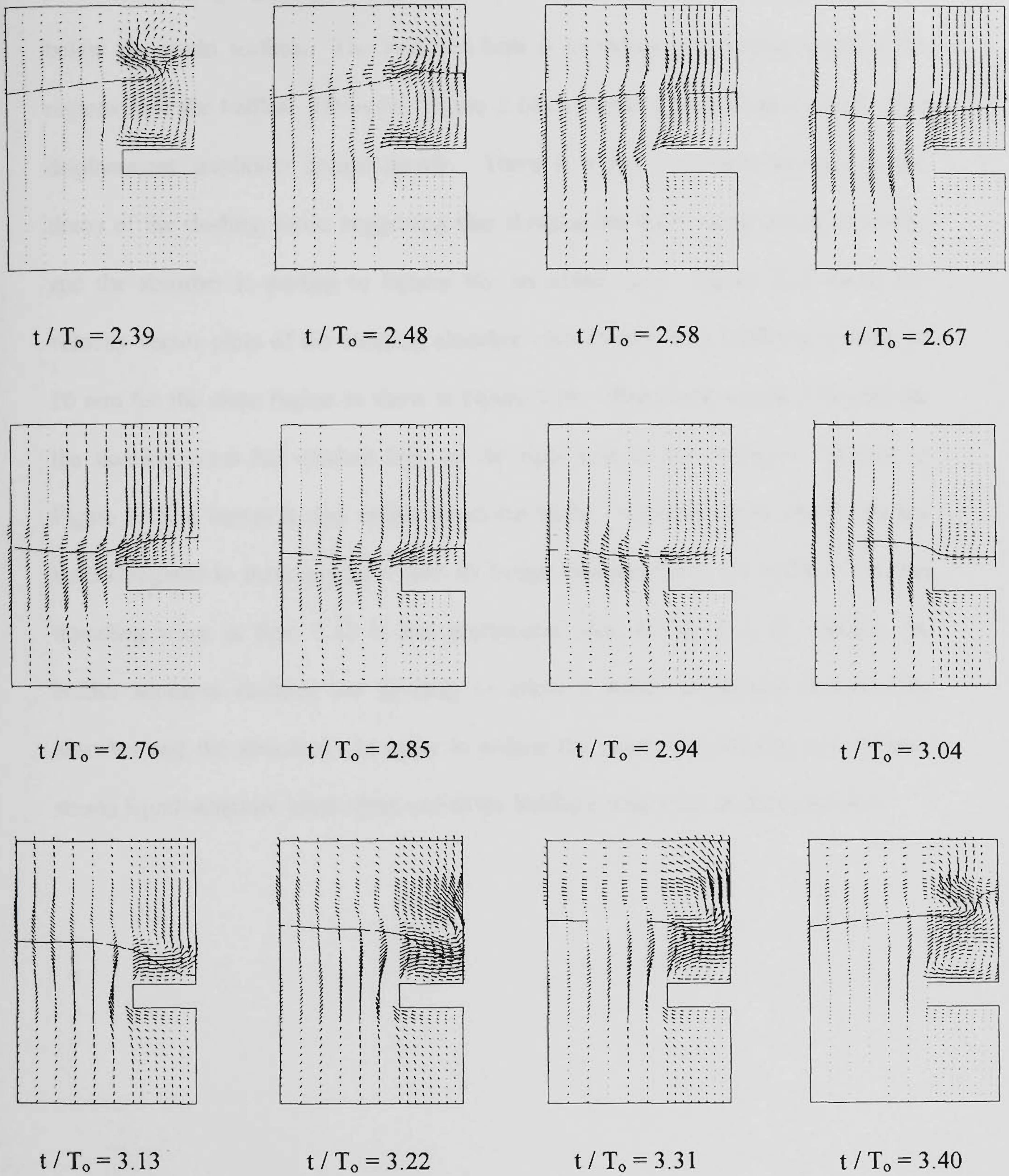

Figure 2.16. Velocity vector plots for a sloshing absorber with two 10 mm baffles submerged 5 mm below the static liquid surface.

In Figure 2.14(c), force and displacement histories are given for a sloshing absorber with 15 mm long baffles placed on both sides of the container at a depth of 10 mm below the liquid surface. The intention here is to induce a travelling wave in the regions near the baffles. However, Figure 2.14(c) shows a poor control effect. The displacement amplitude decays slowly. There is a more dramatic increase in the decay of the sloshing force, suggesting that sloshing has been suppressed excessively, and the absorber is starting to behave like an added mass. Figure 2.17 shows the velocity vector plots of the sloshing absorber with 15 mm long baffles at a depth of 10 mm for the same region as show in Figure 2.16. When time equals 2.39 periods, the sloshing wave has climbed high on the right wall of the container. Similar to Figure 2.16, a vortex is also visible above the baffle. However, here, the vortex has been elongated to form an ellipse with its longer axis parallel to the baffle. Also, the travelling wave at time 3.13 is less pronounced than in Figure 2.16. Hence, the baffles suppress sloshing too severely to allow a strong interaction between the absorber and the structure. In order to reduce the control of sloshing and promote strong liquid-structure interaction, one of the baffles is removed, as discussed next.

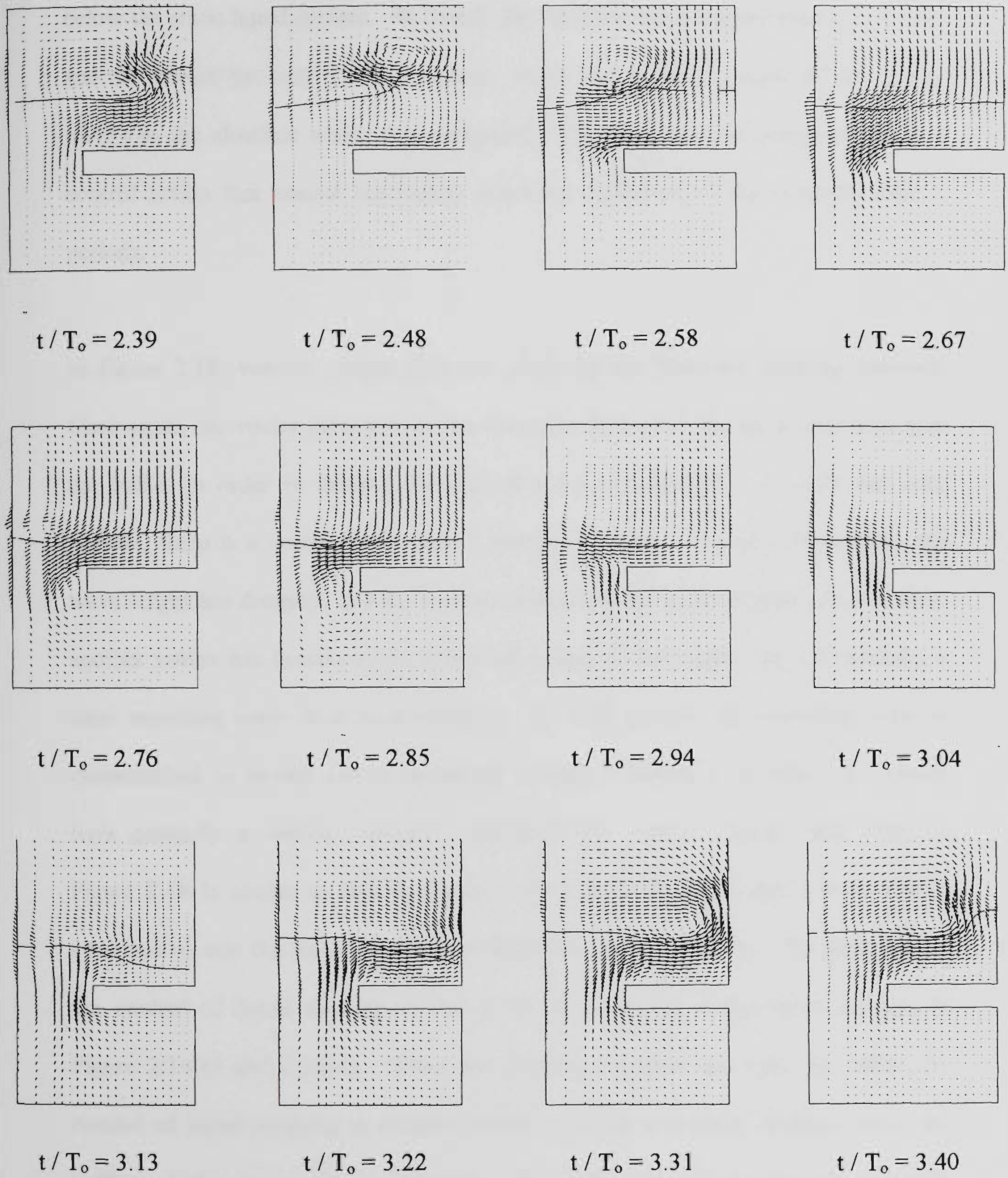

Figure 2.17. Velocity vector plots for a sloshing absorber with two 15 mm baffles submerged 10 mm below the static liquid surface.

In Figure 2.14(d) the displacement and force histories for the improved sloshing absorber are given. This absorber has one 15 mm long baffle submerged 10 mm below the static liquid surface. At time 0, the structure has a displacement of 1.3 mm, and the system has only potential energy. From 0 to 4 periods, some of this energy travels to the absorber where it is dissipated. This dissipation of energy produces a control action that almost completely stops the vibrations of the structure after 6 periods.

In Figure 2.18, velocity vector plots are given for the improved sloshing absorber. Once again, the vector plots are not for the entire flow field, but for a small area near the baffle, in order to achieve the desired level of resolution. At 2.39 and 2.48 periods, there is a vortex in the region above the baffle. At time 2.76 periods, the wave height has dropped, and the vortex above the baffle is not present. At this time, another vortex has formed at the lower left corner of the baffle. At 3.13 periods, a clear travelling wave front is developing. At 3.22 periods, this travelling wave is characterised as having only a horizontal velocity, whereas a standing wave would have primarily a vertical velocity. Although the vector velocity field given in Figure 2.18 is similar to that in Figure 2.17, it must be noted that it is no longer symmetrical, and the level of control of liquid sloshing is different. The difference in the control of liquid sloshing is shown by the variation in the force histories in Figure 2.14(c) and 2.14(d). When the sloshing absorber has only one baffle, the control of liquid sloshing is reduced compared with a sloshing absorber with two baffles of the same size. Therefore, the amplitude of the sloshing force in Figure 2.14(d) (one baffle) is greater than in Figure 2.14(c) (two baffles) from 0 to 4 periods.

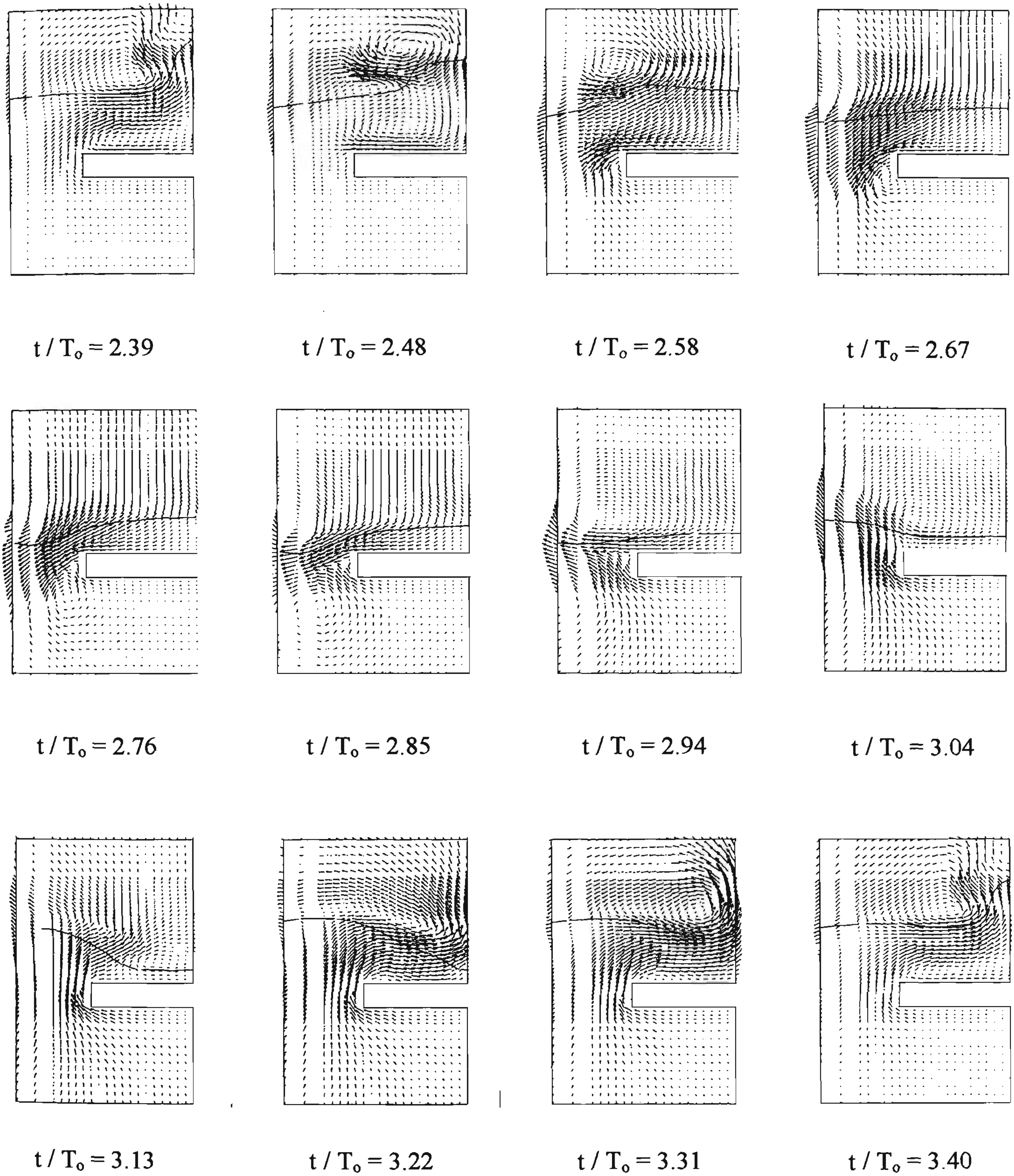

Figure 2.18. Velocity vector plots for a sloshing absorber with one 15 mm baffle submerged 10 mm below the static liquid surface.

2.6. CONCLUSIONS

A sloshing absorber of standing-wave type is proposed as an alternative to a tuned vibration absorber. Liquid storage tanks are likely to have deep levels of liquid which lead to standing-wave type sloshing. A standing wave, on the other hand, has poor energy dissipation characteristics making it an improper choice as a sloshing absorber. The significance of this chapter is that cantilevered baffle plates are employed to enhance the performance of a standing-wave sloshing absorber to control the transient oscillations of a structure. A numerical procedure is described to couple the fluid solution for sloshing with the solution of the structure to be controlled. Simple experiments are performed to verify the accuracy of the numerical predictions. The response of the structure is determined for a transient disturbance. It is expected that a transient disturbance will also indicate the performance of a sloshing absorber for random excitation, such as an earthquake. This correlation between transient and random disturbances is further demonstrated in Section 4.3.2.

When using two baffle plates, the best configuration in a container of 130 mm × 210 mm with 100 mm liquid depth, was found to be 10 mm long 3 mm thick baffle plates placed at 5 mm under the liquid free surface. Experimentally observed performance of this particular case is quite comparable to that of the optimally damped tuned absorber. In contrast to a damped tuned absorber, however, a sloshing absorber is virtually maintenance free.

The results obtained for a small model case are scaled to a larger prototype by ensuring similitude with Froude, Reynolds and Euler numbers. These scaling parameters have been used previously to scale uncontrolled liquid sloshing. The novel approach here is the application of these parameters to a system that has strong fluid-structure interaction between the sloshing liquid and cantilever baffles and also between the sloshing absorber and the structure to be controlled.

Further, the sloshing absorber is re-addressed to identify its energy dissipation mechanisms. For the optimal sloshing absorber with two baffles, vortices formed in the liquid in the region near the baffles. More importantly, the baffles modified the sloshing wave to behave similar to a travelling wave in the region near the baffle plates. Next, these characteristics were encouraged to occur in the sloshing absorber by using a single baffle instead of a pair of baffles. Consequently, the effectiveness of a standing-wave sloshing absorber was improved. The most effective absorber configuration with a container of 130 mm × 210 mm and 100 mm of liquid height has been shown to be a single 15 mm baffle submerged 10 mm below the static liquid surface. By using a single baffle, the energy dissipation characteristics of a travelling sloshing wave can be utilised even more effectively than the case with two baffles. By creating a travelling wave in only part of the absorber, the "tuning" effect of the standing sloshing wave is mostly maintained, resulting in effective control of structural oscillations.

In sloshing absorbers, with either a pair of baffles or a single baffle, the most promising configurations for the control of structural oscillations show vortices in the liquid near the baffles. Both the change from translation to rotation within the liquid above the baffle and the decay of these vortices are suggested to cause the dissipation of energy within the liquid and improve the control action of a sloshing absorber.

The proposed modifications to standing-wave type sloshing absorbers are simple, and inexpensive. Double and single baffles can be added easily to existing containers in practical applications. The biggest advantage of this work is that it may now be possible to modify a liquid storage tank that is already present in a structure, to act as a sloshing absorber to control the oscillations of the structure.

Chapter 3

CONTROL OF LIQUID SLOSHING USING RIGID CANTILEVER BAFFLES AND FLOATING DEVICES†

3.1. INTRODUCTION

In Chapter 2, liquid sloshing was utilised for the purpose of controlling a resonant structure. In this chapter, the focus is shifted to the control of liquid sloshing. Control is important, since there are many applications where uncontrolled liquid sloshing may be detrimental. Transportation of liquid cargo, sloshing in fuel tanks of aircraft and aerospace vehicles and earthquake induced sloshing in storage tanks are some of the common engineering applications where liquid sloshing must be suppressed.

In this chapter, two sloshing control techniques are examined. First, numerical predictions and experiments are presented to determine the control effect of fixed baffle plates for the suppression of liquid sloshing. In Chapter 2, similar baffles cantilevered from the vertical sides of a container, were used to improve the performance of a sloshing absorber as a vibration controller. The second control technique is a simple floating device consisting of two plates in a dumb-bell arrangement (Sharma et al. 1992 and Anderson et al. 1997b). Both of the control techniques examined in this chapter are simple and relatively inexpensive as add-on type of control in containers that are already in service. Therefore, understanding the control action by which these controllers work, is a significant and practically important task.

† The work from this chapter is published in Anderson et al. 1997a, b and c.

As mentioned in Section 2.1 of Chapter 2, cantilever baffles had been investigated experimentally by Muto et al. (1988) who observed that maximum suppression was achieved when the baffle was placed at a critical height. Silverman and Abramson (1966a) investigated rigid and flexible baffles for cylindrical containers. For rigid baffles, they developed an expression for the damping ratio for sloshing wave decay, knowing the initial wave amplitude. Another sloshing control technique was investigated by Hayama and Iwabuchi (1986). They used an inverted U-tube containing liquid to suppress sloshing by tuning liquid motion in the U-tube to oppose the motion of liquid sloshing in a tank. Hara and Shibata (1987) used an active control approach. They injected air bubbles, critically timed to cause enough momentum opposition between the sloshing wave and that of the injected bubbles to suppress sloshing.

For modelling liquid sloshing, either an Eulerian or a Navier Stokes formulation is used. In Eulerian formulations, the liquid is assumed to be inviscid, irrotational and incompressible (Warnitchai and Pinkaew, 1998) to determine the undamped fundamental frequency, free surface shape and hydrodynamic pressure exerted against solid boundaries. Empirical damping is introduced in select cases, where the damping coefficient is determined by matching numerical predictions with experimental results (Bauer, 1990). In inviscid approaches, the free surface representation is governed by two equations, representing the dynamic and kinematic boundary conditions. The dynamic condition sets a constant pressure at the liquid surface. The kinematic condition satisfies equality of velocity at the liquid-gas interface.

The alternative to an inviscid formulation is to consider the effects of viscosity by using the Navier-Stokes equations. Then, the liquid is taken to be rotational. Accounting for the effects of viscosity allows the no-slip condition to be applied on solid boundaries. As indicated in Section 2.4, such effects become important for modelling sloshing control for Re < 10^3.

In a recent example of a viscous formulation, Su and Wang (1990) made extensions to the Volume of Fluid Method to simulate three-dimensional liquid sloshing in arbitrarily shaped containers. They determined the liquid response, including the velocity and pressure distribution of the flow field, as well as the free surface position, for cylindrical containers subjected to arbitrary excitations. To illustrate the capabilities of their code, Su and Wang (1990) simulated the effect of placing blocks on the sides of a container. Each block had a thickness the same as its length.

Chen et al. (1994) determined the free surface position as well as the velocity vectors for liquid sloshing in the spherical fuel tanks of spacecraft. Hung et al. (1993) investigated the dynamic behaviour of fluids affected by asymmetric gravity jitter oscillations determining that the viscous force at liquid and solid interfaces contributed to the damping effect of sloshing.

Although others have investigated the effect of various obstructions to the liquid flow for sloshing problems, the significance of the current investigation for controlling sloshing with cantilever baffles is the description of the control action for baffles of different sizes, that are located at different positions relative to the static liquid height. The container is subjected to a sinusoidal motion. Numerical tests are performed for three excitation amplitudes. In addition to demonstrating the effectiveness of baffles for liquid sloshing control, a limited number of cases were tested experimentally for comparison purposes. A versatile numerical design tool has been prepared to examine various controller and container configurations with different excitation parameters.

A limitation of using baffles is that optimum suppression occurs at a critical liquid height and therefore, variation in liquid depth reduces the effectiveness of the controllers. A possible alternative to cantilever baffles in applications where the volume of liquid varies, may be a dumb-bell controller. The dumb-bell controllers are not fixed to the container, rather they are free floating in the liquid, and as a result, they are less sensitive to variations in liquid depth. It should be emphasised here that dumb-bell controllers are not necessarily suggested to improve the suppression effect. They are simply more suitable controllers when either the structure of the container cannot accommodate baffles due to geometric constraints or the amount of liquid varies considerably. Similarly, when the surface of the liquid must remain as a free-surface, baffles are more suitable controllers than dumb-bells.

The floating nature of the dumb-bell controllers makes their control effect extremely difficult to predict numerically. Therefore, only experimentally evaluated performance is reported in this chapter. However, as a possible first step to predicting the control action of dumb-bell controllers, a numerical procedure is presented in Appendix 3 to determine the fluid-structure interaction between liquid sloshing and a single floating plate.

The experimental setup is described next in Section 3.2. Liquid sloshing control with cantilever baffles is presented in Section 3.3, and with dumb-bell controllers in Section 3.4. The conclusions of this chapter are summarised in Section 3.5.

3.2. EXPERIMENTAL PROCEDURE

Sloshing control with cantilever baffles was investigated in a rectangular container of 130 mm × 210 mm containing water to a depth of 100 mm. This is the same container used for the sloshing absorber in Chapter 2, and it is shown in Figure 2.4, on page 17.

For dumb-bell controllers, two different cylindrical containers were used: a vertical container of 100 mm diameter and a horizontal container of 100 mm diameter and 300 mm length. The static liquid height was kept constant at 75 mm in the vertical container and 63 mm in the horizontal container. The horizontal container was divided into three compartments of approximately 100 mm length, exposing a rectangular free surface area for each compartment as shown in Figure 3.1. This three-compartment arrangement enabled observing the controlled and uncontrolled response simultaneously by leaving at least one of the compartments without a controller. In all trials, the working fluid was water.

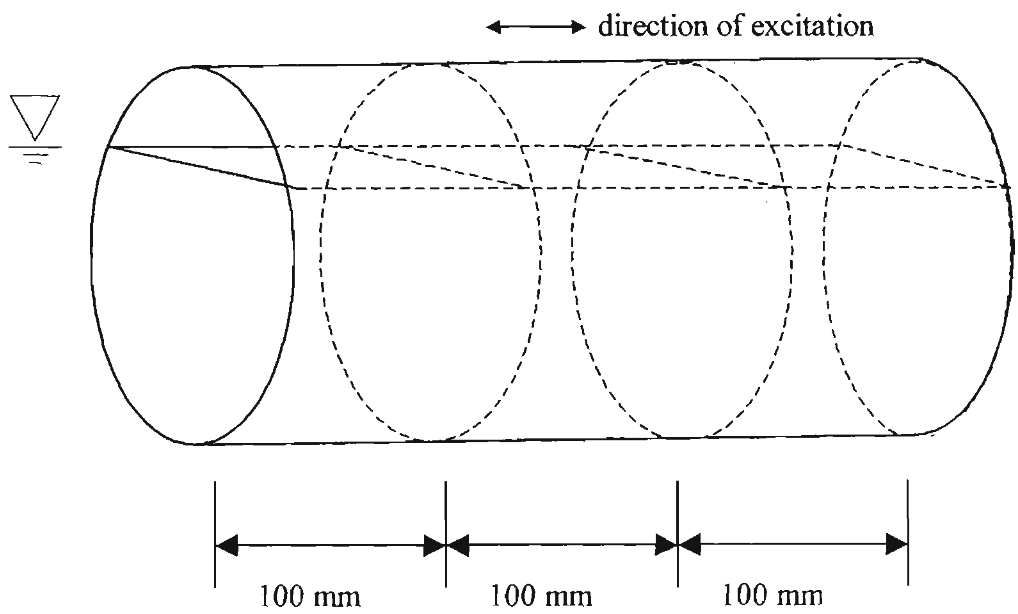

Figure 3.1. The horizontal cylindrical container.

With the rectangular and cylindrical containers, sloshing was induced by the horizontal motion created by an electromagnetic shaker driven by a signal generator. For the rectangular container, a sinusoidal peak-to-peak displacement of 2 ± 1 mm at a frequency of 2.3 ± 0.2 Hz, excited the fundamental mode of sloshing. The container was orientated on a shaking table such that sloshing occurred along the 130 mm dimension of the container. This orientation forced the liquid motion to be a two-dimensional one, as indicated earlier in Section 2.3.1 in Chapter 2.

For the vertical cylindrical container, the peak-to-peak stroke length of the shaking table was also 2 ± 1 mm. For the horizontal cylinder, the stroke length was varied to produce an uncontrolled wave height that reached the top of the container. The frequency of excitation was kept at the fundamental sloshing frequency of 2.8 Hz for both cylindrical containers. This value of the fundamental sloshing frequency, f_n, is in agreement with Milne-Thomson's formulation (1968):

$$f_n = \frac{1}{2\pi}\sqrt{\frac{\pi g}{d}\tanh\frac{\pi H_w}{d}} \tag{3.1}$$

where g is the gravitational acceleration, d is the container diameter for the vertical cylinder (or the partition length for the horizontal cylinder), and H_w is the stationary water height. The unit of f_n is Hz. The derivation of this equation is given in Appendix 2.

For the rectangular container, a range of rigid flat plate baffles of varying cantilever lengths and at different positions from the static free surface was used for the tests. The baffles were constructed from 3 mm thick plywood. Their exposed surfaces were sealed to minimise water absorption. The results of these tests will be discussed in Section 3.3.

For the horizontal and vertical cylindrical containers, the dumb-bell controllers consisted of two plates separated by rigid rods as shown in Figure 3.2. Similar to the baffles, the plates of the dumb-bells were made from 3 mm thick plywood, and the surfaces of the plates were sealed with varnish. The top plate floated on the free surface, whereas the bottom plate was submerged in the water during the experiments. To ensure maximum interference with the sloshing surface wave, circular plates were used in the vertical container and rectangular plates were used in the horizontal container as shown in Figure 3.2. For all the vertical trials and for some of the horizontal trials, the centres of the plates were hollowed out to reduce weight. The hollow square plates had a constant thickness, t, of 20 mm. The thickness of the round plates was varied. The results of the dumb-bell controllers are reported in Section 3.4.

Flow visualization was achieved by video recording the experiment. The viewed image was scaled to enable measuring of the peak-to-peak sloshing amplitude within an estimated accuracy of ± 0.5 mm. A schematic diagram and photograph of the experimental setup is shown in Figure 3.3. A rectangular container is shown in this figure to test the performance of cantilever baffles. The same setup was used with the cylindrical containers for assessing floating dumb-bell controllers.

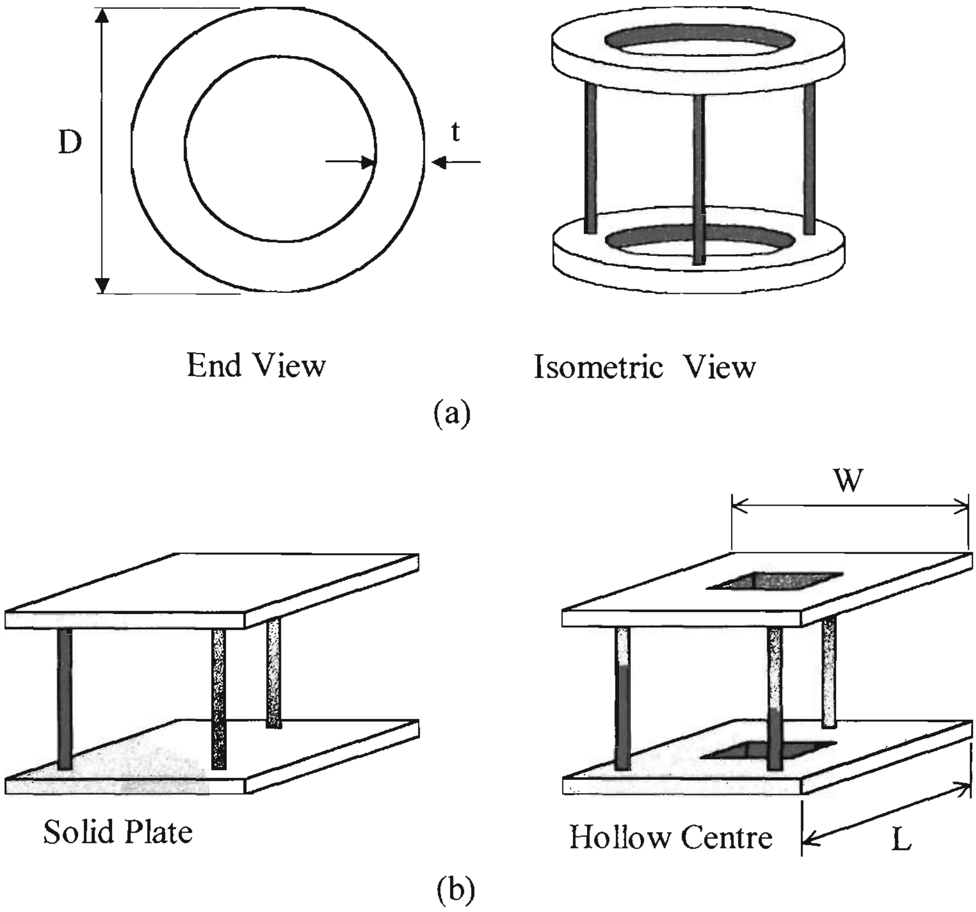

Figure 3.2. Dumb-bell controllers used in (a) the vertical and (b) the horizontal containers.

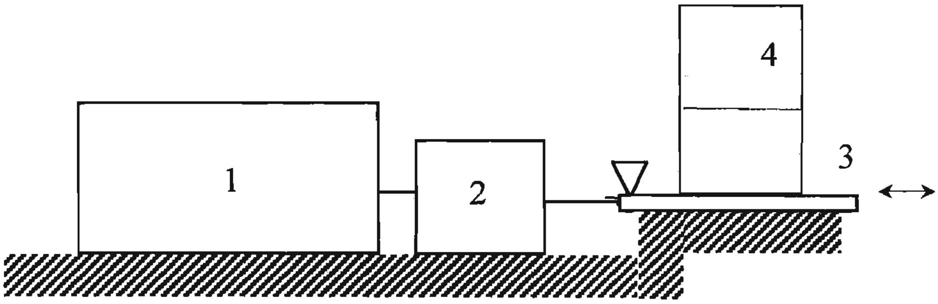

(a)

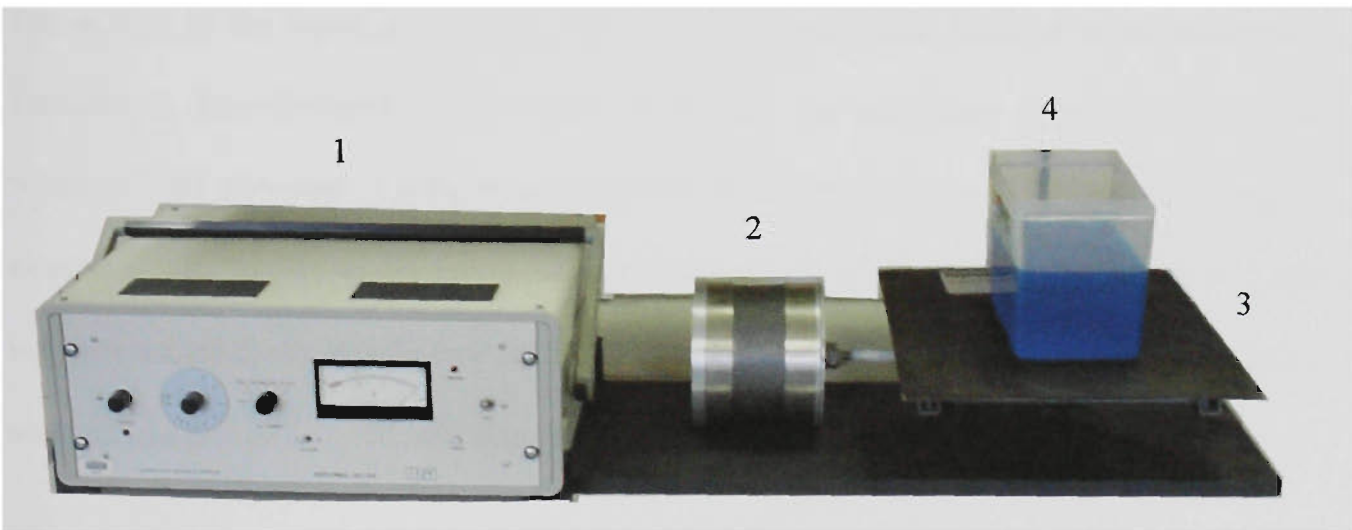

(b)

Figure 3.3. Showing (a) the schematic diagram and (b) photograph of the experimental setup with a rectangular container on the shaking table.
1. Gearing and Watson SS100 signal generator and amplifier, 2. Gearing and Watson Type GWV46 electromagnetic shaker, 3. shaking table (built in house), 4. rectangular container. The liquid free surface shape, shown in (a), represents uncontrolled sloshing at the fundamental mode.

3.3. CONTROL OF SLOSHING WITH CANTILEVER BAFFLES

Both numerical predictions and experimental observations of liquid sloshing with cantilever baffles are given in this section. The same numerical model as in Section 2.3.2 of Chapter 2 for a sloshing absorber is used here. The only difference in the approach is that here, the motion of the container is an imposed sinusoidal displacement instead of a structural response. The numerical procedure is as discussed in Chapter 2, and therefore, only a brief reminder is provided here. The model is two-dimensional, and it is created using CFX 4.1. The motion of the liquid is obtained using the Volume of Fluid Method to solve the two-dimensional, incompressible Navier-Stokes equations. A multiphase simulation is adopted because of the presence of a liquid-gas interface at the free surface. After a grid refinement exercise similar to that in Section 2.3.2, a numerical grid of 26 × 28 cells of 5 mm × 5 mm was determined to be satisfactory for the uncontrolled case. When baffles were included, a non-uniform grid of 64 × 70 cells was required.

Liquid sloshing is a transient phenomenon. As a result, sufficient time is required for the sloshing wave to develop after the container begins to experience an excitation. For the numerical prediction of the uncontrolled case, a sloshing wave was obtained after 10 periods, in good agreement with experiments, with a peak-to-peak excitation amplitude of 2.5 mm at the fundamental sloshing frequency. Subsequently, each simulation case was run for 10 periods starting from rest. A time-step of 0.001 s was the largest possible time-step for accurate numerical predictions for both the uncontrolled and controlled cases.

3.3.1. Results for Cantilever Baffles

Numerical predictions of the uncontrolled surface shape showed close agreement with experimental results as shown in Figure 3.4. In this figure, and in the following two figures, experimental results are shown with a dashed line and numerical predictions are shown with a solid line. In Figure 3.4, as expected in the fundamental mode, the shape of both waves approximates a half sine wave. In the experiments, the uncontrolled peak-to-peak sloshing amplitude was observed to be 35 ± 0.5 mm and the numerically predicted amplitude was 34 ± 0.5 mm, resulting in a difference of only 3%.

In Figure 3.5, a typical comparison between the numerical and experimental results is presented for 10 mm long baffles located at a height of 10 mm above the static liquid surface. The baffles can be identified as the void horizontal areas in the refined band of the grid. The baffles force the wave to have a significantly different shape with a smaller amplitude than in the uncontrolled case. Comparing only the peak–to-peak amplitudes of the two surface shapes, a maximum error of 31% is present between the predicted amplitude of 25 ± 0.5 mm and experimental amplitude of 19 ± 0.5 mm. However, the general shape of the predicted free surface is similar to that observed in the experiments. Figure 3.5 shows that the crests of the waves obtained experimentally and computationally are almost identical as the wave interacts with the left baffle.

When the baffles are on the free surface, there are even larger percentage differences between the predictions and experiments than those in Figures 3.4 and 3.5. Numerical predictions have shown that the wave had a small but measurable amplitude, whereas experiments have shown that for plate sizes ranging from 30 mm to 10 mm, the sloshing amplitude was virtually undetectable. The largest difference was for 10 mm plates as shown in Figure 3.6. For this case, the numerically predicted amplitude (——) was 8.5 mm compared to a zero amplitude of the experiments (-----). Despite this difference, the predicted amplitude was only just large enough for the wave to climb over the edge of the baffle plate.

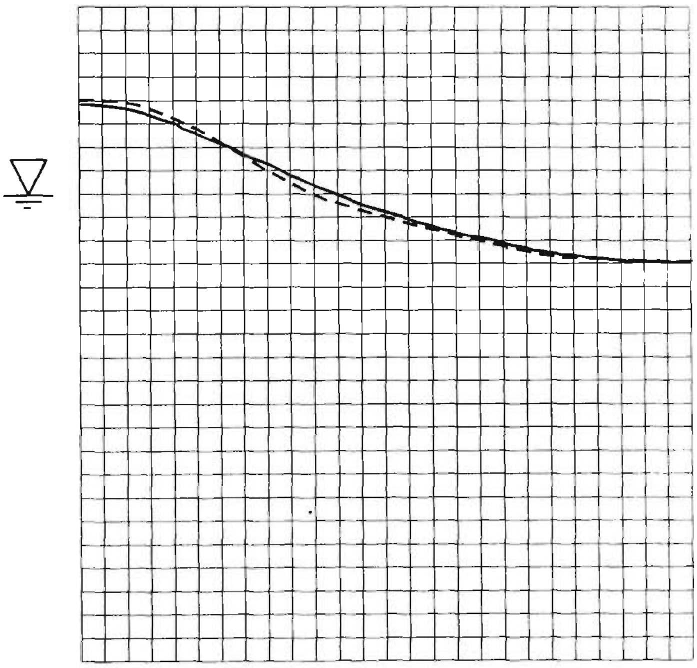

Figure 3.4. Uncontrolled numerical grid with experimental (-----) and numerical (——) surface shapes.

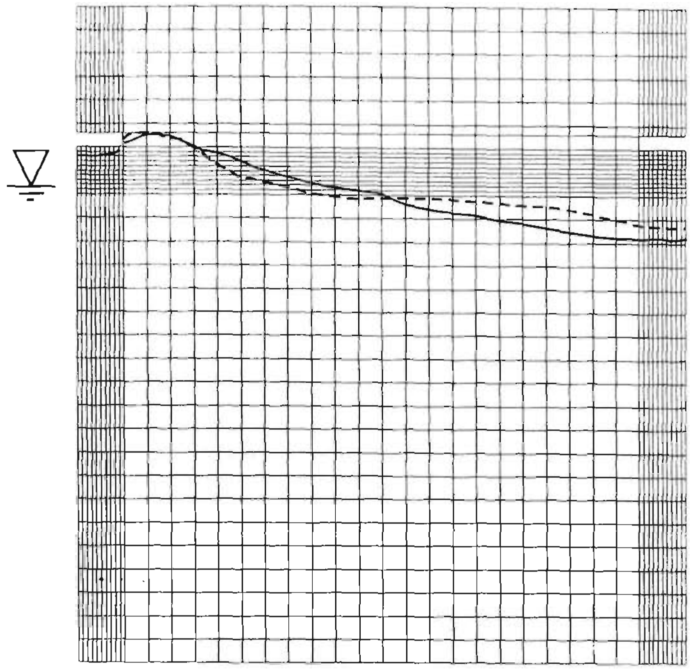

Figure 3.5. Controlled numerical grid with experimental (-----) and numerical. (——) surface shapes for 10 mm baffles located at 10 mm above the static liquid surface.

Experimentally, the presented surface shapes were taken from 10 still frames per period of the video-taped sequence. Numerically, 460 frames per period were available for this purpose. Hence, it was impossible to guarantee that the surface shapes were compared at exactly the same phase experimentally and numerically with respect to the container motion.

The differences between experimental and predicted results in Figure 3.6 may also be attributed to the assumption that in the numerical model, the baffle surfaces and container walls are smooth. No attempt was made to numerically create surface roughness comparable to that of the baffles used experimentally. It is expected that surface roughness should present some resistance to the sloshing wave in contact with the baffle. In addition, surface tension effects were visible in the experiments where the static liquid was observed to climb to the top of the plates located on the liquid surface.

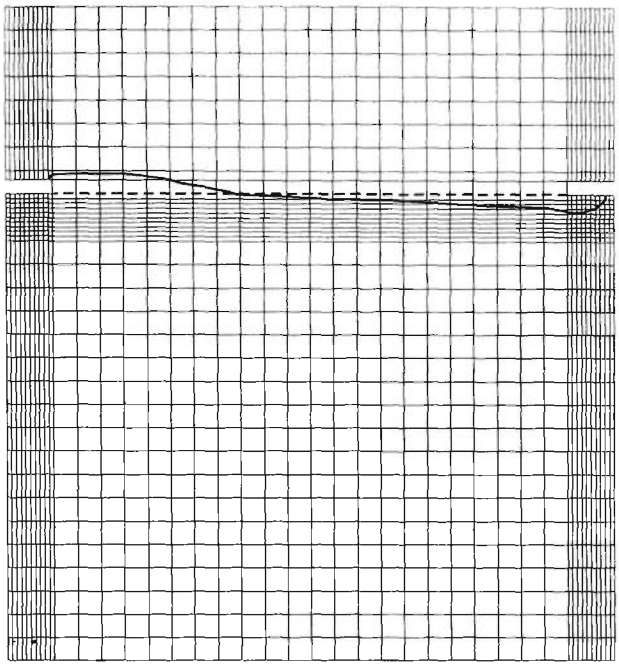

Figure 3.6. Controlled sloshing wave shapes from experiments (-----) and numerical predictions (——), using 10 mm baffles located on the static liquid surface.

The comparison between numerical and experimental results for 10 mm baffles at 10 mm, 5 mm, 0 mm, -5 mm and –10 mm from the static free surface, is shown in Figure 3.7. Figure 3.7 is the same as Figure 2.8 in Chapter 2, and it is repeated here for ease of reference. In an effort to generalise the results, it is appropriate to express the non-dimensional sloshing amplitude as the ratio of the controlled amplitude, A_c, to the uncontrolled amplitude, A_o. The position of the baffles is expressed as the ratio of the distance from the liquid surface, H_b, to the static liquid depth, H_s. Negative H_b/H_s represents submerged baffles.

The trend of experimental and predicted results shows that the baffles are more effective when located on the surface, $H_b/H_s=0$, or just below the surface, $-0.1\leq H_b/H_s<0$, than above the surface[†]. The maximum suppression of approximately 75% numerically and 100% experimentally occurs when $H_b/H_s=0$. When the plates are located above the surface, it is expected that the sloshing amplitude will be at least as high as the location of the baffles. Therefore, the baffles are forced to suppress a wave that already has some motion.

Figure 3.7 shows that the effectiveness of the baffles is observed to be greater experimentally than that predicted numerically. Hence, predicted configurations could be interpreted with some confidence, knowing that in reality, the baffles will be even more effective. The trend shown in Figure 3.7 may be used to produce an advantage in containers where the liquid level drops during operation. For such cases, the baffles should be placed under the liquid surface, for a minimal loss of effectiveness from that of the baffles on the surface. As the liquid level drops, performance of the baffles improves, until the baffles leave the liquid surface, producing a wide range of effectiveness. In this argument for varying levels, the effect of the depth on the behaviour of the liquid is assumed to be insignificant. This assumption was verified with experimental observations.

[†] As indicated earlier in Section 2.3.3 in Chapter 2, the level of effective sloshing control achieved with cantilever baffles at $-0.1 \leq H_b/H_s < 0$ is appropriate for using these configurations also for the control of structural oscillations. The complete or almost complete suppression of liquid sloshing with baffles at $H_b/H_s=0$ makes this case over-damped for structural control. For $H_b/H_s>0$, the slope of the amplitude ratio, A_c/A_o, is much steeper than it is for $H_b/H_s<0$ with a rapidly diminishing effect on the liquid motion, and hence, this part of the curve is not useful for structural control.

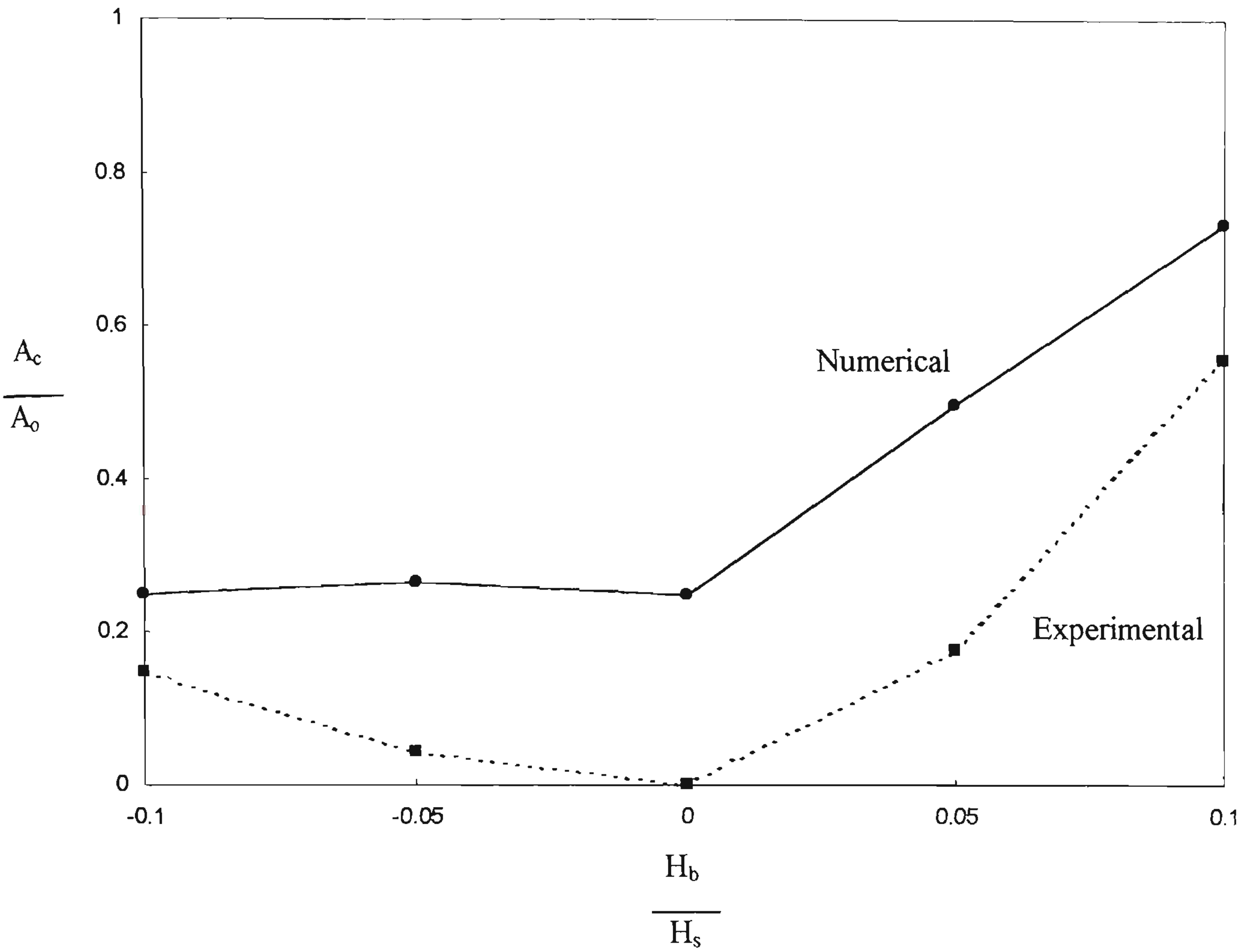

Figure 3.7. Variation of the experimental (■) and numerical (•) non-dimensional sloshing amplitude with non-dimensional height for 10 mm baffles.

With the optimum position of the baffles identified for sloshing control, as on or just below the free surface, it was possible to determine the effect of different plate sizes for a range of excitation amplitudes of 1 mm (▲), 2.5 mm (♦) and 5 mm (■) as shown in Figure 3.8. In this figure, A_c/A_o is again the non-dimensional sloshing amplitude, and $2L'/W'$ is the non-dimensional length of the baffles. Here, L' is the baffle length and W' is the width of the container. The non-dimensional plate size of $2L'/W'=0$ represents the uncontrolled case.

The results in Figure 3.8 generally agree with the expected trends for different stroke lengths. For example, smaller baffles, around $2L'/W'=0$, are generally less effective, $A_c/A_o \cong 1$, than larger baffles. As $2L'/W'$ approaches 0.5, A_c/A_o tends toward 0. For excitation amplitudes of 2.5 mm and 5 mm, the figure shows that as the plate size is reduced to 15% of the container width, $2L'/W'=0.3$, the sloshing amplitude is reduced by at least 80%, $A_c/A_o \leq 0.2$.

In Figure 3.8, experimental results (×) are shown for an excitation amplitude of 2.0 ± 1 mm, where 100% suppression, $A_c/A_o=0$, was achieved for a range of plate sizes from approximately 8% of the container width, $2L'/W'=0.15$, to 23% of the container width, $2L'/W'=0.45$. Although it was not practically possible to make smaller baffles to try experimentally, it is expected that as the baffle size approaches zero, the control performance should deteriorate. In most practical applications, the size of baffles is restricted. For such cases, Figure 3.8 can be used to determine the baffle size for the resulting suppression of a sloshing wave.

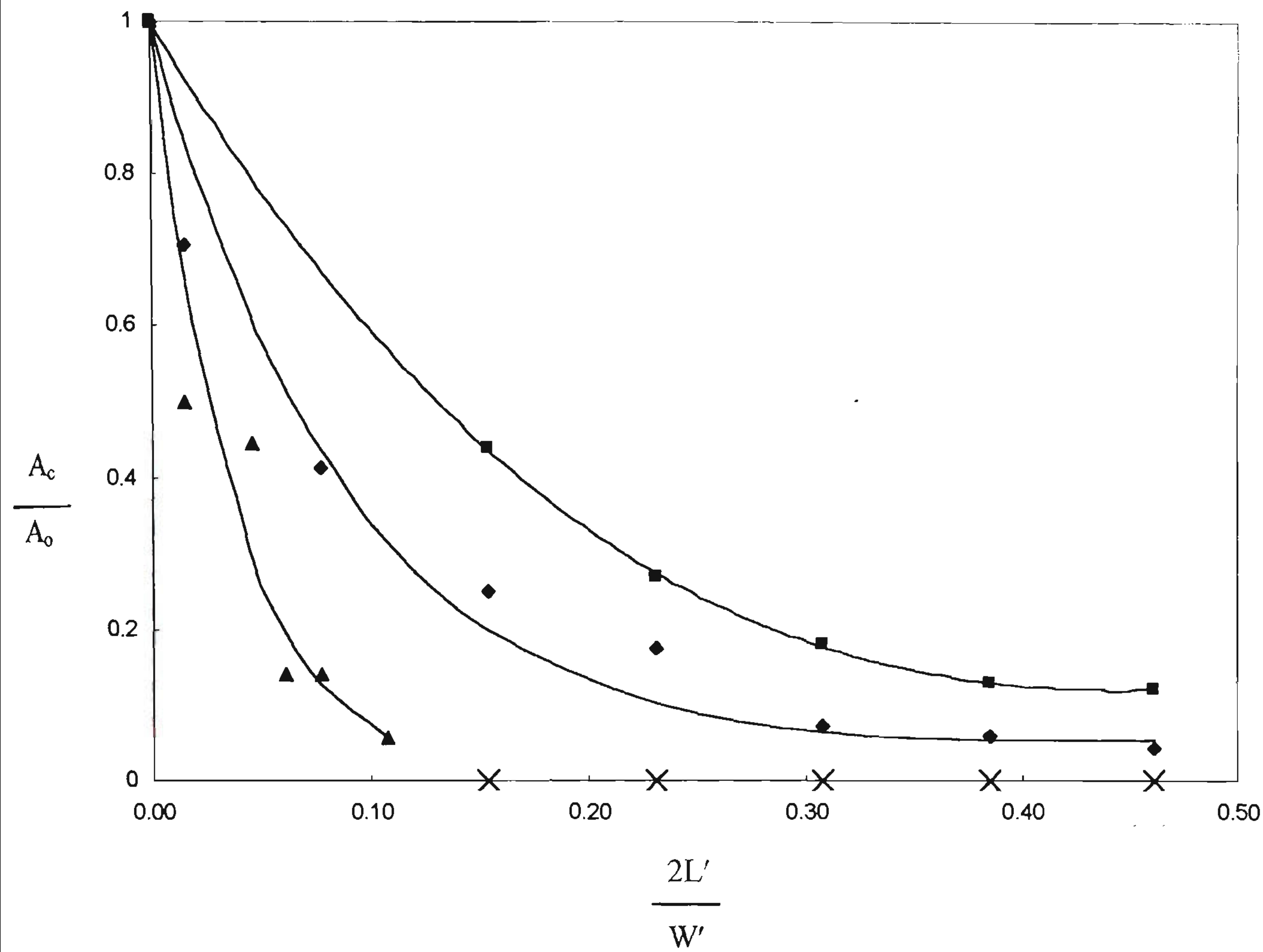

Figure 3.8. Variation of the non-dimensional sloshing amplitude with non-dimensional baffle length. Each line corresponds to a peak-to-peak excitation amplitude of 1 mm (▲), 2.5 mm (♦) and 5 mm (■). Experimental data (×) are given only for an excitation amplitude of 2 ± 1mm.

3.4. CONTROL OF SLOSHING WITH FLOATING DUMB-BELLS

The performance of dumb-bell controllers is discussed in this section. The dumb-bell shaped controllers are positively buoyant when floated on the liquid free surface, having an equilibrium position as shown in Figure 3.9(a). However, when the top plate is forced down into the liquid surface, the controller remains at the second equilibrium position as illustrated in Figure 3.9(b). If the top plate is forced below the surface, the dumb-bell returns to the second equilibrium position. Surface tension was suspected to cause this phenomenon. Surface tension creates a force that acts either upwards or downwards to keep the plate of the dumb-bell in contact with the liquid free surface.

In Figures 3.9(a) or 3.9(b), the surface tension force at the interface of water-air-lower or upper dumb-bell plate, respectively, acts upwards, and it balances the dumb-bell weight together with the upward buoyancy force. For various dumb-bell sizes at these two configurations, the surface tension force was estimated to be 15 to 40% of the buoyancy force, confirming its non-negligible presence. The surface tension force can change direction, and it acts downwards if a dumb-bell is pulled up from its floating position in Figure 3.9(a).

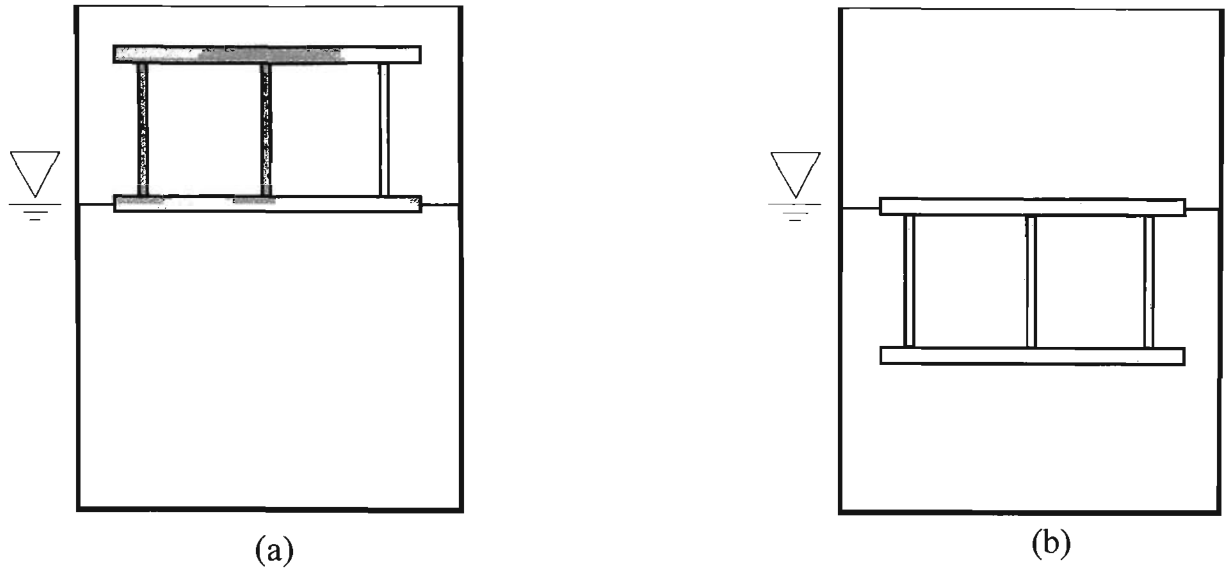

Figure 3.9. Showing the equilibrium positions of the dumb-bells when the bottom plate is (a) floating on the surface and (b) submerged in liquid.

3.4.1. Results for Dumb-Bell Controllers

The results obtained with the vertical container are shown in Figure 3.10. In this figure, different symbols indicate different dumb-bell arrangements. The numbers following the letters D and t indicate the diameter and thickness, respectively, in mm. A_c/A_o is the non-dimensional sloshing amplitude, defined as the ratio of the peak-to-peak sloshing amplitude with the controller, A_c, to without the controller, A_o. A_c/A_o of unity represents uncontrolled sloshing. S is the non-dimensional ratio of the separation distance between the dumb-bell plates to the static water height. S of zero represents a single floating plate on the free surface. Due to the levelling off of the dumb-bell performance as shown in Figure 3.10, the maximum plate separation used in the experiments was 65% of the static liquid height (or 50 mm).

The results in Figure 3.10 suggest that at a critical value of the separation, the submerged bottom plate may act as an anchor for the top plate floating on the free surface. This critical value is around an S of 0.5, which corresponds to a reduction of at least 80 % ($A_c/A_o \cong 0.2$) of the uncontrolled sloshing amplitude. Further increase in S produces quite marginal improvement of the control action. This trend suggests that an inertial liquid region exists at a critical depth. When the bottom plate is immersed in this region, it provides maximum anchoring effect to the top plate. The presence of a deep liquid layer in rigid body motion is mentioned also in Silverman and Abramson (1966b). The results in Figure 3.10 further suggest that starting with a non-dimensional separation distance, S, of approximately 0.25 will allow up to 75% of the liquid to be emptied while maintaining 60% or better sloshing amplitude suppression ($A_c/A_o \leq 0.4$). As the liquid level drops, the value of S will increase, therefore producing smaller values of A_c/A_o and more effective suppression.

Experimental observations presented in Figure 3.10 indicate the critical importance of the separation between the plates for effective control. For different plate configurations, however, it is not possible to maintain the same mass of the controlling dumb-bell device.

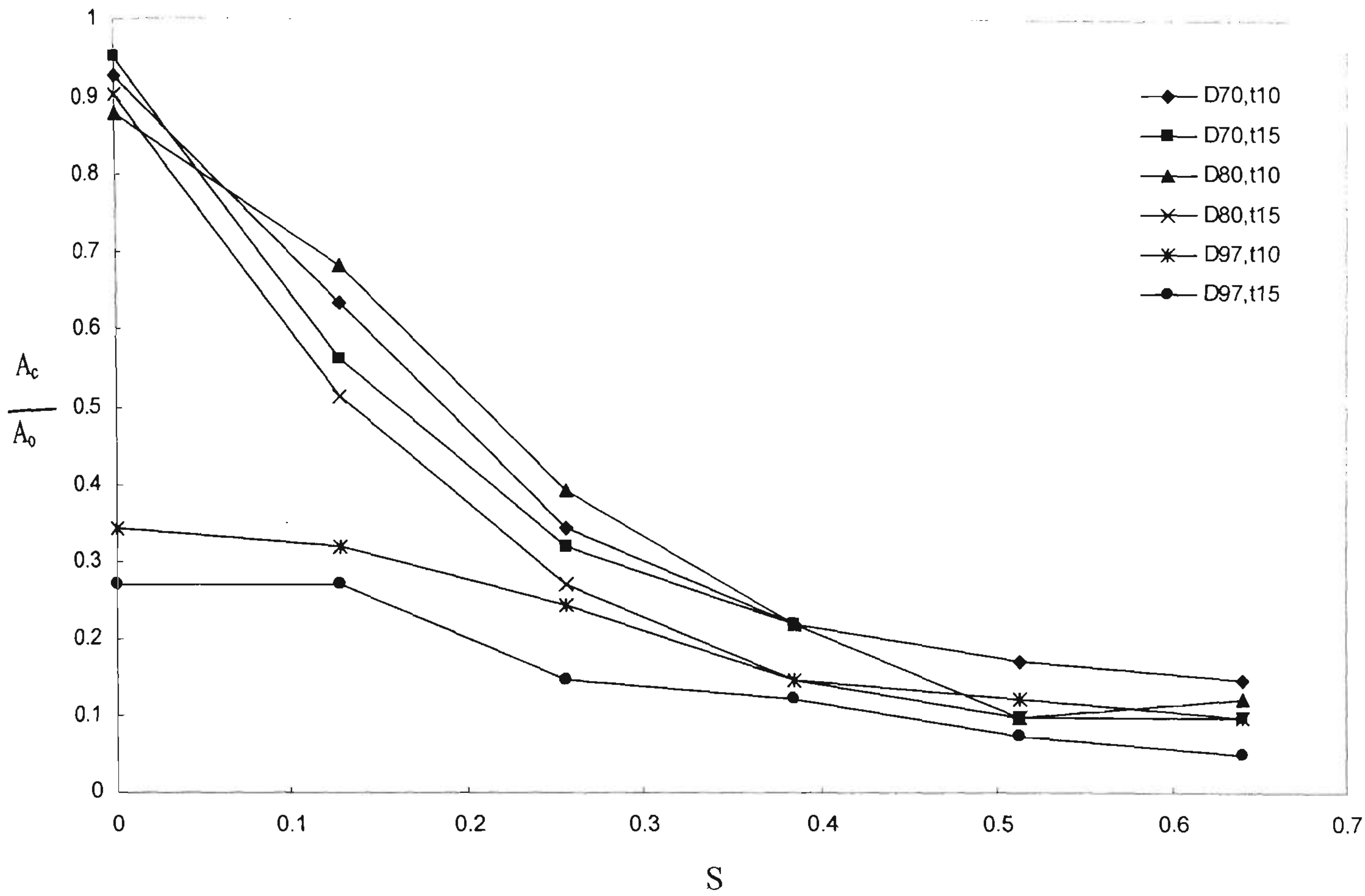

Figure 3.10. Variation of non-dimensional sloshing amplitude, A_c/A_0, with non-dimensional separation distance, S, for the vertical container. Each symbol corresponds to a set of plates with an outer diameter, D, and plate thickness, t, in mm.

The results in Figure 3.10 are presented in a different format in Figure 3.11, in order to separate the effects of controller mass and separation distances. The vertical axis in Figure 3.11 is the same as in Figure 3.10. The horizontal axis represents the ratio of the controller mass to the sloshing liquid mass, m_c/m_l. The results are grouped for three particular S values of 0, 0.26 and 0.65 (corresponding to 0, 20 mm and 50 mm separation distances), and a best fit line is shown for each S value, for demonstration purposes.

For increasing values of S, the control effect improves. For any given mass ratio, along a vertical line, the effectiveness of suppression is significantly larger for larger S. In addition, as S increases, the incremental improvement in A_c/A_0 diminishes. As suggested earlier, beyond an S of 0.5, only slight improvements were observed in the effectiveness of sloshing suppression.

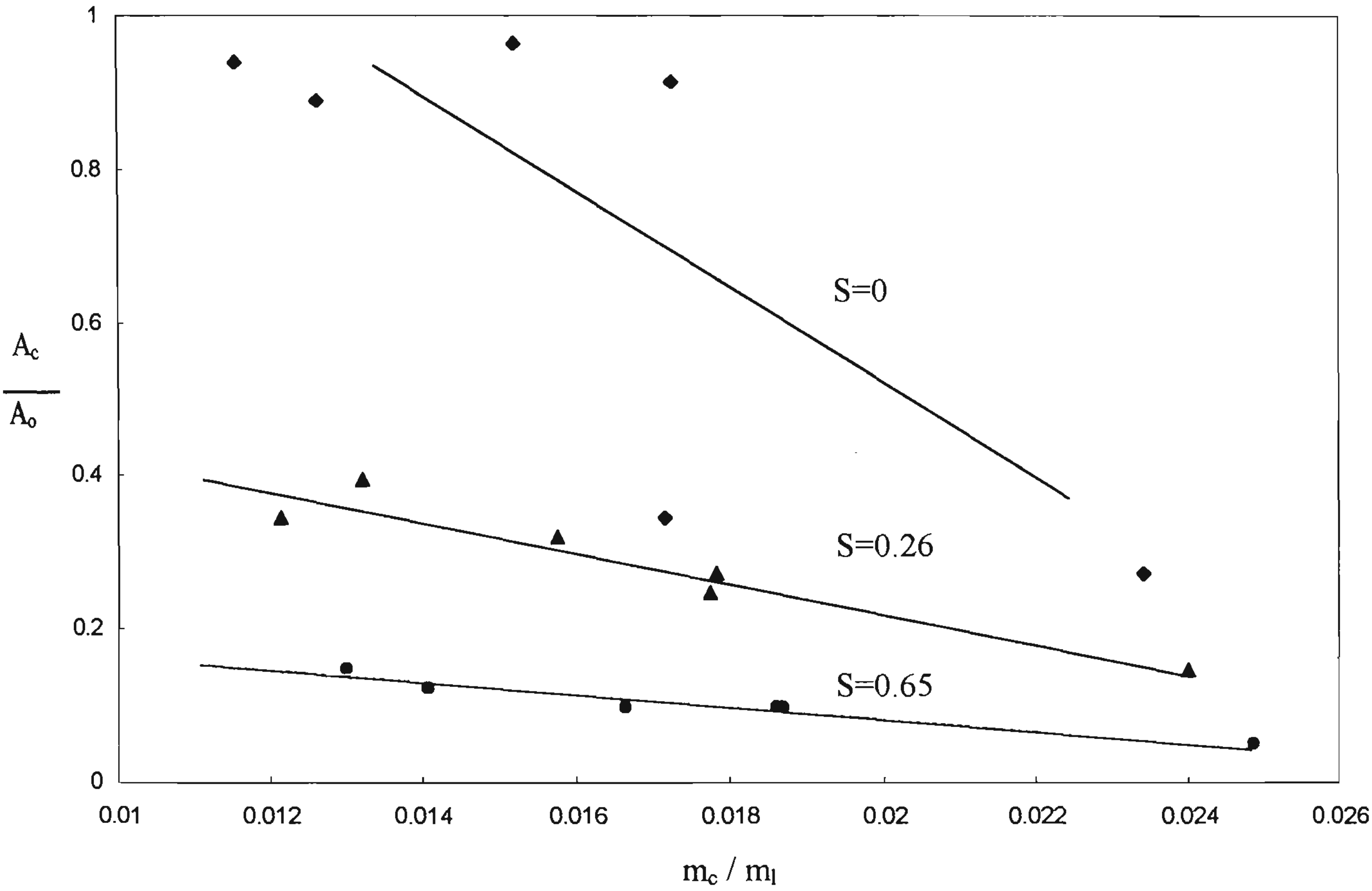

Figure 3.11. Effect of mass ratio on the sloshing wave for non-dimensional separation of the dumb-bell plates, S, of 0, 0.26 and 0.65.

The results for the horizontal container are presented in Figure 3.12, in a similar format to that in Figure 3.10. The numbers following the letters L and W indicate the length and the width of the rectangular plates in mm, respectively, with H indicating hollow plates. For the horizontal container, the controlled sloshing amplitude was approximately linearly proportional to the separation between the two plates. The sloshing was reduced by at least 80% ($A_c/A_o \cong 0.2$) when the plate separation was approximately 60% of the static free surface height of the liquid ($S \cong 0.6$). The reason why a plateau, similar to that in Figure 3.10 for values of S larger than 0.5, could not be observed can be explained with the shape of the bottom of the container. As S increases, the lower plate is immersed in smaller volumes of water, and consequently, anchoring effectiveness decreases. Hence, a critical depth may not exist for a horizontal cylinder, as clearly as for a vertical cylinder.

To examine the absence of a critical depth with its resulting anchoring effect further, two types of rectangular dumb-bell plates were used in experiments with a horizontal cylinder, namely, solid and hollow, as shown in Figure 3.2(b). As seen in Figure 3.12, the difference in sloshing control is not significant between a pair of dumb-bell controllers of the same size, one solid and the other hollow. This trend also indicates that if the results in Figure 3.12 are plotted in the same format as in Figure 3.11, then negligible effect due to mass ratio is observed on sloshing suppression with dumb-bell controllers. The difference observed for the vertical container at varying values of S, diminishes for a horizontal container.

Unlike cantilever baffles, it was not possible to simulate the controlling effect of dumb-bell controllers with CFX 4.1. The reason was that even with the available custom programming capabilities within the CFX environment, the motion of a floating plate could not be predicted, as subsequently confirmed by the CFX programmers. One possible reason is the inability of the program to handle the grid distortion within the liquid with the motion of the floating plate. An attempt is given in Appendix 3 to simulate the effect of a solid plate "floating" on the free surface of a liquid.

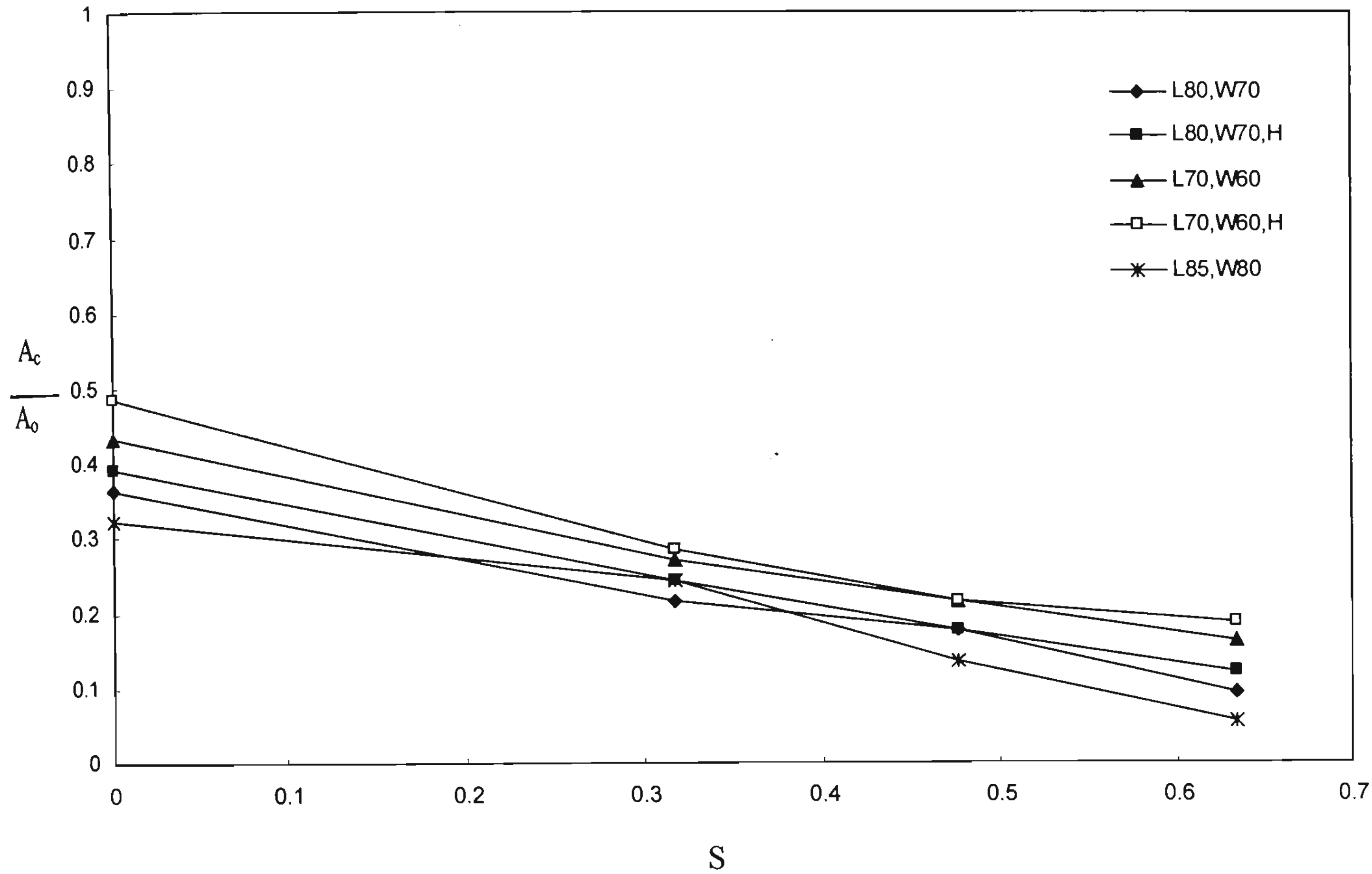

Figure 3.12. Variation of non-dimensional sloshing amplitude, A_c/A_0, with non-dimensional separation distance, S, for the horizontal container. Each symbol corresponds to a set of rectangular plates with a length L, and width W, in mm. H denotes hollow plates with a constant 20 mm thickness.

3.5. CONCLUSIONS

Two types of sloshing control devices are investigated, namely, cantilever baffles and floating dumb-bell controllers. The control of liquid sloshing in a rigid rectangular container using baffle plates has been simulated, and the numerical predictions have been checked experimentally. The control action of the baffles, which are fixed to the vertical walls of a container, is determined. For the uncontrolled case, experimental results matched predicted results to within 3%. For the controlled cases, experimental results showed greater suppression than that could be predicted with numerical simulations. Possible reasons for such differences could be the omission of baffle surface roughness, container wall roughness and surface tension effects in the numerical model. Difficulties in comparing images at exactly the same time-steps may have also resulted in not matching experimental and predicted results at the same phase with respect to the motion of the container.

Despite the differences between numerical predictions of sloshing control with cantilever baffles and limited experimental results reported here, the existing model can be used to design optimum baffles with confidence, since they offer greater suppression than predicted. The most significant contribution of a numerical procedure such as the one presented here, is its versatility. Such a tool is ideally suited to simulating many different configurations in the preliminary design stage. It enables selective promising cases to be isolated to be further tested experimentally and implemented in practice.

The control action of cantilever baffles deteriorates dramatically if the liquid level drops, and the baffles become exposed. Alternatively, the floating nature of dumb-bell controllers makes their control action less sensitive to changes in liquid level. In cases where the liquid level changes, dumb-bell controllers may provide a significant advantage. It was observed that for a vertical cylindrical container, a critical plate separation exists where any further increase could produce only slight improvement of control. This phenomenon can be exploited to allow up to 75% of the liquid to be emptied while still retaining effective sloshing control. For a horizontal cylindrical container, the reduction in sloshing amplitude is almost linearly proportional to the separation between the two plates.

The two passive control techniques investigated in this chapter hold promise. Each controller is suitable for particular applications of either different geometric constraints or varying liquid levels during operation. They both are versatile, inexpensive and easy to implement as add-on type of passive control for liquid sloshing in rigid containers.

Chapter 4

USING CONTAINER FLEXIBILITY AS A TUNED ABSORBER TO CONTROL LIQUID SLOSHING

4.1. INTRODUCTION

In previous chapters, the addition of controllers such as floating devices or baffles in the container is shown to provide effective sloshing control. However, in some practical applications, the addition of such devices may not be possible due to geometric constraints. To this end, this chapter focuses on the interaction between liquid sloshing and flexible wall containers to achieve the required control.

Different configurations of rigid baffles have been shown earlier to provide significant control of liquid sloshing (Anderson et al. 1997a; Su and Wang, 1990; Hung et al. 1993; Gedikli and Erguven, 1999). Furthermore, Stevens (1966), conducted an experimental investigation and determined that flexible baffles could be even more effective than rigid baffles. Stevens found that an optimal flexibility of the baffle existed, after which a further increase in flexibility resulted in a dramatic deterioration of the control effect (because of the baffle's inability to affect the flow).

Flexibility of the container and the fluid-structure interaction that results from the motion of the container were also investigated by Tang (1994), Jeong and Kim (1998), Kana et al. (1966), and Chen and Haroun (1994). However, the primary interest in these works, was the determination of natural frequencies and mode shapes of containers holding liquid. Tang (1994) used numerical simulations to determine the vibration modes of a cylindrical tank containing two liquids. Jeong and Kim (1998) presented an analytical method for determining the natural frequency of shells filled with liquid, and validated the analytical solution with Finite Element Analysis using a commercial code.

Kana et al. (1966) performed experiments to determine the response of a partially filled cylindrical elastic tank. Liquid motion was most easily induced when the liquid free surface level was close to the axial antinode of a breathing mode of the shell. Kana et al. (1966) discovered that significant coupling between a container breathing mode and liquid sloshing occurred when there was a clear separation of the frequencies of the liquid and container. This coupling was identified by a clear beat in the displacement history of an antinode of the container where the elastic shell resonated at a frequency of approximately two orders of magnitude higher than the fundamental sloshing frequency of the liquid.

Chen and Haroun (1994) reported a numerical model for a two-dimensional system consisting of a liquid and a flexible tank. The liquid was considered to be inviscid, incompressible and irrotational. The model required the addition of artificial energy dissipation to stabilize the numerical simulation. Other works simulating inviscid liquid sloshing, also required the addition of artificial damping terms. Yao et al. (1994) simulated three dimensional waves in narrow tanks. Energy dissipation was added to match predicted wave amplitudes to experimental data. Takahara et al. (1994) simulated liquid sloshing in cylindrical tanks subjected to pitching excitation. Equivalent damping terms were added to their formulation to account for the energy dissipation. Fujino et al. (1992) simulated liquid sloshing in a tuned liquid damper for suppressing structural oscillations. Included in their formulation, was also a dissipation term to represent effects of friction at container walls and contamination of the liquid free surface.

In the current investigation, the dynamic interaction of a flexible container and liquid sloshing has been utilised for the purpose of controlling liquid sloshing. The primary concern is the reduction of liquid sloshing, whereas suppressing excessive dynamic deformation of the flexible container is of secondary importance. The technique of using container flexibility to control liquid sloshing is a novel one. The concept of using a flexible container to control oscillations of a liquid is similar to that of using a tuned absorber to control vibrations of an oscillating mass-spring system. This work is potentially important in practical applications involving the transportation of liquid goods where sloshing can either damage the liquid product or compromise the structural integrity of the container.

This chapter starts with experiments to verify the numerical model. Then, numerical predictions are presented to show that the flexibility of the container can be used to control liquid sloshing. For practical applications, the advantages of using a flexible container are two fold. Firstly, liquid sloshing is reduced. Secondly, since the container flexibility is achieved by reducing the wall thickness, a lighter container is used, saving material and cost.

4.2. VALIDATION OF THE NUMERICAL MODEL

In this section, numerical predictions are presented to determine the importance of the interaction between a liquid and its flexible container to control liquid sloshing. A test case is examined experimentally for the purpose of verifying the accuracy of these numerical predictions. Comparisons are presented between the numerically predicted and experimentally measured displacement histories. Instead of such a detailed comparison, taking an average value of the sloshing force on the walls of the tank, for example, would tend to mask differences between experiments and predictions for a sloshing problem where interactions between the container and the liquid are critical. Therefore, the approach adopted here is a conservative one.

4.2.1. Experiments

An aluminium tank was constructed from 1.6 mm thick sheet. The dimensions of the tank were 400 mm x 400 mm x 1600 mm. Mass was added to the container walls at three points as shown in Figure 4.1, in order to tune the natural frequency of the container with that of the fundamental sloshing mode. The container natural frequency could also be lowered by reducing the wall thickness. However, it was seen from the numerical results that a wall thickness of less than about 1 mm would result in buckling.

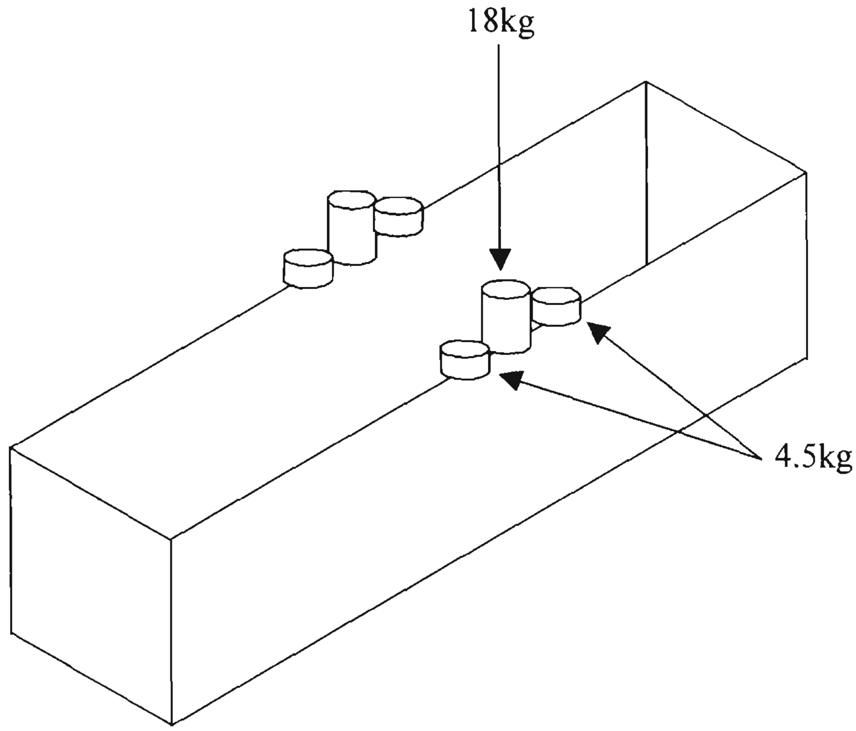

Figure 4.1. Isometric view of the tank with added mass configuration used in the experiment.

The displacement of the walls of the container was measured at one point with a contact displacement transducer. The signal was then recorded with a personal computer. The liquid motion was captured with a video camera and liquid displacements were then measured from still images. A schematic diagram of the experimental set-up is shown in Figure 4.2(a) and a photograph of the setup is shown in Figure 4.2(b). A transient excitation was given by displacing the walls inward by 50 ± 2 mm, from the statically deformed position shown in Figure 4.2(b), at the points where the 18kg mass was attached. The container was then released, and the free vibration response was recorded.

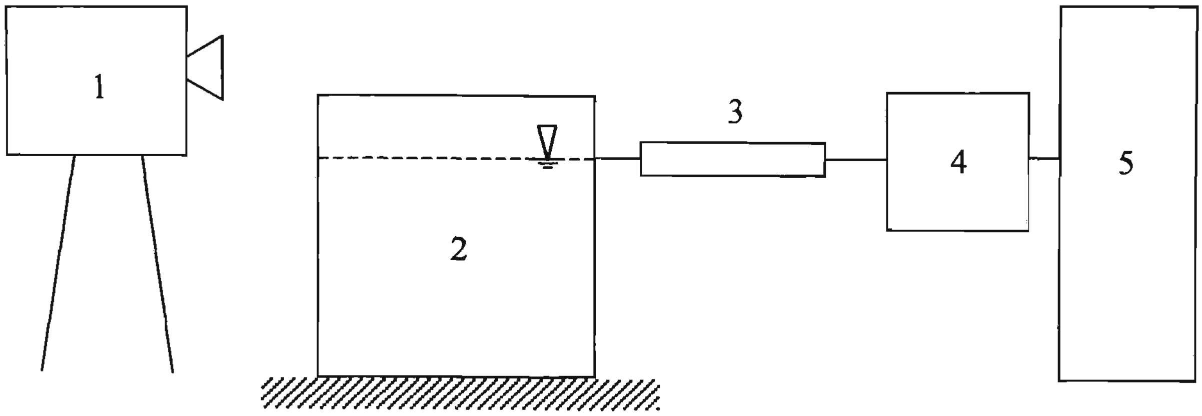

(a)

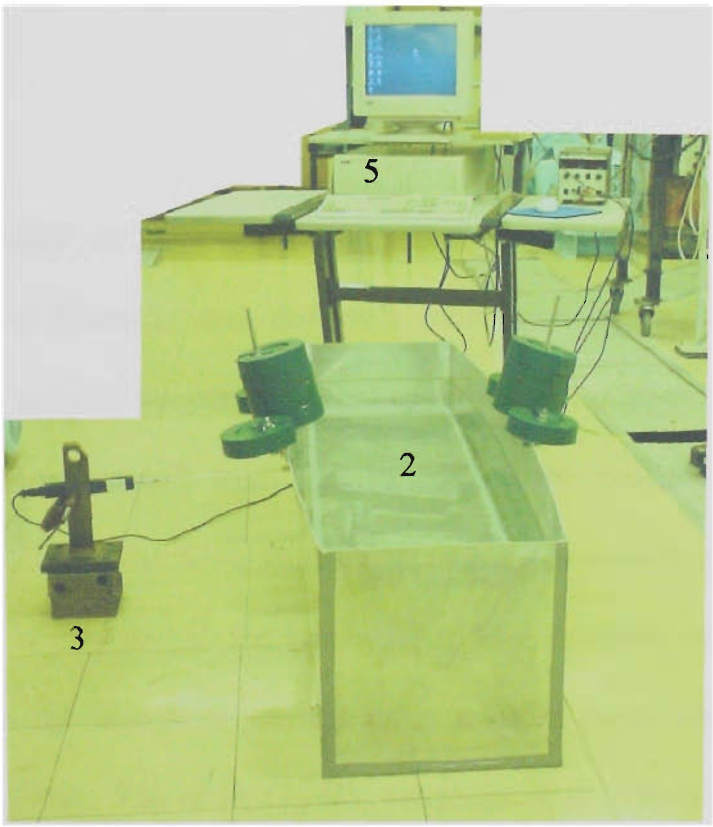

(b)

Figure 4.2. (a) Schematic view and (b) photograph of the experimental setup. 1. Video camera, 2. Tank, 3. Contact displacement transducer (built in house), 4. Analog to digital converter (DT707T), 5. Personal computer (Pentium 200MHz).

4.2.2. Numerical Model

A three-dimensional numerical model of the test case was created using ANSYS 5.3 (ANSYS 5.3, 1994). Two-dimensional rectangular shell elements were used for the container walls, and three-dimensional brick elements for the liquid. Slip wall conditions were used between the container and liquid elements. Here, liquid elements were allowed relative motion in the direction tangent to the wall of the container. Fluid-structure interaction was achieved by coupling the displacement of the liquid and container walls in the direction normal to the walls of the container. The container is shown in Figure 4.3, where the liquid is shown by the grey shaded region.

The material properties for Aluminum were used for the walls of the container. Young's Modulus of Elasticity and Poisson's ratio were set to 70 GPa and 0.3, respectively. These material properties were kept constant for all the numerical trials. Structural damping was varied from 0% to 5% of the critical damping in the fundamental mode without the liquid in the container. The density of the liquid was also kept constant at 998 kg/m^3 for water. Artificial damping of the liquid was included to stabilize the numerical predictions in selected cases, similar to those in Chen and Haroun (1994), Yao et al. (1994), Takahara et al. (1995) and Fujino et al. (1992). The level of artificial damping was chosen to keep the predicted sloshing amplitude similar to the experimental one. Without damping, the sloshing amplitude would increase indefinitely when the tank was excited at the fundamental frequency.

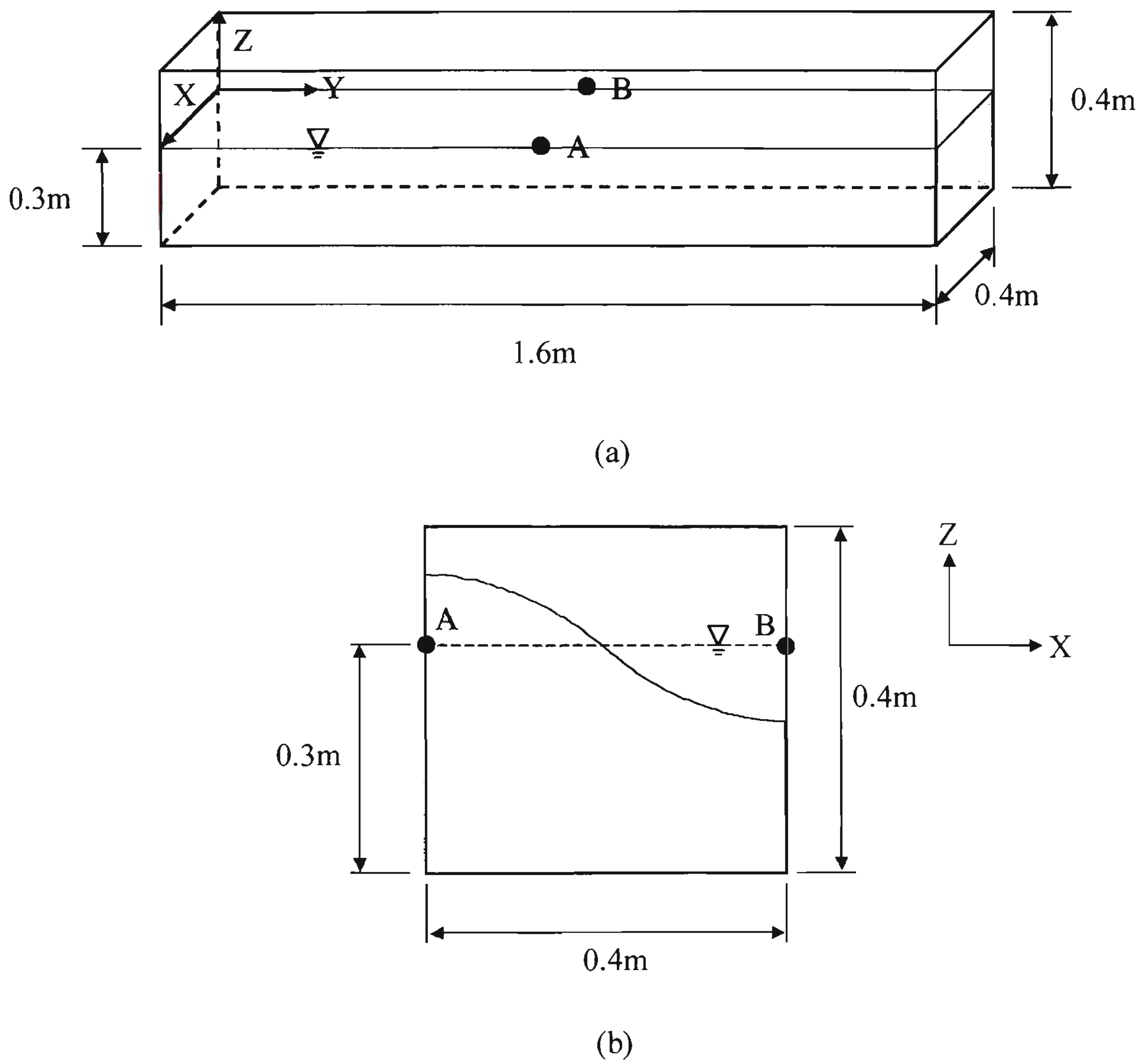

Figure 4.3. Showing (a) container dimensions and initial conditions and (b) the end view of the container with the shape of the fundamental sloshing wave for a rigid container. A and B are the points where displacement histories are observed.

Grid independence of the solution was determined by predicting the sloshing wave amplitude in a rigid container. Grids with cell sizes of 12.5 mm × 12.5 mm, 25 mm × 25 mm, 50 mm × 50 mm and 100 mm × 100 mm were tested. The results of these tests are shown in Table 4.1. The predicted sloshing amplitude is defined as the height difference in the Z direction between displacements of the liquid at points A and B in Figure 4.3. Sloshing was induced by imposing a sinusoidal displacement of

10 mm, peak to peak, on the base of the container in the horizontal X direction. The frequency of excitation was set equal to the fundamental sloshing frequency of 1.34 Hz.

Table 4.1. Predicted sloshing wave amplitude in a rigid container for different grid sizes.

Cell Size [mm]	Total Number of Cells	Sloshing Amplitude [mm]
12.5 × 12.5	768	103.9
25 × 25	192	106.3
50 × 50	48	102.7
100 × 100	12	91.9

For the same grid sizes of 12.5 mm × 12.5 mm, 25 mm × 25 mm, 50 mm × 50 mm and 100 mm × 100 mm, the 1st, 2nd and 3rd natural frequencies were also predicted of the container without liquid. For these trials, the wall thickness was 1.5 mm, and no structural damping was used. These results are shown in Table 4.2. As a result, a grid cell size of 50 mm × 50 mm was selected as sufficient for numerical accuracy for both the liquid and the container. The grids used for the container and liquid are shown in Figures 4.4 and 4.5, respectively.

Table 4.2. Predicted 1st, 2nd and 3rd natural frequencies of the container without liquid for different grid sizes.

Cell Size [mm]	Total Number of Cells	1st Natural Frequency [Hz]	2nd Natural Frequency [Hz]	3rd Natural Frequency [Hz]
12.5	10240	9.5788	9.7071	13.876
25	4098	9.5784	9.7069	13.877
50	640	9.5766	9.7059	13.883
100	160	9.5705	9.7031	13.906

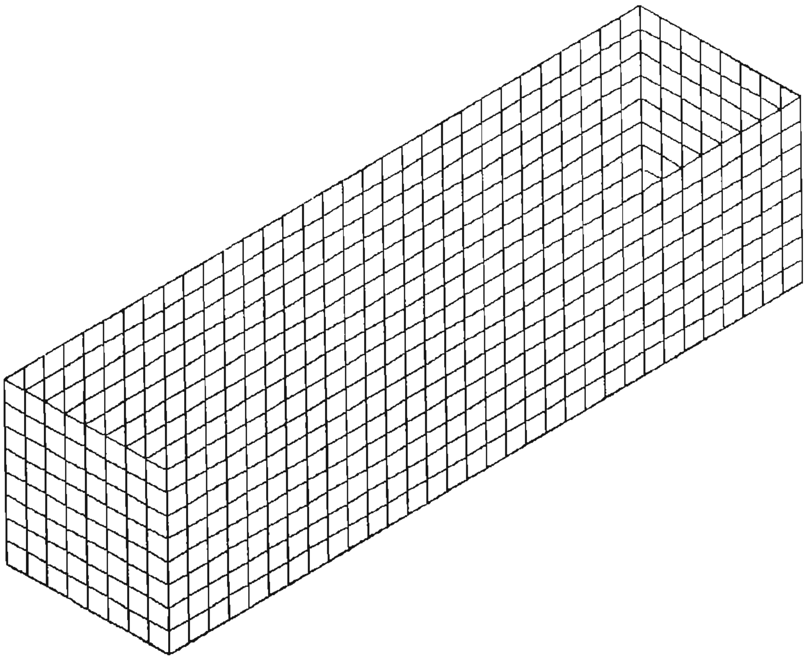

Figure 4.4. Isometric view of the grid used for the container. The cell size is 50 mm × 50 mm.

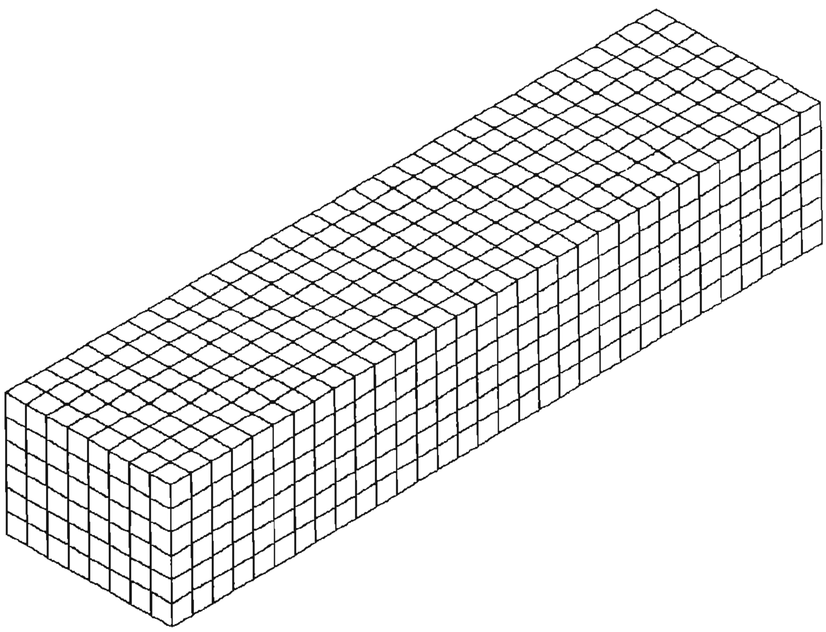

Figure 4.5. Isometric view of the grid used for the liquid. The cell size is 50 mm × 50 mm × 50 mm.

In Table 4.2, there is little difference between the frequency of the 1st and 2nd modes of the container. Mode shapes for the first 3 modes of oscillation of a container with 1.5 mm wall thickness are given in Figure 4.6 to clarify this trend. At the 1st mode, the longest walls of the container oscillated out of phase, and at the 2nd mode, these walls oscillated in phase. Higher modes showed much clearer separation of the frequencies as seen in Figure 4.6(c).

The same amount of mass added to the container in the experiment, was added to corresponding nodes in the numerical grid. A transient disturbance was given to the walls of the container of 50 mm inward at the same points as in the experiment. A transient solution was obtained with a time-step of 0.01 s. When the time-step was reduced to 0.005 s, no detectable difference existed in the displacement histories of the container or liquid.

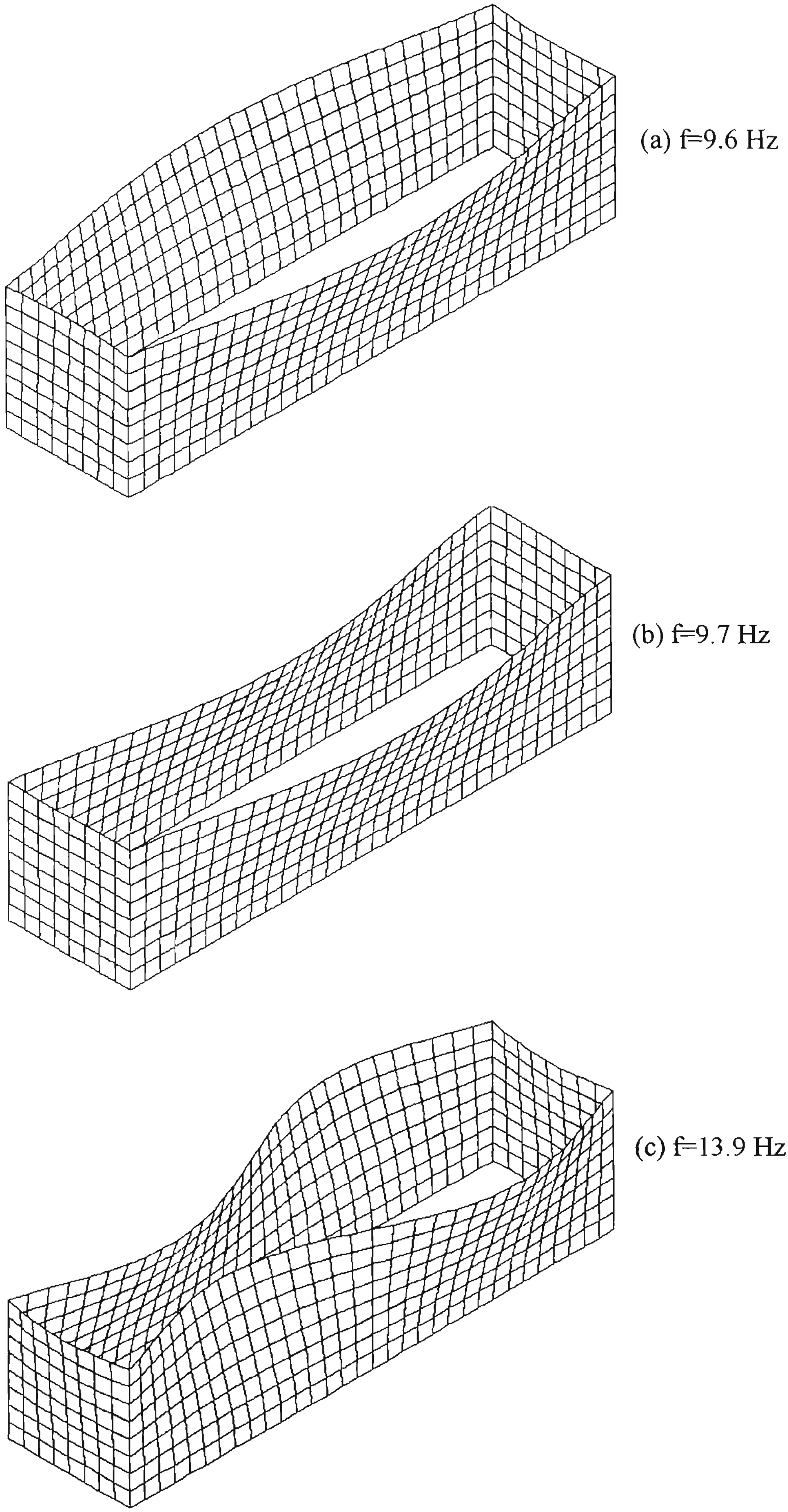

Figure 4.6. Mode shapes of oscillation for a container with 1.5 mm thick walls, no added mass and no liquid a), b) and c) 1^{st} , 2^{nd} and 3^{rd} mode shapes respectively.

4.2.3. Results

For the flexible container with the added mass but without liquid as in Figure 4.1, the natural frequency at the first mode was measured in the experiment to be 1 ± 0.1 Hz with a damping ratio of 2.8 ± 0.2%. The predicted natural frequency for the same case was 1.02 Hz. The damping ratio of the numerical model was set to 2.8%. For the container with liquid, the experimental and predicted displacement histories of the wall of the container are shown in Figure 4.7.

The experimentally observed displacement history of the container is given in Figure 4.7(a). In Figure 4.7(b), the numerically predicted displacement is presented for the case when the liquid is assumed to be inviscid, therefore with no damping. In Figure 4.7(c), the effect of viscosity is approximated with artificial damping in the liquid. When the liquid is undamped, the predicted wall displacement is generally larger than the experimentally determined displacement. A clear beat exists in both the predicted and experimental displacement histories at approximately 2.5 seconds. The beat continues in both histories for the duration of the trial.

The period of the predicted displacement is slightly larger than that in the experiment, resulting in differing beat envelopes after 5 seconds. This difference in the oscillation periods may be due to the presence of the higher modes of sloshing in the experiments. In the predictions, it was possible to initiate two dimensional sloshing in the fundamental mode. In the experiments, however, some liquid motion along the depth of the container could not be avoided.

In the first 25 seconds, the rate of decay of the predicted wall displacement in Figure 4.7(b) is comparable to that in the experiment. From 25 seconds to 40 seconds, there is little decay in the predicted wall amplitude, since the only mechanism for energy dissipation is the 2.8% structural damping in the container.

When the liquid is damped and therefore capable of dissipating energy, there is an improvement in the comparison of the experimental and predicted wall displacements. The beat seen in Figure 4.7(b), over the first 2.5 seconds, is still clearly visible in Figure 4.7(c). From 0 to 10 seconds, the predicted wall displacement has a larger amplitude than that observed in the experiment. From 10 seconds to 20 seconds, the agreement is quite good. After 20 seconds, the amplitude of the predicted wall displacement is smaller than that observed experimentally. This trend may be attributed to the liquid damping in the numerical model being only an approximation to the effect of viscosity. Due to the non-linear nature of liquid sloshing, it is expected that viscous effects would produce a damping effect proportional to the amplitude of liquid motion. In the numerical model, however, the effect from artificial damping is constant. Examining the displacement history of the wall of the container, suggests that the liquid damping should be largest at the start and progressively reduced as the amplitude of the displacement of the walls and liquid decays. However, it is not practically possible to achieve this variation in the numerical trials performed.

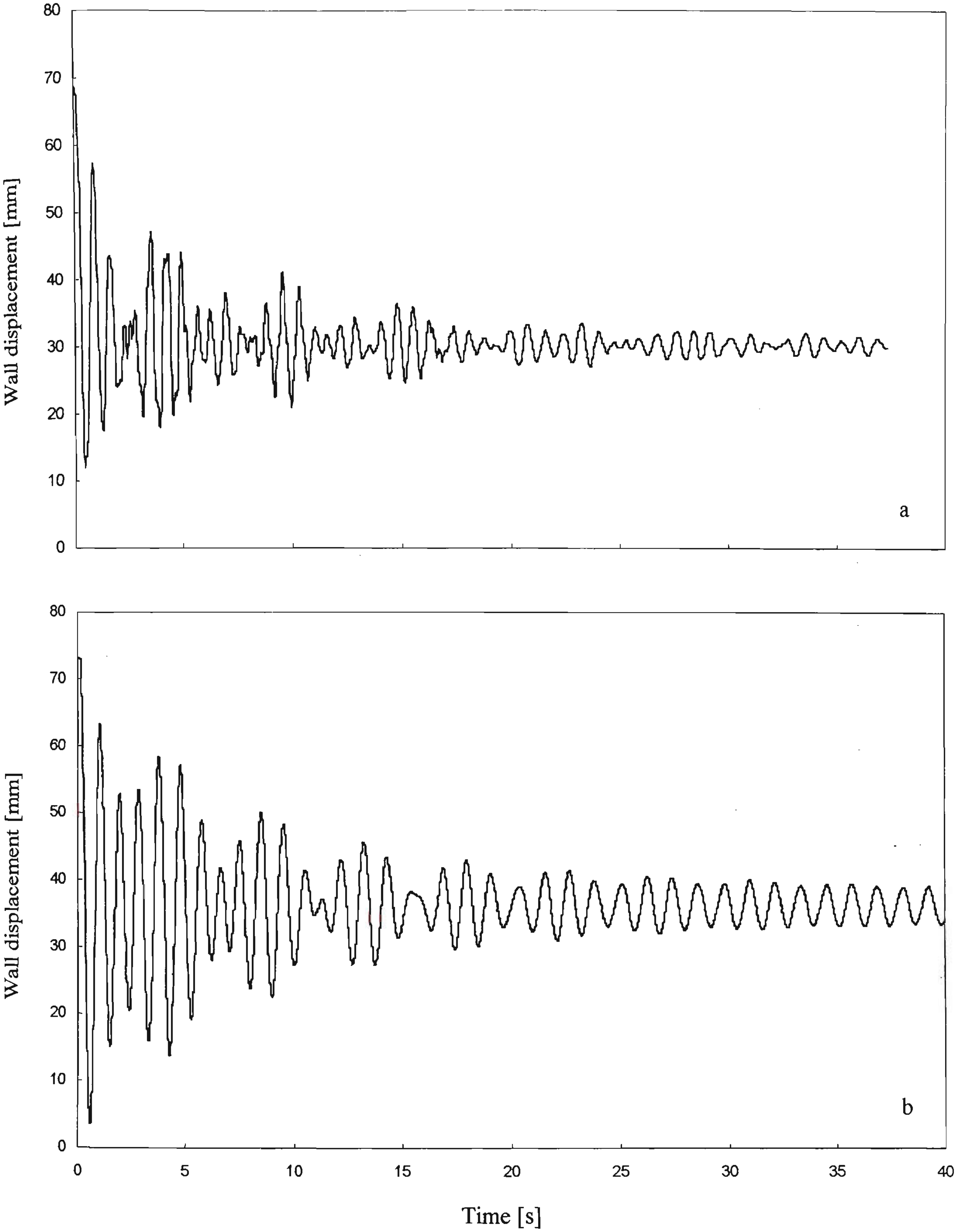

Figure 4.7. Displacement histories for the wall of the container, (a) experimental displacement, (b) predicted displacement when the liquid is inviscid and (c) predicted displacement when the liquid has damping.

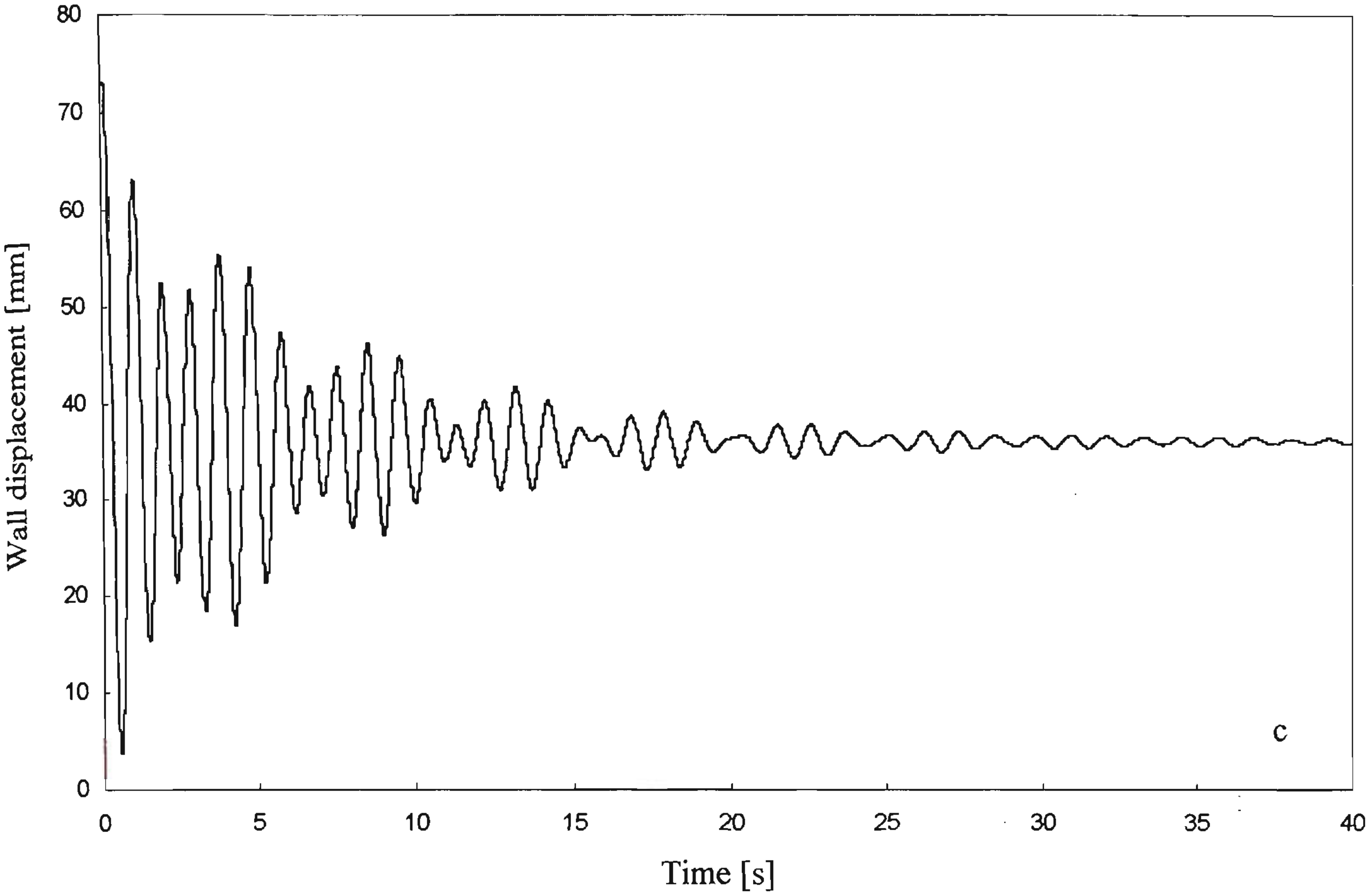

Figure 4.7. Displacement histories for the wall of the container, (a) experimental displacement, (b) predicted displacement when the liquid is inviscid and (c) predicted displacement when the liquid has damping

In Figure 4.8, the experimentally observed and predicted displacement of the liquid is shown for the same cases in Figure 4.7. In the experiment, the liquid displacement history is recorded for the first 15 seconds, and then again from 25 seconds to 30 seconds. In both Figures 4.8(b) and 4.8(c), the amplitude of the numerically predicted liquid displacement is generally smaller than that in the experiment. The difference between the experiments and predictions is large during the first five seconds. Experimentally observed sloshing amplitude exceeds 50 mm around 2.5 seconds where the structural oscillations experience small values. This experimentally observed clear beat could not be predicted numerically, resulting in a smaller amount of oscillatory energy transferred to the sloshing liquid with smaller sloshing amplitudes. Between 25 seconds and 30 seconds, there is improvement in the comparison. Experimental sloshing amplitude is large in Figure 4.8(a) around 27 seconds where there is another clear beat in the structural oscillations in Figure 4.7(a). After this beat, sloshing is quite comparable to that in Figure 4.8(b). Artificial liquid damping in Figure 4.8(c) seems to introduce excessive energy dissipation in the liquid, resulting in consistently small sloshing amplitudes.

The differences between the predicted and experimentally observed liquid displacements may be speculated to be largely due to the assumption in the numerical model that the liquid is inviscid. The effect of viscosity is only approximated by adding artificial damping to the liquid in the predictions. Ideally, a numerical model of the liquid, based on the solution of the Navier-Stokes equations, to include viscous effects would be more appropriate. However, the strong interaction between liquid sloshing and the container makes this approach presently unrealistic. If a viscous solution for the liquid was used at each time-step, as well as a structural solution for the flexible container, the required computational resources would render the numerical model impractical for design purposes.

A second possible reason for the differences discussed above, is the presence of the strong transfer of energy from the liquid to the container and visa versa. As a result, any small difference between the experimental set-up and the numerical model may lead to drastic variations in the displacement histories of both the liquid and the container. Considering the presence of this strong interaction, the comparisons between experiments and numerical predictions here, show reasonable agreement.

Therefore, it is assumed that the numerical model described in this chapter is able to capture the essence of this highly non-linear problem, although there may be differences in the details. This numerical model can be used to indicate important trends in the design of flexible containers. It should always be kept in mind that the suggested designs are only numerical predictions, and they should be verified experimentally. In the next section, extensive numerical test cases are presented to indicate promising trends for sloshing control using the flexibility of the container.

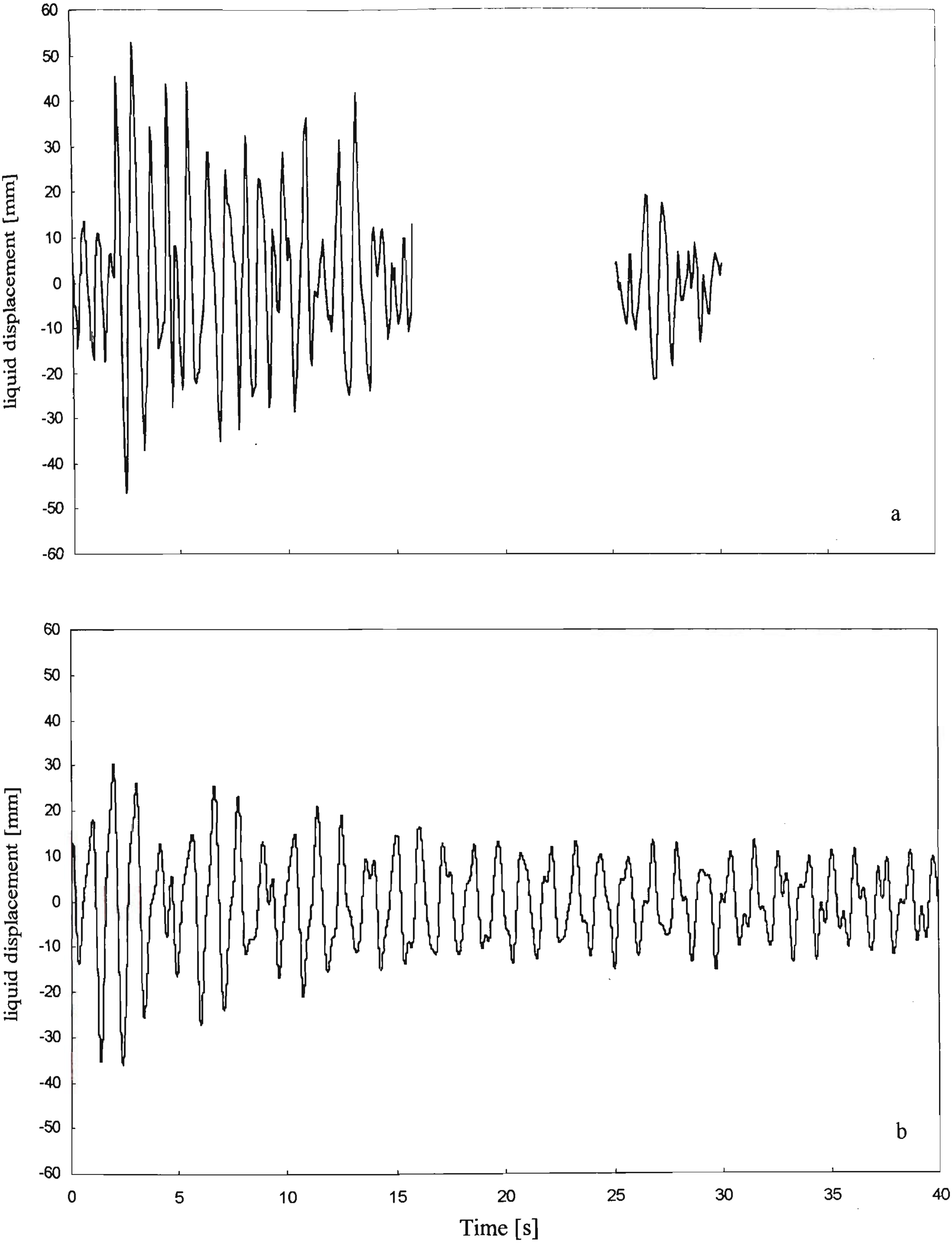

Figure 4.8. Displacement histories for the liquid, (a) experimental displacement, (b) predicted displacement when the liquid is inviscid and (c) predicted displacement when the liquid has damping.

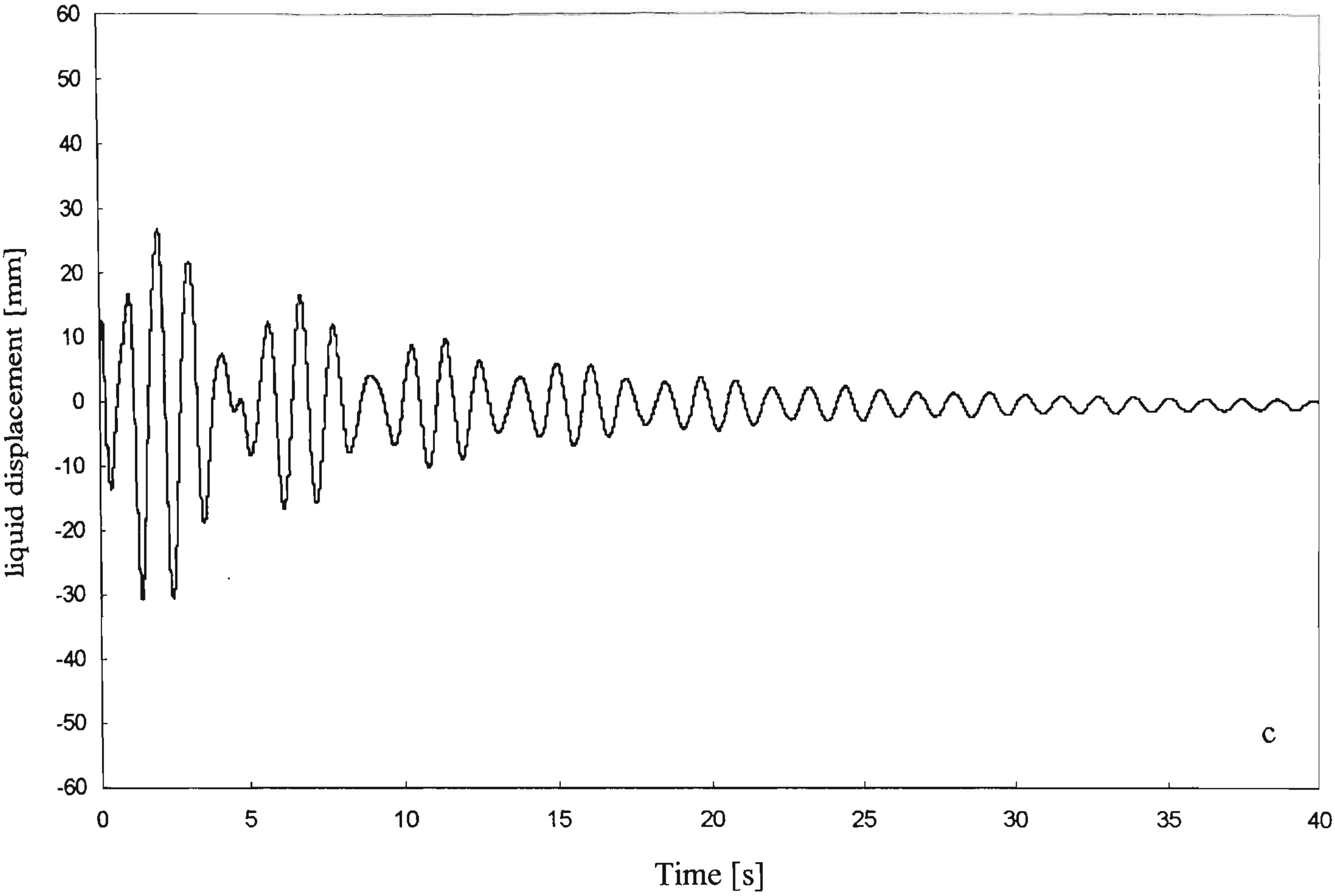

Figure 4.8. Displacement histories for the liquid, (a) experimental displacement, (b) predicted displacement when the liquid is inviscid and (c) predicted displacement when the liquid has damping.

4.3. SLOSHING CONTROL

In this section, results of a series of numerical trials are presented to determine the most promising cases for controlling liquid sloshing using a flexible container. In these trials, the objective was tuning fundamental natural frequency of the flexible container to that of liquid sloshing. Tuning was achieved by adding mass to the top of the longer walls of the container as in Section 4.2.1. Simulations always started with the walls of the container vertical and with a flat liquid free surface. Due to the walls of the container being flexible, and the liquid exerting a static pressure on the walls of the container, the container walls tended to bulge outward immediately after a simulation started. This bulging is similar to the breathing mode of shells. The initial motion of the container also created a liquid motion without any external disturbance. This liquid motion was not of sloshing type, rather the level of the liquid simply changed up and down due to the changes in the volume of the container. For each simulation case, the amplitude of the initial motion was allowed to settle over the first 20 seconds, as the container walls deflected to a static equilibrium position. The system experienced no excitation and was allowed to respond freely during this settling time. After this settling time, two different excitations were investigated, sinusoidal and random. Results for these two types of excitation are discussed separately next.

4.3.1. Sinusoidal Excitation

For all cases in this section, the base of the container experienced a forced sinusoidal displacement in the X direction for one period, from time 20 seconds to 20.75 seconds, with a frequency of 1.34 Hz. The peak-to-peak amplitude of this displacement was 10 mm. The frequency was chosen to excite liquid sloshing at the fundamental mode in the XZ plane. From 20.75 seconds to 36.75 seconds, the system experienced no excitation and was once again allowed to respond freely. It is this free vibration response that is of interest here.

4.3.1.1. Tuning

The sloshing frequency is strongly dependent on the length of the container in the direction of sloshing, which in this case is the horizontal X direction. When the container is flexible, the deformation of the container causes a change in the length of the container in this direction, and therefore, the wavelength of the sloshing wave. For liquid sloshing in flexible containers, previous investigations by Kana et al. (1966) showed that it is not possible to discuss tuning of the container and the liquid separately. Here, what is meant by tuning is the presence of significant energy transfer between the liquid and the container. Typically, a beat in the free vibration response of the two sub-systems indicates tuning (Anderson et al. 1999b). Kana et al. (1966) also classified "tuning" as a beat in the displacement history of the wall of the container. They reported tuned vibrations of the walls of the container, at frequencies approximately twice the frequency of liquid sloshing.

In Figures 4.9, 4.11, 4.13 and 4.15, histories of the numerically predicted displacements of the liquid free surface and the walls of the container are given for various cases. Figure 4.9 is used to demonstrate the problem of liquid sloshing in a rigid container and the effect of tuning the coupled liquid-container system. Figures 4.11, 4.13 and 4.15 show the effects of liquid damping, structural damping and wall flexibility, respectively. As mentioned earlier, the displacement of the liquid and the displacement of the walls of the container are plotted at points A and B shown in Figure 4.3. For the same cases as in Figures 4.9, 4.11, 4.13 and 4.15, the sloshing amplitude history is presented in Figures 4.10, 4.12, 4.14 and 4.16, respectively. The predicted sloshing amplitude is defined as the difference between displacements of the liquid at points A and B.

In Figure 4.9, predictions of the displacement of the container walls and liquid free surface are given for a container with (a) rigid walls, (b), (c), (d), (e) and (f) with 1.5 mm thick flexible walls and total added mass of 0 kg, 52.8 kg, 105.6 kg, 165 kg, and 198 kg, respectively. At points A and B, the displacement of the liquid in the vertical Z direction is shown with a dark line (——) and the displacement of the container walls in the horizontal X direction is shown with a grey line (——). For all the cases shown in Figure 4.9, the liquid is inviscid with no artificial damping. Therefore, there is no mechanism for energy dissipation within the liquid. The added mass is distributed evenly along 33 points at the top of the two longest walls. At each of the 33 points, the added mass in these trials is (b) 0 kg, (c) 0.8 kg, (d) 1.6 kg, (e) 2.5 kg and (f) 3.0 kg. For these cases, the 1^{st} and 3^{rd} natural frequencies of the container without liquid are given in Table 4.3.

Although tuning must be discussed for the coupled liquid-container system, Table 4.3 is included here to show the effect of added mass on reducing the response frequency of the container. The fundamental sloshing frequency in a rigid container was 1.34 Hz. The structural modes of oscillation for the container approach this value for two cases: firstly, when the added mass at each node is 0.8 kg, the oscillation frequency at the 1st mode shape of the container is 1.49 Hz; and secondly, when the added mass is increased to 2.5 kg at each node, the frequency of the 3rd mode of oscillation of the container is reduced to 1.24 Hz.

Table 4.3. Natural frequencies of the 1st and 3rd mode shapes for a container with a wall thickness of 1.5 mm and without liquid.

Added mass at each node along the top wall of the container [kg]	Total added mass [kg]	1st Natural frequency [Hz]	3rd Natural frequency [Hz]
0	0	9.58	13.88
0.8	52.8	1.49	2.18
1.6	105.6	1.06	1.55
2.5	165	0.85	1.24
3.0	198	0.77	1.13

4.3.1.2. Results

Figure 4.9(a) shows liquid displacement histories for sloshing in a rigid container. There is no deformation of the container walls, and therefore, no motion of the liquid free surface during the settling time, from 0 to 20 seconds. A settling time is not even required in this case. However, it is included for consistency. No displacement history is given for the container because the walls have no detectable deflection.

During the excitation period, from 20 seconds to 20.75 seconds, a sloshing wave develops. The two histories shown in Figure 4.9(a), represent the vertical position of the liquid at each side of the container at points A and B, respectively. The two histories are 180° out of phase indicating that when the liquid climbs at one wall, it drops at the other. At the completion of one period of excitation, the liquid has climbed approximately 25 mm on one wall and fallen 25 mm on the opposite wall. The liquid is assumed to be inviscid, and therefore, has no mechanism for energy dissipation. Since there is no wall deformation, there is no structural damping in this case. Therefore, the entire liquid-container system is incapable of dissipating energy. As a result, the sloshing of the liquid continues with a virtually constant amplitude from 20.75 seconds to 36.75 seconds.

The sloshing amplitude for the rigid container is shown in Figure 4.10(a). Again, the sloshing amplitude is defined as the difference between the vertical displacement histories of the liquid at each side of the container. This figure also shows that after the excitation, the envelope of sloshing amplitude does not decay. Therefore, Figures 4.9(a) and 4.10(a) may be used as a comparison base to judge the effectiveness of liquid sloshing control.

In Figure 4.9(b), the container is flexible with a wall thickness of 1.5 mm and no added mass is attached to the container. The structure has a critical damping ratio of 1%, which represents a reasonable inherent level of energy dissipation in the structure. From Table 4.3, the 1st and 3rd resonances of the container without liquid occur at frequencies of 9.58 Hz and 13.88 Hz, respectively. No artificial damping is applied to the liquid.

During the settling time (0 to 20 seconds), Figure 4.9(b) shows the walls of the container oscillating out of phase. This ballooning motion creates a change in the volume of the container, and as a result the liquid surface is forced to move up and down. The vertical liquid motion at the left and right sides of the container is in phase, indicating that the liquid free surface is flat and no sloshing exists. This point was verified by viewing animations of the liquid free surface.

After the excitation, sloshing is induced as indicated by the out of phase motion of the liquid, similar to that in Figure 4.9(a). However, the introduction of flexibility in the container produces a problem worse than that of the rigid case. The absolute displacement of the liquid in the vertical direction reaches 50 mm, whereas in Figure 4.9(a) the maximum vertical displacement is approximately 25 mm. In many practical situations, it is likely that wall thickness and material properties of the container will be insufficient for the container to be rigid. The predictions in Figure 4.9(b) indicate that some flexibility of the container may be even worse than the case of a rigid container. The sloshing amplitude corresponding to the liquid displacement shown in Figure 4.9(b) is shown in Figure 4.10(b). In Figure 4.10(b) the maximum sloshing amplitude of approximately 70 mm, is greater than the 40 mm sloshing amplitude in the rigid wall container. Figure 4.10(b) shows a slight beat in the envelope for the sloshing amplitude, even though the oscillation frequencies of the 1st and 3rd modes for the container (without liquid) are approximately 7 and 10 times greater than the fundamental sloshing frequency in the rigid wall container. However, despite the beat, there is little decay of the sloshing amplitude and the control effect is poor.

In Figure 4.9(c), the natural frequency of the container is lowered by adding 0.8 kg mass at each of the 33 points along each of the two walls, which results in a total mass of 52.8 kg. Without the liquid in the container, the oscillation frequencies of the 1st and 3rd mode are 1.49 Hz and 2.18 Hz, respectively. The patterns in Figures 4.9(b) and 4.9(c) are similar in that the liquid displacements are still out of phase after the excitation period. During the free response, the displacement history for the walls of the container have a peak to peak displacement of approximately 40 mm which is approximately twice as large as that in Figure 4.9(b). The sloshing amplitude for Figure 4.9(c) is shown in Figure 4.10(c). There is a beat in the history of the sloshing amplitude and also a clear decay of the sloshing amplitude. This decay of the sloshing amplitude may be due the larger displacements of the container walls. Energy dissipation can only occur in the container, since the liquid is inviscid. Therefore, the amount of energy dissipation provided by the container is proportional to its displacement amplitude. However, comparing the sloshing amplitude histories of Figure 4.10(a) for the rigid case and Figure 4.10(c) shows that the amplitude of the beat envelope in Figure 4.10(c) is often greater than the sloshing amplitude in the rigid container.

Further reduction of the natural frequency of the container is achieved by adding 1.6 kg at each of the 33 points on the longest walls of the container, which resulted in a total of 105.6 kg of mass added to the container. Adding this mass reduced the oscillation frequency of the 1st mode for the container without liquid to 1.06 Hz and the 3rd mode to 1.55 Hz. The predicted displacement histories are given in Figure 4.9(d). There is a dramatic change, particularly, in the response of the liquid after the excitation period. In contrast to the three earlier cases, the liquid displacement is in phase for much of the predicted response. Also, a beat is starting to develop in the predicted response of the container walls. The predicted sloshing amplitude for this case is shown in Figure 4.10(d). As expected, the in-phase motion of the liquid observed in Figure 4.9(d) results in a good control effect of liquid sloshing. The predicted sloshing amplitude in Figure 4.10(d) has a maximum of 25 mm at 24 seconds, which is approximately only 60% of the sloshing amplitude of the rigid case. However, after 28 seconds, the predicted sloshing amplitude is approximately 15 mm, which is 37.5% of the sloshing amplitude in the rigid container.

In Figure 4.9(e), the displacement histories of the liquid and walls of the container are given for the case of a total added mass of 165 kg, corresponding to 2.5 kg of mass at each node. For this case, the frequencies of oscillation for the 1st and 3rd modes of the container are, 0.85 Hz and 1.24 Hz, respectively. The beat that started to appear in the displacement of the container walls in Figure 4.9(d) is clearly visible in Figure 4.9(e). This beat indicates a strong coupling between the motion of the liquid and the container. This system is assumed to be tuned. The beat represents a transfer of energy from the liquid to the container. Since there is little energy dissipation, the energy returns to the liquid. The sloshing amplitudes shown in Figure 4.10(e) for this case, are comparable to the ones in Figure 4.10(d). However, the tuned case has a more dramatic decay towards the end of the simulation.

A further reduction of the natural frequencies of the container, reduces the control effect of liquid sloshing. The predicted displacements for the container and liquid for a total added mass of 198 kg are given in Figure 4.9(f). At each point along the container walls, 3.0 kg is added to reduce the frequency of the 1st mode to 0.11 Hz and the 3rd mode to 1.13 Hz. The beat observed in Figure 4.9(e) has almost completely disappeared in Figure 4.9(f). The sloshing amplitude for this case is shown in Figure 4.10(f). The control of sloshing has deteriorated when compared with Figure 4.10(e). However, the sloshing amplitudes in Figures 4.9(d), 4.9(e) and 4.9(f) are still lower than the sloshing amplitude in the rigid container in Figure 4.10(a), suggesting a relative insensitivity of the design to the range of required added mass for sloshing control.

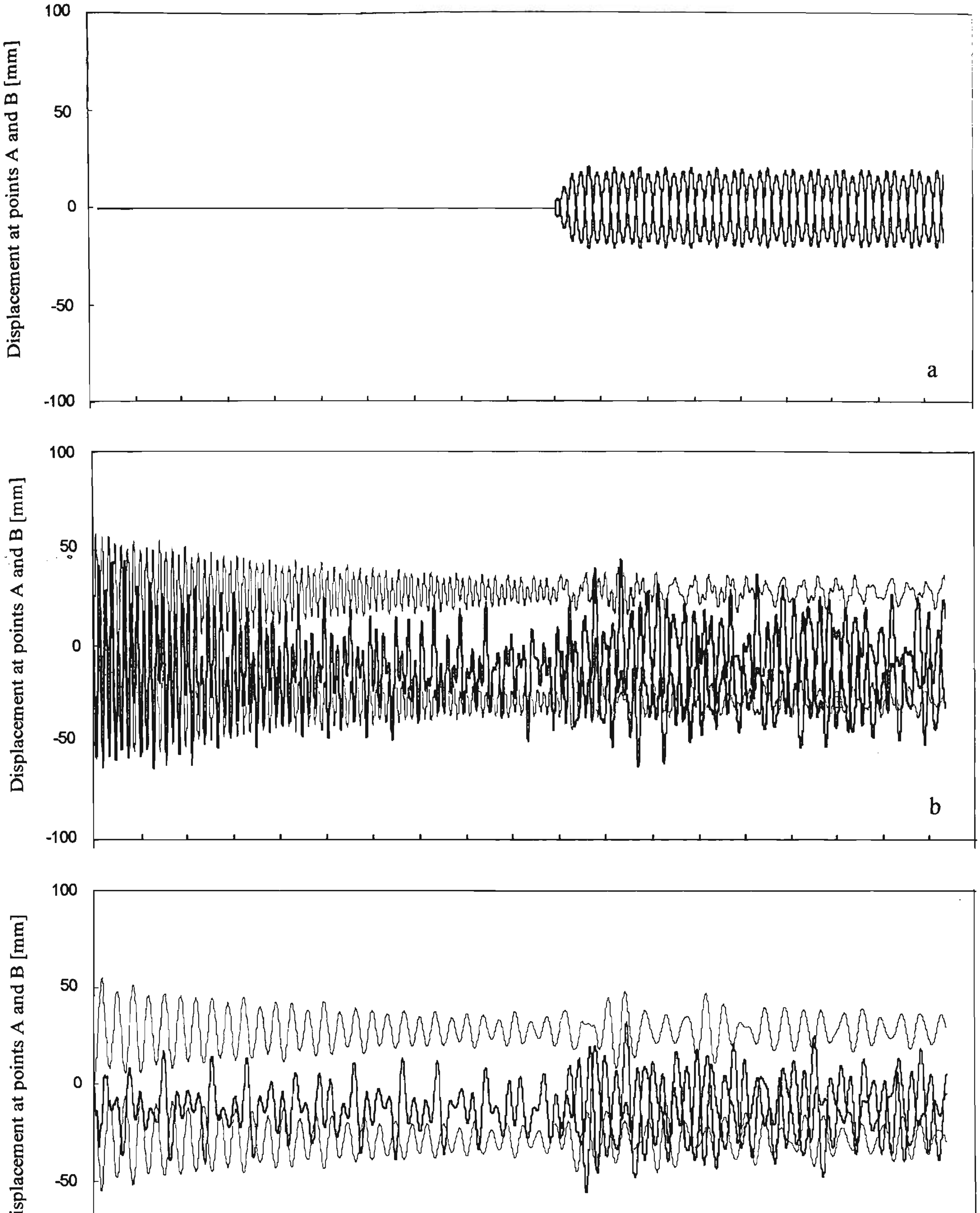

Figure 4.9. Displacement histories of the liquid (——) and container walls (——) for; (a) rigid wall container, (b), (c), (d), (e) and (f) added mass of 0 kg, 52.8 kg, 105.6 kg, 165 kg and 198 kg respectively. The wall thickness is 1.5 mm. The structure has 1% damping and the liquid is undamped.

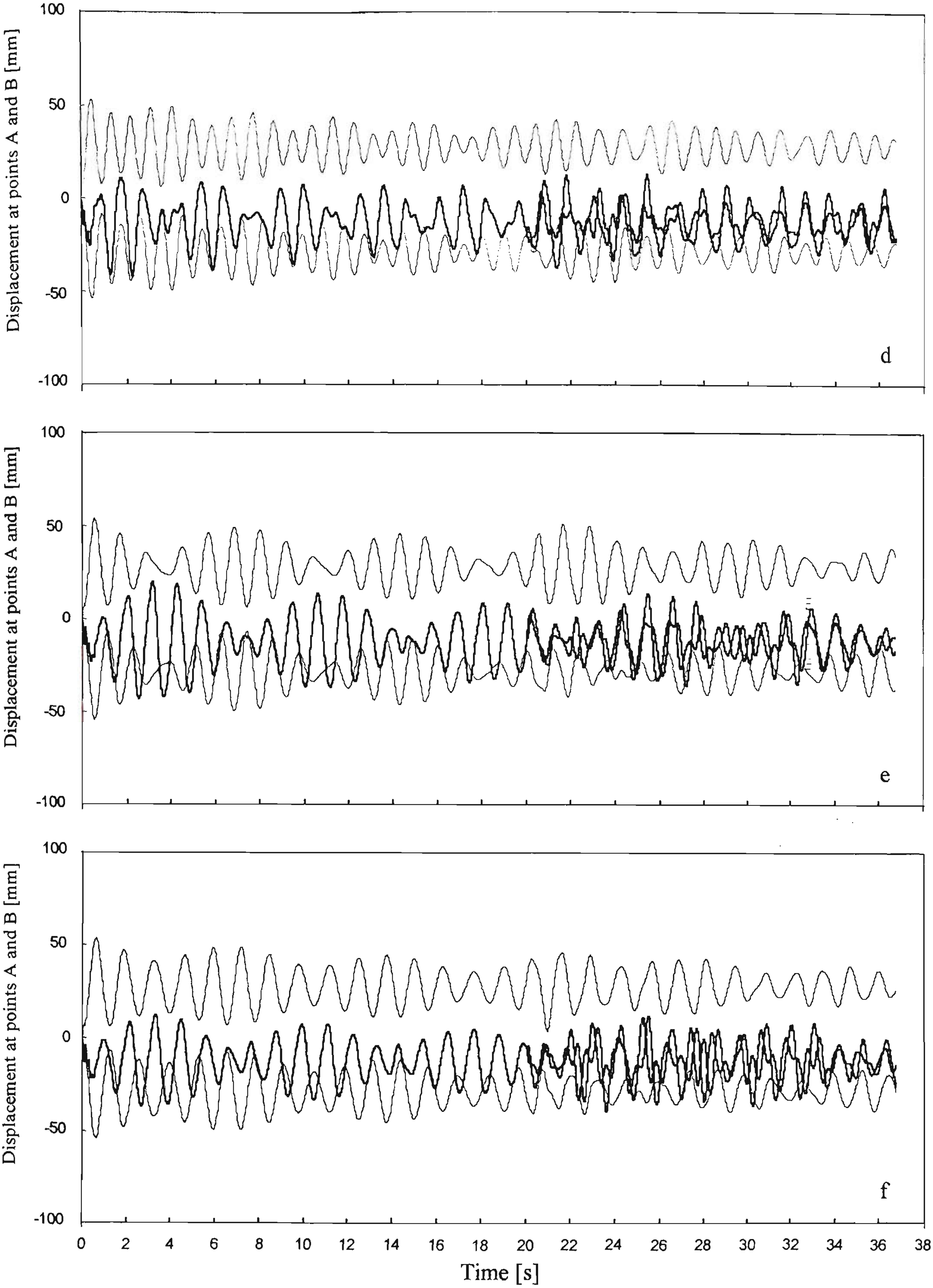

Figure 4.9. Displacement histories of the liquid (——) and container walls (——) for; (a) rigid wall container, (b), (c), (d), (e) and (f) added mass of 0 kg, 52.8 kg, 105.6 kg, 165 kg and 198 kg respectively. The wall thickness is 1.5 mm. The structure has 1% damping and the liquid is undamped.

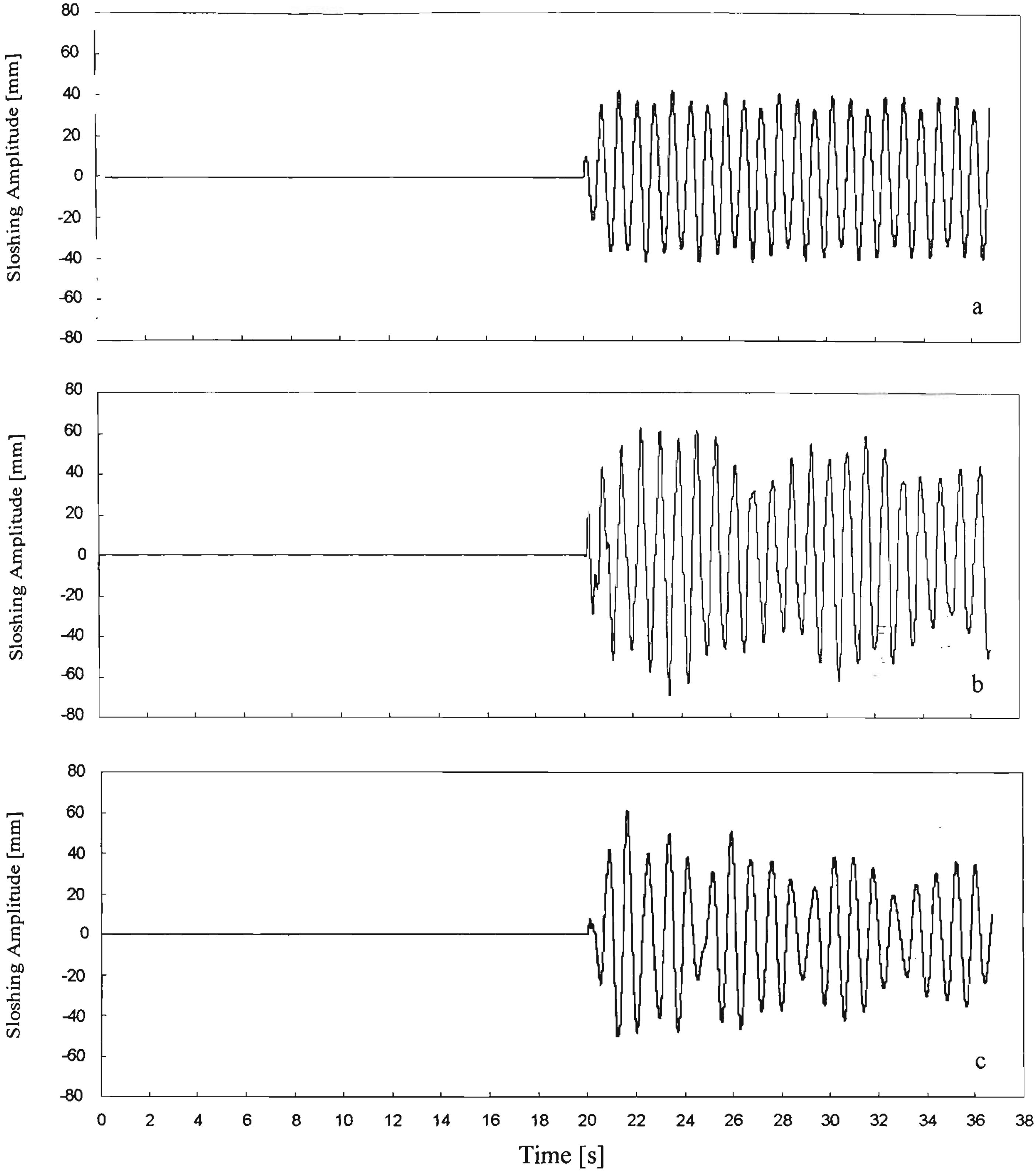

Figure 4.10. Predicted sloshing amplitude for the same cases as shown in Figure 4.9. (a) rigid wall container, (b), (c), (d), (e) and (f) added mass of 0 kg, 52.8 kg, 105.6 kg, 165 kg and 198 kg respectively. The wall thickness is 1.5 mm. The structure has 1% damping and the liquid is undamped.

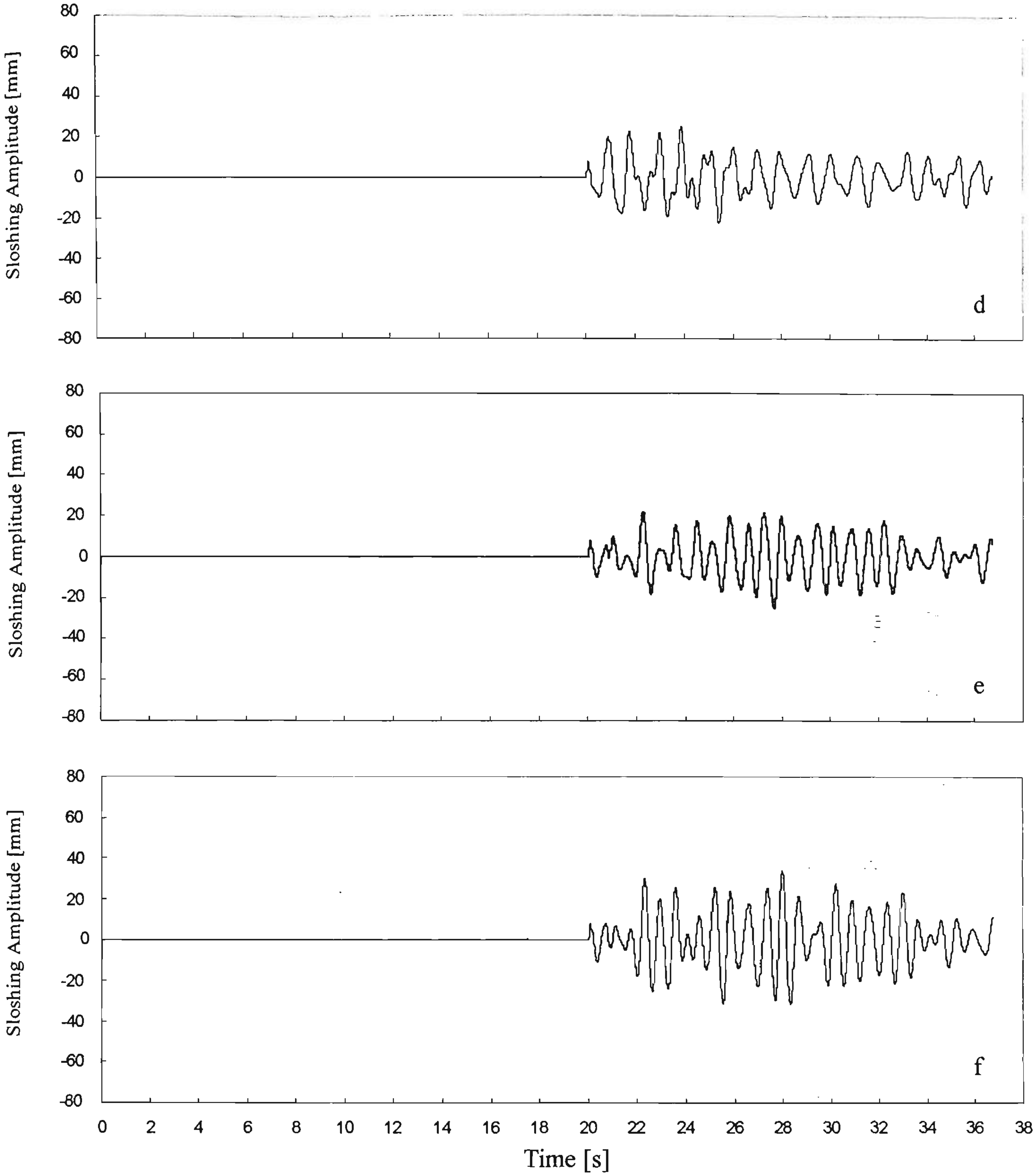

Figure 4.10. Predicted sloshing amplitude for the same cases as shown in Figure 4.9. (a) rigid wall container, (b), (c), (d), (e) and (f) added mass of 0 kg, 52.8 kg, 105.6 kg, 165 kg and 198 kg respectively. The wall thickness is 1.5 mm. The structure has 1% damping and the liquid is undamped.

In Figure 4.11, the same cases in Figure 4.9 are re-examined with the addition of artificial liquid damping similar to those in to Chen and Haroun (1994), Yao et al. (1994), Takahara et al. (1995) and Fujino et al. (1992), as mentioned earlier. The introduction of artificial damping is an attempt to represent the energy dissipation due to viscosity in a highly viscous liquid. In Figure 4.11(a), the walls of the container are rigid. There is a rapid decay of the amplitude of the displacement of the liquid as compared with that in Figure 4.9(a). Once again, Figure 4.11(b) shows the effect of some flexibility in the container with larger sloshing amplitudes than a rigid wall container. Also, same as in Figure 4.9, the optimal tuning is achieved when the added mass is 2.5 kg as shown in Figure 4.11(e). In Figure 4.11(e), the beat in the displacement histories of the liquid and walls of the container, is not as clear as in Figure 4.9(e) because of the energy dissipation both in the liquid and in the container.

When the oscillatory energy is primarily in the structure, there is dissipation due to structural damping. Alternatively, when energy is in the liquid, energy dissipation occurs due to artificial damping. An overall comparison of the results presented in Figures 4.9 and 4.11 clearly shows that the rate of decay of sloshing amplitudes increases with the inclusion of liquid damping. In fact, with such highly dissipative liquids, the best design suggestion would be to maintain the rigidity of the container walls as much as it is possible practically. When rigid walls are not practical, the recommended flexibility in Figure 4.11(e) is effective in restraining liquid motion. This last observation also reinforces a practical aspect of using container flexibility: a properly tuned container is an effective controller of sloshing for a variety of liquids. Its effectiveness is more significant, however, for liquids with low viscosity.

The histories of the sloshing amplitudes for the same cases in Figure 4.11 are shown in Figure 4.12. In Figure 4.12(a), the decay of the sloshing wave in the rigid container is due to the energy dissipation associated with artificial liquid damping. Figure 4.12(e) shows a good control effect when the container and liquid are tuned. The maximum sloshing amplitude between 20 seconds and 36.75 seconds in Figure 4.12(e) is approximately 20 mm, 50% of the maximum sloshing amplitude of 40 mm in the rigid container.

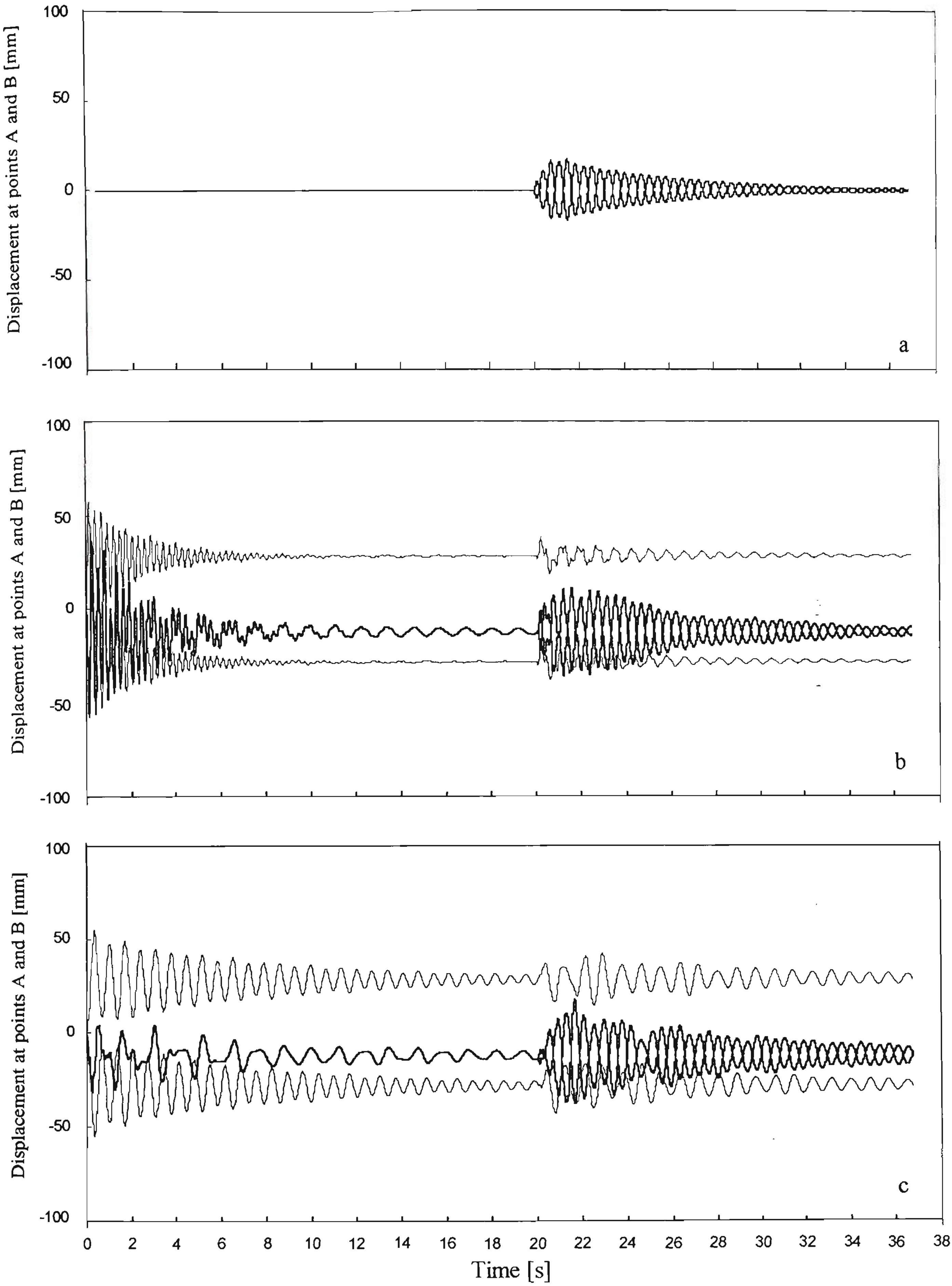

Figure 4.11. Displacement histories of the liquid (——) and container walls (——) for; (a) rigid wall container, (b), (c), (d), (e) and (f) added mass of 0 kg, 52.8 kg, 105.6 kg, 165 kg and 198 kg respectively. The wall thickness is 1.5 mm. The structure has 1% damping and the liquid is damped.

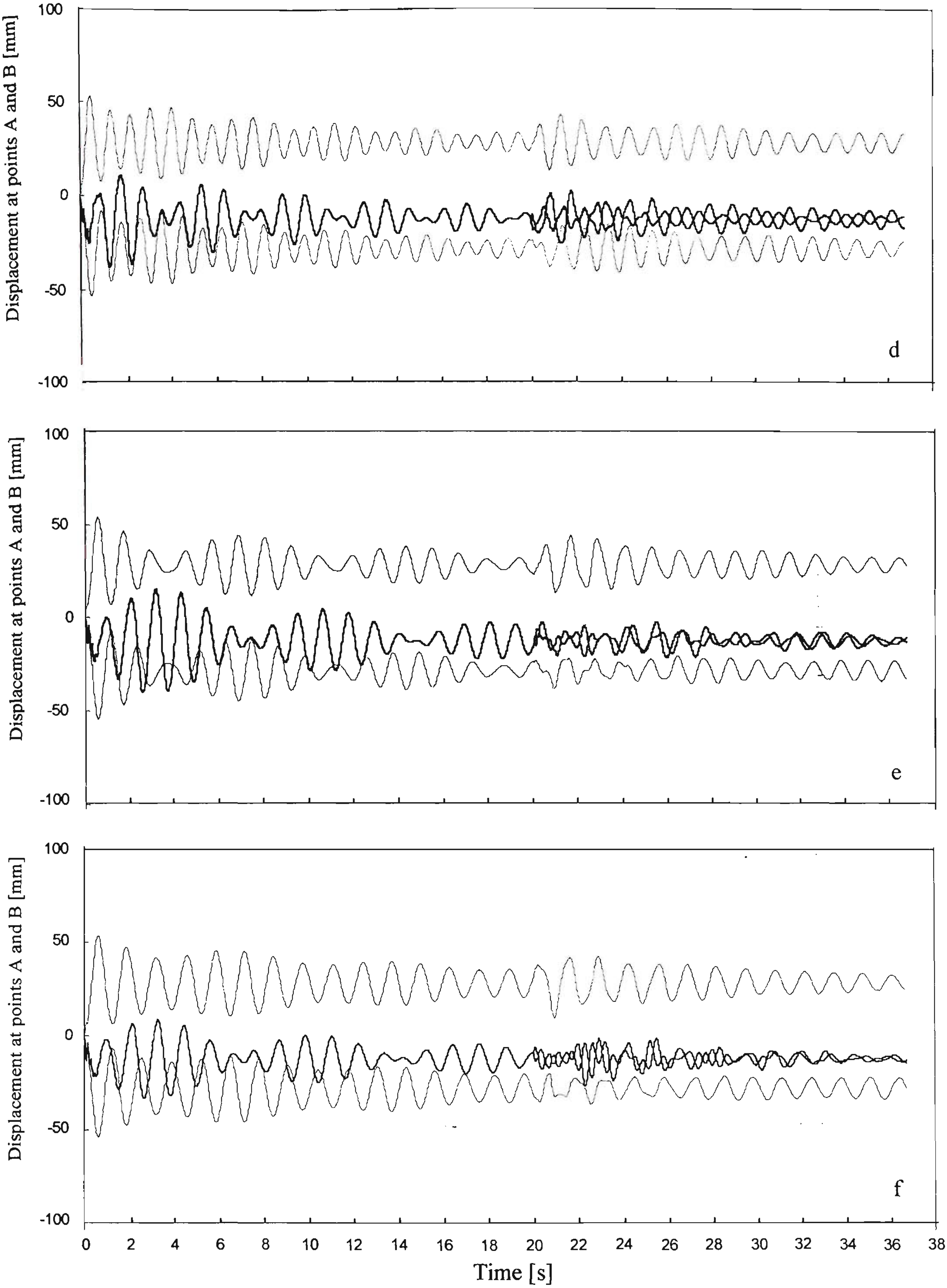

Figure 4.11. Displacement histories of the liquid (——) and container walls (——) for; (a) rigid wall container, (b), (c), (d), (e) and (f) added mass of 0 kg, 52.8 kg, 105.6 kg, 165 kg and 198 kg respectively. The wall thickness is 1.5 mm. The structure has 1% damping and the liquid is damped.

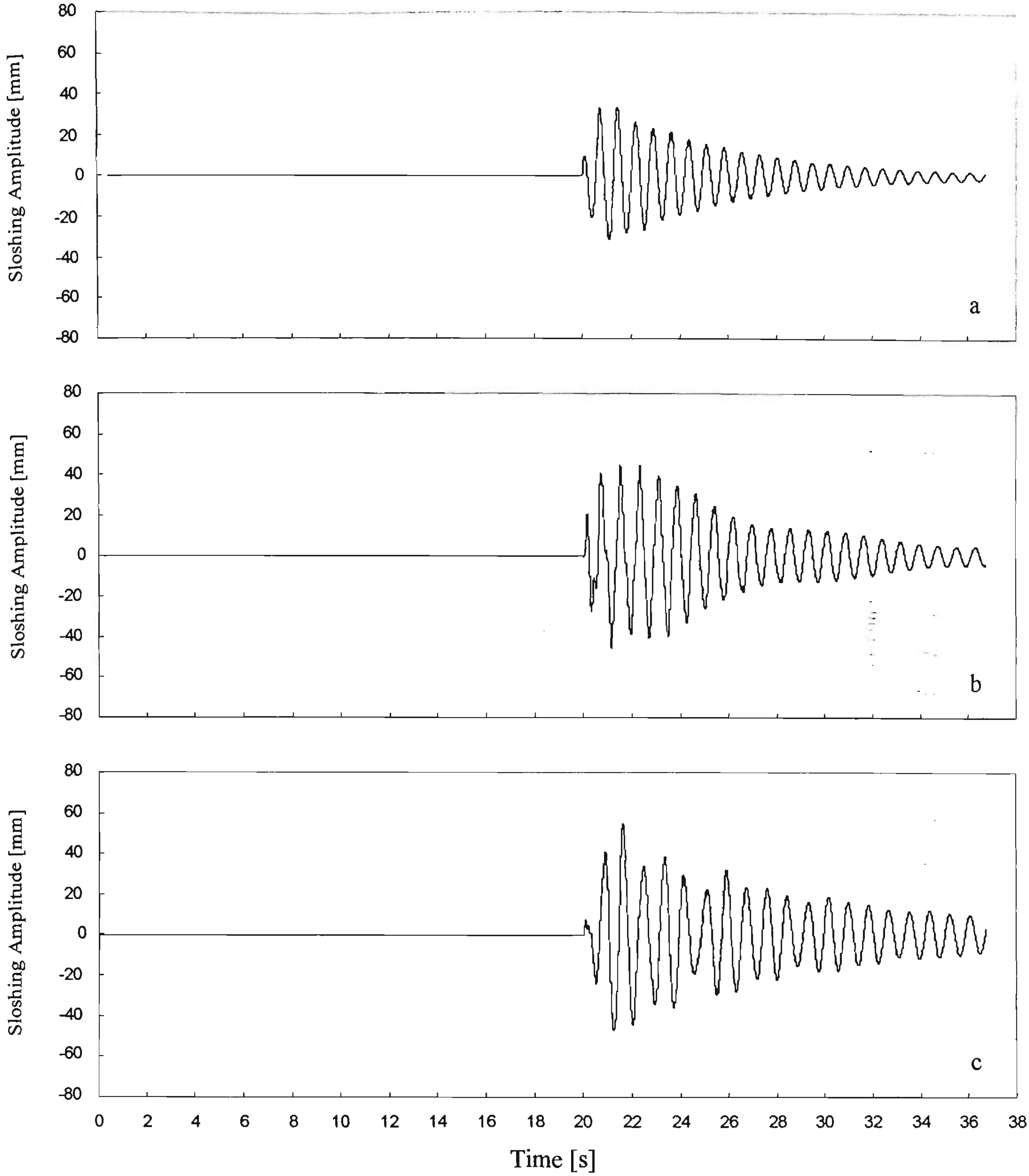

Figure 4.12. Predicted sloshing amplitude for the same cases as shown in Figure 4.11. (a) rigid wall container, (b), (c), (d), (e) and (f) added mass of 0 kg, 52.8 kg, 105.6 kg, 165 kg and 198 kg respectively. The wall thickness is 1.5 mm. The structure has 1% damping and the liquid has artificial damping.

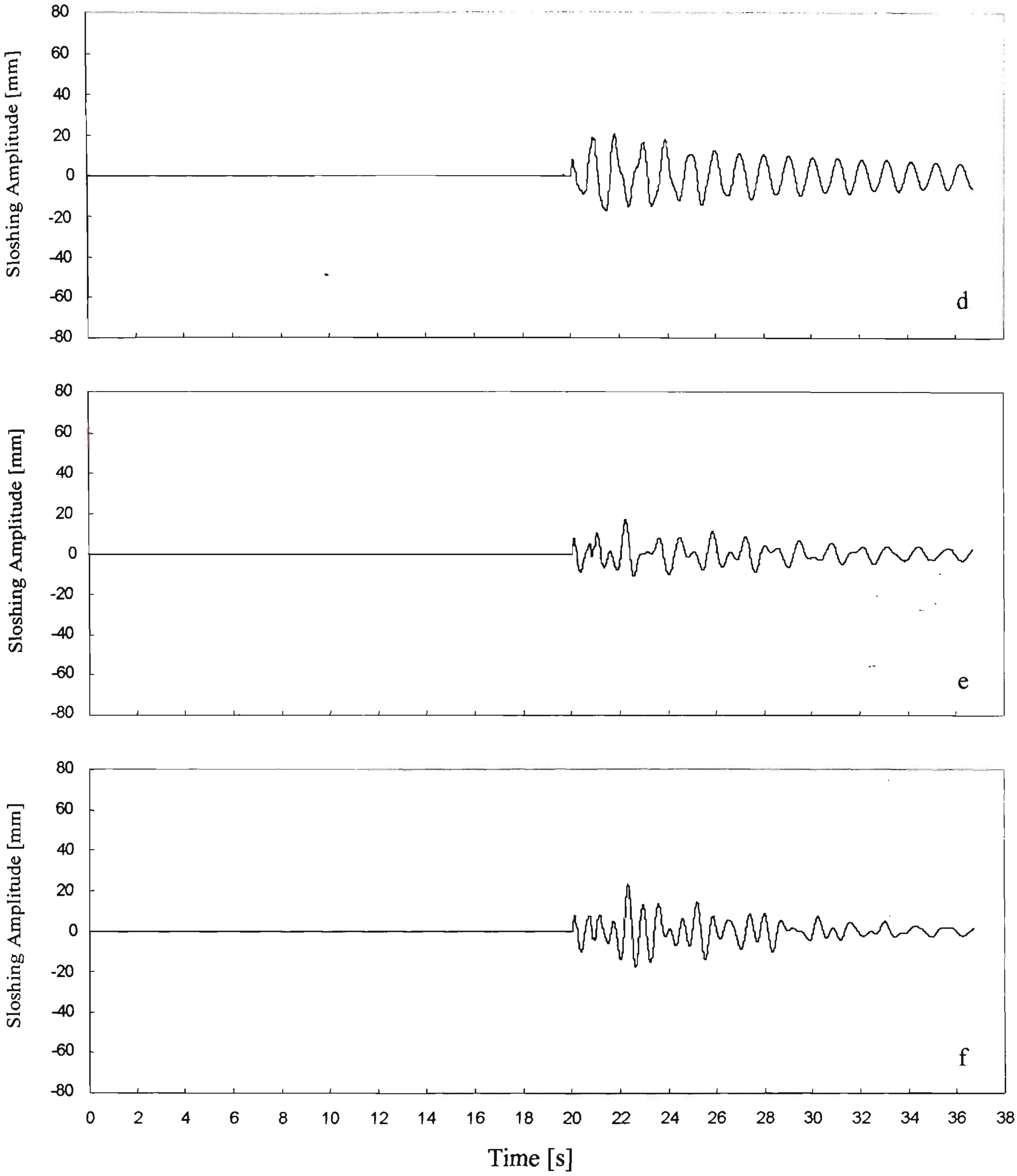

Figure 4.12. Predicted sloshing amplitude for the same cases as shown in Figure 4.11. (a) rigid wall container, (b), (c), (d), (e) and (f) added mass of 0 kg, 52.8 kg, 105.6 kg, 165 kg and 198 kg respectively. The wall thickness is 1.5 mm. The structure has 1% damping and the liquid has artificial damping.

The optimally tuned case is identified, in both Figures 4.9(e) and 4.11(e), when a total of 165 kg of mass is added to the container with a wall thickness of 1.5 mm. This best case is used here to demonstrate the effect of structural damping on the control of liquid sloshing. In Figures 4.13(a), 4.13(b), 4.13(c) and 4.13(d) the structural damping in the fundamental mode is set to critical damping ratios of 0%, 1%, 2% and 5%, respectively. For all the cases in Figure 4.13, the liquid is undamped. In Figure 4.13(a), a clear beat exists in both the displacement of the liquid and the walls of the container. In this case, there is no mechanism for energy dissipation. Energy is readily transferred between the container and the liquid. The introduction of 1% critical damping ratio for the container gives the displacement history shown in Figure 4.13(b) (which is the same as Figure 4.9(e)). Here, there is decay of the amplitude of the beat envelope for both the liquid and structure. The displacement histories of the liquid are in phase for most of the predicted response.

In Figures 4.13(c) and 4.13(d) the critical damping ratio is increased to 2% and 5%, respectively. In Figure 4.13(c), the motion of the structure starts to be restricted by the presence of damping, and the liquid displacement histories start to shift out of phase, particularly from 28 seconds to 32 seconds. In Figure 4.13(d), the structure is overdamped. The motion of the container is restricted to an extent as to cause the liquid displacement histories to be out of phase for almost the entire predicted response. However, even with this restricted container motion, the predicted sloshing amplitude is significantly smaller than for the rigid container case shown in Figure 4.10(a).

The histories of the sloshing amplitudes for the same cases as in Figure 4.13 are given in Figure 4.14. For these cases, 1% structural damping is a reasonably expected value due to inherent damping of the container, whereas a conscious design effort would be required to accomplish the highest value of 5% damping. The results in Figure 4.14 clearly indicate that a lightly damped container, tuned to liquid sloshing, provides sufficient energy dissipation for effective control of sloshing. Increasing the damping level in the container may impede the structural oscillations reverting to a case similar to that of a rigid container.

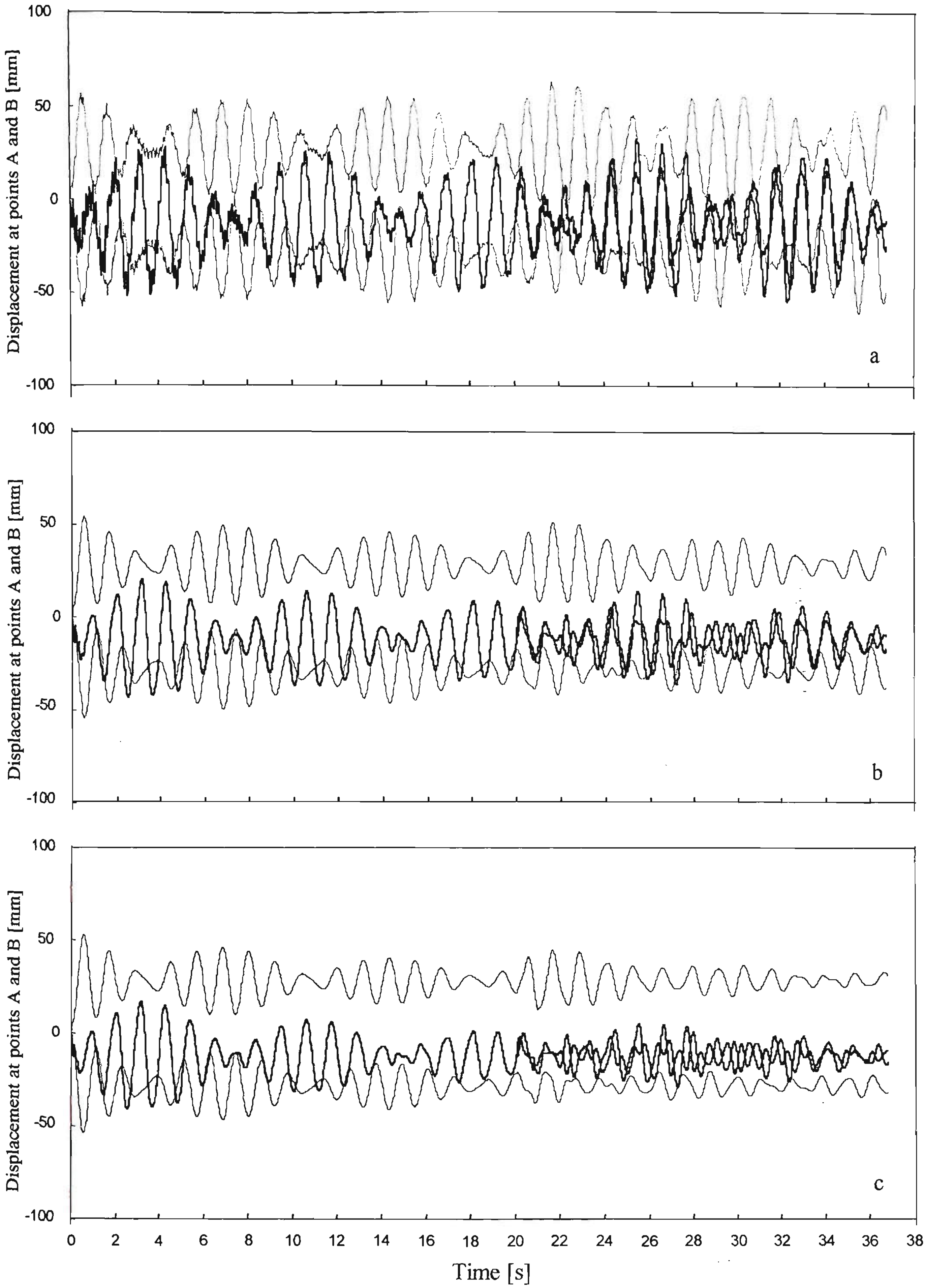

Figure 4.13. Displacement histories of the liquid (—) and container walls (—) for; (a), (b), (c), and (d) 0%, 1%, 2% and 5% structural damping. The wall thickness is 1.5mm. The added mass is 165 kg and the liquid is undamped.

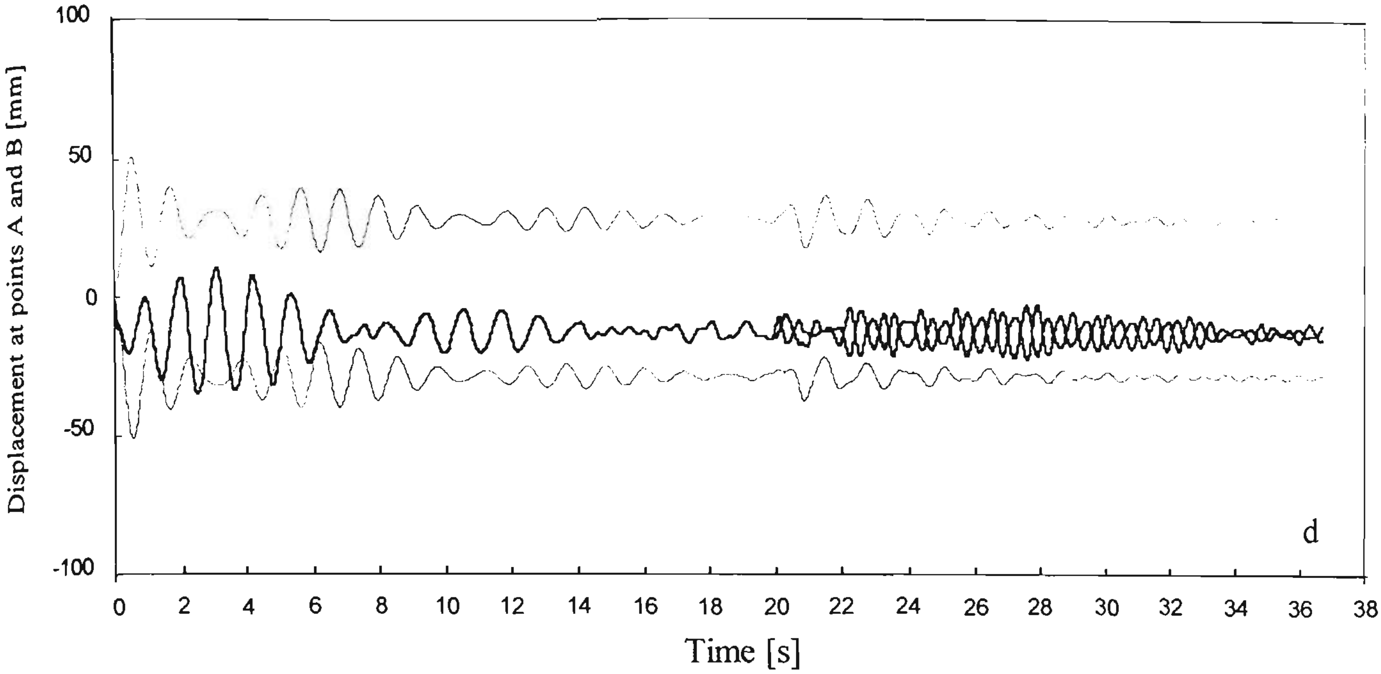

Figure 4.13. Displacement histories of the liquid (—–) and container walls (—–) for; (a), (b), (c), and (d) 0%, 1%, 2% and 5% structural damping. The wall thickness is 1.5mm. The added mass is 165 kg and the liquid is undamped.

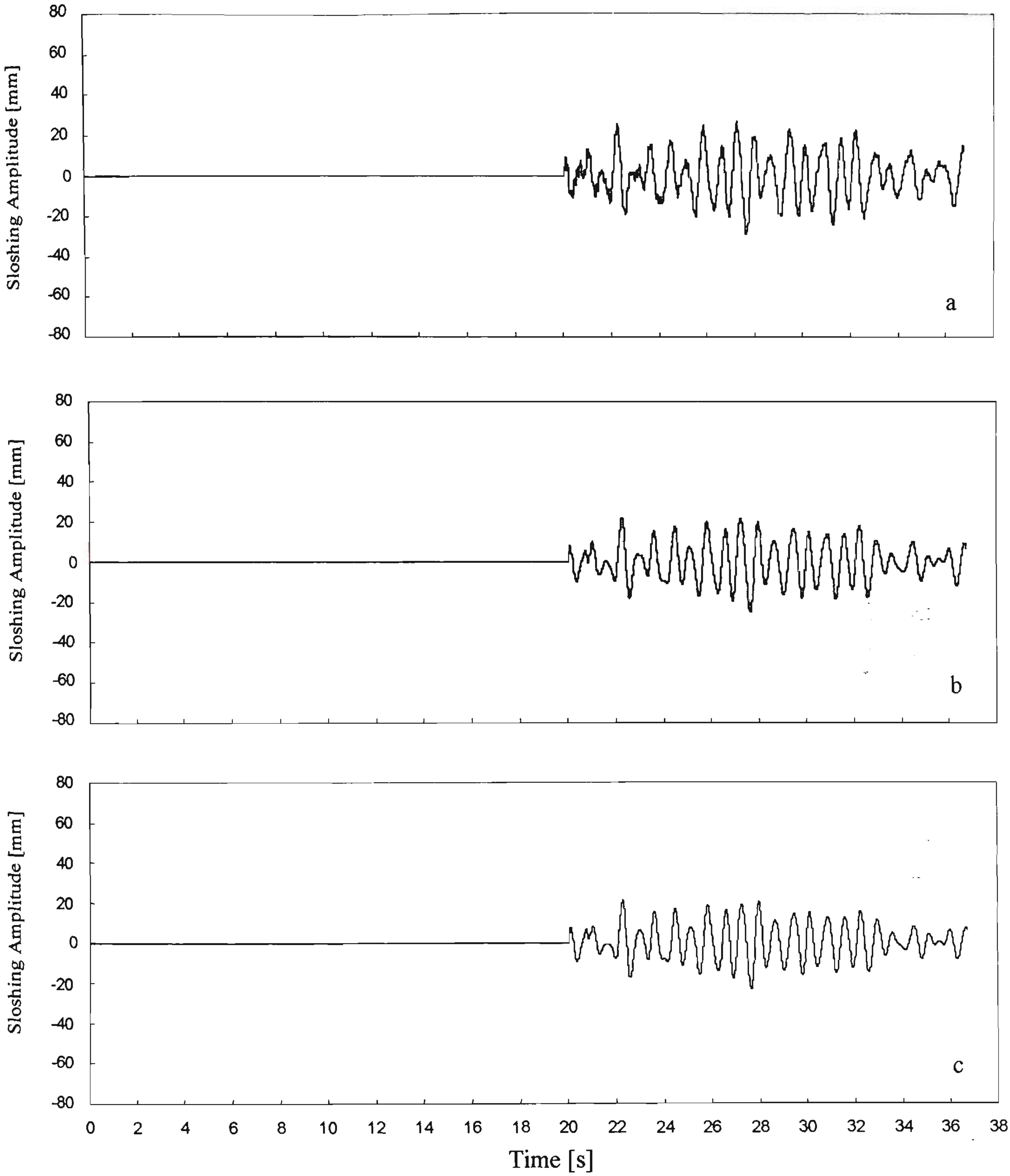

Figure 4.14. Predicted sloshing amplitude for the same cases as shown in Figure 4.13. The container walls are 1.5 mm thick, the total added mass is 165 kg and the critical damping ratio for the container without liquid is (a) 0%, (b) 1%, (c) 2%, and (d) 5%.

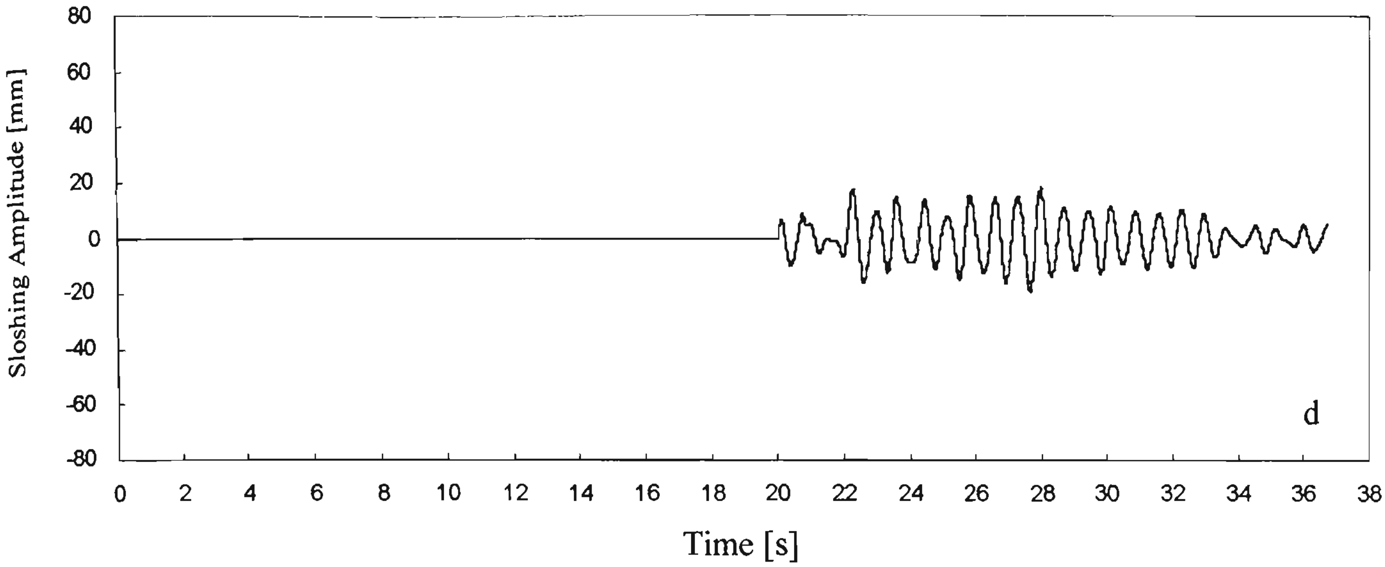

Figure 4.14. Predicted sloshing amplitude for the same cases as shown in Figure 4.13. The container walls are 1.5 mm thick, the total added mass is 165 kg and the critical damping ratio for the container without liquid is (a) 0%, (b) 1%, (c) 2%, and (d) 5%.

In Figure 4.15, predictions are given for a container with a 1 mm wall thickness with 1% structural damping and a total mass of 39.6 kg distributed along the walls of the container. In Figure 4.15(a) the liquid is undamped, whereas in Figure 4.15(b) the liquid has the same damping value as in Figure 4.11. Trials were conducted for other added masses however, only the best case of 39.6 kg is presented here. In Figure 4.15(a), the liquid displacement histories at both sides of the container are generally in phase. Due to this in phase motion, the sloshing amplitudes for the cases shown in Figure 4.15 are relatively small, as shown in Figure 4.16. In Figure 4.16(a), there is a beat in the sloshing amplitude of the liquid. This beat indicates that the liquid and the container frequencies are tuned. In Figure 4.16(b), there is energy dissipation in the liquid due to artificial damping. Due to energy dissipation in the liquid, the beat seen in Figure 4.16(a) has completely disappeared, and the maximum sloshing amplitude of approximately 20 mm is 50% of the maximum sloshing amplitude in the rigid container (of Figure 4.9(a)).

The reduction of the wall thickness from 1.5 mm to 1 mm increases the flexibility of the container. With thinner walls, the static deflection of the container increases as indicated by the separation between the two points of interest, point A and point B on the walls of the container. As a result, the displacement histories for the walls of the structure are shifted further from the zero axis than in the cases for 1.5 mm wall thickness. The advantage of decreased wall thickness is that less added mass is required to "tune" the container to liquid sloshing. This increased flexibility is exploited further by adding mass only in the middle of the longest walls of the container. Figure 4.17 shows an isometric view of the grid used for the container with the added mass at the middle of the container walls.

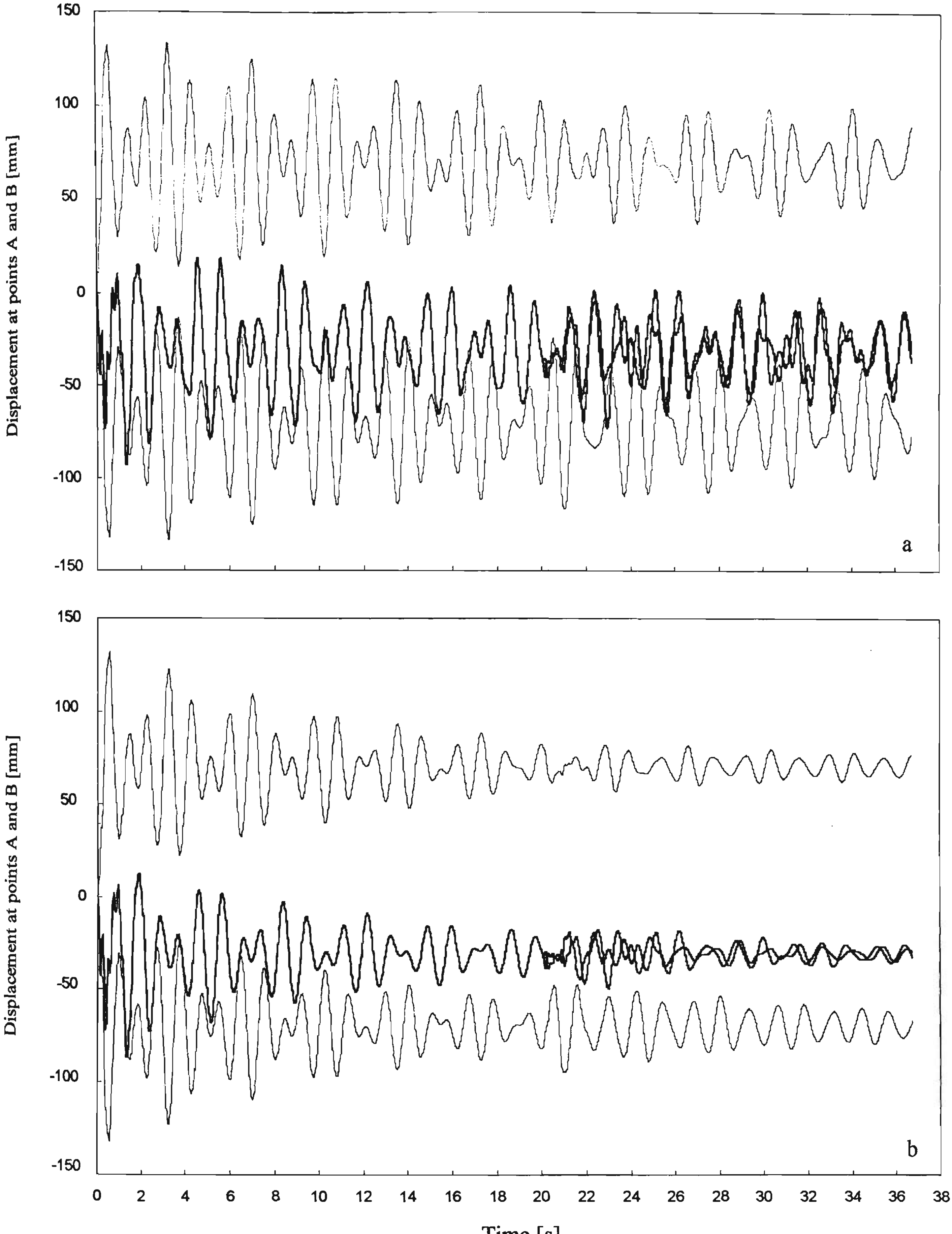

Figure 4.15. Displacement histories of the liquid (——) and container walls (——) for 1 mm wall thickness, 1% Structural damping and 39.6 kg added mass. (a) no liquid damping and (b) liquid damping.

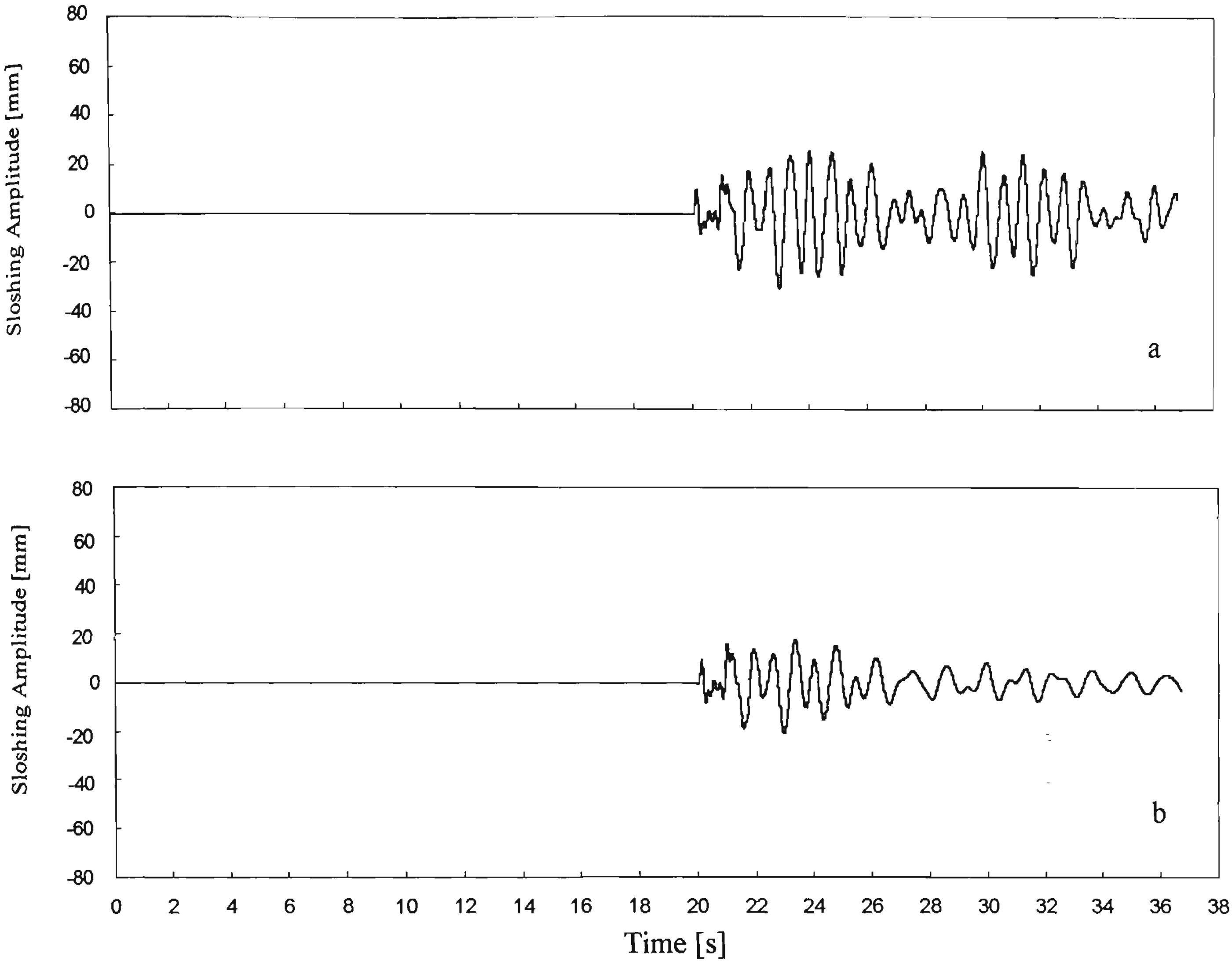

Figure 4.16. Predicted sloshing amplitude for the same cases as shown in Figure 4.15, 1 mm container wall thickness, a total added mass of 39.6 kg, (a) no artificial liquid damping (b) artificial liquid damping.

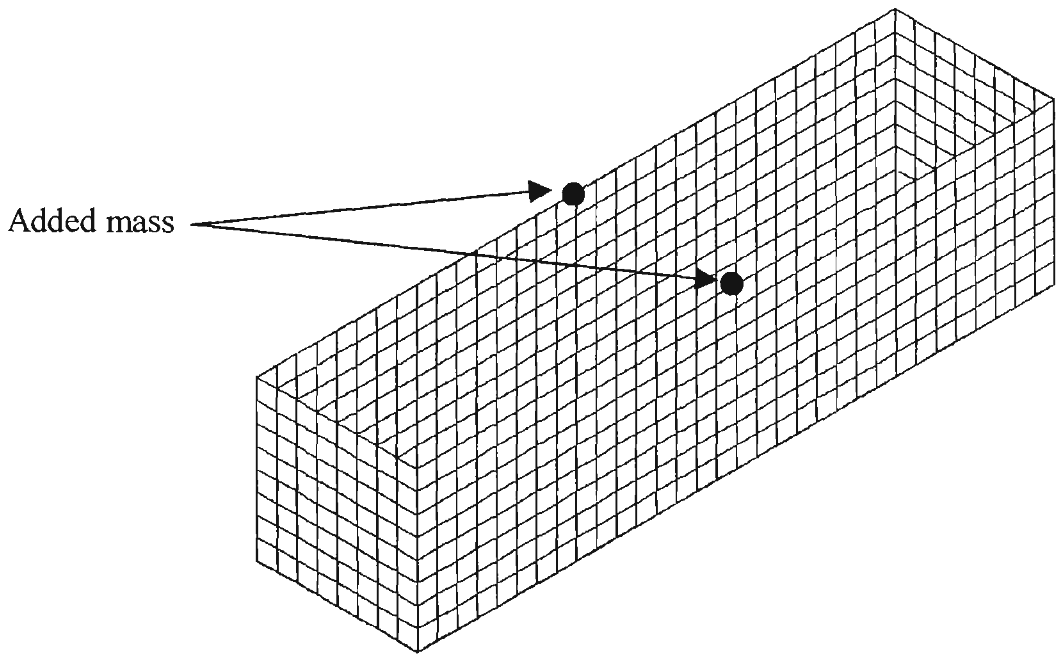

Figure 4.17. Grid used for the container showing added mass in the middle of the longest walls of the container.

In earlier cases, when the wall thickness was 1.5 mm, the container was found to be tuned when the first mode of oscillation of the container (without liquid) was at 0.85 Hz. Similarly, the best case for 1 mm wall thickness had a frequency of 0.94 Hz at the 1st mode. Table 4.4 shows the frequencies of oscillation for the first and third modes of the container without liquid and a wall thickness of 1 mm. Also included as the last row in the table, is the case of two point masses. When point masses are used, only 6 kg is required at each side of the container to reduce the first natural frequency to 1.01 Hz. This case represents a substantially lighter design than all of the earlier cases.

Table 4.4. Natural frequencies of the 1st and 3rd mode shapes for a container with a wall thickness of 1.0 mm and without liquid.

Total added mass [kg]	1st Natural frequency [Hz]	3rd Natural frequency [Hz]
0	6.38	9.26
39.6 [distributed]	0.94	1.37
12 [2 x 6 kg point masses]	1.01	9.26

In Figure 4.18, predictions of the displacement histories for the liquid and the walls of the container are given for a container with 1 mm walls and an added mass of 6 kg at each side of the container as shown in Figure 4.17. At the fundamental mode, this point is an anti-node, and therefore, adding mass at this point has a significant effect on the structural mode of vibration. In this case, the container has 1% structural damping, and the liquid has no artificial energy dissipation. Once again, after the initial settling period, the liquid displacement histories show an in-phase motion at the two sides of the container. The history of the sloshing amplitude for the same case is shown in Figure 4.19. Even without energy dissipation in the liquid, there is good control of liquid sloshing. The maximum sloshing amplitude is approximately

20 mm, which is 50% of the sloshing amplitude in the rigid container. It is seems that when the walls of the container are reduced from 1.5 mm to 1 mm, the increase in the container flexibility allows more movement of the container walls. Since the walls experience large motion, there is a greater amount of energy dissipation due to damping in the container than the case with thicker walls. The net result is a more effective control of sloshing.

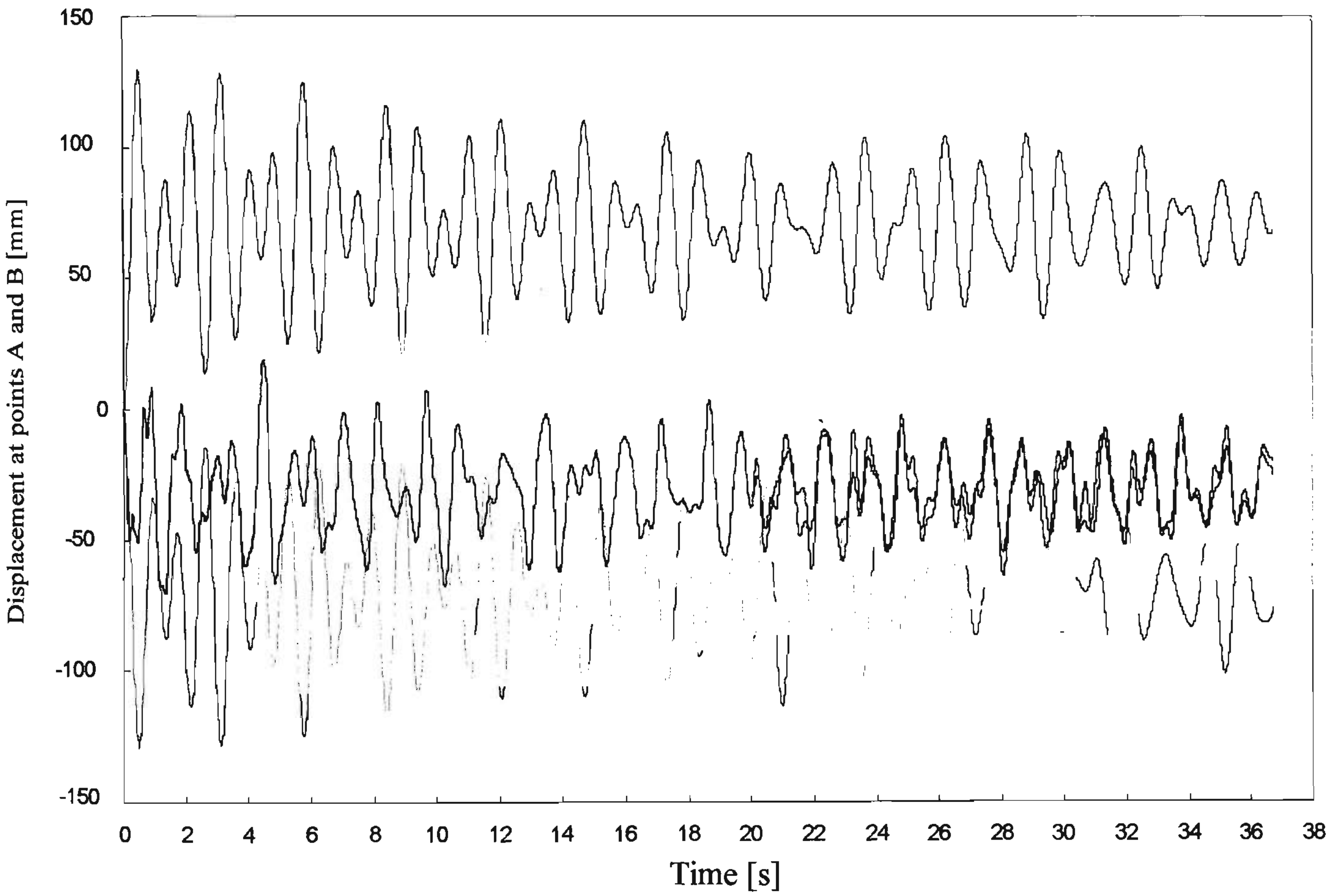

Figure 4.18. Displacement histories of the liquid (——) and container walls (——) for 1 mm wall thickness, 1% structural damping and 12 kg added mass. The liquid is undamped.

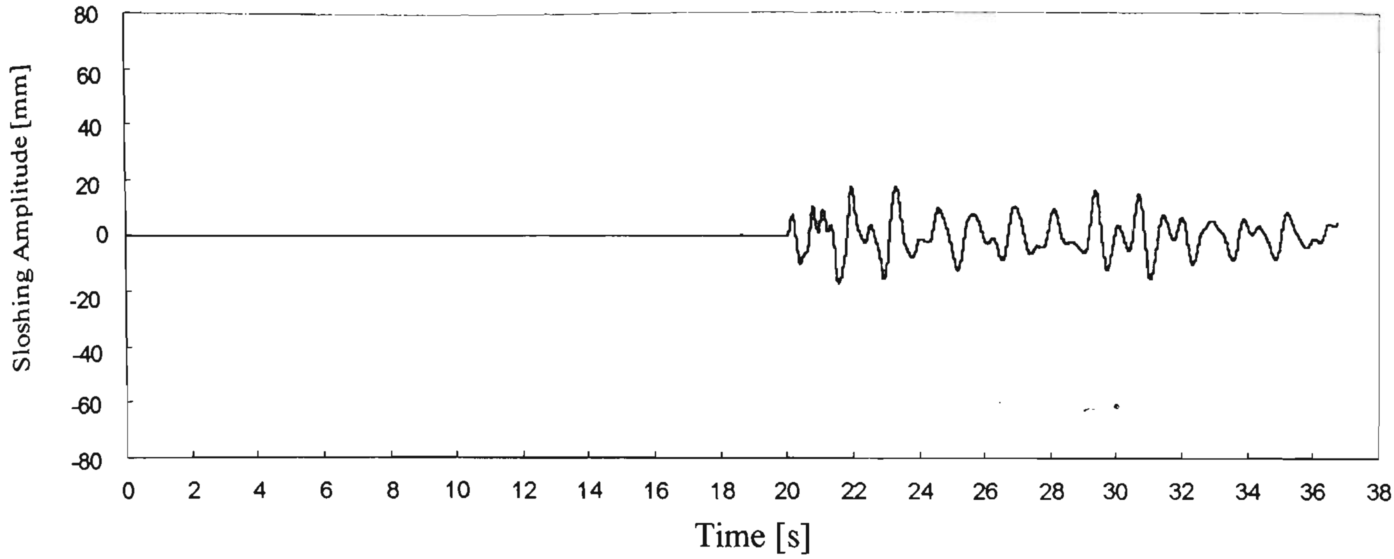

Figure 4.19. Predicted sloshing amplitude for the same case as shown in Figure 4.18. 1 mm wall thickness, 1% structural damping and 12 kg added mass. The liquid is undamped.

4.3.2. Random Excitation

In the previous section, the transient excitation given to the base of the container was sinusoidal and at the natural frequency of the fundamental sloshing mode in a rigid container. However, in many practical applications, the excitation may neither be sinusoidal nor transient. In this section, the two most promising cases predicted earlier along with the rigid container, are subjected to a random excitation.

A limited-band random noise from 0 to 3 Hz (Lee and Byrne, 1987) was employed covering a frequency range approximately twice the value of the fundamental sloshing frequency in the rigid container. Such random excitation may be considered to represent disturbances due to earthquakes and during transport in large vehicles. The primary purpose of presenting these cases is to demonstrate that the control performance in response to a transient disturbance is a close indication to that under a random excitation.

Similar to the previous cases subjected to transient sinusoidal excitation, at the start, the walls of the flexible container are vertical. The container is allowed to respond freely for the first 20 seconds, during this time the base of the container is kept stationary. After this settling time, the base of the container was subjected to the random excitation shown in Figure 4.20 from 20.01 seconds to 35 seconds.

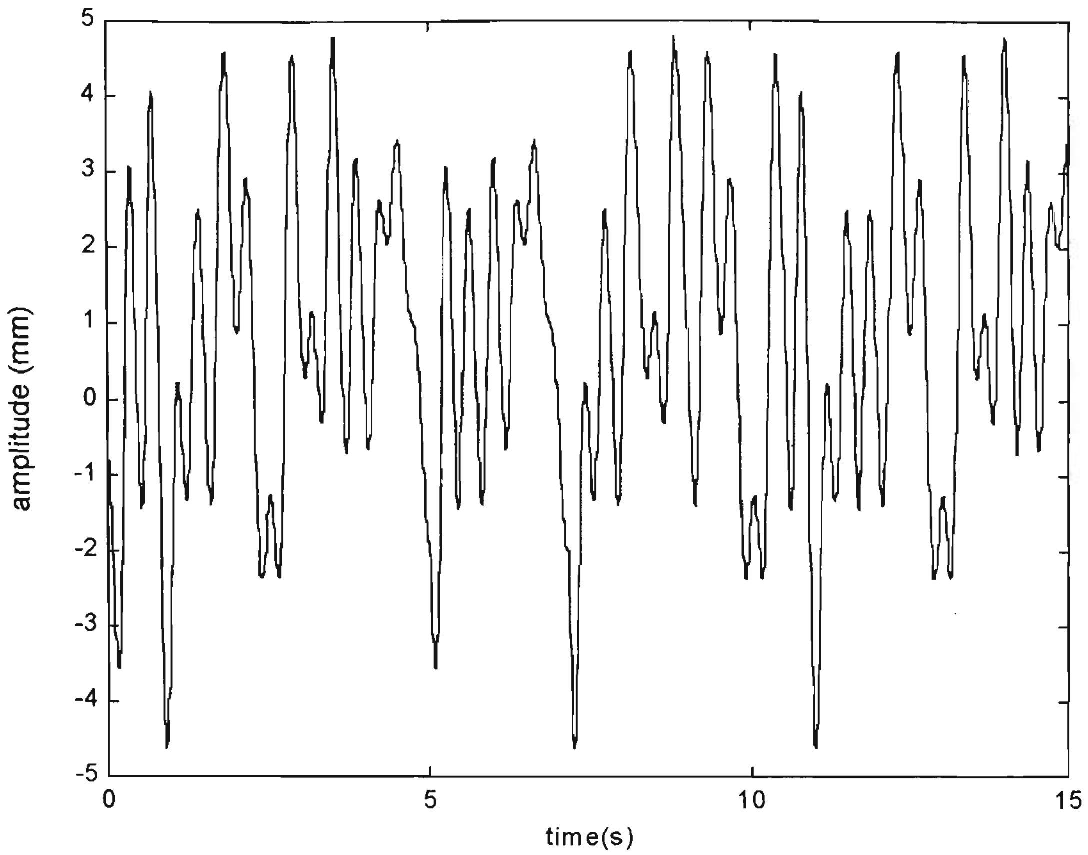

Figure 4.20. Random excitation given to the base of the container.

The Fourier spectrum and probability distribution are shown in Figure 4.21 for the displacement history of the container's base shown in Figure 4.20. The Fourier spectrum in Figure 4.21(a) verifies the intended frequency range, and the probability distribution in Figure 4.21(b) indicates an approximately normal distribution.

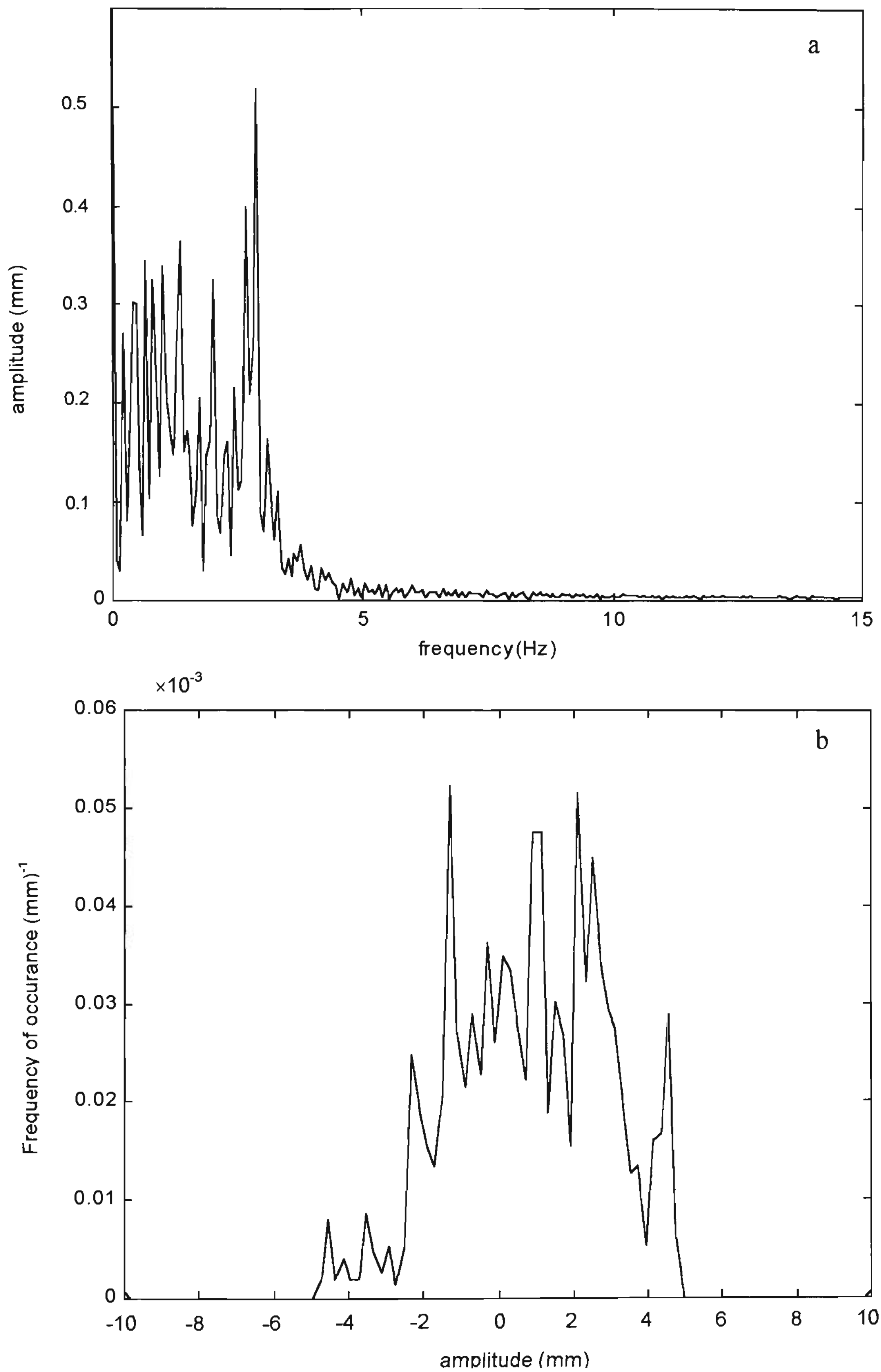

Figure 4.21. (a) Fourier spectrum and (b) probability distribution for the excitation history in Figure 4.20.

The two most promising cases identified earlier, were in Figure 4.9(e), for a wall thickness of 1.5 mm, and in Figure 4.18, for a reduced wall thickness of 1 mm. Displacement histories, for the walls of the container (------) and for the liquid (——), are given in Figures 4.22(a), 4.22(b) and 4.22(c), respectively, for containers with rigid walls, 1.5 mm wall thickness and 1 mm wall thickness when subjected to random excitation. Once again, the displacement histories are given for points A and B on opposite sides of the container shown earlier in Figure 4.3.

In Figure 4.22(a), the histories corresponding to the rigid-wall container are given as a comparison base. For the rigid container, the liquid displacement histories at points A and B are almost perfectly "out of phase" with one another during random excitation. On the other hand, for the two promising cases in Figures 4.22(b) and 4.22(c), the liquid displacement histories are in phase for much of the time after being exposed to the random excitation. The sloshing histories after the initial settling time of 20 seconds, are further discussed next to indicate control performance.

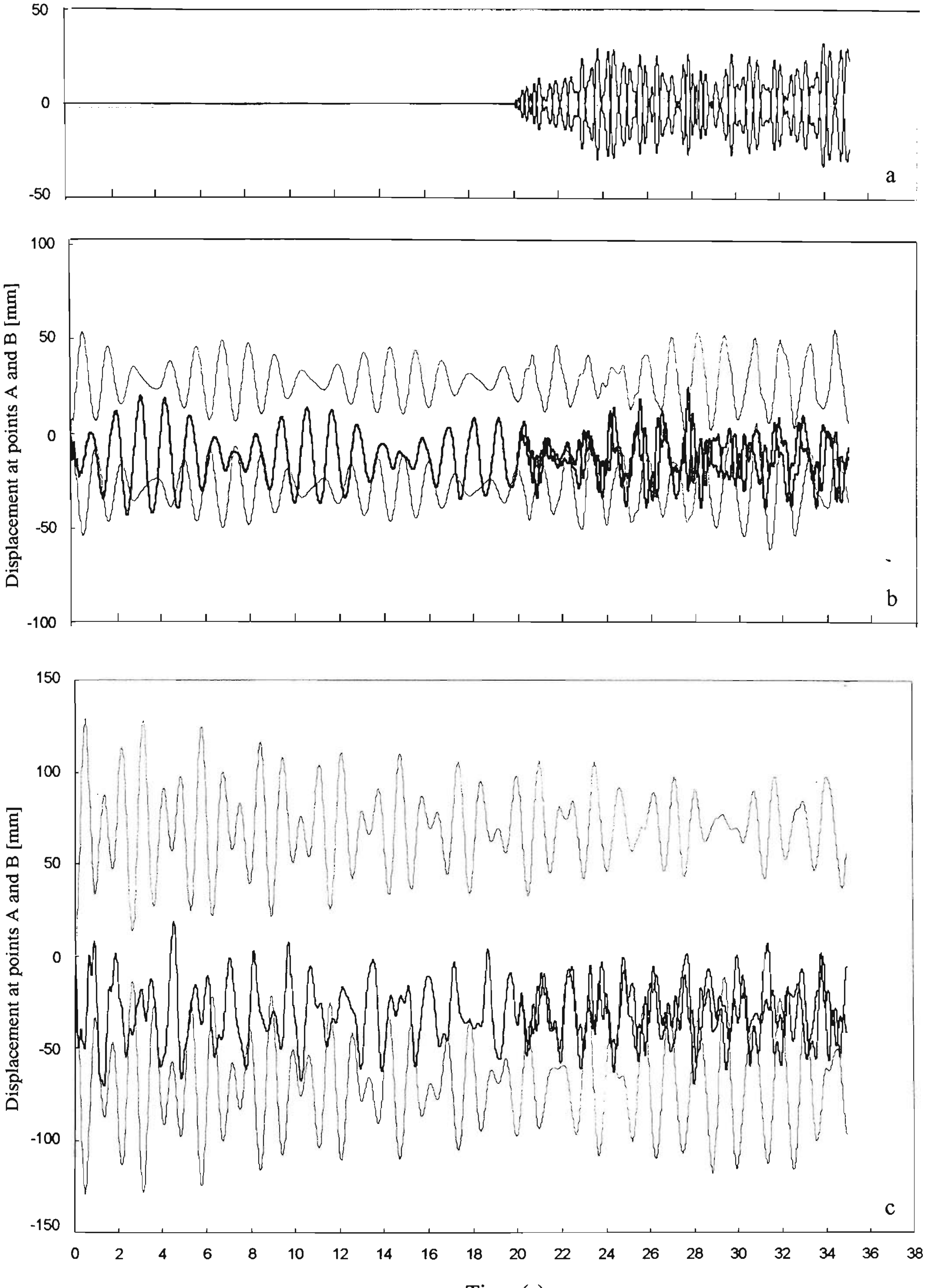

Figure 4.22. Displacement histories of the liquid (——) and container walls (——) for random excitation; (a) rigid wall container, (b) 1.5 mm wall thickness with 165 kg mass added and (c) 1.0 mm wall thickness with 12 kg mass added. Structural damping is 1% and the liquid is undamped.

The sloshing amplitude history, corresponding Fourier spectrum and probability distribution are given in frames (a), (b) and (c) in Figures 4.23, 4.24 and 4.25 for containers with rigid walls, 1.5 mm wall thickness and 1.0 mm wall thickness, respectively. It should be noted here that the 15 second duration in these figures start after the initial 20 second settling period. As expected, the largest sloshing amplitudes can be observed for the rigid container case in Figure 4.23(a). The sloshing history in Figure 4.23(a) clearly displays the characteristic trends of a narrow band process with a clear preference to the fundamental sloshing frequency at approximately 1.3 Hz. This frequency is also marked by the largest spectral amplitude in Figure 4.23(b). In Figure 4.23(c), an approximately normal distribution of the sloshing amplitude indicates a maximum amplitude of around 65 mm (as confirmed also in Figure 4.23(a)).

In Figure 4.24, predictions are given for a container with a 1.5 mm wall thickness. There is a clear improvement in the sloshing amplitude in Figure 4.24(a) compared with that of the rigid wall case. This is confirmed by the probability distribution in Figure 4.24(c), where the sloshing amplitudes are mostly accumulated around zero. In Figure 4.24(b), the first spectral peak in the Fourier spectrum has shifted from 1.3 Hz (in the rigid case) to 0.8 Hz due to the flexibility of the container walls.

For the optimally tuned flexible container of 1 mm wall thickness, the sloshing amplitude history in Figure 4.25(a) loses the clear narrow band character shown for the rigid container. Once again, the fundamental sloshing frequency is around 0.8 Hz, and it is still clearly marked in the frequency spectrum in Figure 4.25(b). The magnitude of this frequency is significantly reduced due to strong interaction with the flexible container. The probability distribution in Figure 4.25(c) confirms the reduction in sloshing amplitude to less than 40 mm, an improvement of 38% compared with the rigid wall case.

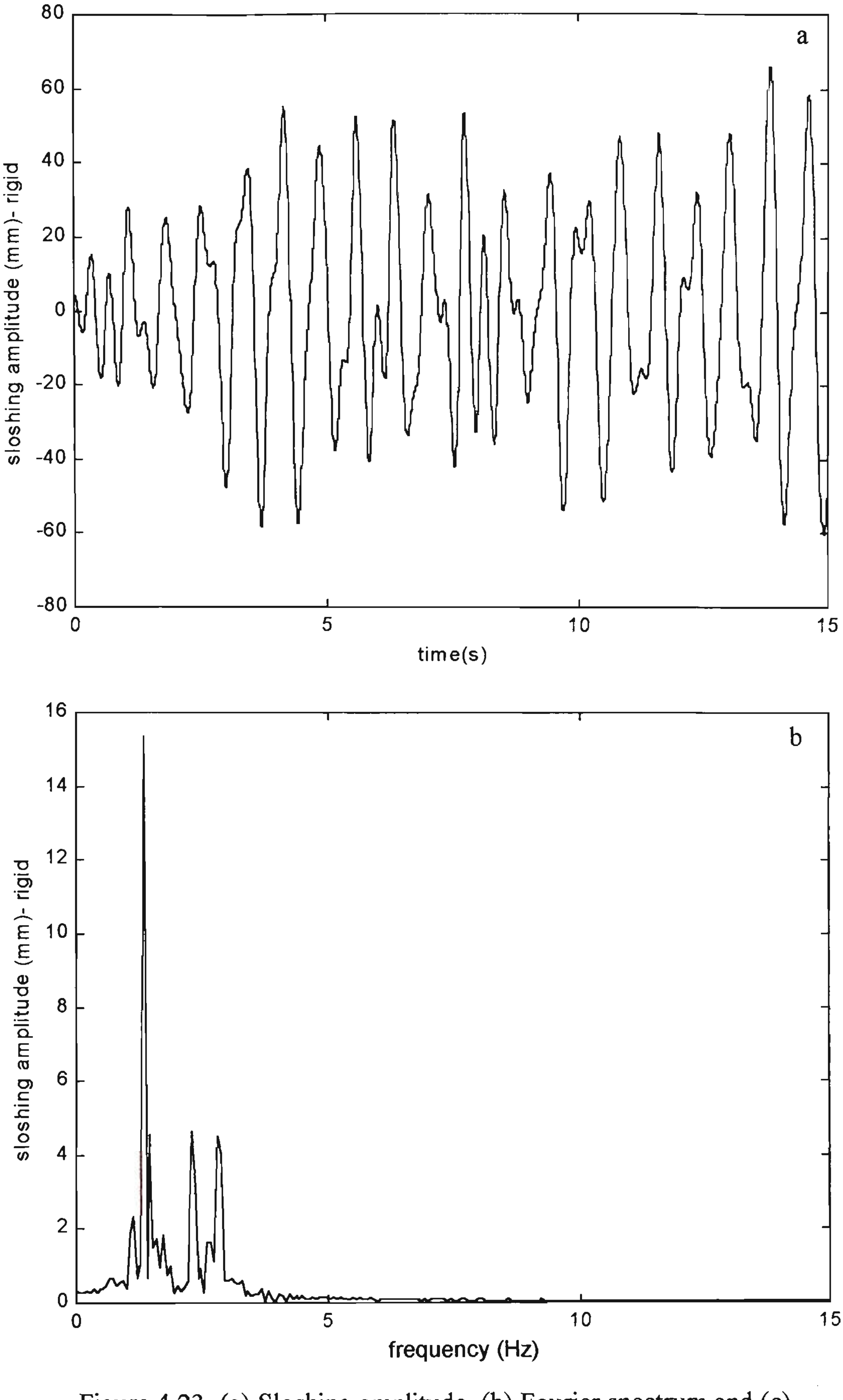

Figure 4.23. (a) Sloshing amplitude, (b) Fourier spectrum and (c) probability distribution for sloshing in a rigid wall container.

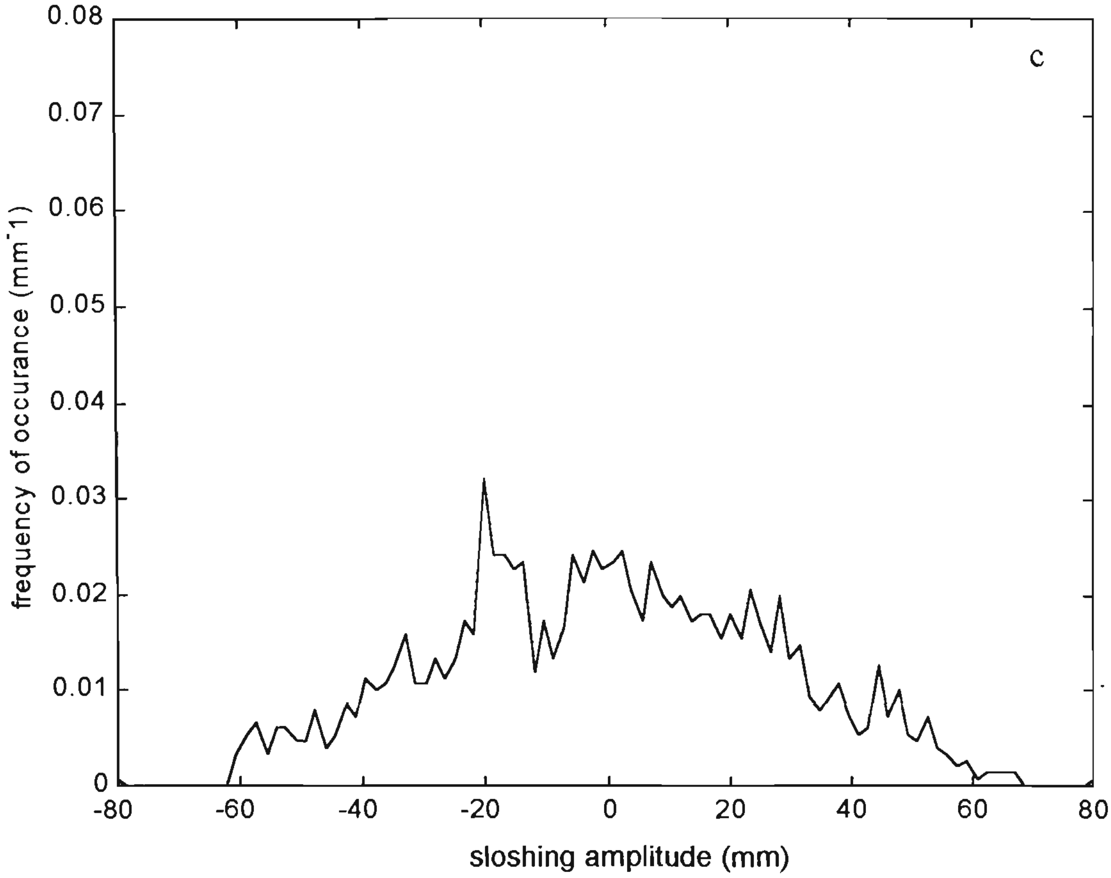

Figure 4.23. (a) Sloshing amplitude, (b) Fourier spectrum and (c) probability distribution for sloshing in a rigid wall container.

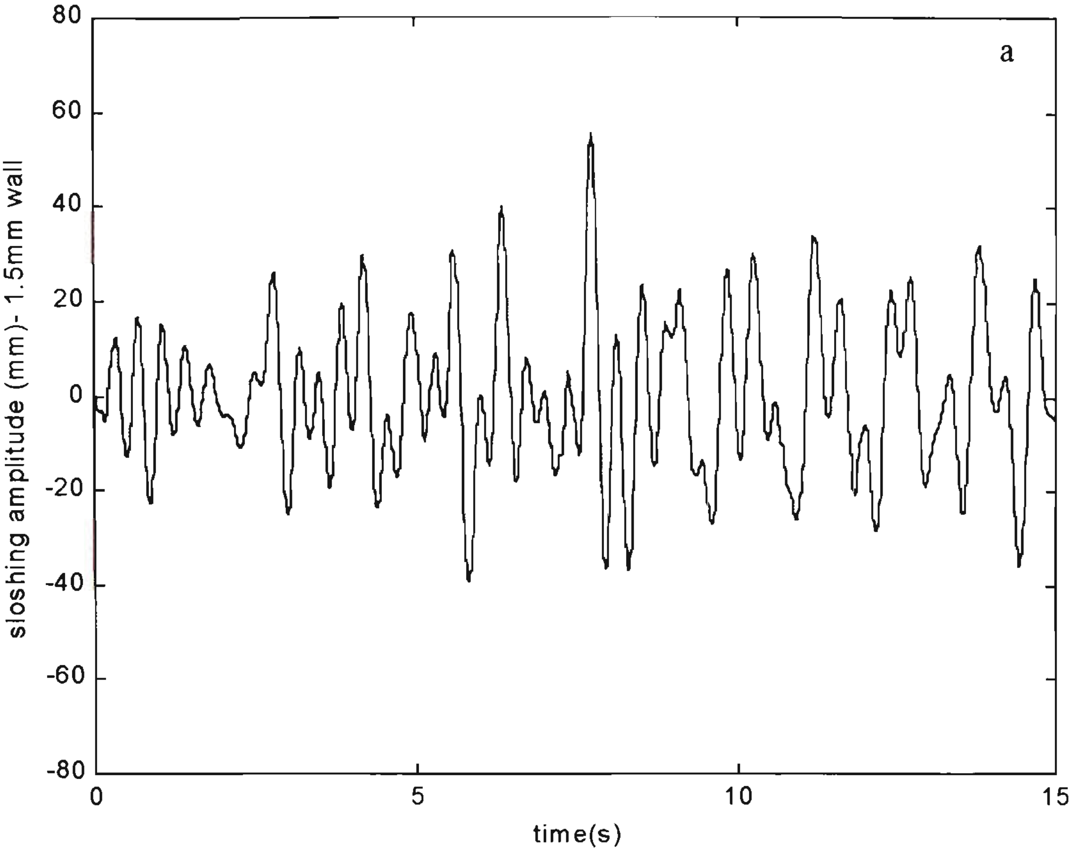

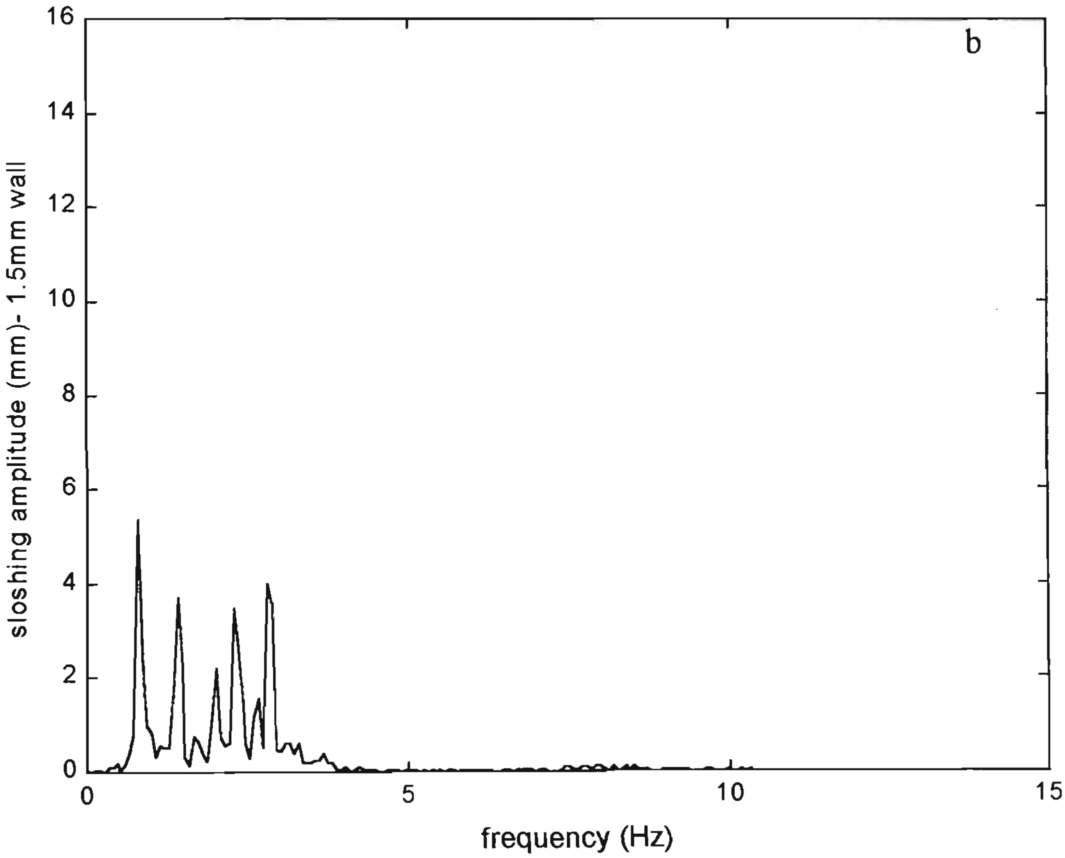

Figure 4.24. (a) Sloshing amplitude, (b) Fourier spectrum and (c) probability distribution for a sloshing in container with 1.5mm thick walls.

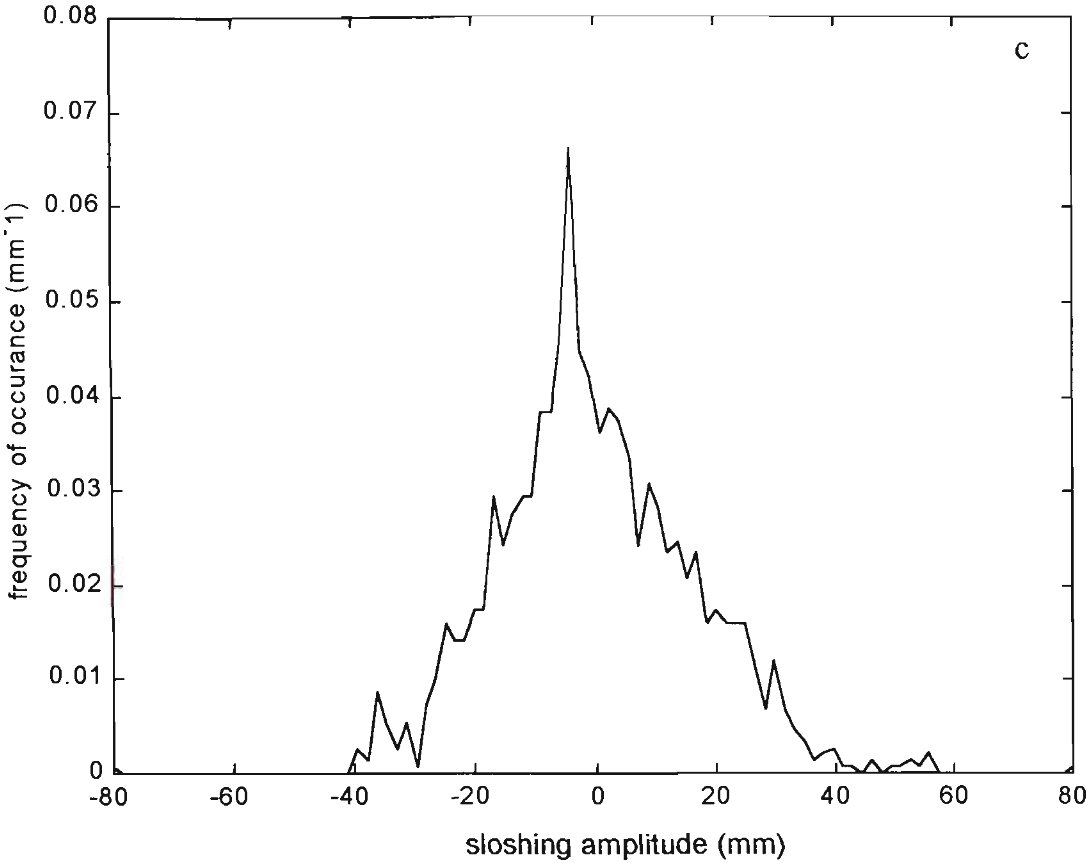

Figure 4.24. (a) Sloshing amplitude, (b) Fourier spectrum and (c) probability distribution for sloshing in a container with 1.5mm thick walls.

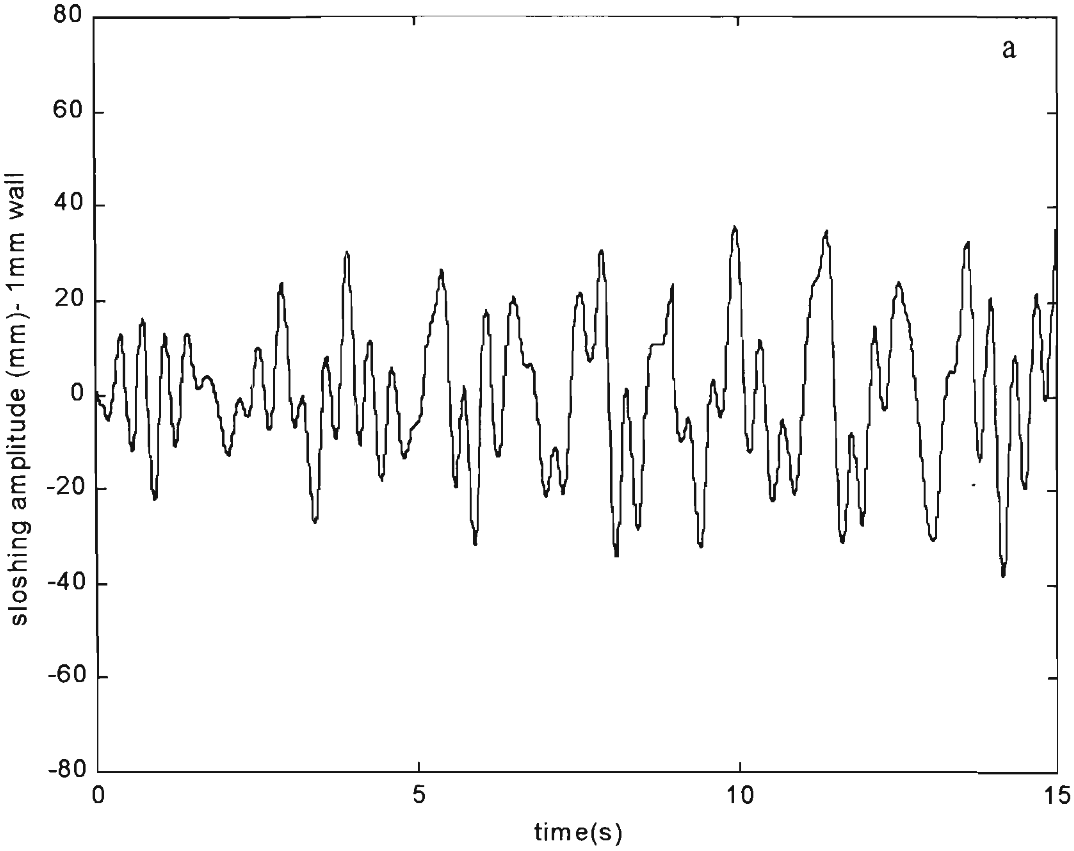

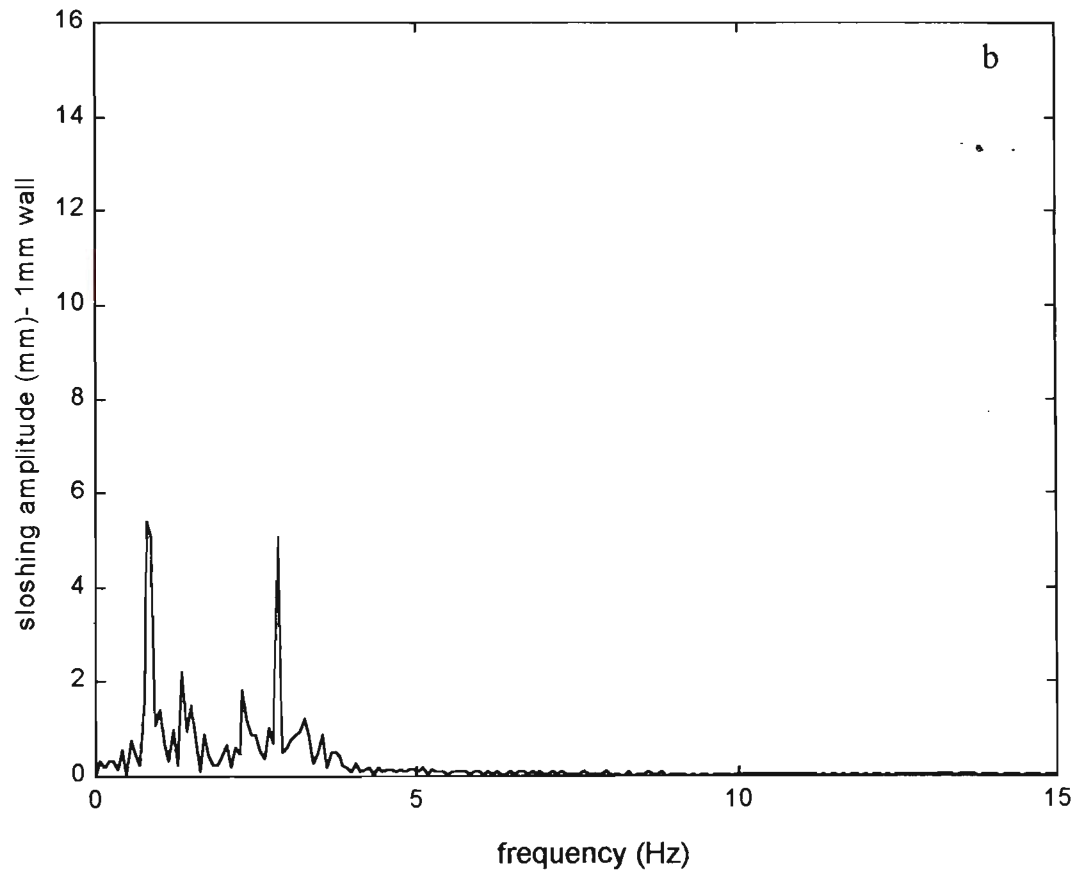

Figure 4.25 (a) Sloshing amplitude, (b) Fourier spectrum and (c) probability distribution for sloshing in a container with 1.0mm thick walls.

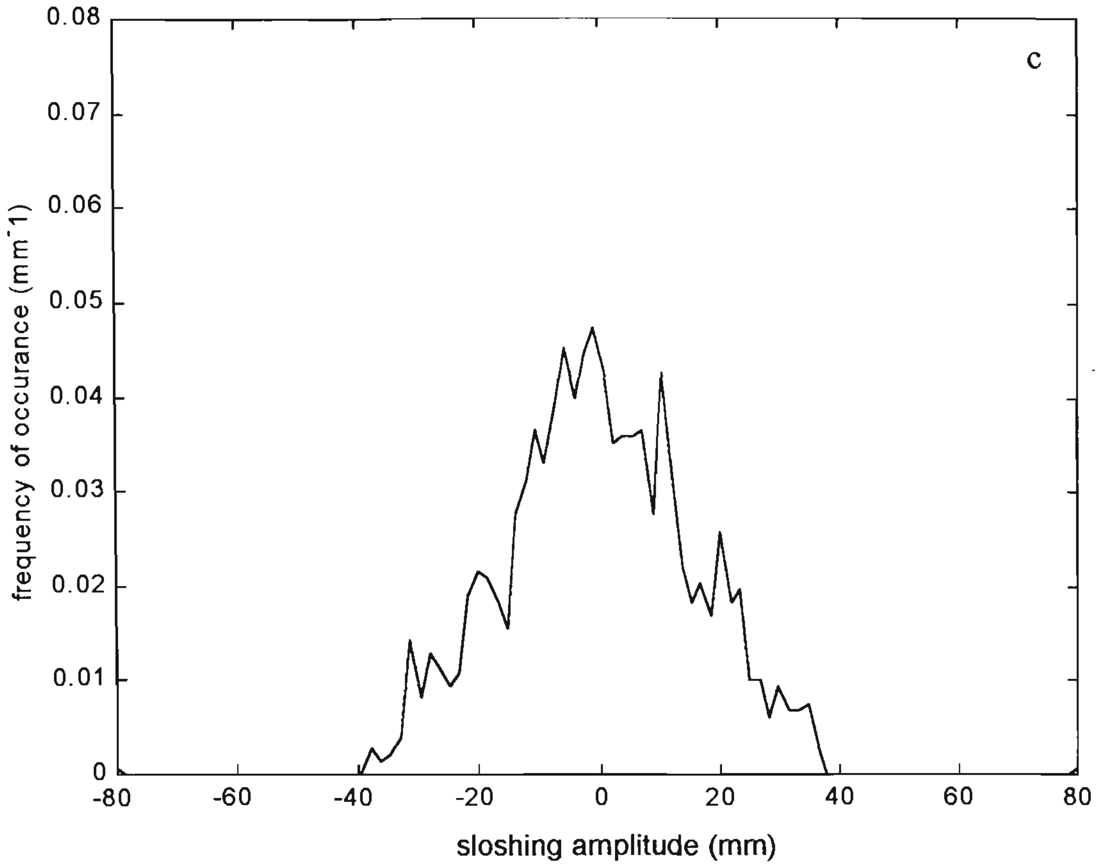

Figure 4.25 (a) Sloshing amplitude, (b) Fourier spectrum and (c) probability distribution for sloshing in a container with 1.0m thick walls.

4.4. CONCLUSIONS

A novel idea is proposed in this chapter to use the flexibility of a container to control liquid sloshing. In some practical applications, the addition of sloshing control devices studied in the earlier chapters may not be practical or even possible. In such situations, it may be possible to reduce the sloshing amplitude significantly by intentionally allowing some flexibility of the container walls.

The numerical predictions in this chapter have been compared with observations from experiments for a selected case. Considering the complex interaction between the liquid and the container and also the non-linear nature of liquid sloshing, the agreement is found to be acceptable. Therefore, the proposed numerical model may be a valuable tool that can be used to identify promising cases for effective control.

The proposed concept of using flexibility of the container walls to reduce liquid sloshing, may lead to significant reductions of the mass of containers, if flexibility is achieved by reducing the container wall thickness. This novel approach for control of liquid sloshing may prove to be an advantage in practical applications involving liquid transportation and storage.

Chapter 5

CONCLUSIONS

The investigations conducted in this thesis are focussed on either the suppression of liquid sloshing or the use of liquid sloshing to control structural oscillations. As a result, contributions are made to the state-of-the-art knowledge of liquid sloshing in engineering applications.

In Chapter 2, a sloshing absorber of standing wave type is proposed as an alternative to a tuned vibration absorber. This type of sloshing absorber is intended to be used as a liquid storage tank, which may also passively control oscillations of the supporting structure. Generally, the geometry of liquid storage tanks leads to standing sloshing waves. A standing wave has poor energy dissipation characteristics which make it an improper choice as a sloshing absorber. The addition of cantilevered baffle plates is shown to enhance the performance of the sloshing absorber to control the transient oscillations of a structure. A numerical procedure is described to couple the fluid solution for sloshing, with the solution of the structure to be controlled. Simple experiments were performed to verify the accuracy of the numerical predictions.

The importance of Chapter 2 is the modification of deep liquid tanks to control structural oscillations. The chapter is a significant contribution to knowledge in this area because previous work focussed almost exclusively on shallow liquid sloshing absorbers, and as a result, travelling sloshing waves. Also, the parameters used previously to scale liquid sloshing, have been applied successfully to a strongly interacting sloshing absorber-structure system.

In many practical applications, it is important to control liquid sloshing. In Chapter 3, rigid cantilever baffles are used to control liquid sloshing in rigid containers. The experimental and predicted results agreed closely. For the uncontrolled case, experimental results matched predicted results to within 3%. For the controlled cases, experimental results showed greater suppression than that predicted with numerical simulations. The predictions in this chapter are useful for design purposes or as a comparison base for other types of sloshing control. In particular, the trends of the control action for different baffle sizes, are identified in a non-dimensionalised form.

A disadvantage of cantilever baffles as sloshing controllers is that their effectiveness deteriorates with varying liquid depths, since the baffles remain fixed at one location. In Chapter 3, floating devices are shown to provide effective sloshing control in cylindrical containers. Experiments suggest that the floating devices, called dumb-bell controllers, may be effective at varying liquid levels. The control action of dumb-bell controllers could not be predicted numerically. A possible first step toward this objective is completed in this thesis for a single floating plate. Appendix 3 is devoted to these numerical modelling attempts. Further development of the numerical procedure would be worthwhile for future work, because the dumb-bell type controllers hold promise in practical applications. They are versatile, inexpensive and easy to implement as add-on type of passive control for violent liquid sloshing in containers.

In some practical applications, the addition of sloshing control devices may not be possible due to existing geometric constraints. In Chapter 4, a different approach to sloshing control is adopted. Rather than considering modifications to the container, the container is made flexible, and its fundamental frequency is tuned to the frequency of liquid sloshing. Such a tuned flexible container should act in a similar fashion to a tuned absorber to control liquid oscillations. Numerical predictions show that the sloshing wave amplitude can be significantly reduced by tuning the interaction of the flexible container with liquid sloshing. The concept of using container flexibility to control liquid sloshing is a novel one, and it is presented here for the first time.

The numerical model in Chapter 4 is tested experimentally. Some differences exist due to the inherent inviscid liquid assumption. Also, the non-linear nature of the problem exaggerates any difference between the experimental and numerical models, regardless of how small the difference may be. Considering the differences, however, it is concluded that the numerical predictions can still be used as a design tool to identify promising cases. The promising cases provide reduced sloshing amplitudes for both sinusoidal and random excitations as compared with those of a rigid container. In addition to providing suppressed sloshing, if flexibility is achieved by a reduction in the wall thickness of the container, then the proposed concept may lead to significant reductions of materials and cost.

The use of container flexibility, as it is presented in this thesis, may still be at its initial stages of development. However, this novel concept represents a significant advancement in the design of liquid containers, towards "smart " packaging which can do more than simply contain cargo.

REFERENCES

Abe, M., Kimura, S. and Fujino, Y., 1996, "Semi-active Tuned Column Damper with Variable Orifice Openings," Third international Conference on Motion and Vibration Control, Chiba, pp. 7-11.

Abiru, H., Tamura, K., Harada, H., Matsamoto, T. and Kondo, H., 1991, "Preventing Vibration in High Rise Structures," Mitsubishi Heavy Industries Ltd., Technical review, Vol. 28, No. 2.

Anderson, J. G., Semercigil, S. E. and Turan, Ö. F., 1999a, "A Standing-wave Type Sloshing Absorber to Control Transient Oscillations," *Accepted for publication in the Journal of Sound and Vibration.*

Anderson, J. G., Semercigil, S. E. and Turan, Ö. F., 1999b, "An Improved Standing-wave Type Sloshing Absorber," *Accepted for publication in the Journal of Sound and Vibration.*

Anderson, J. G., Semercigil, S. E. and Turan, Ö. F., 1999c, "An Improved Standing-wave Type Sloshing Absorber," American Society of Mechanical Engineers, Fluids Engineering Division Summer Meeting, San Francisco, USA, Paper No. FEDSM99-7037.

Anderson, J. G., Semercigil, S. E. and Turan, Ö. F., 1998a, "A Modified Sloshing Absorber to Control Structural Oscillations," American Society of Mechanical Engineers, Fluids Engineering Division Summer Meeting, Washington DC, USA, Paper No. FEDSM98-5096.

Anderson, J. G., Semercigil, S. E., and Turan, Ö. F., 1998b, "Comparison of a Sloshing Absorber and Tuned Absorber for Optimal Vibration Control," Proceedings of The Australasian Conference on Structural Optimisation, Sydney, AUSTRALIA, pp. 199-206.

Anderson, J. G., Semercigil, S. E. and Turan, Ö. F., 1998c, "Scaling of a Novel Sloshing Absorber to Control Structural Vibrations," 13th Australasian Fluid Mechanics Conference, Monash University, Melbourne, AUSTRALIA. pp. 909 – 912.

Anderson, J. G., Turan, Ö. F. and Semercigil, S. E., 1997a, "Control of Liquid Sloshing in Rigid Rectangular Containers Using Rigid Fixed Plate Baffles," Proceedings of the 3rd International Conference on Modelling and Simulation, Melbourne, AUSTRALIA, pp. 414-419.

Anderson, J. G., Turan, Ö. F. and Semercigil, S. E., 1997b, "Control of Sloshing in Rigid Wall Containers; Part I - An Experimental Evaluation with Cylindrical Geometries," American Society of Mechanical Engineers, Fluids Engineering Division Summer Meeting, Vancouver, CANADA, Paper No. FEDSM97-3133.

Anderson, J. G., Turan, Ö. F. and Semercigil, S. E., 1997c, "Control of Sloshing in Rigid Wall Containers; Part II – A Numerical Approach," American Society of Mechanical Engineers, Fluids Engineering Division Summer Meeting, Vancouver, CANADA, Paper No. FEDSM97-3134.

ANSYS 5.3. User manuals, 1994, ANSYS Inc. Houston USA, Copyright 1996 SAS IP, Inc. Proprietary Data.

Bass, R. L., Bowles, E. B., Trudell, R. W., Navickas, J., Peck, J. C., Yoshimura, N., Endo, S. and Pots B. F. M., 1985, "Modelling Criteria for Scaled LNG Sloshing Experiments," Transactions of the ASME, Journal of Fluids Engineering, Vol. 107, pp. 272-280.

Bauer, H. F., 1990, "Oscillatory Response of a Liquid Column to Counter-Rotation Excitation," Journal of Sound and Vibration, Vol. 142, No. 1, pp. 125-133.

CFDS-FLOW3D User Guide, 1994, Computational Fluid Dynamics Services, Oxfordshire, United Kingdom.

Chen, K. H., Kelecy, F. J. and Pletcher, R. H., 1994, "Numerical and Experimental Study of Three-Dimensional Liquid Sloshing Flows," Journal of Thermodynamics and Heat Transfer, Vol. 8, No. 3, July-September, pp. 507-513.

Chen, W. and Haroun, M. A., 1994, "Dynamic Coupling Between Flexible Tanks and Seismically Induced Nonlinear Liquid Sloshing," Fluid Transients ASME, FED-Vol. 198/PVP-Vol. 291.

Fujii, K., Tamura, Y. and Wakahara T., 1990, "Wind-Induced Vibration of Tower and Practical Applications of Tuned Sloshing Damper," Journal of Wind Engineering and Industrial Aerodynamics, Vol. 33, pp. 263-272.

Fujino, Y., Sun, L. M., Pacheco, B. M. and Chaiseri, P., 1992, "Tuned Liquid Damper (TLD) for Suppressing Horizontal Motion of Structures," Journal of Engineering Mechanics, Vol. 118, No. 10, pp. 2017-2030.

Gedikli, A. and Erguven, M. E., 1999, "Seismic Analysis of Liquid Storage Tank with a Baffle," Journal of Sound and Vibration, Vol. 223, No. 1, pp. 141-155.

Hara F. and Shibata H., 1987, "Experimental Study on Active Suppression by Gas Bubble Injection for Earthquake Induced Sloshing in Tanks," Japanese Society of Mechanical Engineers International Journal, Vol. 30, No. 260, pp. 318-323.

Hayama, S. and Iwabuchi, M., 1986, "A Study on the Suppression of Sloshing in a Liquid Tank (1st Report, Suppression of sloshing by means of a reversed U-tube)," Bulletin of JSME, Vol. 29, No. 252, pp. 1834-1841.

Hirt, C. W. and Nichols, B. D., 1981, "Volume of Fluid (VOF) Method for the Dynamics of Free Boundaries," Journal of Computational Physics, Vol. 39, pp 201-225.

Hung, R. J., Lee, C. C. and Leslie, F. W., 1993, "Effect of the Baffle on the Asymmetric Gravity-Jitter Excited Slosh Wave and Spacecraft Moment and Angular Momentum Fluctuations," Proceedings of the Canadian Institution of Mechanical Engineers, Journal of Aerospace Engineering, Vol. 207, pp. 105-120.

Hunt, J. B., 1979, Dynamic Vibration Absorbers, Letchworth, London: The Garden City Limited.

Jeong, K. H. and Kim, K. J., 1998, "Free Vibration of a Circular Cylindrical Shell Filled with Bounded Compressible Fluid," Journal of Sound and Vibration, Vol. 217, No. 2, pp. 197-221.

Kana, D. D., Lindholm, U. S. and Abramson, H. N., 1966, "An Experimental Study of Liquid Instability in a Vibrating Elastic Tank," AIAA Journal of Spacecraft Rockets, Vol. 3, No. 8, pp. 1183-1187.

Kaneko S. and Yoshida O., 1994, "Modelling of Deep Water Type Rectangular Tuned Liquid Damper with Submerged Nets," The American Society of Mechanical Engineers, Sloshing, Fluid-Structure Interaction and Structural Response Due to Shock and Impact Loads, PVP-Vol. 272, pp. 31-42.

Lee, C. H. and Byrne, K. P., 1987, "Impact Statistics for a Random Rattling System," Journal of Sound and Vibration, Vol. 150, pp. 322-329.

Milne-Thomson, L. M., 1968, Theoretical Hydrodynamics 5th ed. Macmillan Press, London, pp. 427-442.

Modi, V. J., and Welt, F., 1984, "Nutation Dampers and Suppression of Wind Induced Instabilities," The American Society of Mechanical Engineers Joint Multidivisional Symposium on Flow-Induced Oscillations, Vol. 1, pp. 173-187.

Muto, K., Kasai, Y. and Nakahara, M, 1988, "Experimental Tests for Suppression Effects of Water Restraint Plates on Sloshing of a Water Pool," Transactions of the ASME, Journal of Pressure and Vessel Technology, Vol. 110, pp. 240-246.

Popov, G., Sankar, S., Sankar, T. S. and Vatistas, G. H., 1992, "Liquid Sloshing in Rectangular Road Containers," Computers in Fluids, Vol. 21, pp. 551-569.

Popov, G., Sankar, S., Sankar, T. S., and Vatistas, G. H., 1993, "Dynamics of Liquid Sloshing in Horizontal Cylindrical Road Containers," Proceedings of the Canadian Institution of Mechanical Engineers, Vol. 207, pp. 399-406.

Rao S. S., 1990, Mechanical Vibrations, New York: Addison-Wesley Publishing Co., second edition, pp. 712-715.

Schlichting, H., 1979, Boundary Layer Theory, New York: McGraw Hill, seventh edition, pp. 537 and 663.

Seto, M. L., and Modi, V. J., 1997, "A Numerical Approach to Liquid Sloshing Dynamics and Control of Fluid-Structure Interaction Instabilities," The American Society of Mechanical Engineers, Fluids Engineering Division Summer Meeting, Paper no. FEDSM97-3302.

Sharma, R., Semercigil, S. E. and Turan Ö. F., 1992, "Floating and Immersed Plates to Control Sloshing in a Cylindrical Container at the Fundamental Mode," Journal of Sound and Vibration, Vol. 155, No. 2, pp. 365-370.

Silverman, S., and Abramson, H. M., 1966a, "Damping of Liquid Motions and Lateral Sloshing," The Dynamic Behavior of Liquids in Moving Containers with Applications to Space Vehicle Technology, NASr-94(07), pp. 121-140.

Silverman, S. and Abramson, H. N., 1966b, "Lateral Sloshing in Moving Containers," The Dynamic Behavior of Liquids in Moving Containers with Applications to Space Vehicle Technology, NASr-94(07), pp. 13-78.

Snowdon, J. C., 1968, Vibration and Shock in Damped Mechanical Systems, New York: John Wiley & Sons, pp. 87-90.

Stevens, D. G., 1966, "Flexible Baffles for Slosh Damping," AIAA Journal of Spacecraft Rockets, Vol. 3, No. 5, pp. 765-766.

Su, T.C. and Wang, Y., 1990, "Numerical Simulation of Three-Dimensional Large Amplitude Liquid Sloshing in Cylindrical Tanks Subjected to Arbitrary Excitations," Flow Structure Vibration and Sloshing, 4th Symposium – Pressure Vessels and Piping Conference, pp. 127-148.

Takahara, H., Kimura, K. and Sakata, M., 1995, "Frequency Response of Sloshing in a Circular Cylindrical Tank Subjected to Pitching Excitation," Proceedings of Asia Pacific Vibration Conference, Kuala Lumpur, pp. 703-708.

Tang, Y., 1994, "Free-Vibration Analysis of Tank Containing Two Liquids," Journal of Engineering Mechanics, Vol. 20, No. 3, pp. 618-636.

Warnitchai, P. and Pinkaew, T., 1998, "Modelling of Liquid Sloshing in Rectangular Tanks with Flow-dampening Devices," Engineering Structures, Vol. 20, No. 7, pp. 593-600.

Yao, Y., Tulin, M. P. and Kolaini, A. R., 1994, "Theoretical and Experimental Studies of Three-Dimensional Wavemaking in Narrow Tanks, Including Nonlinear Phenomena Near Resonance," Journal of Fluid Mechanics, Vol. 276, pp. 211-232.

Appendix 1

CFX4.1 FILES FOR A SLOSHING ABSORBER IN CHAPTER TWO

A1.1. SOURCE CODE

In Chapter 2, numerical predictions for a sloshing absorber are presented using a commercial code, CFX 4.1. Within the CFX environment, two files were used to create a model of the sloshing absorber. In this Appendix, a listing of these two files is given for completeness. These files are a Command file and a User Fortran file. The Command file is used to create the numerical grid and to set boundary conditions that are standard in the CFX environment. More complex boundary conditions must be set within a User Fortran file. In this investigation, a User Fortran file is used to set the initial depth of the liquid and non-slip velocity conditions at the walls of the sloshing absorber. The User Fortran file is also used to determine the fluid-structure interaction between the sloshing absorber and the structure to be controlled. This interaction is determined from the control force, meaning the resultant pressure force of a sloshing liquid at the moving boundary of the container. The Command file and User Fortran file for a typical sloshing absorber are given next, corresponding to the results presented in Figures 2.7 and 2.14.

A1.1.1. Command File

```
>>CFX4
  >>SET LIMITS
    MEDIUM
  >>OPTIONS
    TWO DIMENSIONS
    RECTANGULAR GRID
    CARTESIAN COORDINATES
```

```
    LAMINAR FLOW
    BUOYANT FLOW
    TRANSIENT FLOW
    TRANSIENT GRID
    NUMBER OF PHASES 2
  >>USER FORTRAN
    USRBCS
    USRGRD
    USRINT
>>MODEL TOPOLOGY
  >>CREATE BLOCK
    BLOCK NAME 'DUCT'
    BLOCK DIMENSIONS 78 71 1
  >>CREATE PATCH
    PATCH NAME 'TOP'
    BLOCK NAME 'DUCT'
    PATCH TYPE 'PRESSURE BOUNDARY'
    PATCH LOCATION 2 77 71 71 1 1
    HIGH J
  >>CREATE PATCH
    PATCH NAME 'WALLS'
    BLOCK NAME 'DUCT'
    PATCH TYPE 'SOLID'
    PATCH LOCATION 1 1 1 71 1 1
  >>CREATE PATCH
    PATCH NAME 'WALLS'
    BLOCK NAME 'DUCT'
    PATCH TYPE 'SOLID'
    PATCH LOCATION 2 77 1 1 1 1
  >>CREATE PATCH
    PATCH NAME 'WALLS'
    BLOCK NAME 'DUCT'
    PATCH TYPE 'SOLID'
    PATCH LOCATION 78 78 1 71 1 1
  >>CREATE PATCH
    PATCH NAME 'RT'
    BLOCK NAME 'DUCT'
    PATCH TYPE 'SOLID'
    PATCH LOCATION 63 77 42 47 1 1
  >>CREATE PATCH
    PATCH NAME 'LT'
    BLOCK NAME 'DUCT'
    PATCH TYPE 'SOLID'
    PATCH LOCATION 2 16 42 47 1 1
>>MODEL DATA
  >>AMBIENT VARIABLES
    PHASE NAME 'PHASE1'
    VOLUME FRACTION 1.0000E+00
  >>AMBIENT VARIABLES
    PHASE NAME 'PHASE2'
    VOLUME FRACTION 0.0000E+00
  >>TITLE
    PROBLEM TITLE 'AF=0.95 X=0.00125'
  >>PHYSICAL PROPERTIES
    >>BUOYANCY PARAMETERS
      GRAVITY VECTOR 0.000000E+00 -9.810000E+00 0.000000E+00
      BUOYANCY REFERENCE DENSITY 1.2090E+00
    >>FLUID PARAMETERS
      PHASE NAME 'PHASE1'
      VISCOSITY 1.8000E-05
```

```
      DENSITY 1.2090E+00
    >>FLUID PARAMETERS
      PHASE NAME 'PHASE2'
      VISCOSITY 1.0000E-03
      DENSITY 1.0200E+03
    >>MULTIPHASE PARAMETERS
      >>PHASE DESCRIPTION
        PHASE NAME 'PHASE1'
        GAS
        CONTINUOUS
      >>PHASE DESCRIPTION
        PHASE NAME 'PHASE2'
        LIQUID
        CONTINUOUS
      >>MULTIPHASE MODELS
        >>MOMENTUM
          HOMOGENEOUS
          SURFACE SHARPENING ALGORITHM
        >>HOMOGENEOUS
          SURFACE SHARPENING ALGORITHM
          SURFACE SHARPENING LEVEL 2
    >>TRANSIENT PARAMETERS
      >>FIXED TIME STEPPING
        TIME STEPS 1000* 1.000000E-03
>>SOLVER DATA
  >>PROGRAM CONTROL
    MAXIMUM NUMBER OF ITERATIONS 50
    MASS SOURCE TOLERANCE 1.0000E-06
>>CREATE GRID
  >>SIMPLE GRID
    BLOCK NAME 'DUCT'
    DX 1* 5.000000E-03 20* 1.000000E-03 +
       36* 2.500000E-03 20* 1.000000E-03 1* +
       5.000000E-03
    DY 1* 5.000000E-03 16* 5.000000E-03 +
       10* 1.000000E-03 36* 5.000000E-04 5* +
       1.000000E-03 3* 5.000000E-03
    DZ 1.000000E+00
    X START 1.2500E-03
    Y START 0.0000E+00
    Z START 0.0000E+00
>>MODEL BOUNDARY CONDITIONS
>>OUTPUT OPTIONS
  >>PRINT OPTIONS
    >>WHAT
      NO VARIABLES
      NO WALL PRINTING
      NO RESIDUAL HISTORY
  >>DUMP FILE OPTIONS
    PHASE NAME 'PHASE2'
    TIME STEP INTERVAL 100
    GEOMETRY DATA
    U VELOCITY
    V VELOCITY
    W VELOCITY
    PRESSURE
    VOLUME FRACTION
>>STOP
```

A1.1.2. User Fortran File

```
      SUBROUTINE USRINT(U,V,W,P,VFRAC,DEN,VIS,TE,ED,RS,T,H,RF,SCAL
     +                  ,CONV,XC,YC,ZC,XP,YP,ZP
     +                  ,VOL,AREA,VPOR,ARPOR,WFACT,DISWAL,IPT
     +
,IBLK,IPVERT,IPNODN,IPFACN,IPNODF,IPNODB,IPFACB
     +                  ,WORK,IWORK,CWORK)
C*********************************************************************
C   UTILITY SUBROUTINE FOR USER-SUPPLIED INITIAL FIELD.
C*********************************************************************
C   THIS SUBROUTINE IS CALLED BY THE FOLLOWING SUBROUTINE
C       CUSR  INIT
C*********************************************************************
C   CREATED
C       13/06/90 ADB
C   MODIFIED
C       07/08/91 IRH   NEW STRUCTURE
C       10/09/91 IRH   CORRECTION TO IUSED
C       26/09/91 IRH   ALTER ARGUMENT LIST
C       01/10/91 DSC   REDUCE COMMENT LINE GOING OVER COLUMN 72.
C       03/10/91 IRH   CORRECT COMMENTS
C       28/01/92 PHA   UPDATE CALLED BY COMMENT, ADD RF ARGUMENT,
C                      CHANGE LAST DIMENSION OF RS TO 6 AND IVERS TO 2
C       03/06/92 PHA   ADD PRECISION FLAG AND CHANGE IVERS TO 3
C       08/02/93 NSW   REMOVE REDUNDANT COMMENTS
C       23/11/93 CSH   EXPLICITLY DIMENSION IPVERT ETC.
C       03/02/94 PHA   CHANGE FLOW3D TO CFDS-FLOW3D, REMOVE COMMA
C                      FROM BEGINNING OF DIMENSION STATEMENT
C       03/03/94 FHW   CORRECTION OF SPELLING MISTAKE
C       09/08/94 NSW   CORRECT SPELLING
C                      MOVE 'IF(IUSED.EQ.0) RETURN' OUT OF USER AREA
C       19/12/94 NSW   CHANGE FOR CFX-F3D
C       30/01/95 NSW   INCLUDE NEW EXAMPLE
C
C*********************************************************************
C   SUBROUTINE ARGUMENTS
C
C     U       - U COMPONENT OF VELOCITY
C     V       - V COMPONENT OF VELOCITY
C     W       - W COMPONENT OF VELOCITY
C     P       - PRESSURE
C     VFRAC   - VOLUME FRACTION
C     DEN     - DENSITY OF FLUID
C     VIS     - VISCOSITY OF FLUID
C     TE      - TURBULENT KINETIC ENERGY
C     ED      - EPSILON
C     RS      - REYNOLD STRESSES
C     T       - TEMPERATURE
C     H       - ENTHALPY
C     RF      - REYNOLD FLUXES
C     SCAL    - SCALARS (THE FIRST 'NCONC' OF THESE ARE MASS
FRACTIONS)
C     CONV    - CONVECTION COEFFICIENTS
C     XC      - X COORDINATES OF CELL CORNERS
C     YC      - Y COORDINATES OF CELL CORNERS
C     ZC      - Z COORDINATES OF CELL CORNERS
C     XP      - X COORDINATES OF CELL CENTRES
C     YP      - Y COORDINATES OF CELL CENTRES
```

```
C      ZP     - Z COORDINATES OF CELL CENTRES
C      VOL    - VOLUME OF CELLS
C      AREA   - AREA OF CELLS
C      VPOR   - POROUS VOLUME
C      ARPOR  - POROUS AREA
C      WFACT  - WEIGHT FACTORS
C      DISWAL - DISTANCE OF CELL CENTRE FROM WALL
C
C      IPT    - 1D POINTER ARRAY
C      IBLK   - BLOCK SIZE INFORMATION
C      IPVERT - POINTER FROM CELL CENTERS TO 8 NEIGHBOURING VERTICES
C      IPNODN - POINTER FROM CELL CENTERS TO 6 NEIGHBOURING CELLS
C      IPFACN - POINTER FROM CELL CENTERS TO 6 NEIGHBOURING FACES
C      IPNODF - POINTER FROM CELL FACES TO 2 NEIGHBOURING CELL CENTERS
C      IPNODB - POINTER FROM BOUNDARY CENTERS TO CELL CENTERS
C      IPFACB - POINTER FROM BOUNDARY CENTERS TO BOUNDARY FACES
C
C      WORK   - REAL WORKSPACE ARRAY
C      IWORK  - INTEGER WORKSPACE ARRAY
C      CWORK  - CHARACTER WORKSPACE ARRAY
C
C    SUBROUTINE ARGUMENTS PRECEDED WITH A '*' ARE ARGUMENTS THAT MUST
C    BE SET  BY THE USER IN THIS ROUTINE.
C
C    LOGICAL VARIABLE LRDISK IN COMMON BLOCK IOLOGC INDICATES WHETHER
C    THE RUN IS A RESTART AND CAN BE USED SO THAT INITIAL INFORMATION
C    IS ONLY SET WHEN STARTING A RUN FROM SCRATCH.
C
C    NOTE THAT OTHER DATA MAY BE OBTAINED FROM CFX-F3D USING THE
C    ROUTINE GETADD, FOR FURTHER DETAILS SEE THE VERSION 4
C    USER MANUAL.
C
C**********************************************************************
      LOGICAL LDEN,LVIS,LTURB,LTEMP,LBUOY,LSCAL,LCOMP
     +       ,LRECT,LCYN,LAXIS,LPOROS,LTRANS
      LOGICAL LRDISK,LWDISK
C
      CHARACTER*(*) CWORK
C
C+++++++++++++++ USER AREA 1
++++++++++++++++++++++++++++++++++++++++
C---- AREA FOR USERS EXPLICITLY DECLARED VARIABLES
C
C+++++++++++++++ END OF USER AREA 1
++++++++++++++++++++++++++++++++
C
      COMMON
     + /ALL/    NBLOCK,NCELL,NBDRY,NNODE,NFACE,NVERT,NDIM
     + /ALLWRK/ NRWS,NIWS,NCWS,IWRFRE,IWIFRE,IWCFRE
     + /ADDIMS/ NPHASE,NSCAL,NVAR,NPROP
     +         ,NDVAR,NDPROP,NDXNN,NDGEOM,NDCOEF,NILIST,NRLIST,NTOPOL
     + /CHKUSR/ IVERS,IUCALL,IUSED
     + /DEVICE/ NREAD,NWRITE,NRDISK,NWDISK
     + /IDUM/   ILEN,JLEN
     + /IOLOGC/ LRDISK,LWDISK
     + /LOGIC/  LDEN,LVIS,LTURB,LTEMP,LBUOY,LSCAL,LCOMP
     +         ,LRECT,LCYN,LAXIS,LPOROS,LTRANS
     + /MLTGRD/ MLEVEL,NLEVEL,ILEVEL
     + /SGLDBL/ IFLGPR,ICHKPR
     + /TRANSI/ NSTEP,KSTEP,MF,INCORE
```

```
     + /TRANSR/ TIME,DT,DTINVF,TPARM
C
C+++++++++++++++ USER AREA 2
++++++++++++++++++++++++++++++++++++++++
C---- AREA FOR USERS TO DECLARE THEIR OWN COMMON BLOCKS
C     THESE SHOULD START WITH THE CHARACTERS 'UC' TO ENSURE
C     NO CONFLICT WITH NON-USER COMMON BLOCKS
C
C+++++++++++++++ END OF USER AREA 2
++++++++++++++++++++++++++++++++++
C
      DIMENSION
     + U(NNODE,NPHASE),V(NNODE,NPHASE),W(NNODE,NPHASE)
     +,P(NNODE,NPHASE),VFRAC(NNODE,NPHASE)
     +,TE(NNODE,NPHASE),ED(NNODE,NPHASE),RS(NNODE,NPHASE,6)
     +,T(NNODE,NPHASE),H(NNODE,NPHASE),RF(NNODE,NPHASE,4)
     +,SCAL(NNODE,NPHASE,NSCAL)
     +,DEN(NNODE,NPHASE),VIS(NNODE,NPHASE),CONV(NFACE,NPHASE)
      DIMENSION
     + XC(NVERT),YC(NVERT),ZC(NVERT),XP(NNODE),YP(NNODE),ZP(NNODE)
     +,VOL(NCELL),AREA(NFACE,3),VPOR(NCELL),ARPOR(NFACE,3)
     +,WFACT(NFACE),DISWAL(NCELL)
      DIMENSION
     + IPT(*),IBLK(5,NBLOCK)

+,IPVERT(NCELL,8),IPNODN(NCELL,6),IPFACN(NCELL,6),IPNODF(NFACE,4)
     +,IPNODB(NBDRY,4),IPFACB(NBDRY)
      DIMENSION
     + IWORK(NIWS),WORK(NRWS),CWORK(NCWS)
C
C+++++++++++++++ USER AREA 3
++++++++++++++++++++++++++++++++++++++++
C---- AREA FOR USERS TO DIMENSION THEIR ARRAYS
C
C---- AREA FOR USERS TO DEFINE DATA STATEMENTS
C
C+++++++++++++++ END OF USER AREA 3
++++++++++++++++++++++++++++++++++
C
C---- STATEMENT FUNCTION FOR ADDRESSING
      IP(I,J,K)=IPT((K-1)*ILEN*JLEN+(J-1)*ILEN+I)
C
C----VERSION NUMBER OF USER ROUTINE AND PRECISION FLAG
C
      IVERS=3
      ICHKPR = 1
C
C+++++++++++++++ USER AREA 4
++++++++++++++++++++++++++++++++++++++++
C---- TO USE THIS USER ROUTINE FIRST SET IUSED=1
C
       IUSED=1
C
C+++++++++++++++ END OF USER AREA 4
++++++++++++++++++++++++++++++++++
C
       IF (IUSED.EQ.0) RETURN
C
C---- FRONTEND CHECKING OF USER ROUTINE
      IF (IUCALL.EQ.0) RETURN
```

```
C
C+++++++++++++++ USER AREA 5
+++++++++++++++++++++++++++++++++++++++
C
C---- AREA FOR INITIALISING VARIABLES U,V,W,P,VFRAC,TE,ED,RS,T,SCAL
C     ONLY.
C
      FULL=1.0
      EMPTY=1.E-10
C

      CALL IPREC('DUCT','BLOCK','CENTRES',IPT,ILEN,JLEN,KLEN,
     +           CWORK,IWORK)
C
      DO 90 K=1,KLEN
        DO 90 J=1,JLEN
          DO 90 I=2,ILEN-1

            INODE=IP(I,J,K)
            VFRAC(INODE,1)=FULL
            VFRAC(INODE,2)=EMPTY
  90      CONTINUE

      DO 95 K=1,KLEN
        DO 95 I=2,ILEN-1
          DO 95 J=1,47

            INODE=IP(I,J,K)
            VFRAC(INODE,1)=EMPTY
            VFRAC(INODE,2)=FULL
  95      CONTINUE
C
C+++++++++++++++ END OF USER AREA 5
++++++++++++++++++++++++++++++++
C
      RETURN
      END
      SUBROUTINE USRBCS(VARBCS,VARAMB,A,B,C,ACND,BCND,CCND
     +                  ,IWGVEL,NDVWAL
     +                  ,FLOUT,NLABEL,NSTART,NEND,NCST,NCEN
     +                  ,U,V,W,P,VFRAC,DEN,VIS,TE,ED,RS,T,H,RF,SCAL
     +                  ,XP,YP,ZP,VOL,AREA,VPOR,ARPOR,WFACT,IPT
     +
,IBLK,IPVERT,IPNODN,IPFACN,IPNODF,IPNODB,IPFACB
     +                  ,WORK,IWORK,CWORK)
C
C**********************************************************************
***
C
C  USER ROUTINE TO SET REALS AT BOUNDARIES.
C
C   >>> IMPORTANT
<<<
C   >>>
<<<
C   >>> USERS MAY ONLY ADD OR ALTER PARTS OF THE SUBROUTINE WITHIN
<<<
C   >>> THE DESIGNATED USER AREAS
<<<
C
```

```
C*******************************************************************
***
C
C  THIS SUBROUTINE IS CALLED BY THE FOLLOWING SUBROUTINE
C    CUSR  SRLIST
C
C*******************************************************************
***
C   CREATED
C      30/11/88 ADB
C   MODIFIED
C      08/09/90 ADB  RESTRUCTURED FOR USER-FRIENDLINESS.
C      10/08/91 IRH  FURTHER RESTRUCTURING ADD ACND BCND CCND
C      22/09/91 IRH  CHANGE ICALL TO IUCALL + ADD /SPARM/
C      10/03/92 PHA  UPDATE CALLED BY COMMENT, ADD RF ARGUMENT,
C                    CHANGE LAST DIMENSION OF RS TO 6 AND IVERS TO 2
C      03/06/92 PHA  ADD PRECISION FLAG AND CHANGE IVERS TO 3
C      30/06/92 NSW  INCLUDE FLAG FOR CALLING BY ITERATION
C                    INSERT EXTRA COMMENTS
C      03/08/92 NSW  MODIFY DIMENSION STATEMENTS FOR VAX
C      21/12/92 CSH  INCREASE IVERS TO 4
C      02/08/93 NSW  INCORRECT AND MISLEADING COMMENT REMOVED
C      05/11/93 NSW  INDICATE USE OF FLOUT IN MULTIPHASE FLOWS
C      23/11/93 CSH  EXPLICITLY DIMENSION IPVERT ETC.
C      01/02/94 NSW  SET VARIABLE POINTERS IN WALL EXAMPLE.
C                    CHANGE FLOW3D TO CFDS-FLOW3D.
C                    MODIFY MULTIPHASE MASS FLOW BOUNDARY TREATMENT.
C      03/03/94 FHW  CORRECTION OF SPELLING MISTAKE
C      02/07/94 BAS  SLIDING GRIDS - ADD NEW ARGUMENT IWGVEL
C                    TO ALLOW VARIANTS OF TRANSIENT-GRID WALL BC
C                    CHANGE VERSION NUMBER TO 5
C      09/08/94 NSW  CORRECT SPELLING
C                    MOVE 'IF(IUSED.EQ.0) RETURN' OUT OF USER AREA
C      19/12/94 NSW  CHANGE FOR CFX-F3D
C      02/02/95 NSW  CHANGE COMMON /IMFBMP/
C
C*******************************************************************
***
C
C   SUBROUTINE ARGUMENTS
C
C     VARBCS - REAL BOUNDARY CONDITIONS
C     VARAMB - AMBIENT VALUE OF VARIABLES
C     A      - COEFFICIENT IN WALL BOUNDARY CONDITION
C     B      - COEFFICIENT IN WALL BOUNDARY CONDITION
C     C      - COEFFICIENT IN WALL BOUNDARY CONDITION
C     ACND   - COEFFICIENT IN CONDUCTING WALL BOUNDARY CONDITION
C     BCND   - COEFFICIENT IN CONDUCTING WALL BOUNDARY CONDITION
C     CCND   - COEFFICIENT IN CONDUCTING WALL BOUNDARY CONDITION
C     IWGVEL - USAGE OF INPUT VELOCITIES (0 = AS IS,1 = ADD GRID
MOTION)
C     NDVWAL - FIRST DIMENSION OF ARRAY IWGVEL
C     FLOUT  - MASS FLOW/FRACTIONAL MASS FLOW
C     NLABEL - NUMBER OF DISTINCT OUTLETS
C     NSTART - ARRAY POINTER
C     NEND   - ARRAY POINTER
C     NCST   - ARRAY POINTER
C     NCEN   - ARRAY POINTER
C     U      - U COMPONENT OF VELOCITY
C     V      - V COMPONENT OF VELOCITY
```

```
C      W       - W COMPONENT OF VELOCITY
C      P       - PRESSURE
C      VFRAC   - VOLUME FRACTION
C      DEN     - DENSITY OF FLUID
C      VIS     - VISCOSITY OF FLUID
C      TE      - TURBULENT KINETIC ENERGY
C      ED      - EPSILON
C      RS      - REYNOLD STRESSES
C      T       - TEMPERATURE
C      H       - ENTHALPY
C      RF      - REYNOLD FLUXES
C      SCAL    - SCALARS (THE FIRST 'NCONC' OF THESE ARE MASS
FRACTIONS)
C      XP      - X COORDINATES OF CELL CENTRES
C      YP      - Y COORDINATES OF CELL CENTRES
C      ZP      - Z COORDINATES OF CELL CENTRES
C      VOL     - VOLUME OF CELLS
C      AREA    - AREA OF CELLS
C      VPOR    - POROUS VOLUME
C      ARPOR   - POROUS AREA
C      WFACT   - WEIGHT FACTORS
C
C      IPT     - 1D POINTER ARRAY
C      IBLK    - BLOCK SIZE INFORMATION
C      IPVERT - POINTER FROM CELL CENTERS TO 8 NEIGHBOURING VERTICES
C      IPNODN - POINTER FROM CELL CENTERS TO 6 NEIGHBOURING CELLS
C      IPFACN - POINTER FROM CELL CENTERS TO 6 NEIGHBOURING FACES
C      IPNODF - POINTER FROM CELL FACES TO 2 NEIGHBOURING CELL CENTERS
C      IPNODB - POINTER FROM BOUNDARY CENTERS TO CELL CENTERS
C      IPFACB - POINTER TO NODES FROM BOUNDARY FACES
C
C      WORK    - REAL WORKSPACE ARRAY
C      IWORK   - INTEGER WORKSPACE ARRAY
C      CWORK   - CHARACTER WORKSPACE ARRAY
C
C    SUBROUTINE ARGUMENTS PRECEDED WITH A '*' ARE ARGUMENTS THAT MUST
C    BE SET  BY THE USER IN THIS ROUTINE.
C
C    NOTE THAT OTHER DATA MAY BE OBTAINED FROM CFX-F3D USING THE
C    ROUTINE GETADD, FOR FURTHER DETAILS SEE THE VERSION 4
C    USER MANUAL.
C
C*******************************************************************
***
      LOGICAL LDEN,LVIS,LTURB,LTEMP,LBUOY,LSCAL,LCOMP
     +        ,LRECT,LCYN,LAXIS,LPOROS,LTRANS
C
      CHARACTER*(*) CWORK
C
C++++++++++++++++ USER AREA 1
+++++++++++++++++++++++++++++++++++++++++
C---- AREA FOR USERS EXPLICITLY DECLARED VARIABLES
C
C++++++++++++++++ END OF USER AREA 1
++++++++++++++++++++++++++++++++++
C
      COMMON
     + /ALL/    NBLOCK,NCELL,NBDRY,NNODE,NFACE,NVERT,NDIM
     + /ALLWRK/ NRWS,NIWS,NCWS,IWRFRE,IWIFRE,IWCFRE
     + /ADDIMS/ NPHASE,NSCAL,NVAR,NPROP
```

```
     +          ,NDVAR,NDPROP,NDXNN,NDGEOM,NDCOEF,NILIST,NRLIST,NTOPOL
     + /BCSOUT/ IFLOUT
     + /CHKUSR/ IVERS,IUCALL,IUSED
     + /DEVICE/ NREAD,NWRITE,NRDISK,NWDISK
     + /IDUM/   ILEN,JLEN
     + /IMFBMP/ IMFBMP,JMFBMP
     + /LOGIC/  LDEN,LVIS,LTURB,LTEMP,LBUOY,LSCAL,LCOMP
     +          ,LRECT,LCYN,LAXIS,LPOROS,LTRANS
     + /MLTGRD/ MLEVEL,NLEVEL,ILEVEL
     + /SGLDBL/ IFLGPR,ICHKPR
     + /SPARM/  SMALL,SORMAX,NITER,INDPRI,MAXIT,NODREF,NODMON
     + /TRANSI/ NSTEP,KSTEP,MF,INCORE
     + /TRANSR/ TIME,DT,DTINVF,TPARM
     + /UBCSFL/ IUBCSF
C
C++++++++++++++++ USER AREA 2
+++++++++++++++++++++++++++++++++++++++++
C---- AREA FOR USERS TO DECLARE THEIR OWN COMMON BLOCKS
C     THESE SHOULD START WITH THE CHARACTERS 'UC' TO ENSURE
C     NO CONFLICT WITH NON-USER COMMON BLOCKS
C
C++++++++++++++++ END OF USER AREA 2
++++++++++++++++++++++++++++++++++
C
      DIMENSION
     + VARBCS(NVAR,NPHASE,NCELL+1:NNODE),VARAMB(NVAR,NPHASE)
     +,A(4+NSCAL,NPHASE,NSTART:*)
     +,B(4+NSCAL,NPHASE,NSTART:*),C(4+NSCAL,NPHASE,NSTART:*)
     +,FLOUT(*),ACND(NCST:*),BCND(NCST:*),CCND(NCST:*)
     +,IWGVEL(NDVWAL,NPHASE)
C
      DIMENSION
     +
U(NNODE,NPHASE),V(NNODE,NPHASE),W(NNODE,NPHASE),P(NNODE,NPHASE)
     +,VFRAC(NNODE,NPHASE),DEN(NNODE,NPHASE),VIS(NNODE,NPHASE)
     +,TE(NNODE,NPHASE),ED(NNODE,NPHASE),RS(NNODE,NPHASE,6)
     +,T(NNODE,NPHASE),H(NNODE,NPHASE),RF(NNODE,NPHASE,4)
     +,SCAL(NNODE,NPHASE,NSCAL)
C
      DIMENSION
     + XP(NNODE),YP(NNODE),ZP(NNODE)

+,VOL(NCELL),AREA(NFACE,3),VPOR(NCELL),ARPOR(NFACE,3),WFACT(NFACE)
     +,IPT(*),IBLK(5,NBLOCK)

+,IPVERT(NCELL,8),IPNODN(NCELL,6),IPFACN(NCELL,6),IPNODF(NFACE,4)
     +,IPNODB(NBDRY,4),IPFACB(NBDRY)
     +,IWORK(*),WORK(*),CWORK(*)
C
C++++++++++++++++ USER AREA 3
+++++++++++++++++++++++++++++++++++++++++
C---- AREA FOR USERS TO DIMENSION THEIR ARRAYS
C
C---- AREA FOR USERS TO DEFINE DATA STATEMENTS
C
C++++++++++++++++ END OF USER AREA 3
++++++++++++++++++++++++++++++++++
C
C---- STATEMENT FUNCTION FOR ADDRESSING
      IP(I,J,K)=IPT((K-1)*ILEN*JLEN+(J-1)*ILEN+I)
```

```
C
C----VERSION NUMBER OF USER ROUTINE AND PRECISION FLAG
C
      IVERS=5
      ICHKPR = 1
C
C+++++++++++++++++ USER AREA 4
+++++++++++++++++++++++++++++++++++++++++
C---- TO USE THIS USER ROUTINE FIRST SET IUSED=1
C     AND SET IUBCSF FLAG:
C     BOUNDARY CONDITIONS NOT CHANGING                      IUBCSF=0
C     BOUNDARY CONDITIONS CHANGING WITH ITERATION           IUBCSF=1
C     BOUNDARY CONDITIONS CHANGING WITH TIME                IUBCSF=2
C     BOUNDARY CONDITIONS CHANGING WITH TIME AND ITERATION  IUBCSF=3
C
       IUSED=1
       IUBCSF=2
C
C+++++++++++++++++ END OF USER AREA 4
++++++++++++++++++++++++++++++++++
C
       IF (IUSED.EQ.0) RETURN
C
C---- FRONTEND CHECKING OF USER ROUTINE
      IF (IUCALL.EQ.0) RETURN
C
C+++++++++++++++++ USER AREA 5
+++++++++++++++++++++++++++++++++++++++++
C
C---- AREA FOR SETTING VALUES AT INLETS, PRESSURE BOUNDARIES
C     AND OUTLETS. (NOTE THAT THE MASS FLOW AT OUTLETS IS
C     SPECIFIED IN USER AREA 7)
C
C     IF USING A REYNOLDS STRESS OR FLUX MODEL, NOTE THAT AT INLETS
C     IT IS IMPORTANT THAT THE USER SETS ALL COMPONENTS OF THE
C     REYNOLDS STRESS AND FLUX AND THE TURBULENT KINETIC ENERGY
C     AS WELL AS THE ENERGY DISSIPATION RATE.
C
C     SET THE VALUES IN VARBCS(NVAR,NPHASE,ILEN,JLEN,KLEN)
C
C
C+++++++++++++++++ END OF USER AREA 5
++++++++++++++++++++++++++++++++++
C
C+++++++++++++++++ USER AREA 6
+++++++++++++++++++++++++++++++++++++++++
C
C---- AREA FOR SETTING VALUES AT WALLS
C
C     USE A(2+NSCAL,NPHASE,ILEN,JLEN,KLEN)
C     WHERE NSCAL = NO. OF SCALARS, AND NPHASE = NO. OF PHASES.
C
C     THE CONVENTION FOR VARIABLE NUMBERS IS DIFFERENT IN THIS
ROUTINE
C     FROM THAT IN THE REST OF THE PROGRAM. IT IS:
C
C     IU = 1, IV = 2 , IW = 3, IT = 4, IS = 5
C

C--- SET IWGVEL FLAG
```

```
      DO 150 I=1, NDVWAL
        DO 140 J=1,NPHASE
           IWGVEL(I,J)=1
  140 CONTINUE
  150 CONTINUE

C
C+++++++++++++++++ END OF USER AREA 6
++++++++++++++++++++++++++++++++++
C
C
C+++++++++++++++++ USER AREA 7
+++++++++++++++++++++++++++++++++++++++
C
C----- DEFINE FLOW AT OUTLETS (MASS FLOW BOUNDARIES)
C       (TO TEMPERATURES AND SCALARS AT MASS FLOW BOUNDARIES USE
C        USER AREA 5)
C
C      SET PARAMETER IFLOUT:
C      IFLOUT = 1  ==> MASS FLOW SPECIFIED AT LABELLED OUTLETS.
C      IFLOUT = 2  ==> FRACTIONAL MASS FLOW SPECIFIED AT LABELLED
OUTLETS
C      IFLOUT = 2
C
C      SET OUTLET FLOW RATES:
C      FLOUT(LABEL) = MASS FLOW OUT OF OUTLETS LABELLED LABEL
(IFLOUT=1).
C      FLOUT(LABEL) = FRACTIONAL MASS FLOW OUT OF OUTLETS LABELLED
LABEL
C                     (IFLOUT=2).
C      FOR MULTIPHASE FLOWS IT IS NECESSARY TO SET
C      EITHER
C                     FLOUT(LABEL) = TOTAL MASS FLOW
C                     IFLOUT = 1
C                     IMFBMP = 0
C      OR
C                     FLOUT(LABEL + (IPHASE-1)*NLABEL) FOR EACH PHASE
C                     IFLOUT = 1 OR 2
C                     IMFBMP = 1
C
C---- EXAMPLE: EQUIDISTRIBUTION OF FRACTIONAL MASS FLOW AMONGST
OUTLETS
C
C      IFLOUT=2
C      FRAC = 1.0 / MAX( 1.0, FLOAT(NLABEL) )
C      DO 300 ILABEL = 1, NLABEL
C         FLOUT(ILABEL) = FRAC
C300  CONTINUE
C
C----END OF EXAMPLE
C
C+++++++++++++++++ END OF USER AREA 7
++++++++++++++++++++++++++++++++++
C
      RETURN
      END
      SUBROUTINE USRGRD(U,V,W,P,VFRAC,DEN,VIS,TE,ED,RS,T,H,RF,SCAL,
     +                  XP,YP,ZP,VOL,AREA,VPOR,ARPOR,WFACT,
     +                  XCOLD,YCOLD,ZCOLD,XC,YC,ZC,IPT,
```

```
     +
IBLK,IPVERT,IPNODN,IPFACN,IPNODF,IPNODB,IPFACB,
     +                   WORK,IWORK,CWORK)
C
C*******************************************************************
**
C
C   USER SUBROUTINE TO ALLOW USERS TO GENERATE A GRID FOR CFX-F3D
C
C   >>> IMPORTANT
<<<
C   >>>
<<<
C   >>> USERS MAY ONLY ADD OR ALTER PARTS OF THE SUBROUTINE WITHIN
<<<
C   >>> THE DESIGNATED USER AREAS
<<<
C
C*******************************************************************
**
C
C   THIS SUBROUTINE IS CALLED BY THE FOLLOWING SUBROUTINES
C      CREATE  CUSR
C
C*******************************************************************
**
C   CREATED
C      27/04/90  ADB
C   MODIFIED
C      05/08/91  IRH  NEW STRUCTURE
C      09/09/91  IRH  CORRECT EXAMPLE
C      01/10/91  DSC  REDUCE COMMENT LINE GOING OVER 72 COLUMNS.
C      29/11/91  PHA  UPDATE CALLED BY COMMENT, ADD RF ARGUMENT,
C                     CHANGE LAST DIMENSION OF RS TO 6 AND IVERS TO 2
C      03/06/92  PHA  ADD PRECISION FLAG AND CHANGE IVERS TO 3
C      03/07/92  DSC  CORRECT COMMON MLTGRD.
C      23/11/93  CSH  EXPLICITLY DIMENSION IPVERT ETC.
C      03/02/94  PHA  CHANGE FLOW3D TO CFDS-FLOW3D
C      03/03/94  FHW  CORRECTION OF SPELLING MISTAKE
C      22/08/94  NSW  MOVE 'IF(IUSED.EQ.0) RETURN' OUT OF USER AREA
C      19/12/94  NSW  CHANGE FOR CFX-F3D
C
C*******************************************************************
**
C
C   SUBROUTINE ARGUMENTS
C
C     U      - U COMPONENT OF VELOCITY
C     V      - V COMPONENT OF VELOCITY
C     W      - W COMPONENT OF VELOCITY
C     P      - PRESSURE
C     VFRAC  - VOLUME FRACTION
C     DEN    - DENSITY OF FLUID
C     VIS    - VISCOSITY OF FLUID
C     TE     - TURBULENT KINETIC ENERGY
C     ED     - EPSILON
C     RS     - REYNOLD STRESSES
C     T      - TEMPERATURE
C     H      - ENTHALPY
C     RF     - REYNOLD FLUXES
```

```
C     SCAL   - SCALARS (THE FIRST 'NCONC' OF THESE ARE MASS
FRACTIONS)
C     XP     - X COORDINATES OF CELL CENTRES
C     YP     - Y COORDINATES OF CELL CENTRES
C     ZP     - Z COORDINATES OF CELL CENTRES
C     VOL    - VOLUME OF CELLS
C     AREA   - AREA OF CELLS
C     VPOR   - POROUS VOLUME
C     ARPOR  - POROUS AREA
C     WFACT  - WEIGHT FACTORS
C  *  XC     - X COORDINATES OF CELL VERTICES
C  *  YC     - Y COORDINATES OF CELL VERTICES
C  *  ZC     - Z COORDINATES OF CELL VERTICES
C     XCOLD  - X COORDINATES OF CELL VERTICES AT START OF TIME STEP
C     YCOLD  - Y COORDINATES OF CELL VERTICES AT START OF TIME STEP
C     ZCOLD  - Z COORDINATES OF CELL VERTICES AT START OF TIME STEP
C
C     IPT    - 1D POINTER ARRAY
C     IBLK   - BLOCK SIZE INFORMATION
C     IPVERT - POINTER FROM CELL CENTERS TO 8 NEIGHBOURING VERTICES
C     IPNODN - POINTER FROM CELL CENTERS TO 6 NEIGHBOURING CELLS
C     IPFACN - POINTER FROM CELL CENTERS TO 6 NEIGHBOURING FACES
C     IPNODF - POINTER FROM CELL FACES TO 2 NEIGHBOURING CELL CENTERS
C     IPNODB - POINTER FROM BOUNDARY CENTERS TO CELL CENTERS
C     IPFACB - POINTER FROM BOUNDARY CENTERS TO BOUNDARY FACESS
C
C     WORK   - REAL WORKSPACE ARRAY
C     IWORK  - INTEGER WORKSPACE ARRAY
C     CWORK  - CHARACTER WORKSPACE ARRAY
C
C   SUBROUTINE ARGUMENTS PRECEDED WITH A '*' ARE ARGUMENTS THAT MUST
C   BE SET  BY THE USER IN THIS ROUTINE.
C
C   NOTE THAT OTHER DATA MAY BE OBTAINED FROM CFX-F3D USING THE
C   ROUTINE GETADD, FOR FURTHER DETAILS SEE THE VERSION 4
C   USER MANUAL.
C
C***********************************************************************
**
C
      LOGICAL LDEN,LVIS,LTURB,LTEMP,LBUOY,LSCAL,LCOMP
     +       ,LRECT,LCYN,LAXIS,LPOROS,LTRANS
C
      CHARACTER*(*) CWORK
C
C++++++++++++++++ USER AREA 1
++++++++++++++++++++++++++++++++++++++++
C---- AREA FOR USERS EXPLICITLY DECLARED VARIABLES
C
C++++++++++++++++ END OF USER AREA 1
++++++++++++++++++++++++++++++++
C
      COMMON
     + /ALL/    NBLOCK,NCELL,NBDRY,NNODE,NFACE,NVERT,NDIM
     + /ALLWRK/ NRWS,NIWS,NCWS,IWRFRE,IWIFRE,IWCFRE
     + /ADDIMS/ NPHASE,NSCAL,NVAR,NPROP
     +         ,NDVAR,NDPROP,NDXNN,NDGEOM,NDCOEF,NILIST,NRLIST,NTOPOL
     + /CHKUSR/ IVERS,IUCALL,IUSED
     + /CONC/   NCONC
     + /DEVICE/ NREAD,NWRITE,NRDISK,NWDISK
```

```
     + /IDUM/   ILEN,JLEN
     + /LOGIC/  LDEN,LVIS,LTURB,LTEMP,LBUOY,LSCAL,LCOMP
     +          ,LRECT,LCYN,LAXIS,LPOROS,LTRANS
     + /MLTGRD/ MLEVEL,NLEVEL,ILEVEL
     + /SGLDBL/ IFLGPR,ICHKPR
     + /SPARM/  SMALL,SORMAX,NITER,INDPRI,MAXIT,NODREF,NODMON
     + /TIMUSR/ DTUSR
     + /TRANSI/ NSTEP,KSTEP,MF,INCORE
     + /TRANSR/ TIME,DT,DTINVF,TPARM
C
C++++++++++++++++ USER AREA 2
++++++++++++++++++++++++++++++++++++++++
C---- AREA FOR USERS TO DECLARE THEIR OWN COMMON BLOCKS
C     THESE SHOULD START WITH THE CHARACTERS 'UC' TO ENSURE
C     NO CONFLICT WITH NON-USER COMMON BLOCKS
C
C++++++++++++++++ END OF USER AREA 2
+++++++++++++++++++++++++++++++++
C
      DIMENSION
     +
U(NNODE,NPHASE),V(NNODE,NPHASE),W(NNODE,NPHASE),P(NNODE,NPHASE)
     +,VFRAC(NNODE,NPHASE),DEN(NNODE,NPHASE),VIS(NNODE,NPHASE)
     +,TE(NNODE,NPHASE),ED(NNODE,NPHASE),RS(NNODE,NPHASE,6)
     +,T(NNODE,NPHASE),H(NNODE,NPHASE),RF(NNODE,NPHASE,4)
     +,SCAL(NNODE,NPHASE,NSCAL)
      DIMENSION
     + XP(NNODE),YP(NNODE),ZP(NNODE),XC(NVERT),YC(NVERT),ZC(NVERT)
     +,XCOLD(NVERT),YCOLD(NVERT),ZCOLD(NVERT)
     +,VOL(NCELL),AREA(NFACE,3),VPOR(NCELL),ARPOR(NFACE,3)
     +,WFACT(NFACE)
     +,IPT(*),IBLK(5,NBLOCK)

+,IPVERT(NCELL,8),IPNODN(NCELL,6),IPFACN(NCELL,6),IPNODF(NFACE,4)
     +,IPNODB(NBDRY,4),IPFACB(NBDRY)
     +,IWORK(*),WORK(*),CWORK(*)
C
C++++++++++++++++ USER AREA 3
++++++++++++++++++++++++++++++++++++++++
C---- AREA FOR USERS TO DIMENSION THEIR ARRAYS
      DIMENSION
     + FRCEPR(2),DISP(2),VEL(2),ACC(2)
C---- AREA FOR USERS TO DEFINE DATA STATEMENTS
       REAL FRLEFT,FRRIGHT
     + ,STIFF,C,M,KX,TIME_ST,Z,DELF,DELFX,DLDISP,DLVEL,DLACC

C     FRLEFT = TOTAL PRESSURE ON LEFT WALL
C     FRRIGHT = TOTAL PRESSURE ON RIGHT WALL
C     STIFF = SPRING STIFFNESS
C     C = DAMPING CO-EFFICIENT
C     M = MASS OF WATER AND STRUCTURE
C     KX = K STAR EQN 7.16A
C     DELF = DELTA F IN EQN 7.16B
C     DELFX = DELTA F STAR EQN 7.16B
C       TIME_ST = TIME STEP
C       DLDISP = DELTA DISPLACEMENT
C     DLVEL = DELTA VELOCITY
C       DLACC = DELTA ACCELERATION
C++++++++++++++++ END OF USER AREA 3
+++++++++++++++++++++++++++++++++
```

```
C
C---- STATEMENT FUNCTION FOR ADDRESSING
      IP(I,J,K)=IPT((K-1)*ILEN*JLEN+(J-1)*ILEN+I)
C
C---- VERSION NUMBER OF USER ROUTINE AND PRECISION FLAG
C
      IVERS=3
      ICHKPR = 1
C
C++++++++++++++++ USER AREA 4
++++++++++++++++++++++++++++++++++++++++
C---- TO USE THIS USER ROUTINE FIRST SET IUSED=1
C
       IUSED=1
C
C++++++++++++++++ END OF USER AREA 4
+++++++++++++++++++++++++++++++++
C
       IF (IUSED.EQ.0) RETURN
C
C---- FRONTEND CHECKING OF USER ROUTINE
       IF (IUCALL.EQ.0) RETURN
C
C++++++++++++++++ USER AREA 5
++++++++++++++++++++++++++++++++++++++++
C
      OPEN(UNIT=13,FILE='DATA',STATUS='NEW')
C
C
C-- SET MOVING GRID
C-- USE IPREC TO FIND ADDRESSES

      CALL IPREC('DUCT','BLOCK','VERTICES',IPT,ILEN,JLEN,
     +           KLEN,CWORK,IWORK)
C-- LOOP OVER BLOCK

       DO 280 K=1,KLEN
         DO 280 J=1,JLEN
            DO 280 I=1,ILEN
C-- USE STATEMENT FUNCTION IP TO GET ADDRESSES
            INODE = IP(I,J,K)
C-- DEFINE LOCATION OF GRID VERTICES

       XC(INODE)=XCOLD(INODE)+DLDISP

  280 CONTINUE

C     PROGRAM to determine the
C     response of a single degree
C     of freedom oscillator
C     SET VALUES FOR STIFF,C,M, AND TIME STEP

      STIFF=6374
      C=0.0
      TIME_ST = 0.001

C     M is the Total mass of water
C     and structure
      M=30.8
C     USE CTR AS A COUNTER
```

```
      ICTR = ICTR + 1
      IF(ICTR.EQ.1) THEN
C     SET INTIAL DISPLACEMENT, VELOCITY and PRESSURE FORCE
      DISP(1) = 0.00125
      VEL(1)= 0
      FRCEPR(1)=0
      FRCEPR(2)=0
C     SOLVE INITIAL ACCELERATION "ACC(1)" USING EQUATION 7.18

      ACC(1) = (1/M)*(FRCEPR(1)-C*VEL(1)-STIFF*DISP(1))

      WRITE(13,*)'TIME      DISP        VEL        ACC      FORCE'

      END IF

      IF(ICTR.GT.1) THEN

C     SET PREVIOUS VALUES OF DISP, VEL, ACC AND FORCE TO
C     FIRST POSITIONS IN THE ARRAYS

      DISP(1)   = DISP(2)
      VEL(1)    = VEL(2)
      ACC(1)    = ACC(2)
      FRCEPR(1) = FRCEPR(2)

      END IF

C     FORM K STAR USING EQ 7.16A

      KX = STIFF + ( (2*C)/TIME_ST ) + ( (4*M)/TIME_ST**2 )

C     FORM DELTA F STAR USING EQ 7.16B

      Z = (4*M/TIME_ST) + 2*C

C -- LOOP OVER BLOCK TO OBTAIN PRESSURE DISTRIBUTION
C   AT CELLS ALONG THE LEFT AND RIGHT WALLS

C   LOOP OVER LEFT SIDE WALL
C   FRLEFT AND FRRIGHT ARE THE
C   SUMS OF THE PRESSURE AT EACH CELL OF THE
C   LEFT AND RIGHT WALLS RESPECTIVELY

C   NOTE ONLY PRESSURE VALUES FOR PHASE 2
C   PRESSURE VALUES FOR PHASE 1 WERE FOUND
C   TO BE IDENTICAL TO PHASE 2

       FRLEFT=0
       FRRIGHT=0

      CALL IPREC('DUCT','BLOCK','CENTRES',IPT,ILEN,JLEN,
     +            KLEN,CWORK,IWORK)

       DO 370 K=1,KLEN
         DO 370 J=1,JLEN
            DO 370 I=2,2

            INODE = IP(I,J,K)

            FRLEFT = FRLEFT + P(INODE,2)*AREA(INODE,1)*0.210
```

```
  370  CONTINUE

C       LOOP OVER RIGHT SIDE WALL

        DO 375 K=1,KLEN
          DO 375 J=1,JLEN
             DO 375 I=ILEN-1,ILEN-1

             INODE = IP(I,J,K)

             FRRIGHT = FRRIGHT + P(INODE,2)*AREA(INODE,1)*0.210

  375  CONTINUE

C      CALCULATE FORCE FROM FLUID ON WALLS

       FRCEPR(2) = FRRIGHT - FRLEFT

C      LET DELF = DELTA F

       DELF = FRCEPR(2) - FRCEPR(1)

C     LET DELFX = DELTA F STAR IN EQN 7.16B

       DELFX = DELF + Z*VEL(1) + 2*M*ACC(1)

C     SOLVE FOR DELTA DISP EQ 7.15

       DLDISP= DELFX/KX

C      SOLVE FOR DELTA ACC AND DELTA VEL
C      USING EQNS 7.12 AND 7.13

       DLACC = (4/(TIME_ST**2))*
      & (DLDISP-(VEL(1)*TIME_ST))-(2*ACC(1))

       DLVEL=(2/TIME_ST) * DLDISP - 2*VEL(1)

C      SOLVE FOR DISP(I+1), VEL(I+1) AND ACC(I+1)
C      USING EQN 7.17

       DISP(2) = DISP(1) + DLDISP
       VEL(2) = VEL(1) + DLVEL
       ACC(2) = ACC(1) + DLACC

       WRITE(13,*)TIME,DISP(1),VEL(1),ACC(1),FRCEPR(2)

C++++++++++++++++ END OF USER AREA 5
++++++++++++++++++++++++++++++++
C
       RETURN

       END
```

Appendix 2

DERIVATION OF THEORETICAL FUNDAMENTAL SLOSHING FREQUENCY

In Chapter 3, a closed form solution for the fundamental sloshing frequency is given in Equation 3.1. In this Appendix, the derivation of this equation is presented from (Milne-Thomson, 1968), for completeness.

The fundamental sloshing frequency is derived with the help of a kinematic and a dynamic condition which must be satisfied at the liquid surface. These two conditions will be presented next for the geometry given in Figure A2.1.

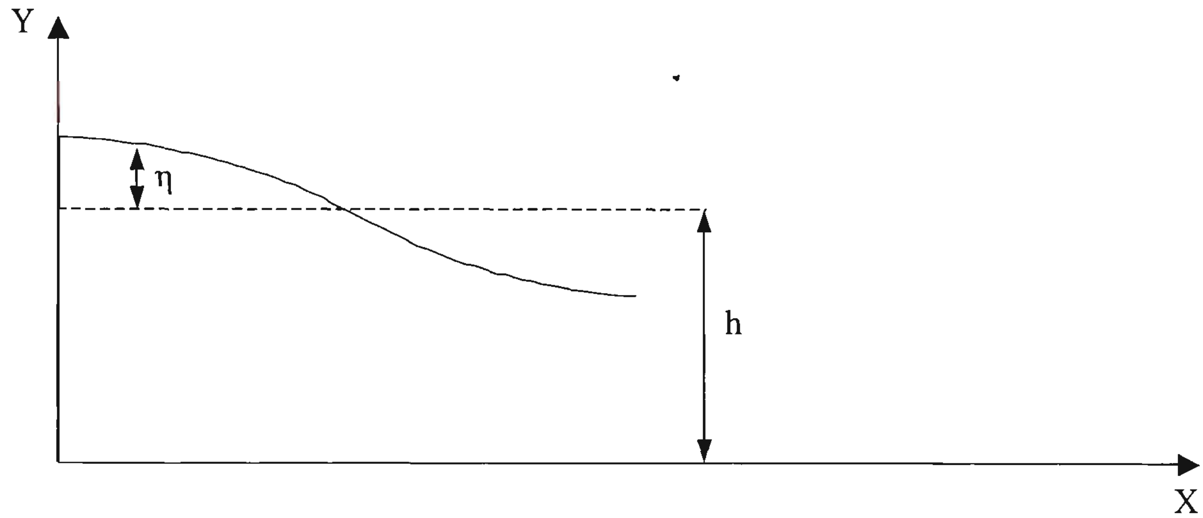

Figure A2.1. A two-dimensional standing sloshing wave.

In Figure A2.1, the position of the liquid surface is indicated with η where the depth of the liquid is h. The velocity of the free surface, v, may then be expressed as

$$v = \frac{d\eta}{dt} = \frac{\partial\eta}{\partial t} + \frac{\partial x}{\partial t}\frac{\partial\eta}{\partial x} \qquad \text{(A2.1)}$$

If the slope of $\frac{\partial\eta}{\partial x}$ is assumed to be small,

$$\frac{\partial\eta}{\partial t} = v \qquad \text{(A2.2)}$$

Defining a stream function φ such that $\frac{\partial\varphi}{\partial x} = v$, Equation A2.2 becomes,

$$\frac{\partial\eta}{\partial t} = \frac{\partial\varphi}{\partial x} \qquad \text{(A2.3)}$$

Equation A2.3 is the kinematic condition for wave profiles of small amplitude.

Next, a complex potential function, w, is defined as

$$w = b\,\mathrm{Cos}(mz - nt) \qquad \text{(A2.4)}$$

where b is the magnitude of w, z is a complex number, t is time, and m and n are related to the wavelength $\lambda = \frac{2\pi}{m}$ and period $T = \frac{2\pi}{n}$ such that $c = \frac{n}{m}$ becomes the speed of wave propagation in the x-direction.

Since the stream function φ and velocity potential ϕ are always perpendicular to each other, the real and imaginary components of w may be taken as

$$\mathrm{Im}(w) = \varphi = -b\,\mathrm{Sin}\,(mx - nt)\,\mathrm{Sinh}(mh) \qquad \text{(A2.5a)}$$

$$\mathrm{Re}(w) = \phi = b\,\mathrm{Cos}\,(mx - nt)\,\mathrm{Cosh}(mh) \qquad \text{(A2.5b)}$$

Therefore, Equation A2.5a may be differentiated in x to obtain

$$\frac{\partial\varphi}{\partial x} = -mb\,\mathrm{Cos}(mx - nt)\,\mathrm{Sinh}(mh) \qquad \text{(A2.6)}$$

the right-hand-side of Equation A2.3. The next step is to determine the left-hand-side term $\frac{\partial\eta}{\partial t}$.

The shape of the free surface in Figure A2.1 may be represented by a harmonic function as

$$\eta = a\,\mathrm{Sin}(mx - nt) \qquad \text{(A2.7)}$$

where a is an arbitrary magnitude. Differentiating Equation A2.7 in t

$$\frac{\partial \eta}{\partial t} = -an\,\mathrm{Cos}(mx - nt) \qquad \text{(A2.8)}$$

gives the left-hand-side of Equation A2.3. Hence, Equation A2.3 may be written as

$$-an\,\mathrm{Cos}(mx - nt) = -bm\,\mathrm{Cos}(mx - nt)\,\mathrm{Sinh}(mh) \qquad \text{(A2.9)}$$

$-an = -bm\,\mathrm{Sinh}(mh)$ and

$$b = \frac{an}{m\,\mathrm{Sinh}(mh)}$$

(A2.10)

Since speed of wave propagation $c = \dfrac{n}{m}$,

$$b = \frac{ac}{\mathrm{Sinh}(mh)} \qquad \text{(A2.11)}$$

b may now be substituted in the stream function φ and velocity potential ϕ in Equations A2.5 as

$$\varphi = -ac\,\mathrm{Sin}\,(mx - nt) \qquad \text{(A2.12a)}$$

$$\phi = \frac{ac}{\tanh(mh)}\mathrm{Cos}\,(mx - nt) \qquad \text{(A2.12b)}$$

These last two expressions will be used in association with the dynamic boundary condition which will be given next.

Since the only body force on the sloshing liquid is the gravity force (in the negative y-direction),

$$\frac{\partial \varphi}{\partial t} - g\eta = \frac{1}{2}(\nabla \varphi)^2 \qquad \text{(A2.13)}$$

$(\nabla \varphi)^2 = 0$ in potential flow. Therefore,

$$\frac{\partial \varphi}{\partial t} = g\eta \qquad \text{(A2.14)}$$

Partially differentiating Equation A2.14 with respect to time

$$\frac{1}{g}\frac{\partial^2 \phi}{\partial t^2} = \frac{\partial \eta}{\partial t} \qquad \text{(A2.15)}$$

$\frac{\partial \eta}{\partial t}$ may be substituted from the kinematic condition in Equation A2.3 to give

$$\frac{1}{g}\frac{\partial^2 \phi}{\partial t^2} = \frac{\partial \varphi}{\partial x} \qquad \text{(A2.16)}$$

The components of Equation A2.16 are determined from Equations 2.12a and 2.12b as

$$\varphi = -ac\,\mathrm{Sin}\,(mx - nt)$$

$$\frac{\partial \varphi}{\partial x} = -mac\,\mathrm{Cos}(mx - nt) \qquad \text{(A2.17)}$$

and

$$\phi = \frac{ac}{\tanh(mh)}\mathrm{Cos}\,(mx - nt)$$

$$\frac{\partial^2 \phi}{\partial t^2} = -\frac{acn^2}{\tanh(mh)}\mathrm{Cos}(mx - nt) \qquad \text{(A2.18)}$$

Equations A2.17 and A2.18 can be substituted into Equation A2.16 to give

$$\frac{1}{g}\frac{\partial^2\phi}{\partial t^2} = \frac{\partial\varphi}{\partial x}$$

$$-\frac{1}{g}\frac{acn^2}{\tanh(mh)}\mathrm{Cos}(mx - nt) = -mac\,\mathrm{Cos}(mx - nt)$$

$$n^2 = gm\tanh(mh)$$

$$\frac{n^2}{m^2} = \frac{g}{m}\tanh(mh)$$

Since $c = \dfrac{n}{m}$ and $\lambda = \dfrac{2\pi}{m}$,

$$c^2 = \frac{g\lambda}{2\pi}\tanh\left(\frac{2\pi h}{\lambda}\right) \qquad \text{(A2.19)}$$

Now the fundamental sloshing frequency can be determined for the case shown in Figure A2.2, where d is either the container diameter (for a cylindrical container) or the container length (for a rectangular container). The shaded area represents sloshing liquid at its fundamental mode.

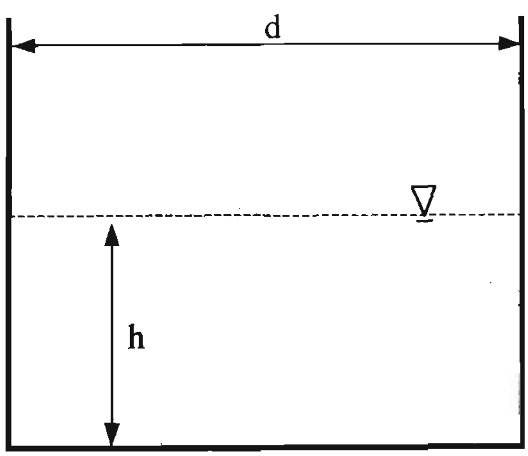

Figure A2.2. Sloshing at its fundamental mode.

The full wavelength of the sloshing wave is equal to twice the available distance in the container, $\lambda = 2d$. Therefore, the fundamental sloshing frequency $f = \frac{c}{\lambda}$ may be written from Equation A2.19 as

$$c^2 = \frac{g\lambda}{2\pi} \tanh\left(\frac{2\pi h}{\lambda}\right)$$

$$f^2 = \frac{1}{\lambda^2} \frac{g\lambda}{2\pi} \tanh\left(\frac{2\pi h}{\lambda}\right)$$

$$f^2 = \frac{1}{4d^2} \frac{g2d}{2\pi} \tanh\left(\frac{2\pi h}{2d}\right)$$

$$f^2 = \frac{g\pi}{4d\pi^2} \tanh\left(\frac{\pi h}{d}\right)$$

$$f = \frac{1}{2\pi} \sqrt{\frac{g\pi}{d} \tanh\left(\frac{\pi h}{d}\right)} \qquad \text{(A2.20)}$$

Equation A2.20 gives the closed form expression of fundamental sloshing frequency in Hz for a container with length d, filled to a depth of h and acceleration due to gravity g.

Appendix 3

NUMERICAL PREDICTIONS AND CFX4.1 FILES FOR SLOSHING CONTROL WITH FLOATING PLATES IN CHAPTER THREE

A3.1. DETAILS OF THE NUMERICAL MODEL

The purpose of this Appendix is to present the numerical procedure devised to handle a floating plate on the free surface of a liquid in a container. Representative results from these numerical simulations and the source code of the program in the CFX environment are also included for completeness.

Experimental observations for the control of liquid sloshing with dumb-bell devices are given in Chapter 3. Although it is clearly recognized that what is needed is to model the performance of dumb-bell devices, their complex geometry and partially submerged and partially floating nature, make it very challenging to obtain an acceptable representation of the required fluid-structure interaction. The numerical simulations presented in this section correspond to the simplified geometry shown in Figure A3.1. Hence, the information presented in this section should be interpreted as a preliminary attempt rather than being conclusive. Despite the significant simplifications, these preliminary predictions are still valuable to indicate trends for sloshing control.

The same tank used for sloshing control with cantilever baffles is used in this investigation. Since the details of the two-dimensional numerical model (including grid refinement and time step dependency) are given in Chapter 2, only a brief description is included here. The predictions were obtained using CFX4.1. The COMMAND and FORTRAN files needed to represent the geometry in the CFX environment are given in Section A3.3 of this Appendix. The Volume of Fluid (V.O.F.) method was used to discretise the liquid and gas domains. A surface sharpening algorithm was used to improve the definition of the liquid free surface. The solution included viscous effects and a time step of 0.001s, as used previously, was used here.

A three dimensional view of the tank and floating plate and the two dimensional grid used for the numerical predictions are given in Figures A3.1 and A3.2, respectively. Sloshing was induced by imposing a sinusoidal displacement on the container along the 130 mm width. The amplitude of the container displacement was 2.5 mm peak-to-peak at the fundamental sloshing frequency of 2.175Hz. With this excitation, the uncontrolled peak-to-peak sloshing amplitude was 34 mm.

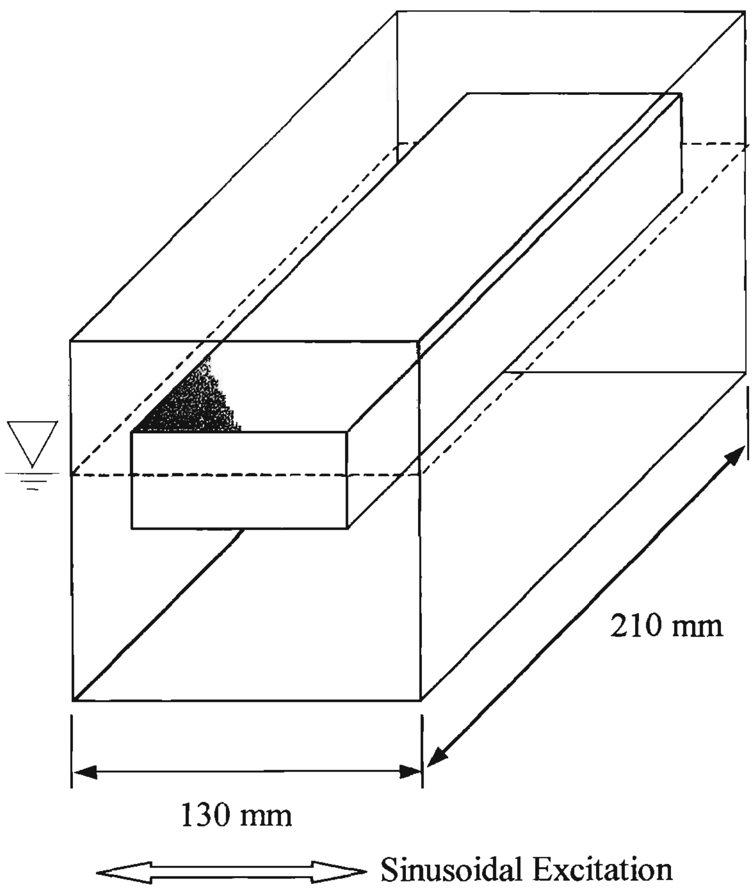

Figure A3.1. Three dimensional view of the tank and floating plate.

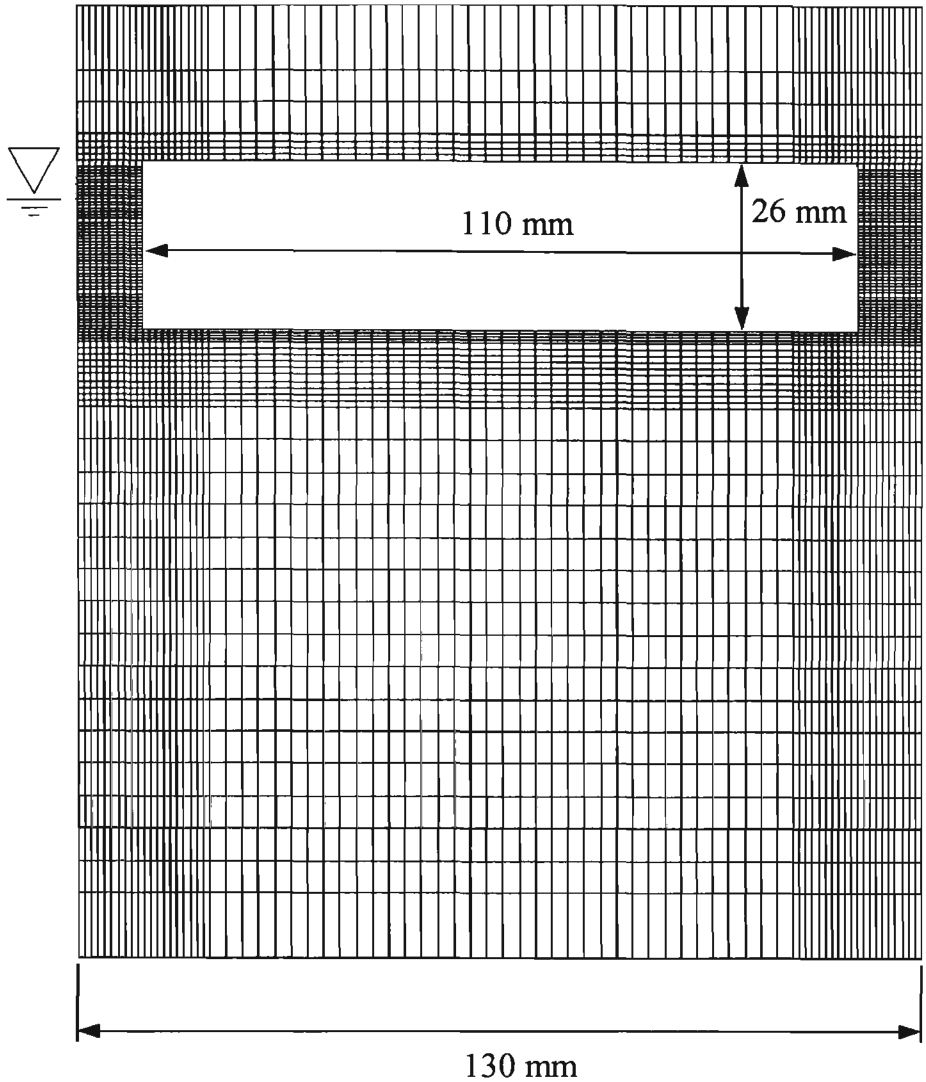

Figure A3.2. Grid used for the numerical predictions.

In Figure A3.2, the floating plate is represented as the 110 mm × 26 mm void in the numerical grid. Similar to the walls of the container, the no-slip velocity boundary condition is applied at the edges of the plate. Both the container and the plate are modelled for a depth, normal to the view, of 210 mm. The mass of the plate is 0.51kg to represent a plate made from wood. The plate has two degrees of freedom which are the vertical displacement in the Y direction and rotation θ as shown in Figure A3.3(a). A typical pressure distribution, on the submerged surface of the plate, is shown schematically in Figure A3.3(b). The effect of such a pressure distribution is to create a resultant turning moment M_0 and a resultant vertical force F_v.

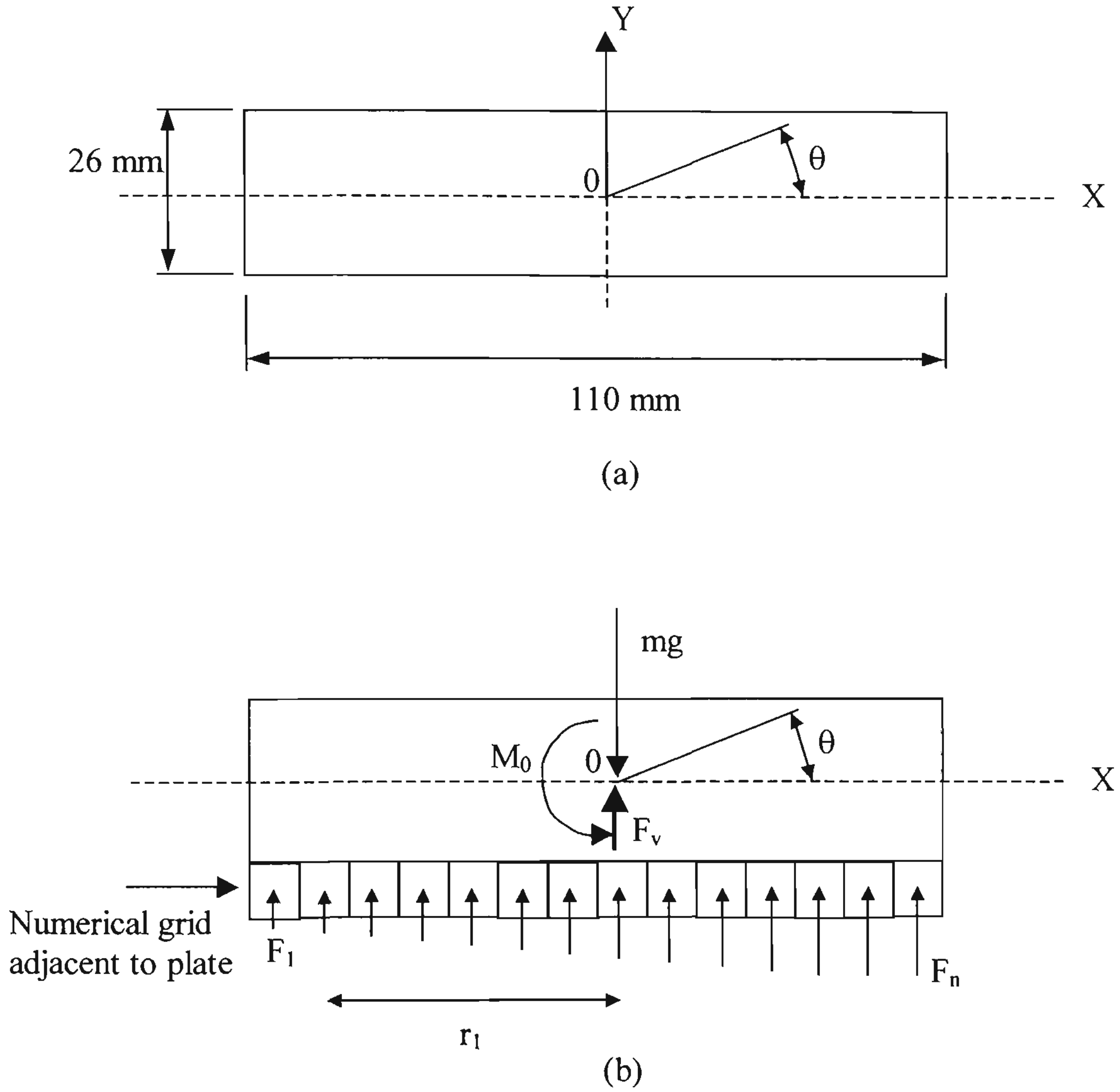

Figure A3.3. Floating plate showing (a) two degrees of freedom and (b) forces acting on the plate. The mass of the plate is m and acceleration due to gravity is g. M_0 is the resultant moment about point 0 due to the pressure force F_i acting in each cell, for $i = 1$ to n.

The size of the liquid cells shown under the plate in Figure A3.3(b), is exaggerated for clarity of explanation. The force F_i, due to pressure in each cell, was determined by multiplying the pressure at the boundary interface by the corresponding cell area. The sum of these forces was then added algebraically to the weight of the plate to determine the resultant vertical force, F_v, as given by equation A3.1.

During simulations, unusually large pressures were detected in the cells near the submerged corners of the plate. The reason for these large pressure values could not be determined, although cell distortion with the plate motion was suspected to be the cause, as stated in Section 3.4.1. If a simulation was allowed to proceed with these unreasonably large pressures, immediate numerical instability resulted due to the step-by-step nature of the numerical integration. The cells away from the sharp corners of the plates seemed to have reasonable magnitudes (comparable values to expected buoyancy force). It should be stated here that there is no other rationale than a simple order-of-magnitude analysis for the "reasonable' assertion. In order to be able to proceed with simulations, the cells in the region near the left and right submerged corners of the plate were ignored, with F_1 and F_n. This ignored region on each side was 10% of the total plate length. Hence, F_v was calculated as follows:

$$F_v = -mg + \sum_{i=2}^{n-1} F_i \cos\theta \qquad \text{(A3.1)}$$

The moment about the mid point of the plate due to each force was determined from the product of each cell's force and its distance from the center of the plate. To determine the length of the moment arm, r, the pressure force was assumed to act in the center of each cell. The resultant moment was then determined by using Equation A3.2 as the sum of the moments at each cell:

$$M_0 = \sum_{i=2}^{n-1} F_i r_i \qquad \text{(A3.2)}$$

The rotation and vertical displacement of the plate was then determined by assuming constant acceleration over each integration step, and by solving Equations A3.3 and A3.4, respectively. In these equations, t is time, α, ω and θ are the angular acceleration, velocity and displacement, respectively. I is the mass moment of inertia about the center of the plate in Figure A3.3. For the vertical motion, a, V and Y are the vertical acceleration, velocity and displacement of the plate, respectively. Δ indicates an incremental change in time.

$$\alpha = \frac{M_0}{I}$$

$$\Delta\omega = \alpha\Delta t$$

$$\Delta\theta = \omega\Delta t + \frac{1}{2}\alpha\Delta t^2 \qquad \text{(A3.3)}$$

$$a = \frac{F_v}{m}$$

$$\Delta V = a\Delta t$$

$$\Delta Y = V\Delta t + \frac{1}{2}a\Delta t^2 \qquad \text{(A3.4)}$$

The equations of motion for the plate were solved at every second time step. To avoid excessive distortion of the liquid cells between the edges of the plate and the walls of the container, the edges of the plate were kept vertical at all times

For the plate, the mass moment of inertia was defined as,

$$I = \frac{1}{12} m(L^2 + B^2) \qquad \text{(A3.5)}$$

where m is the mass of the plate and L and B are the length and thickness of the container respectively. For a plate of length 110 mm and thickness 26 mm, the mass moment of inertia is approximately 6×10^{-4} kgm^2.

A3.2. Typical Results

A series of predictions were obtained for plates with mass moments of inertia of 6×10^{-4} kgm^2, 10×10^{-4} kgm^2, 15×10^{-4} kgm^2 and 20×10^{-4} kgm^2 to determine the sensitivity of the control action to I. Of course, other parameters such as plate dimensions will affect the control action, and they should therefore deserve future investigation. In each trial here, the plate dimensions were kept constant. Since the plate occupies much of the liquid free surface, the angular displacement history of the plate is a reasonable indication of the liquid motion near the surface. These histories are shown in Figure A3.4.

In Figure A3.4(a), when I=6×10^{-4} kgm^2, the amplitude of the angular displacement increases for the duration of the prediction to a maximum of greater than 0.1 radians. In Figures A3.4(b), A3.4(c) and A3.4(d) the amplitude of the angular displacement decreases as the mass moment of inertia for the floating plate is increased. In Figure A3.4(d) the maximum amplitude approaches 0.025 radians, indicating that plates with a larger mass moment of inertia are promising for sloshing control.

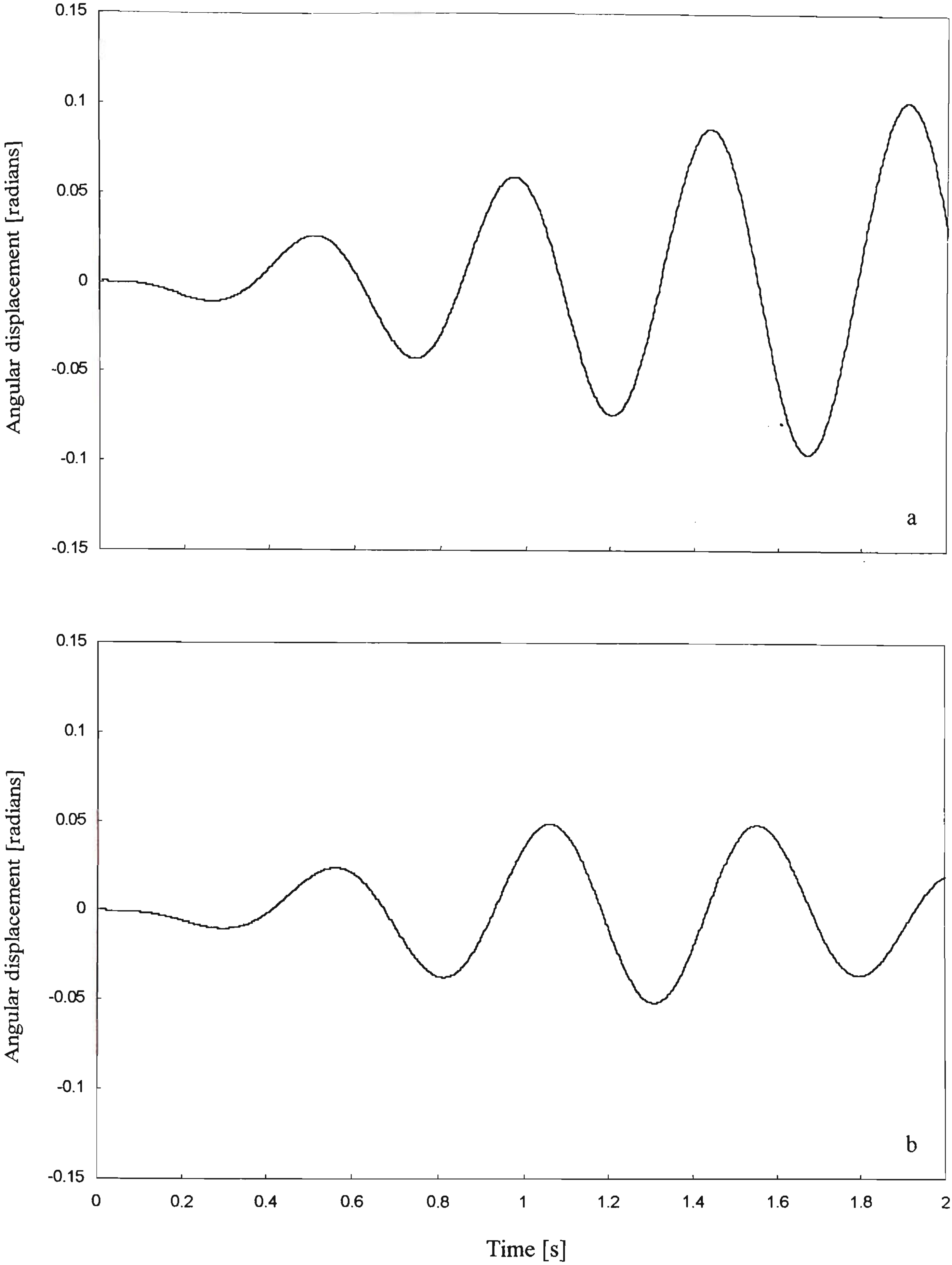

Figure A3.4. Angular displacement histories for a single floating plate with (a) I = 6×10^{-4} kgm^2, (b) I = 10×10^{-4} kgm^2, (c) I= 15×10^{-4} kgm^2 and (d) I= 20×10^{-4} kgm^2.

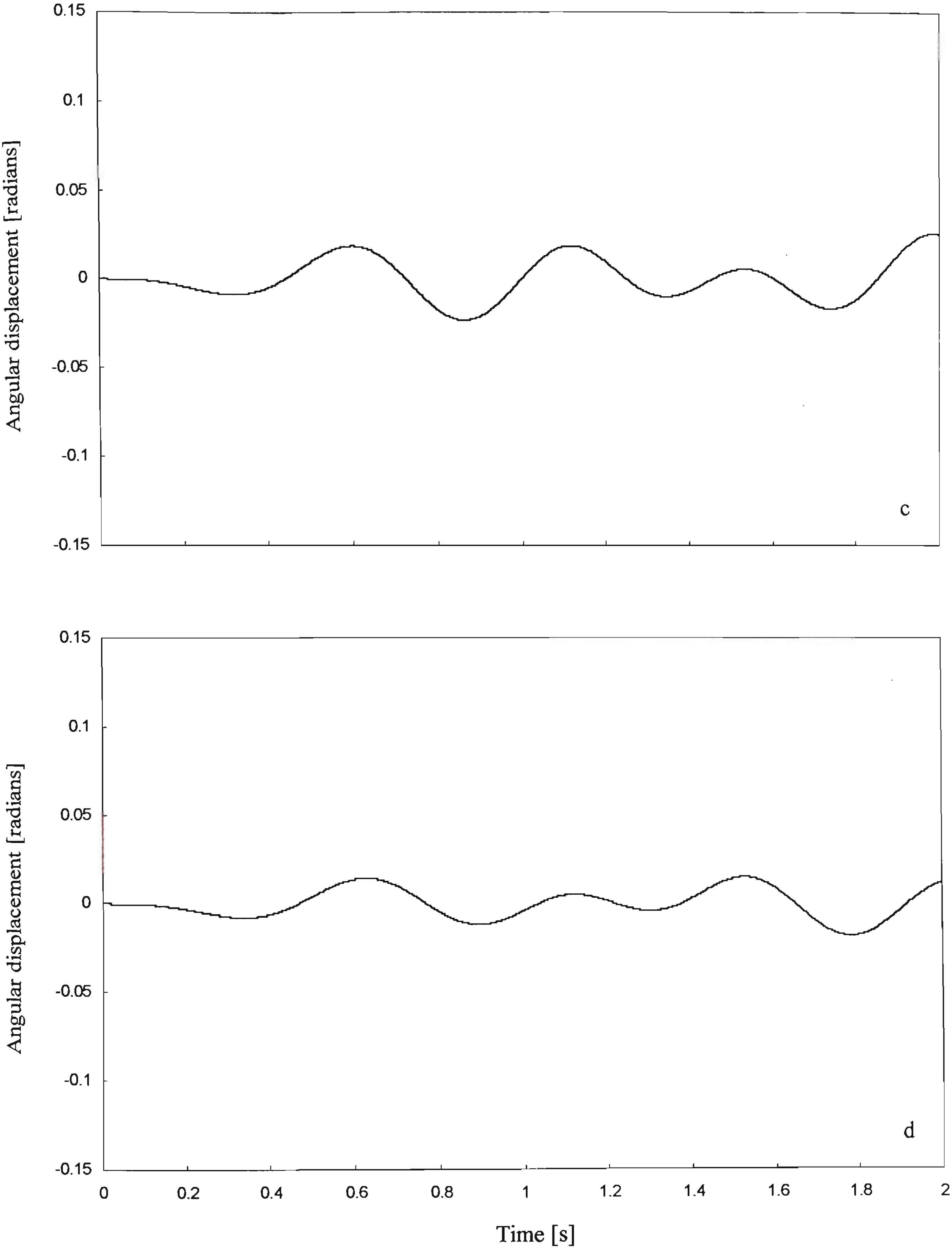

Figure A3.4. Angular displacement histories for a single floating plate with (a) $I = 6 \times 10^{-4}$ kgm^2, (b) $I = 10 \times 10^{-4}$ kgm^2, (c) $I = 15 \times 10^{-4}$ kgm^2 and (d) $I = 20 \times 10^{-4}$ kgm^2.

A3.3. Source Code

The two files used in the CFX environment consist of the Command and User Fortran files. The Command file controls the geometry and fluid properties, while the User Fortran file consists of three sub-routines to define liquid depth, to set wall boundary conditions and to move the grid as the floating plate changes position. The files used for floating plates are similar to those given in Appendix 1 for a sloshing absorber.

A3.3.1. Command File

```
>>CFX4
  >>SET LIMITS
    MEDIUM
  >>OPTIONS
    TWO DIMENSIONS
    RECTANGULAR GRID
    CARTESIAN COORDINATES
    LAMINAR FLOW
    BUOYANT FLOW
    TRANSIENT FLOW
    TRANSIENT GRID
    NUMBER OF PHASES 2
  >>USER FORTRAN
    USRBCS
    USRGRD
    USRINT
>>MODEL TOPOLOGY
  >>CREATE BLOCK
    BLOCK NAME 'DUCT'
    BLOCK DIMENSIONS 78 89 1
  >>CREATE PATCH
    PATCH NAME 'TOP'
    BLOCK NAME 'DUCT'
    PATCH TYPE 'PRESSURE BOUNDARY'
    PATCH LOCATION 2 77 89 89 1 1
    HIGH J
  >>CREATE PATCH
    PATCH NAME 'WALLS'
    BLOCK NAME 'DUCT'
    PATCH TYPE 'SOLID'
    PATCH LOCATION 1 1 1 89 1 1
  >>CREATE PATCH
    PATCH NAME 'WALLS'
    BLOCK NAME 'DUCT'
    PATCH TYPE 'SOLID'
    PATCH LOCATION 2 77 1 1 1 1
  >>CREATE PATCH
    PATCH NAME 'WALLS'
```

```
    BLOCK NAME 'DUCT'
    PATCH TYPE 'SOLID'
    PATCH LOCATION 78 78 1 89 1 1
  >>CREATE PATCH
    PATCH NAME 'RT'
    BLOCK NAME 'DUCT'
    PATCH TYPE 'SOLID'
    PATCH LOCATION 12 67 32 82 1 1
>>MODEL DATA
  >>AMBIENT VARIABLES
    PHASE NAME 'PHASE1'
    VOLUME FRACTION 1.0000E+00
  >>AMBIENT VARIABLES
    PHASE NAME 'PHASE2'
    VOLUME FRACTION 0.0000E+00
  >>TITLE
    PROBLEM TITLE 'TEST FLOAT'
  >>PHYSICAL PROPERTIES
    >>BUOYANCY PARAMETERS
      GRAVITY VECTOR 0.000000E+00 -9.810000E+00 0.000000E+00
      BUOYANCY REFERENCE DENSITY 1.2090E+00
    >>FLUID PARAMETERS
      PHASE NAME 'PHASE1'
      VISCOSITY 1.8000E-05
      DENSITY 1.2090E+00
    >>FLUID PARAMETERS
      PHASE NAME 'PHASE2'
      VISCOSITY 1.0000E-03
      DENSITY 1.0200E+03
    >>MULTIPHASE PARAMETERS
      >>PHASE DESCRIPTION
        PHASE NAME 'PHASE1'
        GAS
        CONTINUOUS
      >>PHASE DESCRIPTION
        PHASE NAME 'PHASE2'
        LIQUID
        CONTINUOUS
      >>MULTIPHASE MODELS
        >>MOMENTUM
          HOMOGENEOUS
          SURFACE SHARPENING ALGORITHM
        >>HOMOGENEOUS
          SURFACE SHARPENING ALGORITHM
          SURFACE SHARPENING LEVEL 2
    >>TRANSIENT PARAMETERS
      >>FIXED TIME STEPPING
        TIME STEPS 3000* 1.000000E-03
>>SOLVER DATA
  >>PROGRAM CONTROL
    MAXIMUM NUMBER OF ITERATIONS 50
    OUTPUT MONITOR POINT 20 5 1
    MASS SOURCE TOLERANCE 1.0000E-06
>>CREATE GRID
  >>SIMPLE GRID
    BLOCK NAME 'DUCT'
    DX 21* 1.000000E-03
       36* 2.500000E-03
       21* 1.000000E-03
    DY 1*  5.000000E-03
```

```
        1*  1.000000E-02
        15* 5.000000E-03
        10* 1.000000E-03
        54* 5.000000E-04
        5* 1.000000E-03
        2* 5.000000E-03
        1* 1.000000E-02
     DZ 1.000000E+00
     X START 0.0000E+00
     Y START 0.0000E+00
     Z START 0.0000E+00
>>MODEL BOUNDARY CONDITIONS
>>OUTPUT OPTIONS
  >>PRINT OPTIONS
    >>WHAT
      PHASE NAME 'PHASE1'
      NO VARIABLES
      NO WALL PRINTING
      NO RESIDUAL HISTORY
  >>DUMP FILE OPTIONS
    PHASE NAME 'PHASE2'
    TIME STEP INTERVAL 100
    GEOMETRY DATA
    U VELOCITY
    V VELOCITY
    W VELOCITY
    PRESSURE
    VOLUME FRACTION
>>STOP
```

A3.3.2. User Fortran File

```
      SUBROUTINE USRINT(U,V,W,P,VFRAC,DEN,VIS,TE,ED,RS,T,H,RF,SCAL
     +                  ,CONV,XC,YC,ZC,XP,YP,ZP
     +                  ,VOL,AREA,VPOR,ARPOR,WFACT,DISWAL,IPT
     +
,IBLK,IPVERT,IPNODN,IPFACN,IPNODF,IPNODB,IPFACB
     +                  ,WORK,IWORK,CWORK)
C
C*********************************************************************
**
C
C   UTILITY SUBROUTINE FOR USER-SUPPLIED INITIAL FIELD.
C
C*********************************************************************
**
C
C   THIS SUBROUTINE IS CALLED BY THE FOLLOWING SUBROUTINE
C      CUSR  INIT
C
C*********************************************************************
**
C   CREATED
C      13/06/90 ADB
C   MODIFIED
C      07/08/91 IRH   NEW STRUCTURE
C      10/09/91 IRH   CORRECTION TO IUSED
C      26/09/91 IRH   ALTER ARGUMENT LIST
```

```
C       01/10/91 DSC   REDUCE COMMENT LINE GOING OVER COLUMN 72.
C       03/10/91 IRH   CORRECT COMMENTS
C       28/01/92 PHA   UPDATE CALLED BY COMMENT, ADD RF ARGUMENT,
C                      CHANGE LAST DIMENSION OF RS TO 6 AND IVERS TO 2
C       03/06/92 PHA   ADD PRECISION FLAG AND CHANGE IVERS TO 3
C       08/02/93 NSW   REMOVE REDUNDANT COMMENTS
C       23/11/93 CSH   EXPLICITLY DIMENSION IPVERT ETC.
C       03/02/94 PHA   CHANGE FLOW3D TO CFDS-FLOW3D, REMOVE COMMA
C                      FROM BEGINNING OF DIMENSION STATEMENT
C       03/03/94 FHW   CORRECTION OF SPELLING MISTAKE
C       09/08/94 NSW   CORRECT SPELLING
C                      MOVE 'IF(IUSED.EQ.0) RETURN' OUT OF USER AREA
C       19/12/94 NSW   CHANGE FOR CFX-F3D
C       30/01/95 NSW   INCLUDE NEW EXAMPLE
C
C*********************************************************************
**
C
C    SUBROUTINE ARGUMENTS
C
C      U      - U COMPONENT OF VELOCITY
C      V      - V COMPONENT OF VELOCITY
C      W      - W COMPONENT OF VELOCITY
C      P      - PRESSURE
C      VFRAC  - VOLUME FRACTION
C      DEN    - DENSITY OF FLUID
C      VIS    - VISCOSITY OF FLUID
C      TE     - TURBULENT KINETIC ENERGY
C      ED     - EPSILON
C      RS     - REYNOLD STRESSES
C      T      - TEMPERATURE
C      H      - ENTHALPY
C      RF     - REYNOLD FLUXES
C      SCAL   - SCALARS (THE FIRST 'NCONC' OF THESE ARE MASS
FRACTIONS)
C      CONV   - CONVECTION COEFFICIENTS
C      XC     - X COORDINATES OF CELL CORNERS
C      YC     - Y COORDINATES OF CELL CORNERS
C      ZC     - Z COORDINATES OF CELL CORNERS
C      XP     - X COORDINATES OF CELL CENTRES
C      YP     - Y COORDINATES OF CELL CENTRES
C      ZP     - Z COORDINATES OF CELL CENTRES
C      VOL    - VOLUME OF CELLS
C      AREA   - AREA OF CELLS
C      VPOR   - POROUS VOLUME
C      ARPOR  - POROUS AREA
C      WFACT  - WEIGHT FACTORS
C      DISWAL - DISTANCE OF CELL CENTRE FROM WALL
C
C      IPT    - 1D POINTER ARRAY
C      IBLK   - BLOCK SIZE INFORMATION
C      IPVERT - POINTER FROM CELL CENTERS TO 8 NEIGHBOURING VERTICES
C      IPNODN - POINTER FROM CELL CENTERS TO 6 NEIGHBOURING CELLS
C      IPFACN - POINTER FROM CELL CENTERS TO 6 NEIGHBOURING FACES
C      IPNODF - POINTER FROM CELL FACES TO 2 NEIGHBOURING CELL CENTERS
C      IPNODB - POINTER FROM BOUNDARY CENTERS TO CELL CENTERS
C      IPFACB - POINTER FROM BOUNDARY CENTERS TO BOUNDARY FACES
C
C      WORK   - REAL WORKSPACE ARRAY
C      IWORK  - INTEGER WORKSPACE ARRAY
```

```
C     CWORK  - CHARACTER WORKSPACE ARRAY
C
C   SUBROUTINE ARGUMENTS PRECEDED WITH A '*' ARE ARGUMENTS THAT MUST
C   BE SET  BY THE USER IN THIS ROUTINE.
C
C   LOGICAL VARIABLE LRDISK IN COMMON BLOCK IOLOGC INDICATES WHETHER
C   THE RUN IS A RESTART AND CAN BE USED SO THAT INITIAL INFORMATION
C   IS ONLY SET WHEN STARTING A RUN FROM SCRATCH.
C
C   NOTE THAT OTHER DATA MAY BE OBTAINED FROM CFX-F3D USING THE
C   ROUTINE GETADD, FOR FURTHER DETAILS SEE THE VERSION 4
C   USER MANUAL.
C
C**********************************************************************
**
      LOGICAL LDEN,LVIS,LTURB,LTEMP,LBUOY,LSCAL,LCOMP
     +       ,LRECT,LCYN,LAXIS,LPOROS,LTRANS
      LOGICAL LRDISK,LWDISK
C
      CHARACTER*(*) CWORK
C
C+++++++++++++++++ USER AREA 1
+++++++++++++++++++++++++++++++++++++++++
C---- AREA FOR USERS EXPLICITLY DECLARED VARIABLES
C
C+++++++++++++++++ END OF USER AREA 1
+++++++++++++++++++++++++++++++++++
C
      COMMON
     + /ALL/    NBLOCK,NCELL,NBDRY,NNODE,NFACE,NVERT,NDIM
     + /ALLWRK/ NRWS,NIWS,NCWS,IWRFRE,IWIFRE,IWCFRE
     + /ADDIMS/ NPHASE,NSCAL,NVAR,NPROP
     +         ,NDVAR,NDPROP,NDXNN,NDGEOM,NDCOEF,NILIST,NRLIST,NTOPOL
     + /CHKUSR/ IVERS,IUCALL,IUSED
     + /DEVICE/ NREAD,NWRITE,NRDISK,NWDISK
     + /IDUM/   ILEN,JLEN
     + /IOLOGC/ LRDISK,LWDISK
     + /LOGIC/  LDEN,LVIS,LTURB,LTEMP,LBUOY,LSCAL,LCOMP
     +         ,LRECT,LCYN,LAXIS,LPOROS,LTRANS
     + /MLTGRD/ MLEVEL,NLEVEL,ILEVEL
     + /SGLDBL/ IFLGPR,ICHKPR
     + /TRANSI/ NSTEP,KSTEP,MF,INCORE
     + /TRANSR/ TIME,DT,DTINVF,TPARM
C
C+++++++++++++++++ USER AREA 2
+++++++++++++++++++++++++++++++++++++++++
C---- AREA FOR USERS TO DECLARE THEIR OWN COMMON BLOCKS
C     THESE SHOULD START WITH THE CHARACTERS 'UC' TO ENSURE
C     NO CONFLICT WITH NON-USER COMMON BLOCKS
C
C+++++++++++++++++ END OF USER AREA 2
+++++++++++++++++++++++++++++++++++
C
      DIMENSION
     + U(NNODE,NPHASE),V(NNODE,NPHASE),W(NNODE,NPHASE)
     +,P(NNODE,NPHASE),VFRAC(NNODE,NPHASE)
     +,TE(NNODE,NPHASE),ED(NNODE,NPHASE),RS(NNODE,NPHASE,6)
     +,T(NNODE,NPHASE),H(NNODE,NPHASE),RF(NNODE,NPHASE,4)
     +,SCAL(NNODE,NPHASE,NSCAL)
     +,DEN(NNODE,NPHASE),VIS(NNODE,NPHASE),CONV(NFACE,NPHASE)
```

```
      DIMENSION
     + XC(NVERT),YC(NVERT),ZC(NVERT),XP(NNODE),YP(NNODE),ZP(NNODE)
     +,VOL(NCELL),AREA(NFACE,3),VPOR(NCELL),ARPOR(NFACE,3)
     +,WFACT(NFACE),DISWAL(NCELL)
      DIMENSION
     + IPT(*),IBLK(5,NBLOCK)
+,IPVERT(NCELL,8),IPNODN(NCELL,6),IPFACN(NCELL,6),IPNODF(NFACE,4)
     +,IPNODB(NBDRY,4),IPFACB(NBDRY)
      DIMENSION
     + IWORK(NIWS),WORK(NRWS),CWORK(NCWS)
C
C+++++++++++++++ USER AREA 3
+++++++++++++++++++++++++++++++++++++++
C---- AREA FOR USERS TO DIMENSION THEIR ARRAYS
C
C---- AREA FOR USERS TO DEFINE DATA STATEMENTS
C
C++++++++++++++++ END OF USER AREA 3
+++++++++++++++++++++++++++++++++
C
C---- STATEMENT FUNCTION FOR ADDRESSING
      IP(I,J,K)=IPT((K-1)*ILEN*JLEN+(J-1)*ILEN+I)
C
C----VERSION NUMBER OF USER ROUTINE AND PRECISION FLAG
C
      IVERS=3
      ICHKPR = 1
C
C++++++++++++++++ USER AREA 4
+++++++++++++++++++++++++++++++++++++++
C---- TO USE THIS USER ROUTINE FIRST SET IUSED=1
C
       IUSED=1
C
C++++++++++++++++ END OF USER AREA 4
+++++++++++++++++++++++++++++++++
C
       IF (IUSED.EQ.0) RETURN
C
C---- FRONTEND CHECKING OF USER ROUTINE
      IF (IUCALL.EQ.0) RETURN
C
C++++++++++++++++ USER AREA 5
+++++++++++++++++++++++++++++++++++++++
C
C---- AREA FOR INITIALISING VARIABLES U,V,W,P,VFRAC,TE,ED,RS,T,SCAL
C     ONLY.
C
      FULL=1.0
      EMPTY=1.E-10
C

      CALL IPREC('DUCT','BLOCK','CENTRES',IPT,ILEN,JLEN,KLEN,
     +           CWORK,IWORK)
C
      DO 90 K=1,KLEN
        DO 90 J=1,JLEN
          DO 90 I=2,ILEN-1
```

```
            INODE=IP(I,J,K)
            VFRAC(INODE,1)=FULL
            VFRAC(INODE,2)=EMPTY
  90      CONTINUE

      DO 95 K=1,KLEN
        DO 95 I=2,ILEN-1
          DO 95 J=1,71

            INODE=IP(I,J,K)
            VFRAC(INODE,1)=EMPTY
            VFRAC(INODE,2)=FULL
  95      CONTINUE
C
C++++++++++++++++ END OF USER AREA 5
++++++++++++++++++++++++++++++++
C
      RETURN
      END
      SUBROUTINE USRBCS(VARBCS,VARAMB,A,B,C,ACND,BCND,CCND
     +                  ,IWGVEL,NDVWAL
     +                  ,FLOUT,NLABEL,NSTART,NEND,NCST,NCEN
     +                  ,U,V,W,P,VFRAC,DEN,VIS,TE,ED,RS,T,H,RF,SCAL
     +                  ,XP,YP,ZP,VOL,AREA,VPOR,ARPOR,WFACT,IPT
     +
,IBLK,IPVERT,IPNODN,IPFACN,IPNODF,IPNODB,IPFACB
     +                  ,WORK,IWORK,CWORK)
C
C*******************************************************************
***
C
C  USER ROUTINE TO SET REALS AT BOUNDARIES.
C
C   >>> IMPORTANT USERS MAY ONLY ADD OR ALTER PARTS OF THE SUBROUTINE
WITHIN THE DESIGNATED USER AREAS
C
C*******************************************************************
***
C
C  THIS SUBROUTINE IS CALLED BY THE FOLLOWING SUBROUTINE
C    CUSR  SRLIST
C
C*******************************************************************
***
C   CREATED
C      30/11/88 ADB
C   MODIFIED
C      08/09/90 ADB  RESTRUCTURED FOR USER-FRIENDLINESS.
C      10/08/91 IRH  FURTHER RESTRUCTURING ADD ACND BCND CCND
C      22/09/91 IRH  CHANGE ICALL TO IUCALL + ADD /SPARM/
C      10/03/92 PHA  UPDATE CALLED BY COMMENT, ADD RF ARGUMENT,
C                    CHANGE LAST DIMENSION OF RS TO 6 AND IVERS TO 2
C      03/06/92 PHA  ADD PRECISION FLAG AND CHANGE IVERS TO 3
C      30/06/92 NSW  INCLUDE FLAG FOR CALLING BY ITERATION
C                    INSERT EXTRA COMMENTS
C      03/08/92 NSW  MODIFY DIMENSION STATEMENTS FOR VAX
C      21/12/92 CSH  INCREASE IVERS TO 4
C      02/08/93 NSW  INCORRECT AND MISLEADING COMMENT REMOVED
C      05/11/93 NSW  INDICATE USE OF FLOUT IN MULTIPHASE FLOWS
C      23/11/93 CSH  EXPLICITLY DIMENSION IPVERT ETC.
```

```
C       01/02/94 NSW  SET VARIABLE POINTERS IN WALL EXAMPLE.
C                     CHANGE FLOW3D TO CFDS-FLOW3D.
C                     MODIFY MULTIPHASE MASS FLOW BOUNDARY TREATMENT.
C       03/03/94 FHW  CORRECTION OF SPELLING MISTAKE
C       02/07/94 BAS  SLIDING GRIDS - ADD NEW ARGUMENT IWGVEL
C                     TO ALLOW VARIANTS OF TRANSIENT-GRID WALL BC
C                     CHANGE VERSION NUMBER TO 5
C       09/08/94 NSW  CORRECT SPELLING
C                     MOVE 'IF(IUSED.EQ.0) RETURN' OUT OF USER AREA
C       19/12/94 NSW  CHANGE FOR CFX-F3D
C       02/02/95 NSW  CHANGE COMMON /IMFBMP/
C
C**********************************************************************
***
C
C   SUBROUTINE ARGUMENTS
C
C     VARBCS - REAL BOUNDARY CONDITIONS
C     VARAMB - AMBIENT VALUE OF VARIABLES
C     A      - COEFFICIENT IN WALL BOUNDARY CONDITION
C     B      - COEFFICIENT IN WALL BOUNDARY CONDITION
C     C      - COEFFICIENT IN WALL BOUNDARY CONDITION
C     ACND   - COEFFICIENT IN CONDUCTING WALL BOUNDARY CONDITION
C     BCND   - COEFFICIENT IN CONDUCTING WALL BOUNDARY CONDITION
C     CCND   - COEFFICIENT IN CONDUCTING WALL BOUNDARY CONDITION
C     IWGVEL - USAGE OF INPUT VELOCITIES (0 = AS IS,1 = ADD GRID
MOTION)
C     NDVWAL - FIRST DIMENSION OF ARRAY IWGVEL
C     FLOUT  - MASS FLOW/FRACTIONAL MASS FLOW
C     NLABEL - NUMBER OF DISTINCT OUTLETS
C     NSTART - ARRAY POINTER
C     NEND   - ARRAY POINTER
C     NCST   - ARRAY POINTER
C     NCEN   - ARRAY POINTER
C     U      - U COMPONENT OF VELOCITY
C     V      - V COMPONENT OF VELOCITY
C     W      - W COMPONENT OF VELOCITY
C     P      - PRESSURE
C     VFRAC  - VOLUME FRACTION
C     DEN    - DENSITY OF FLUID
C     VIS    - VISCOSITY OF FLUID
C     TE     - TURBULENT KINETIC ENERGY
C     ED     - EPSILON
C     RS     - REYNOLD STRESSES
C     T      - TEMPERATURE
C     H      - ENTHALPY
C     RF     - REYNOLD FLUXES
C     SCAL   - SCALARS (THE FIRST 'NCONC' OF THESE ARE MASS
FRACTIONS)
C     XP     - X COORDINATES OF CELL CENTRES
C     YP     - Y COORDINATES OF CELL CENTRES
C     ZP     - Z COORDINATES OF CELL CENTRES
C     VOL    - VOLUME OF CELLS
C     AREA   - AREA OF CELLS
C     VPOR   - POROUS VOLUME
C     ARPOR  - POROUS AREA
C     WFACT  - WEIGHT FACTORS
C
C     IPT    - 1D POINTER ARRAY
C     IBLK   - BLOCK SIZE INFORMATION
```

```
C     IPVERT - POINTER FROM CELL CENTERS TO 8 NEIGHBOURING VERTICES
C     IPNODN - POINTER FROM CELL CENTERS TO 6 NEIGHBOURING CELLS
C     IPFACN - POINTER FROM CELL CENTERS TO 6 NEIGHBOURING FACES
C     IPNODF - POINTER FROM CELL FACES TO 2 NEIGHBOURING CELL CENTERS
C     IPNODB - POINTER FROM BOUNDARY CENTERS TO CELL CENTERS
C     IPFACB - POINTER TO NODES FROM BOUNDARY FACES
C
C     WORK   - REAL WORKSPACE ARRAY
C     IWORK  - INTEGER WORKSPACE ARRAY
C     CWORK  - CHARACTER WORKSPACE ARRAY
C
C   SUBROUTINE ARGUMENTS PRECEDED WITH A '*' ARE ARGUMENTS THAT MUST
C   BE SET  BY THE USER IN THIS ROUTINE.
C
C   NOTE THAT OTHER DATA MAY BE OBTAINED FROM CFX-F3D USING THE
C   ROUTINE GETADD, FOR FURTHER DETAILS SEE THE VERSION 4
C   USER MANUAL.
C
C**********************************************************************
***
      LOGICAL LDEN,LVIS,LTURB,LTEMP,LBUOY,LSCAL,LCOMP
     +       ,LRECT,LCYN,LAXIS,LPOROS,LTRANS
C
      CHARACTER*(*) CWORK
C
C++++++++++++++++ USER AREA 1
+++++++++++++++++++++++++++++++++++++++++
C---- AREA FOR USERS EXPLICITLY DECLARED VARIABLES
C
C++++++++++++++++ END OF USER AREA 1
++++++++++++++++++++++++++++++++++
C
      COMMON
     + /ALL/    NBLOCK,NCELL,NBDRY,NNODE,NFACE,NVERT,NDIM
     + /ALLWRK/ NRWS,NIWS,NCWS,IWRFRE,IWIFRE,IWCFRE
     + /ADDIMS/ NPHASE,NSCAL,NVAR,NPROP
     +         ,NDVAR,NDPROP,NDXNN,NDGEOM,NDCOEF,NILIST,NRLIST,NTOPOL
     + /BCSOUT/ IFLOUT
     + /CHKUSR/ IVERS,IUCALL,IUSED
     + /DEVICE/ NREAD,NWRITE,NRDISK,NWDISK
     + /IDUM/   ILEN,JLEN
     + /IMFBMP/ IMFBMP,JMFBMP
     + /LOGIC/  LDEN,LVIS,LTURB,LTEMP,LBUOY,LSCAL,LCOMP
     +         ,LRECT,LCYN,LAXIS,LPOROS,LTRANS
     + /MLTGRD/ MLEVEL,NLEVEL,ILEVEL
     + /SGLDBL/ IFLGPR,ICHKPR
     + /SPARM/  SMALL,SORMAX,NITER,INDPRI,MAXIT,NODREF,NODMON
     + /TRANSI/ NSTEP,KSTEP,MF,INCORE
     + /TRANSR/ TIME,DT,DTINVF,TPARM
     + /UBCSFL/ IUBCSF
C
C++++++++++++++++ USER AREA 2
+++++++++++++++++++++++++++++++++++++++++
C---- AREA FOR USERS TO DECLARE THEIR OWN COMMON BLOCKS
C     THESE SHOULD START WITH THE CHARACTERS 'UC' TO ENSURE
C     NO CONFLICT WITH NON-USER COMMON BLOCKS
C
C++++++++++++++++ END OF USER AREA 2
++++++++++++++++++++++++++++++++++
C
```

```
      DIMENSION
     + VARBCS(NVAR,NPHASE,NCELL+1:NNODE),VARAMB(NVAR,NPHASE)
     +,A(4+NSCAL,NPHASE,NSTART:*)
     +,B(4+NSCAL,NPHASE,NSTART:*),C(4+NSCAL,NPHASE,NSTART:*)
     +,FLOUT(*),ACND(NCST:*),BCND(NCST:*),CCND(NCST:*)
     +,IWGVEL(NDVWAL,NPHASE)
C
      DIMENSION
     +
U(NNODE,NPHASE),V(NNODE,NPHASE),W(NNODE,NPHASE),P(NNODE,NPHASE)
     +,VFRAC(NNODE,NPHASE),DEN(NNODE,NPHASE),VIS(NNODE,NPHASE)
     +,TE(NNODE,NPHASE),ED(NNODE,NPHASE),RS(NNODE,NPHASE,6)
     +,T(NNODE,NPHASE),H(NNODE,NPHASE),RF(NNODE,NPHASE,4)
     +,SCAL(NNODE,NPHASE,NSCAL)
C
      DIMENSION
     + XP(NNODE),YP(NNODE),ZP(NNODE)

+,VOL(NCELL),AREA(NFACE,3),VPOR(NCELL),ARPOR(NFACE,3),WFACT(NFACE)
     +,IPT(*),IBLK(5,NBLOCK)

+,IPVERT(NCELL,8),IPNODN(NCELL,6),IPFACN(NCELL,6),IPNODF(NFACE,4)
     +,IPNODB(NBDRY,4),IPFACB(NBDRY)
     +,IWORK(*),WORK(*),CWORK(*)
C
C+++++++++++++++++ USER AREA 3
+++++++++++++++++++++++++++++++++++++++
C---- AREA FOR USERS TO DIMENSION THEIR ARRAYS
C
C---- AREA FOR USERS TO DEFINE DATA STATEMENTS
C
C+++++++++++++++++ END OF USER AREA 3
++++++++++++++++++++++++++++++++
C
C---- STATEMENT FUNCTION FOR ADDRESSING
      IP(I,J,K)=IPT((K-1)*ILEN*JLEN+(J-1)*ILEN+I)
C
C----VERSION NUMBER OF USER ROUTINE AND PRECISION FLAG
C
      IVERS=5
      ICHKPR = 1
C
C+++++++++++++++++ USER AREA 4
+++++++++++++++++++++++++++++++++++++++
C---- TO USE THIS USER ROUTINE FIRST SET IUSED=1
C     AND SET IUBCSF FLAG:
C     BOUNDARY CONDITIONS NOT CHANGING                        IUBCSF=0
C     BOUNDARY CONDITIONS CHANGING WITH ITERATION             IUBCSF=1
C     BOUNDARY CONDITIONS CHANGING WITH TIME                  IUBCSF=2
C     BOUNDARY CONDITIONS CHANGING WITH TIME AND ITERATION    IUBCSF=3
C
       IUSED=1
       IUBCSF=2
C
C+++++++++++++++++ END OF USER AREA 4
++++++++++++++++++++++++++++++++
C
       IF (IUSED.EQ.0) RETURN
C
C---- FRONTEND CHECKING OF USER ROUTINE
```

```
      IF (IUCALL.EQ.0) RETURN
C
C+++++++++++++++++ USER AREA 5
+++++++++++++++++++++++++++++++++++++++++
C
C---- AREA FOR SETTING VALUES AT INLETS, PRESSURE BOUNDARIES
C     AND OUTLETS. (NOTE THAT THE MASS FLOW AT OUTLETS IS
C     SPECIFIED IN USER AREA 7)
C
C     IF USING A REYNOLDS STRESS OR FLUX MODEL, NOTE THAT AT INLETS
C     IT IS IMPORTANT THAT THE USER SETS ALL COMPONENTS OF THE
C     REYNOLDS STRESS AND FLUX AND THE TURBULENT KINETIC ENERGY
C     AS WELL AS THE ENERGY DISSIPATION RATE.
C
C     SET THE VALUES IN VARBCS(NVAR,NPHASE,ILEN,JLEN,KLEN)
C
C
C+++++++++++++++++ END OF USER AREA 5
++++++++++++++++++++++++++++++++++
C
C+++++++++++++++++ USER AREA 6
+++++++++++++++++++++++++++++++++++++++++
C
C---- AREA FOR SETTING VALUES AT WALLS
C
C     USE A(2+NSCAL,NPHASE,ILEN,JLEN,KLEN)
C     WHERE NSCAL = NO. OF SCALARS, AND NPHASE = NO. OF PHASES.
C
C     THE CONVENTION FOR VARIABLE NUMBERS IS DIFFERENT IN THIS
ROUTINE
C     FROM THAT IN THE REST OF THE PROGRAM. IT IS:
C
C     IU = 1, IV = 2 , IW = 3, IT = 4, IS = 5
C
C---- EXAMPLE: SETTING FREE SLIP BOUNDARY CONDITIONS AT ALL WALLS
C              AND SETTING T=300.0 AND SCALAR1 AND SCALAR2 =0.0
C              ON WALL1. SET T=400.0 ON CONDUCTING SOLID BOUNDARY
WALL2


C--- SET IWGVEL FLAG

      DO 150 I=1, NDVWAL
        DO 140 J=1,NPHASE
           IWGVEL(I,J)=1
  140 CONTINUE
  150 CONTINUE

C
C+++++++++++++++++ END OF USER AREA 6
++++++++++++++++++++++++++++++++++
C
C
C+++++++++++++++++ USER AREA 7
+++++++++++++++++++++++++++++++++++++++++
C
C----- DEFINE FLOW AT OUTLETS (MASS FLOW BOUNDARIES)
C      (TO TEMPERATURES AND SCALARS AT MASS FLOW BOUNDARIES USE
C       USER AREA 5)
C
```

```
C      SET PARAMETER IFLOUT:
C      IFLOUT = 1  ==> MASS FLOW SPECIFIED AT LABELLED OUTLETS.
C      IFLOUT = 2  ==> FRACTIONAL MASS FLOW SPECIFIED AT LABELLED
OUTLETS
C      IFLOUT = 2
C
C      SET OUTLET FLOW RATES:
C      FLOUT(LABEL) = MASS FLOW OUT OF OUTLETS LABELLED LABEL
(IFLOUT=1).
C      FLOUT(LABEL) = FRACTIONAL MASS FLOW OUT OF OUTLETS LABELLED
LABEL
C                        (IFLOUT=2).
C      FOR MULTIPHASE FLOWS IT IS NECESSARY TO SET
C      EITHER
C                        FLOUT(LABEL) = TOTAL MASS FLOW
C                        IFLOUT = 1
C                        IMFBMP = 0
C      OR
C                        FLOUT(LABEL + (IPHASE-1)*NLABEL) FOR EACH PHASE
C                        IFLOUT = 1 OR 2
C                        IMFBMP = 1
C
C---- EXAMPLE: EQUIDISTRIBUTION OF FRACTIONAL MASS FLOW AMONGST
OUTLETS
C
C      IFLOUT=2
C      FRAC = 1.0 / MAX( 1.0, FLOAT(NLABEL) )
C      DO 300 ILABEL = 1, NLABEL
C         FLOUT(ILABEL) = FRAC
C300  CONTINUE
C
C----END OF EXAMPLE
C
C++++++++++++++++ END OF USER AREA 7
++++++++++++++++++++++++++++++++
C
      RETURN
      END
      SUBROUTINE USRGRD(U,V,W,P,VFRAC,DEN,VIS,TE,ED,RS,T,H,RF,SCAL,
     +                  XP,YP,ZP,VOL,AREA,VPOR,ARPOR,WFACT,
     +                  XCOLD,YCOLD,ZCOLD,XC,YC,ZC,IPT,
     +
IBLK,IPVERT,IPNODN,IPFACN,IPNODF,IPNODB,IPFACB,
     +                  WORK,IWORK,CWORK)
C
C*******************************************************************
**
C
C   USER SUBROUTINE TO ALLOW USERS TO GENERATE A GRID FOR CFX-F3D
C
C   >>> USERS MAY ONLY ADD OR ALTER PARTS OF THE SUBROUTINE WITHIN
THE DESIGNATED USER AREAS                          <<<
C
C*******************************************************************
**
C
C   THIS SUBROUTINE IS CALLED BY THE FOLLOWING SUBROUTINES
C      CREATE  CUSR
C
```

```
C***********************************************************************
**
C   CREATED
C       27/04/90  ADB
C   MODIFIED
C       05/08/91  IRH  NEW STRUCTURE
C       09/09/91  IRH  CORRECT EXAMPLE
C       01/10/91  DSC  REDUCE COMMENT LINE GOING OVER 72 COLUMNS.
C       29/11/91  PHA  UPDATE CALLED BY COMMENT, ADD RF ARGUMENT,
C                      CHANGE LAST DIMENSION OF RS TO 6 AND IVERS TO 2
C       03/06/92  PHA  ADD PRECISION FLAG AND CHANGE IVERS TO 3
C       03/07/92  DSC  CORRECT COMMON MLTGRD.
C       23/11/93  CSH  EXPLICITLY DIMENSION IPVERT ETC.
C       03/02/94  PHA  CHANGE FLOW3D TO CFDS-FLOW3D
C       03/03/94  FHW  CORRECTION OF SPELLING MISTAKE
C       22/08/94  NSW  MOVE 'IF(IUSED.EQ.0) RETURN' OUT OF USER AREA
C       19/12/94  NSW  CHANGE FOR CFX-F3D
C
C***********************************************************************
**
C
C   SUBROUTINE ARGUMENTS
C
C     U      - U COMPONENT OF VELOCITY
C     V      - V COMPONENT OF VELOCITY
C     W      - W COMPONENT OF VELOCITY
C     P      - PRESSURE
C     VFRAC  - VOLUME FRACTION
C     DEN    - DENSITY OF FLUID
C     VIS    - VISCOSITY OF FLUID
C     TE     - TURBULENT KINETIC ENERGY
C     ED     - EPSILON
C     RS     - REYNOLD STRESSES
C     T      - TEMPERATURE
C     H      - ENTHALPY
C     RF     - REYNOLD FLUXES
C     SCAL   - SCALARS (THE FIRST 'NCONC' OF THESE ARE MASS
FRACTIONS)
C     XP     - X COORDINATES OF CELL CENTRES
C     YP     - Y COORDINATES OF CELL CENTRES
C     ZP     - Z COORDINATES OF CELL CENTRES
C     VOL    - VOLUME OF CELLS
C     AREA   - AREA OF CELLS
C     VPOR   - POROUS VOLUME
C     ARPOR  - POROUS AREA
C     WFACT  - WEIGHT FACTORS
C   * XC     - X COORDINATES OF CELL VERTICES
C   * YC     - Y COORDINATES OF CELL VERTICES
C   * ZC     - Z COORDINATES OF CELL VERTICES
C     XCOLD  - X COORDINATES OF CELL VERTICES AT START OF TIME STEP
C     YCOLD  - Y COORDINATES OF CELL VERTICES AT START OF TIME STEP
C     ZCOLD  - Z COORDINATES OF CELL VERTICES AT START OF TIME STEP
C
C     IPT    - 1D POINTER ARRAY
C     IBLK   - BLOCK SIZE INFORMATION
C     IPVERT - POINTER FROM CELL CENTERS TO 8 NEIGHBOURING VERTICES
C     IPNODN - POINTER FROM CELL CENTERS TO 6 NEIGHBOURING CELLS
C     IPFACN - POINTER FROM CELL CENTERS TO 6 NEIGHBOURING FACES
C     IPNODF - POINTER FROM CELL FACES TO 2 NEIGHBOURING CELL CENTERS
C     IPNODB - POINTER FROM BOUNDARY CENTERS TO CELL CENTERS
```

```
C      IPFACB - POINTER FROM BOUNDARY CENTERS TO BOUNDARY FACESS
C
C      WORK   - REAL WORKSPACE ARRAY
C      IWORK  - INTEGER WORKSPACE ARRAY
C      CWORK  - CHARACTER WORKSPACE ARRAY
C
C    SUBROUTINE ARGUMENTS PRECEDED WITH A '*' ARE ARGUMENTS THAT MUST
C    BE SET  BY THE USER IN THIS ROUTINE.
C
C    NOTE THAT OTHER DATA MAY BE OBTAINED FROM CFX-F3D USING THE
C    ROUTINE GETADD, FOR FURTHER DETAILS SEE THE VERSION 4
C    USER MANUAL.
C
C*********************************************************************
**
C
      LOGICAL LDEN,LVIS,LTURB,LTEMP,LBUOY,LSCAL,LCOMP
     +        ,LRECT,LCYN,LAXIS,LPOROS,LTRANS
C
      CHARACTER*(*) CWORK
C
C++++++++++++++++ USER AREA 1
++++++++++++++++++++++++++++++++++++++
C---- AREA FOR USERS EXPLICITLY DECLARED VARIABLES
C
C++++++++++++++++ END OF USER AREA 1
++++++++++++++++++++++++++++++++
C
      COMMON
     + /ALL/    NBLOCK,NCELL,NBDRY,NNODE,NFACE,NVERT,NDIM
     + /ALLWRK/ NRWS,NIWS,NCWS,IWRFRE,IWIFRE,IWCFRE
     + /ADDIMS/ NPHASE,NSCAL,NVAR,NPROP
     +          ,NDVAR,NDPROP,NDXNN,NDGEOM,NDCOEF,NILIST,NRLIST,NTOPOL
     + /CHKUSR/ IVERS,IUCALL,IUSED
     + /CONC/   NCONC
     + /DEVICE/ NREAD,NWRITE,NRDISK,NWDISK
     + /IDUM/   ILEN,JLEN
     + /LOGIC/  LDEN,LVIS,LTURB,LTEMP,LBUOY,LSCAL,LCOMP
     +          ,LRECT,LCYN,LAXIS,LPOROS,LTRANS
     + /MLTGRD/ MLEVEL,NLEVEL,ILEVEL
     + /SGLDBL/ IFLGPR,ICHKPR
     + /SPARM/  SMALL,SORMAX,NITER,INDPRI,MAXIT,NODREF,NODMON
     + /TIMUSR/ DTUSR
     + /TRANSI/ NSTEP,KSTEP,MF,INCORE
     + /TRANSR/ TIME,DT,DTINVF,TPARM
C
C++++++++++++++++ USER AREA 2
++++++++++++++++++++++++++++++++++++++
C---- AREA FOR USERS TO DECLARE THEIR OWN COMMON BLOCKS
C     THESE SHOULD START WITH THE CHARACTERS 'UC' TO ENSURE
C     NO CONFLICT WITH NON-USER COMMON BLOCKS

C++++++++++++++++ END OF USER AREA 2
++++++++++++++++++++++++++++++++
C
      DIMENSION
     +
U(NNODE,NPHASE),V(NNODE,NPHASE),W(NNODE,NPHASE),P(NNODE,NPHASE)
     +,VFRAC(NNODE,NPHASE),DEN(NNODE,NPHASE),VIS(NNODE,NPHASE)
     +,TE(NNODE,NPHASE),ED(NNODE,NPHASE),RS(NNODE,NPHASE,6)
```

```
     +,T(NNODE,NPHASE),H(NNODE,NPHASE),RF(NNODE,NPHASE,4)
     +,SCAL(NNODE,NPHASE,NSCAL)
      DIMENSION
     + XP(NNODE),YP(NNODE),ZP(NNODE),XC(NVERT),YC(NVERT),ZC(NVERT)
     +,XCOLD(NVERT),YCOLD(NVERT),ZCOLD(NVERT)
     +,VOL(NCELL),AREA(NFACE,3),VPOR(NCELL),ARPOR(NFACE,3)
     +,WFACT(NFACE)
     +,IPT(*),IBLK(5,NBLOCK)

+,IPVERT(NCELL,8),IPNODN(NCELL,6),IPFACN(NCELL,6),IPNODF(NFACE,4)
     +,IPNODB(NBDRY,4),IPFACB(NBDRY)
     +,IWORK(*),WORK(*),CWORK(*)
C
C+++++++++++++++++ USER AREA 3
+++++++++++++++++++++++++++++++++++++++++
C---- AREA FOR USERS TO DIMENSION THEIR ARRAYS
      DIMENSION
     + OMEGA(2),THETA(2),VRTVEL(2),FRCEPR(2),DELYB(500)

C---- AREA FOR USERS TO DEFINE DATA STATEMENTS

      REAL
     + MOMNT,ALPHA,INERTIA,TIME_ST,RDIST,DELYA,OTIMEST,VRTACC
     +,MPLATE,FRRIGHT,FRLEFT,VRTFRCE,DELTHTA,DELDST
     +,UCAREA,RADIUS,IMPNTA,IMPNTB

C+++++++++++++++++ END OF USER AREA 3
+++++++++++++++++++++++++++++++++
C
C---- STATEMENT FUNCTION FOR ADDRESSING
      IP(I,J,K)=IPT((K-1)*ILEN*JLEN+(J-1)*ILEN+I)
C
C---- VERSION NUMBER OF USER ROUTINE AND PRECISION FLAG
C
      IVERS=3
      ICHKPR = 1
C
C+++++++++++++++++ USER AREA 4
+++++++++++++++++++++++++++++++++++++++++
C---- TO USE THIS USER ROUTINE FIRST SET IUSED=1
C
       IUSED=1
C
C+++++++++++++++++ END OF USER AREA 4
+++++++++++++++++++++++++++++++++
C
       IF (IUSED.EQ.0) RETURN
C
C---- FRONTEND CHECKING OF USER ROUTINE
       IF (IUCALL.EQ.0) RETURN
C
C+++++++++++++++++ USER AREA 5
+++++++++++++++++++++++++++++++++++++++++
C

C-- THIS SECTION DETERMINES THE NEW POSITION FOR THE FLOATING PLATE
C-- THE GRID IS ALSO MOVED AS IF IT IS ATTACHED TO A SHAKING TABLE

C-- FOR THE SHAKING TABLE THE GRID IS MOVED AT EACH TIME STEP
```

```
C-- WHEREAS FOR THE FLOATING PLATE THE GRID IS MOVED AT COARSER
INTERVALS
C-- DETERMINED BY OTIMEST

C-- THIS IS DONE TO ALLOW THE PRESSURE TO SETTLE AFTER EACH MOVEMENT
OF THE PLATE

C-- VARIABLE NAMES
C      ALPHA = ANGULAR PLATE ACCELERATION
C      OMEGA = ANGULAR PLATE VELOCITY
C      THETA = ANGULAR PLATE DISPLACEMENT
C      INERTIA = PLATE MASS MOMENT OF INERTIA
C                  ABOUT ITS MID POINT (1/12)M*(L^2+B^2)
C      MOMNT = SUM OF MOMENTS ABOUT PLATE CENTER
C                CLOCKWISE IS POSITIVE
C      VRTFCE = PRESSURE FORCE IN Y DIRECTION
C      MPLATE = MASS OF PLATE
C      VRTACC = VERTICAL PLATE ACCELERATION
C      VRTVEL = VERTICAL PLATE VELOCITY
C        DELYA = DELTA VERTICAL DISPLACEMENT CENTER OF MASS
C        DELYB = DELTA VERTICAL DISPLACEMENT FROM ROTATION
C      TIME_ST = TIME STEP FOR FLUID SOLUTION
C      OTIMEST = TIME STEP INTERVAL WHEN PLATE SOLUTION IS PERFORMED


C-- SET INITIAL CONDITIONS
      MOMNT=0
      VRTFRCE=0
      INERTIA=6E-04
      MPLATE=0.51
      TIME_ST=1.0E-03
      OTIMEST=2.0E-03

      IF(TIME.LT.0.001)THEN
      ALPHA=0
      VRTACC=0
      OMEGA(1)=0
      THETA(1)=0
      VRTVEL(1)=0
      DELYA=0
      THETA(1)=0
      THETA(2)=0
      ENDIF
C-- ENDIF TIME LESS THAN 0.002


      OPEN(UNIT=13,FILE='VERT',STATUS='NEW')
      OPEN(UNIT=14,FILE='ROT',STATUS='NEW')
      OPEN(UNIT=15,FILE='PRESS',STATUS='NEW')

      IF(KSTEP.GT.4) THEN

      KINT=KSTEP/2*2

      IF(KINT.NE.KSTEP) GO TO 400

C--*****************************************************
C-- ROTATION SECTION
C--*****************************************************
```

```
C-- NOW DETERMINE AMOUNT OF ROTATION DUE
C-- TO SUM OF MOMENTS MOMNT=PRESS*AREA*DISTANCE
C-- ALSO THE FORCE IN THE VERTICAL DIRECTION
C-- IS DETERMINED HERE VRTFRCE=PRESS*AREA

C-- ALPHA = ANGULAR ACCELERATION
C-- OMEGA = ANGULAR VELOCITY ARRAY
C-- THETA = ANGULAR DISPLACEMENT ARRAY

       CALL IPREC('DUCT','BLOCK','CENTRES',IPT,ILEN,JLEN,
     +             KLEN,CWORK,IWORK)


          DO 200 J=31,31
             DO 200 I=22,57

             INODE = IP(I,J,1)
             IMPNTA=IP(39,1,1)
             IMPNTB=IP(40,1,1)

             RADIUS=((XP(IMPNTA)+XP(IMPNTB))/2)-XP(INODE)
             UCAREA=5.25E-04

             MOMNT=MOMNT+P(INODE,2)*UCAREA*RADIUS

             VRTFRCE=VRTFRCE+P(INODE,2)*UCAREA*COS(THETA(1))

             WRITE(15,*)TIME,I,P(INODE,2),MOMNT

  200   CONTINUE

       VRTFRCE=VRTFRCE/0.8

             WRITE(15,*)TIME,'TOTAL',MOMNT

       ALPHA = MOMNT/INERTIA

       OMEGA(2) = OMEGA(1)+ALPHA*OTIMEST

        DELTHTA = OMEGA(1)*OTIMEST+0.5*ALPHA*(OTIMEST*OTIMEST)


       THETA(2)=THETA(1)+DELTHTA/2

       WRITE(14,*)TIME,ALPHA,OMEGA(1),THETA(2)

C--*************************************************
C-- END OF ROTATION SECTION
C--*************************************************

C--*************************************************
C-- VERTICAL DISPLACEMENT SECTION
C--*************************************************

       VRTACC= (VRTFRCE-MPLATE*9.81)/MPLATE

       VRTVEL(2) = VRTVEL(1) + VRTACC*OTIMEST

       DELYA = VRTVEL(1)*OTIMEST +
```

```
     +        0.5*VRTACC*(OTIMEST*OTIMEST)

      DELDST=DELYA/2

      WRITE(13,*)TIME,VRTACC,VRTVEL(1),DELYA
C--*************************************************
C-- END OF VERTICAL DISPLACEMENT SECTION
C--*************************************************

C--*************************************************
C-- SECTION TO SET NEW CO-ORDINATES OF CELL VERTICES
C--*************************************************


C-- DETERMINE NEW Y CO-ORDINATES FOR EACH CELL

C-- USE IPREC TO FIND CELL ADDRESSES

      CALL IPREC('DUCT','BLOCK','VERTICES',IPT,ILEN,JLEN,
     +             KLEN,CWORK,IWORK)

        DO 300 K=1,KLEN
          DO 300 J=17,87
             DO 300 I=2,ILEN-1
C-- USE STATEMENT FUNCTION IP TO GET ADDRESSES
             INODE = IP(I,J,K)
             IMPNT = IP(40,1,1)

C-- DEFINE LOCATION OF GRID VERTICES
        DELYB(I)=( XC(INODE)-XC(IMPNT) )*( TAN(THETA(2))-TAN(THETA(1))
)

        YC(INODE)=YCOLD(INODE)+DELDST-DELYB(I)

  300 CONTINUE


        DO 301 K=1,KLEN
          DO 301 J=15,16
             DO 301 I=2,ILEN-1
C-- USE STATEMENT FUNCTION IP TO GET ADDRESSES
             INODE = IP(I,J,K)
             IMPNT = IP(40,1,1)

C-- DEFINE LOCATION OF GRID VERTICES
        DELYB(I)=( XC(INODE)-XC(IMPNT) )*( TAN(THETA(2))-TAN(THETA(1))
)

        YC(INODE)=YCOLD(INODE)+0.7*DELDST-0.7*DELYB(I)

  301 CONTINUE

        DO 302 K=1,KLEN
          DO 302 J=88,JLEN-1
             DO 302 I=2,ILEN-1
C-- USE STATEMENT FUNCTION IP TO GET ADDRESSES
             INODE = IP(I,J,K)
             IMPNT = IP(40,1,1)

C-- DEFINE LOCATION OF GRID VERTICES
```

```
      DELYB(I)=( XC(INODE)-XC(IMPNT) )*( TAN(THETA(2))-TAN(THETA(1))
)

      YC(INODE)=YCOLD(INODE)+0.7*DELDST-0.7*DELYB(I)

  302 CONTINUE

C-- SET CURRENT VALUES TO FIRST POSITON IN ARRAYS
C-- TO BE USED NEXT TIME STEP


      OMEGA(1)=OMEGA(2)
      THETA(1)=THETA(2)
      VRTVEL(1)=VRTVEL(2)

  400 CONTINUE

C-- SECOND TIME STEP CONSTANT MOTION

      IF(KINT.NE.KSTEP) THEN

      CALL IPREC('DUCT','BLOCK','CENTRES',IPT,ILEN,JLEN,
     +             KLEN,CWORK,IWORK)

         DO 401 J=29,29
            DO 401 I=22,57

            INODE = IP(I,J,1)

            WRITE(15,*)TIME,I,P(INODE,2)
  401 CONTINUE

      THETA(2)=THETA(1)+DELTHTA/2

      CALL IPREC('DUCT','BLOCK','VERTICES',IPT,ILEN,JLEN,
     +             KLEN,CWORK,IWORK)

       DO 199 K=1,KLEN
         DO 199 J=17,87
            DO 199 I=2,ILEN-1
C-- USE STATEMENT FUNCTION IP TO GET ADDRESSES
            INODE = IP(I,J,K)
            IMPNT = IP(40,1,1)
       DELYB(I)=( XC(INODE)-XC(IMPNT) )*( TAN(THETA(2))-TAN(THETA(1))
)

       YC(INODE)=YCOLD(INODE)+DELDST-DELYB(I)

  199 CONTINUE


       DO 410 K=1,KLEN
         DO 410 J=15,16
            DO 410 I=2,ILEN-1
C-- USE STATEMENT FUNCTION IP TO GET ADDRESSES
            INODE = IP(I,J,K)
            IMPNT = IP(40,1,1)

C-- DEFINE LOCATION OF GRID VERTICES
```

```
       DELYB(I)=( XC(INODE)-XC(IMPNT) )*( TAN(THETA(2))-TAN(THETA(1))
)

       YC(INODE)=YCOLD(INODE)+0.7*DELDST-0.7*DELYB(I)

  410 CONTINUE

       DO 411 K=1,KLEN
         DO 411 J=88,JLEN-1
            DO 411 I=2,ILEN-1
C-- USE STATEMENT FUNCTION IP TO GET ADDRESSES
            INODE = IP(I,J,K)
            IMPNT = IP(40,1,1)

C-- DEFINE LOCATION OF GRID VERTICES
       DELYB(I)=( XC(INODE)-XC(IMPNT) )*( TAN(THETA(2))-TAN(THETA(1))
)

       YC(INODE)=YCOLD(INODE)+0.7*DELDST-0.7*DELYB(I)

  411 CONTINUE


       THETA(1)=THETA(2)

       ENDIF

C ENDIF KINT NE KSTEP

      ENDIF
C-- ENDIF KSTEP GREATER THAN 4

C-- ****************************************************************
C-- SECTION FOR HORIZONTAL CONTAINER MOTION
C-- ****************************************************************

      CALL IPREC('DUCT','BLOCK','VERTICES',IPT,ILEN,JLEN,
     +            KLEN,CWORK,IWORK)

C-- LOOP OVER BLOCK

       DO 500 K=1,KLEN
         DO 500 J=1,JLEN
            DO 500 I=1,ILEN

            INODE = IP(I,J,K)
          XC(INODE)=XCOLD(INODE)+0.0005*SIN(2*3.14159*2.175*TIME)
     +                 -0.0005*SIN(2*3.14159*2.175*(TIME-0.001))

  500 CONTINUE

C++++++++++++++++ END OF USER AREA 5
++++++++++++++++++++++++++++++++++
C
      RETURN

      END
```